

國立臺灣大學生命科學院生命科學系



博士論文

Department of Life Science

College of Life Science

National Taiwan University

Doctoral Dissertation

核內中間神經元對小鼠藍斑核正腎上腺素細胞

自發相位性放電活性調控角色之功能性研究

Local Interneurons Regulate Spontaneous Phasic  
Activity of Noradrenergic Neurons in Mouse Locus  
Coeruleus and Functional Implications

郭昭成

Chao-Cheng Kuo

指導教授：閔明源 博士

Advisor: Ming-Yuan Min, Ph.D.

中華民國 109 年 8 月

August, 2020



國立臺灣大學博士學位論文  
口試委員會審定書

核內中間神經元對小鼠藍斑核正腎上腺素細胞  
自發相位性放電活性調控角色之功能性研究

Local Interneurons Regulate Spontaneous Phasic  
Activity of Noradrenergic Neurons in Mouse Locus  
Coeruleus and Functional Implications

本論文係郭昭成君（學號 D03B21007）在國立臺灣大學  
生命科學系、所完成之博士學位論文，於民國 109 年 7 月 28  
日承下列考試委員審查通過及口試及格，特此證明

口試委員：

劉明源

（簽名）

（指導教授）

陳志忠

劉明源

楊清雲

陳永國

吳玉威

連正喜

黃偉邦

（簽名）

生命科學系 系主任



# 致謝



謹以此論文，感謝與紀念幫助我完成研究的人事物。

尤其要感謝是閔明源老師，作為帶領我進入神經科學領域的啟蒙老師，老師對生理議題的思維構築方式與對學術事務的堅持，深遠地影響了我對於科學的想像。

也由衷感謝其他老師與學長姐們的提攜與教導；感謝師母楊琇雯老師帶給我有關

電子顯微鏡與神經型態學的訓練；感謝陳志成老師與陳世國老師指導我們製作與

使用腺病毒相關的材料；感謝姚皓傑老師指導我們進行動物行為的實驗；感謝連

正章老師與吳玉威學長對我的論文與口試的指導；感謝陳瑞芬老師給我有關生理

學的教導；感謝吳高逸老師給我的解剖學與動物標本處理的訓練；感謝經倫與昕

偉學長在美國開會時給我的指導；感謝信忠學長、瀚穎學長與怡嫻學姐在我還剛

學習做實驗的時候給我的指導。感謝連老師、Yanagawa與Yoshihara老師慷慨提

供Vglut2<sup>cre</sup>小鼠、GADGFP小鼠與WGA質體給我們。也感謝Techcomm提供的技術協助。

另外也要感謝幫助我一同完成論文研究的同儕與學弟妹，感謝戎建幫忙有關腺病

毒製造與神經追蹤相關實驗的部分；感謝幸君幫忙有關動物行為實驗的部分；感

謝育嫻幫忙有關遠端神經追蹤相關實驗的部分；感謝瑋辰學長與我對於科學的各

種共同討論、也感謝詹鎬、雨銘、品寰、珮瑜、冠廷、蓓萱、景萃、Daniel、姊

姊、謝秉與Wego陪我度過了在實驗室裏面美好的時光。最後要感謝我的家人與親

愛的芮妮給我的長期支持，讓我能順利完成博士班學業與論文研究。

# 中文摘要



藍斑核正腎上腺素細胞廣泛性投射軸突到幾乎整個大腦，在遭遇環境的新感官刺激或是行為實驗任務相關的訊息時，這些細胞能透過放射相位性叢集狀的動作電位組合來促成一個對感官刺激的導向性行為或是增進已熟稔的正向實驗任務表現。然而對相位性動作電位叢集來說，其細胞層次的產生機制尚未明瞭。在此我們報告了在小鼠腦切片中的藍斑核正腎上腺素細胞能夠產生類似活體中相位性動作電位叢集的自發性反應，被稱為自發性類相位性活化。我們團隊發現阻斷興奮性與抑制性的神經傳導可以消除或增幅自發性類相位性活化的現象，這樣的結果顯示藍斑核區域內存在一個小的迴路以產生此自發性類相位性活化，且迴路內興奮性與抑制性傳導會達成互動平衡以進一步調控這些自發性類相位性活化。我們從這樣的結果發想，我們找到了一群主要位於藍斑核內側的抑制性中間神經元能夠透過伽馬氨基丁酸與甘氨酸來對正腎上腺素藍斑核細胞行使前饋抑制。使用化學性遺傳學方法來專一性抑制這些核內抑制性中間神經元可以增幅自發性類相位性活化與前脈衝抑制行為。再者，框額葉皮質與前邊緣皮質這兩個跟支出與報酬審視的腦區投射軸突到藍斑核正腎上腺素細胞與上述的核內抑制性中間神經元。綜上所述，這些發現揭示了核內抑制性中間神經元能夠幫助藍斑核正腎上腺素細胞整合額葉來的訊息以及控管相位性動作電位叢集的出現。除了核內抑制性中間神經元之外，我也展示了一些與核內興奮性中間神經元有關的活



體腦切片實驗結果。利用光遺傳學的實驗方法確認了近藍斑核興奮性神經元至藍斑核正腎上腺素細胞的麩氨酸突觸傳導，且進一步使用鈣離子影像方法將具有活性的此些興奮性神經元區分為相位性與持續性放電族群。最後，我與團隊成員在細胞型態與鈣離子影像上的初步結果提供了一些線索，顯示藍斑核興奮性中間神經元對藍斑核相位性放電調控角色的可能性。

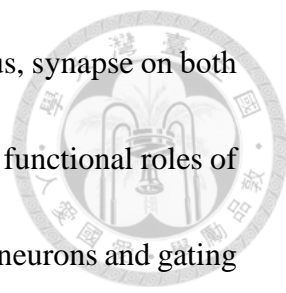
## 關鍵字：

化學遺傳學、光遺傳學、眶額皮質、前邊緣皮質、前脈衝抑制作用、全細胞記錄

# Abstract



Noradrenergic (NA) neurons in the locus coeruleus (LC) have global axonal projection to the brain. These neurons discharge action potentials phasically in response to either novel stimuli in the environment to initiate an orienting behavior or stimuli representing the outcome of task-related decision processes to facilitate ensuing behaviors and help optimize task performance. Nevertheless, the cellular mechanisms underlying the generation and regulation of phasic LC activation remain unknown. Our group report here that LC-NA neurons recorded in brain slices exhibit bursts of action potentials that resembled the phasic activation-pause profile observed in animals. The activity was referred to as spontaneous phasic-like activity (sPLA) and was suppressed and enhanced by blocking excitatory and inhibitory synaptic transmissions, respectively. These results suggest the existence of a local circuit to drive PLA, and the activity could be regulated by the excitatory-inhibitory balance of the circuit. In support of this notion, I and my colleagues located a population of inhibitory interneurons (I-INs) in the medial part of the peri-LC that exerted feedforward inhibition of LC-NA neurons through GABAergic and glycinergic transmissions. Selective inhibition of peri-LC I-INs with chemogenetic methods could enhance the sPLA in brain slices and increase prepulse inhibition in animals. Moreover, axons from the orbitofrontal and prelimbic cortices,



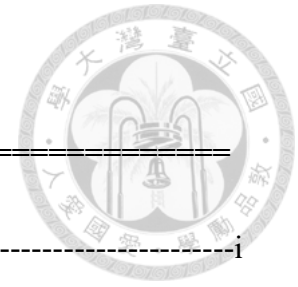
which play important roles in evaluating the cost/reward of a stimulus, synapse on both peri-LC I-INs and LC-NA neurons. These observations demonstrate functional roles of peri-LC I-INs in integrating inputs of the frontal cortex onto LC-NA neurons and gating the phasic LC output. In addition to the peri-LC I-INs, this thesis also show preliminary results of E-INs using brain slice recordings. In this part, I and my colleagues found the functional glutamatergic contacts from these E-INs onto LC-NA neurons by optogenetics approaches and morphology reconstructions, the E-IN population was classified into the burst and tonic E-INs according to the fluctuation pattern of calcium imaging. Finally, my results of the cell morphology and calcium imageing provide a positive evidence supporting the role of LC E-INs in driving sPLAs.

**Keywords:**

Chemogenetic, Optogenetic, Orbitofrontal cortex, Prelimbic cortex, Prepulse inhibition,

Whole-cell patch

# Contents



---

口試委員會審定書	i
致謝	iii
中文摘要	iv
Abstract	vi
Contents	viii
Abbreviations	x
Introduction	1
Section 1: Anatomy of LC NA Neurons	3
Section 2: Physiology of Locus Coeruleus	16
Section 3: Effects of NA on Synaptic Transmission	28
Section 4: Functional Implications of LC Discharging Patterns	40
Section 5: Local Regulation of the LC Phasic Activity	53
Specific Aim	62

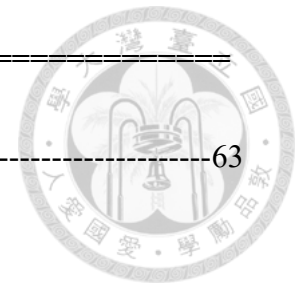
---

---

---

Materials and Methods-----	63
Results-----	85
Section 1: Identification of LC Local Circuit-----	87
Figures-----	95
Section 2: Role of peri-LC I-IN in Regulation of sPLA-----	116
Figures-----	131
Section 3: Functional Implications of peri-LC I-IN-----	167
Figures-----	174
Section 4: Positive Evidence of near LC ENs in Regulation of LC Phasic Activation-----	198
Figures-----	208
Discussion-----	226
Tables-----	252
Reference-----	259

---



# Abbreviations



## #

4-AP : 4-aminopyridine

5-HT : Serotonin

6-OHDA : 6-hydroxydopamine

6n : Abducens nerve

7n, Facial nerve

$\alpha_1$ -AR :  $\alpha_1$  adrenergic receptor

$\alpha_2$ -AR :  $\alpha_2$  adrenergic receptor

$\beta$ -AR :  $\beta$ -adrenergic receptor

## A

A1 : Primary auditory cortex

AAV : Adeno-associated virus

ACC : Anterior cingulate cortex

Ach : Acetylcholine

AchE : Acetylcholinesterase

AchR : Acetylcholinergic receptors

aco: Anterior commissure

aCSF : Artificial cerebrospinal fluid

AD : adenylyl cyclase

AIC: Anterior insular cortex

AHP : Afterhyperpolarization

AON: Anterior olfactory nucleus

AP : Action potential

AR : adrenoceptor

AU : Arbitrary unit



## **B**

Bar : Barrington nucleus

BLA : Basolateral amygdala

BM : Bicuculline methochloride

BSA : Bovine serum albumin

## **C**

CaMKII : Calmodulin kinase type II

cAMP : Cyclic AMP

cc: Corpus callosum

CeA : central nucleus of the amygdala

Cg1: Anterior cingulate cortex

ChAT : Choline acetyltransferase

ChR2 : channelrhodopsin 2

ChriR-tdT : ChrimsonR tagged with tdtomato

CNO : Clozapine-N-oxide

CRF : Corticotropin-releasing factor

CRH : Corticotropin-releasing hormone

CS : Conditioned stimulus

## **D**

DA : Dopamine

DAB : Diaminobenzidine

DBH : Dopamine  $\beta$  hydroxylase

DDM : Drift diffusion model

DIO : double-floxed inverse orientation

DREADD : designer receptors exclusively activated by the designer drugs

## **E**

E-IN : excitatory interneurons

EEG : electroencephalograph

eYFP : enhanced yellow fluorescent proteins



## **F**

fMRI : Functional magnetic resonance imaging

## **G**

GABA<sub>A</sub>R : GABA<sub>A</sub> receptor

GAD : Glutamic acid decarboxylase

GFP : Green fluorescent protein

GlyR : Glycine receptor

## **H**

HCN : Hyperpolarization-activated cyclic nucleotide-gated channels

HEK-293 : Human embryonic kidney 293 (a line of cell culture)

hM3DqR : hM3Dq receptor

hM4DiR : hM4Di receptor

HW : Half width

## **I**

I-clamp : Current clamp

I-IN : inhibitory interneurons

IC : Inferior colliculus

I<sub>CNO</sub> : Outward CNO-sensitive current

I<sub>h</sub> current : Hyperpolarization-activated cation current

IHC : Immunohistochemistry

ILA: Infra-limbic cortex  
IN : Interneuron  
IP : Intraperitoneal  
IP<sub>3</sub> : 1,4,5-triphosphate  
IPSC : Inhibitory postsynaptic currents  
ir : Immunoreactive  
IRt : Intermediate reticular nucleus



## **K**

KA : Kynurenic acid

## **L**

large sEPSC : Spontaneously large EPSC  
LC : locus coeruleus  
LDTg : laterodorsal tegmental nucleus  
IOFC : Lateral orbitofrontal cortex  
lot: Lateral olfactory tract  
LPB : Lateral parabrachial nucleus  
LPGN : Dorsal lateral geniculate nucleus  
LTD : Long-term depression  
LTP : Long-term potentiation

## **M**

M1 : Primary motor cortex  
M2 : Secondary motor cortex  
Me5 : Mesencephalic trigeminal nucleus  
Mo5 : Motor trigeminal nucleus  
mOFC : Medial orbitofrontal cortex



## **N**

NA : Noradrenaline

NDS : Normal donkey serum

NE : Norepinephrine

NMDG : N-methyl-D-glucose

NPY : Neuropeptide Y

## **O**

OFC : Orbitofrontal cortex

OT: Olfactory tubercle

## **P**

PB : Phosphate buffer

PBS : Phosphate buffer saline

PBST : 0.3% Triton X-100 in PBS

PCRtA : Parvicellular reticular nucleus, alpha

peri-LC : Pericerulear dendritic zone of LC nucleus

peri-LC I-IN : Inhibitory interneuron located in Pericerulear dendritic zone of LC  
nucleus

PFC : Prefrontal cortex

PGN : Gerigeniculate reticular nucleus

PIR: Piriform cortex

PLC : phospholipase C

PPI : Prepulse inhibition

PPTg : pedunculopontine nucleus

PnC : Nucleus reticularis pontis caudalis

Pr5 : Principal sensory trigeminal nucleus

PrL : Prelimbic cortex

PTN : Parataenial thalamic nucleus

## **R**

RMS : Root mean square

ROI : Region of interest

RT : Rising time



## **S**

S1 : Primary somatosensory cortex

scp : Superior cerebellar peduncle

SD : Standard deviation

SEM : Standard error

sEPSC : Spontaneous excitatory synaptic current

sPLA : Spontaneous phasic-like activity

STDP : Spike timing dependent plasticity

STN : Subthalamic nucleus

Stry : Strychnine

Syn : Synaptophysin

## **T**

TCR : Truncated conditioned reflex

TEA : tetraethylammonium

TH : Tyrosine hydroxylase

TranN : Transneuronal

TRN : thalamic reticular nucleus

TTX : Tetrodotoxin

## **U**

US : Unconditioned stimulus

## **V**

V-clamp : Voltage clamp

Vgat : Vesicular GABA transporter

Vglut2 : Vesicular glutamate transporter 2

VLPO : ventrolateral preoptic area

vOFC : Ventral orbitofrontal cortex

VTA : Ventral tegmental area



## **W**

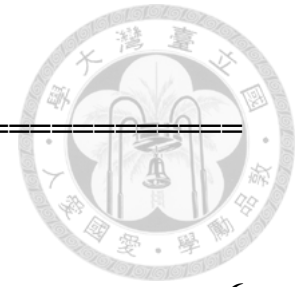
WGA : Wheat germ agglutinin

WT : Wild type

# INTRODUCTION

---

---



## Section 1: Anatomy of LC NA Neurons

1.1 Sky Blue Place in Brain-----	6
1.2 General Anatomy-----	6
1.3 Global Efferents-----	7
1.4 Afferents to Locus Coeruleus-----	11

## Section 2: Physiology of Locus Coeruleus

2.1 Spontaneous Activity of LC-NA Neurons-----	17
2.2 Autoregulation of LC-NA Neurons-----	20
2.3 LC-NA Activity and Wakefulness-----	21
2.4 Two Firing Modes of LC-----	23

## Section 3: Effects of NA on Synaptic Transmission

3.1 Adrenergic Receptors-----	28
3.2 Noradrenergic Effects in Cortex and Hippocampus-----	30
3.3 Noradrenergic Effects in Subcortical Area-----	34

---

---



---

---

**3.4 Co-release of Dopamine from Noradrenergic Terminals-----36**

**Section 4: Functional Implications of LC Discharging Patterns**

**4.1 Roles of LC-NA System in Sensory Processing-----39**

**4.2 Adaptive Gain Theory-----42**

**4.3 Network Reset Theory-----45**

**4.4 Functional Interpretation of LC Activities in Cognition-----48**

**Section 5: Local Regulation of the LC Phasic Activity**

**5.1 General Regulations of LC Activity-----51**

**5.2 Direct and Indirect Mechanisms Underlying LC Phasic  
Activity-----53**

**5.3 Possible Role of Local Circuit-----54**

# Section 1



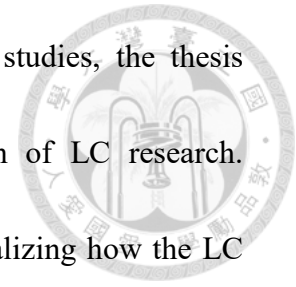
## Anatomy of LC NA Neurons

In order to know the physiology of the LC, the fundamental work of scientists was to build a knowledge of the anatomy. Based on that, many works further build our understanding of the LC. As the pioneers had done, the basic anatomy of LC-NA neurons should be introduced in the beginning of this thesis, including the general anatomy, efferents, and afferents.

## 1.1 Sky Blue Place in Brain

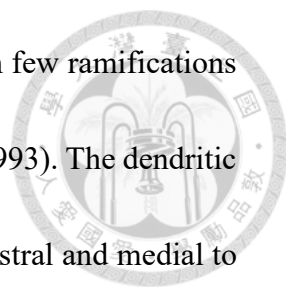
This thesis contains my works that focuses on the locus coeruleus nucleus (LC). Such a small nucleus maintains a wildspread axonal projection and offers its huge impact on the individual behavior. The oldest literature record of LC nuclei appeared in the late 18<sup>th</sup> century, the era of the first industrial revolution, when Félix Vicq d’Azyr (Félix Vicq d’Azyr, 1793), a French anatomist, made the very first description of this blue-colored brain area (Shane R. et al., 2011) and his work and denomination of the LC are still in use nowadays. In that time, the term “locus coeruleus”, meaning “sky-blue or dark-blue place” in Latin, was used to describe the region with an azure appearance in the unstained brain tissue. Not until the latter half of the 20<sup>th</sup> century, scientists learned that such a blue color is due to the cytoplasmic organelle storage of a polymeric compound, neuromelanin, which is derived from catecholic metabolites and found in rich quantities in LC, as well as other brain regions comprising of dense catecholaminergic cells (Kazumasa et al., 2015). It was not until the emergence of catecholamine histochemistry in the 1960s that the LC was discovered to contain a large amount of monoaminergic cells and be the primary brain region for the synthesis of noradrenaline (NA), also known as norepinephrine (NE) (Carlsson et al., 1962; Joe and Russell, 1964). Nowadays, the LC has accumulated decades of research works and

become a popular research target for scientists. Like the prior studies, the thesis demonstrates scientific results and contributes to the campaign of LC research. Personally, I wish this work can provide some new insights in realizing how the LC works and acts as an operation centre of attention and motivation.



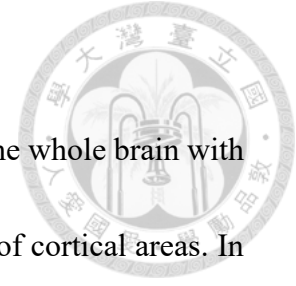
## 1.2 General Anatomy

In rodents, there are seven noradrenergic nuclei identified across the brainstem (A1 to A7) and similar correspondents are also found in humans, showing the conserved noradrenergic system in mammalian (Dahlström and Fuxe, 1964; Bogerts, 1981). In fact, the LC (A6) is the largest noradrenergic nucleus providing a principle supply for the entire neocortex, thalamus, hippocampus, cerebellum, as well as the spinal cord. In human, the LC is located in the floor of the 4<sup>th</sup> ventricle and predominantly composed with medium sized (35-45  $\mu\text{m}$ ) noradrenergic cells, displaying normally bipolar fusiform or multipolar in somatic morphology. The majority of the LC noradrenergic (LC-NA) neurons tend to form a tight assembly mixing with a few of the non-noradrenergic neurons which are usually small in size. This dense arrangement of LC-NA neurons is referred to as the LC-proper, and this anatomic feature is also found in other mammalian. Studies using golgi stain or immunohistochemistry (IHC) of human

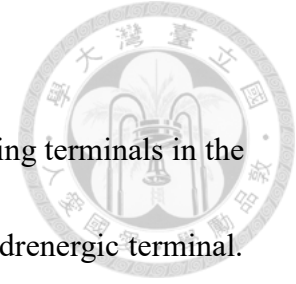


LC-NA neurons exhibited the typically 3-4 long, thin dendrites with few ramifications and branches (Chan-Palay and Asan, 1989; Patt S. and Gerhard L. 1993). The dendritic architecture of preferentially occupies the pontine tegmental area rostral and medial to the LC nuclei (rostromedial pericoerulear region), while a small portion of dendrites extend in to both the caudomedial (caudal juxtaependymal pericoerulear region), and the dorsolateral to the LC nuclei near the 4<sup>th</sup> ventricle (Shipley et al., 1996; Bangasser et al., 2011). Moreover, a sparse population of noradrenergic neurons which distributes in the ventral region of the LC nuclei and subcoeruleus region was found to make the descending innervations to the brainstem and spinal cord. Such a subset of the LC-NA neurons favoring the descending projection was further revealed by using the modern viral tracing techniques in mice (Westlund and Coulter, 1980; Schwarz et al., 2015; Hirschberg et al., 2017). The distribution pattern and functional implications of the groups of LC-NA neurons with different projecting preference has been further reported recently (Hirschberg et al., 2017; Uematsu et al., 2017).

### 1.3 Global Efferents



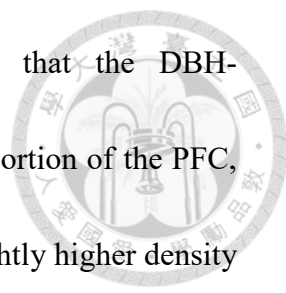
In contrast, the LC-NA neurons project their axons to almost the whole brain with extensive arborizations, especially the branch innervate to the vast of cortical areas. In primate, the organization of the LC axon can be divided into three bundles near the rostral tegmental region that is not far from the rostromedial dendritic field, then subsequently give rise into the many axonal collaterals along the long distance projection: (1) the dorsal noradrenergic bundle responsible to the ascending pathway that eventually innervates to the forebrain structure, including the entire neocortex, thalamus, limbic system, and midbrain. (2) the superior cerebellar bundle mainly projects to the cerebellum. (3) the descending bundle sends axons to the lower brainstem regions and all the columns of the spinal cord (Szabadi, 2013). Studies using the immunohistochemistry of dopamine  $\beta$  hydroxylase (DBH), a necessary enzyme for the NA synthesis, demonstrated that even single noradrenergic axon travels across cortices for the heterogeneous brain functions. In addition to the anatomy reports, antidromic action potentials (APs) were recorded from the LC-NA neurons in response to the electrical stimulation in the different cortical and thalamic locations, and served as an early criteria of the LC in vivo unit in rat (Segal et al., 1983; Aston-Jones et al., 1985; Foote S. L. and Morrison J. H., 1987; Nakazato, 1987).



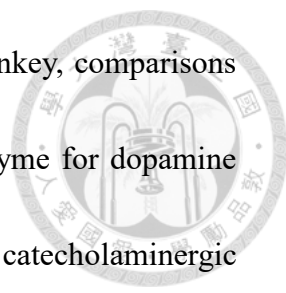
The electronic microscopic investigations of the DBH expressing terminals in the monkey prefrontal cortex (PFC) revealed the fine structure of noradrenergic terminal.

Enlarged portions of noradrenergic fibers (usually up to 500 nm) with accumulating clear and abundant vesicles, were considered as functional varicosities. Most of the synaptic junction formed by the DBH immunoreactive components did not associate toward an identifiable post-synaptic component, neither the encapsulating synaptic cleft by the astrocytic processes, and only 5-10% of them exhibited typical features of a junctional complex. The ultrastructural evidence suggests that the NA likely act as a volumetric neurotransmitter which results in a broader spatiotemporal effect than the point-to-point fast transmission (Descarries et al., 1997; Aoki et al., 1998).

Despite the global innervation, the LC-NA axons distribute in a heterogeneous manner and show regional specificity, as this feature was reported in rodent and primate using IHC in the late 70s to 80s. In general, there are relatively dense varicosities in some regions of the PFC, including the primary motor cortex (M1) and some of the sensory cortices. In addition to the difference across the cortices, a considerable laminar variation is far greater in a primate than in a rodent. Morrison and his colleagues



performed a series IHC experiment in monkey, and found that the DBH-immunoreactive (ir) fibers made extensive innervations in a large portion of the PFC, with relatively less but tangential fibers in the superficial layer; slightly higher density in layers II/III; the most abundant fibers in layer V and slightly lower density in layer VI. The Brodmann area 8b demonstrated the most abundant noradrenergic innervations among the entire monkey neocortex, while the Brodmann areas 9 and 10 showed the lowest in density. Interestingly, the Brodmann area 8b, part of the medial frontal cortex, was found to correlate with increasing uncertainty using the functional magnetic resonance imaging (fMRI) (Volz et al., 2005). These findings provided evidence for the functional implications of the LC when facing an uncertain choice. Furthermore, Lewis and Morrison focused on the primary somatosensory cortex (S1) located in the postcentral gyrus (Brodmann areas 3,1,2), and found another type of laminar difference, as layer I contained smaller tangential fibers and also some radial and oblique fibers extending to layers II/III; layers IV/V, and layer VI were marked by extensive varicosities and a dense band of tangential fibers parallel to the white matter, respectively. Noradrenergic fibers in the M1 located in the monkey precentral gyrus (Brodmann area 4) showed a similar pattern when compared to those in the S1, with general innervations in all of the layers but fairly higher density in the deeper layers.

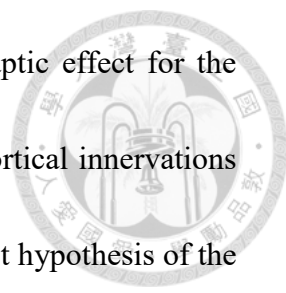


Following the findings of Morrison and his colleagues in monkey, comparisons among the DBH- and TH- (tyrosine hydroxylase, a necessary enzyme for dopamine (DA) and NA syntheses) IHC profiles demonstrated that these two catecholaminergic projections shared a high similarity, and few interesting differences. For example, dopaminergic fibers were found more extensive than noradrenergic fibers in the M1 but fairly sparse in the S1 showing noradrenergic-rich, as this difference was reckoned as the distinct functions between the two catecholamergic systems (Morrison et al., 1982b; Lewis et al., 1987; Lewis and Morrison, 1989; Berger et al., 1988). Compared to the primate, the noradrenergic fibers showed relatively uniform but the same distributing tendency in the rodent cortices, with slightly higher fibers in the PFC and M1. Studies using IHC displayed that the DBH-ir fibers arranged as a grid-like tangential pattern in the superficial layer with slightly higher density than the deeper layers, and the white matter-paralleling fibers in layer VI across the rat cerebral cortex (Morrison et al., 1978; Morrison and Magistretti, 1983; Agster et al., 2013).

## 1.4 Afferents to Locus Coeruleus

In spite of the widespread projection, the LC receives massive synaptic afferents from the selective brain regions. Abundant innervations from the several nuclei corresponded to the various brain functions, coupled with the expression of wide types of receptors. The complexity of the afferent indicates that the LC-NA neurons display a diversified pattern of activity by receiving the delicate, multi-level regulations when engaged in different behaviors and physiological states.

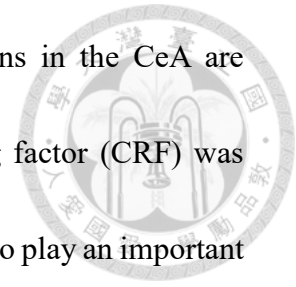
The PFC is the most well-known cortical area forming reciprocal connections to the LC, as studies using the IHC combining the tracing method on primates revealed this feature of a selective descending projection and a broad ascending projection. Besides the PFC, the LC also receives limited afferents from other cortical areas. Terminals of cortical afferents are dense in the rostromedial aspect of the LC, particularly in regions medial to the LC-proper (Porrino and Goldman-Rakic, 1982; Arnsten and Goldman-Rakic, 1984; Aston-Jones and Cohen, 2005). Jodo and Aston-jones published papers using the unit recording together with electrical or pharmacological stimulation in the medial prefrontal cortex that showed an excitatory effect to the LC which expressed ~35ms as median of latency onsets through the



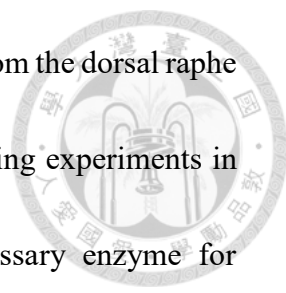
glutamatergic transmission in rat. They supposed a complex synaptic effect for the variation of onset latency comprising of both direct and indirect cortical innervations (Jodo and Aston-Jones, 1997; Jodo et al., 1998). This is the very first hypothesis of the LC local interneurons (INs). Moreover, electrical stimulations in the LC consistently evoked antidromic activations in the rat prefrontal cortex unit, and provided evidence of direct cortical projection to the LC (Branchereau et al., 1996).

The amygdalo-brainstem projection terminates in many catecholaminergic nuclei and is involved in the defensive or stress related behaviors. Like the PFC, the amygdala also forms a reciprocal connection to the LC. In rodents, the amygdalar axonal projection originates from the central nucleus of the amygdala (CeA), and the reciprocal noradrenergic projection mainly terminates in the basolateral amygdala (BLA) (Wallace et al., 1989; Price and Amaral, 1981; Valentino and Van Bockstaele, 2008; McCall et al., 2015; McCall et al., 2017). Interestingly, afferents from the CeA occupy the dorsolateral aspect of the LC and continues with those innervations in the parabrachial nucleus, and only a small patch of arborizations is directly located in the medial to the LC-proper. Distributions of the afferents arising from the PFC and the amygdala reflect a possible spatial discrimination in the integration of these inputs

(Valentino and Van Bockstaele, 2008). The LC-projecting neurons in the CeA are mainly GABAergic, the coreleasing of the corticotropin-releasing factor (CRF) was also reported by several studies, and this CRFergic input was found to play an important role in stress, anxiety, and aversive behaviors (Van Bockstaele et al., 1998; Van Bockstaele et al., 1999; McCall et al., 2015).

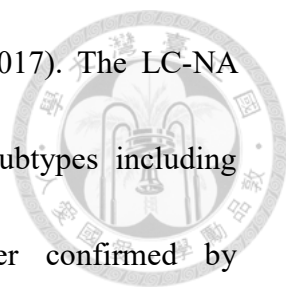


Dopaminergic neurons located in the ventral tegmental area (VTA), a midbrain nucleus, send a dense innervation to the LC. Actually, the NA is derived from the DA, thus, it cannot be excluded from the self-supply of dopamine-NA co-releasing from the LC-NA neurons. One of following section will discuss the co-releasing of the DA and NA. In rats, studies using the IHC showed that the VTA projected extensively to the LC and lesions of the VTA removed a large portion of the dopaminergic fibers in the dorsal pontine area (Swanson, 1982; Ornstein et al., 1987; Maeda et al., 1994; Kitahama et al., 2000). The expression of the dopaminergic receptors showed the functional transmission of the DA onto the LC-NA neurons. Furthermore, the infusion of agonists of the dopaminergic receptors affected the exploring and morphine withdrawal behavior in rodents (Weine et al., 1991; Lazarov et al., 1998; Dizgah et al., 2005; Lin et al., 2008).



The LC-NA neurons also receive dense serotonergic inputs from the dorsal raphe nucleus and forms a reciprocal connection between them. The tracing experiments in rats combining the IHC of the tryptophan hydroxylase, a necessary enzyme for serotonin syntheses, revealed a topological serotonergic projection to the LC from the majority of the posterior raphe nuclei (Pickel et al., 1997; Imai et al. 1986; Miller et al., 2011). This projection was later supported by examinations of the serotonergic pharmacology of the different receptors on LC-NA neurons. In conclusion, the net effect of the serotonergic inputs onto rodent LC-NA neurons was to provide a tonic inhibition of membrane potential and decrease the excitability (Aston-Jones et al., 1991; Pudovkina et al., 2002; Ortega et al., 2012; de Freitas et al., 2016).

In addition, LC-NA neurons receive inputs of acetylcholine (Ach) from the cholinergic neurons of the pedunclopontine nucleus (PPTg) and the laterodorsal tegmental nucleus (LDTg), as both of them are tegmental nuclei, actually the LDTg is located in the dorsomedial region adjacent to the LC nuclei. The immunoreactive signal of the choline acetyltransferase (ChAT, an essential enzyme for Ach production), and acetylcholinesterase (AChE, a critical enzyme for removing the Ach from the synaptic cleft) showed copious cholinergic afferents in the LC area of rats and cats (Jones B. E.



1990, Sutin and Jacobowitz, 1991; Mena-Segovia and Bolam, 2017). The LC-NA neurons were found to express various Ach receptor (AchR) subtypes including nicotinic and muscarinic receptors, this finding was further confirmed by electrophysiological approaches in rats and cats (Baghdoyan et al., 1994; Léna et al., 1999). Applications of the AchRs agonists or simply Ach increased the firing rate of the LC-NA neurons in both in vivo and in vitro investigations. Hence, the cholinergic agonists acted as a pharmacological activator for rodent LC-NA neurons in many studies (Egan and North, 1986; Berridge C. W. and Foote, 1991; Shen and North, 1992; Alsene and Bakshi, 2011). My unpublished data in mice showed that the AchR agonist induced a muscarinic AchR subtype 1, 3, but not 2, 4, mediated the depolarization in the LC-NA neurons, and similar results were obtained from local INs. The cholinergic system plays an important role in expressing the sleep-awake cycle, many cholinergic neurons in the tegmental area are active during the waking state and REM sleep, as lesions of them lead to an elimination of the paradoxal sleep in rats and cats (Jones B. E. 1991a; 1991b; Torontali et al., 2014). The nearly silent activity of the LC during sleep is proposed to be regulated by distal and local GABAergic innervations, which could be triggered by the widespread Ach efferent in rodents and cats (Nitz and Siegel, 1997; Gervasoni et al., 1998; Mallick et al., 2001; Pal and Mallick, 2007).

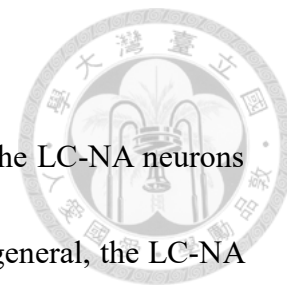
## Section 2



## Physiology of Locus Coeruleus

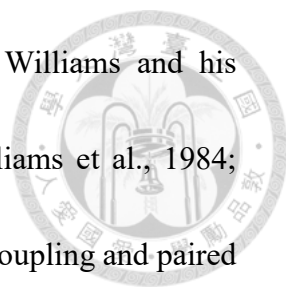
Based on the unique characteristics in anatomy, the LC-NA neurons also have their own physiological property which keeps the background releasing of the NA, but a quick response to the external inputs then put themselves into a transient activation. Many general features directly linked to the neural activity of the LC-NA neurons will be reviewed and discussed in this section.

## 2.1 Spontaneous Activity of LC-NA Neurons

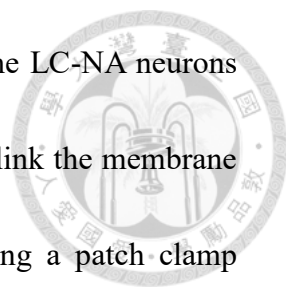


Both *in vivo* and *in vitro* electrophysiological recordings on the LC-NA neurons showed a fairly homogeneous cell property and neural activity. In general, the LC-NA neurons shared a relatively synchronous firing activity as the similar mean firing frequency and considerable variation among the individual cells (Foote et al., 1980; Grant et al., 1988; Wang et al., 2015). As aforementioned, it has been found that the antidromic activations could trigger the APs with a longer duration (2-3 ms) and biphasic waveform in the LC-NA unit, such an experiment revealed a slower axonal conduction velocity, usually 1-5 m/s in primates and cats (Segal et al., 1983; Nakazato, 1987; Foote and Berridge, 2019). Studies in rats and monkeys using the electron microscope provided a complementary result showing characteristics of the smaller diameter unmyelinated DBH-ir fibers and varicosities in variable sizes among several brain regions, echoed to the slow conducting velocity of noradrenergic axons (Morrison and Foote, 1986; Farb et al., 2010).

The most important cell property of the LC-NA neurons is that they exhibit spontaneous APs even those present in the blocking of the fast synaptic transmission, so it is considered as an endogenous property related to the channel composition but



not the synaptic inputs. And this feature was first reported by Williams and his colleagues, similar results was also observed by our groups (Williams et al., 1984; Alvarez et al., 2002; Wu et al., 2020). Studies in rodents using dye coupling and paired recordings demonstrated that many LC-NA neurons share a synchronous firing and the oscillation of membrane potential via electrical connections, the frequent appearance of spikelets at peaks of fluctuation were also found. The broad but weak expression of gap junction subtypes was also found between the LC dendrites as well as between the LC-NA neurons and glia in the postnatal rat (Christi and Jelinek, 1993; Ishimatsu and Williams, 1996; Alvarez-Maubecin et al., 2000; Van Bockstaele et al., 2004; Rash et al., 2007). The electrical couplings help to maintain the synchronous firing and integrate synaptic events in the dendrites when afferent inputs arrive. The presence of a gap junction blocker abolishes the spontaneous spikelet and the oscillation of membrane potential in postnatal rats (Wu. et al., 2020). Moreover, paired recordings of rat adult LC-NA neurons showed a subthreshold oscillation which tends to synchronize the neural activity when the overall firing rate becomes too low, although the adult LC-NA neurons exhibit a weaker electrical coupling with each other. Whereas the postnatal LC-NA neurons show a higher synchronicity of neural activity regardless of the presented firing rate (Christie et al., 1989; Alvarez et al., 2002).



A detailed understanding of the pace making mechanism of the LC-NA neurons has not, as yet, been established, albeit many studies have tried to link the membrane property to the spontaneous firing ability. Studies in rodents using a patch-clamp recording on rats suggested that the persistent calcium current, the tetrodotoxin (TTX) sensitive sodium current, tetraethylammonium (TEA) sensitive potassium current, as well as the L/T-type calcium current, and the calcium activated potassium current, built a gradual depolarization during the inter-spike interval of spontaneous APs (Williams et al., 1984; Stocker and Pedarzani, 2000; de Oliveira et al., 2011; Matschke et al., 2015; Matschke et al., 2018). The higher persistent TTX resistant sodium current was also detected in adult mice and resulted in an increase of voltage fluctuations within the inter-spike interval and was thought as a possible pace generator (de Oliveira et al., 2011). Besides, many pontine noradrenergic neurons share a feature of the strong expression of voltage gated transient potassium channel (A-type potassium channel), which results in a significant delay of firing after the hyperpolarized steps and contributes to the fluctuations that drive the AP firing (Forsythe et al., 1992; Min et al., 2010). The data from our group in rats and mice showed that the LC-NA neurons largely increased the background firing rate in the presence of 4-aminopyridine (4AP, an A

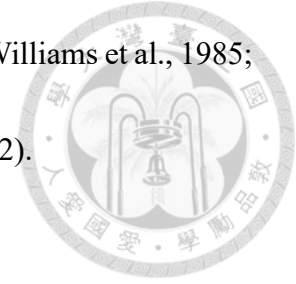
channel blocker), and further supported the role of the A channels in the regulation of the LC firing rate.



## 2.2 Autoregulation of LC-NA Neurons

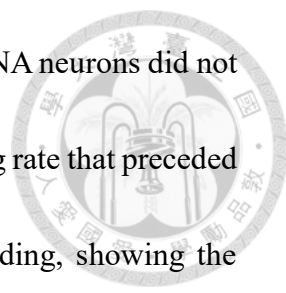
The  $\alpha 2$  adrenoreceptor (AR) was found on the somata, dendrites, and presynaptic components of the axon terminals of the LC-NA neurons. Combining the evidence of the dendritic and somatic NA releasing in rats show an autoregulation of the LC-NA neurons through the NA released from themselves (Aghajanian and VanderMaelen, 1982; Vila-Porcile et al., 2009; Huang et al., 2012). The fine structure of rat LC-NA neurons revealed that the distribution of specific  $\alpha 2$  subtypes, which were primarily located at the extrasynaptic and subcellular sites across the TH-ir components, while some  $\alpha 2$  subtypes were also found in some of the glia process (Lee et al., 1998a; Lee et al., 1998b). I will introduce the different ARs in Section 3. Shortly, the activation of the  $\alpha 2$  AR yielded a hyperpolarized effect on the LC-NA neurons through an increasing of the potassium conductance by the Gi protein signal pathway and subsequent inhibition of adenylate cyclase. Together, these findings suggest an activity dependent on autoregulation against the hyperactivity of the LC-NA neurons themselves for

maintaining a proper firing intensity and global NA concentration (Williams et al., 1985; Aghajanian and Wang, 1986; Jedema et al., 2008; Huang et al., 2012).



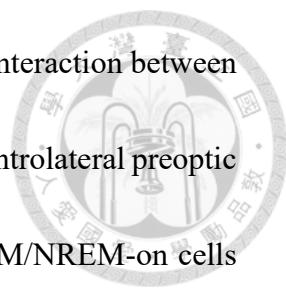
### **2.3 LC-NA Activity and Wakefulness**

The microdialysis examination in rat showed the linear relationship of the cortical NA concentration and the firing rate of the LC-NA neurons (Berridge and Abercrombie, 1999), and the LC-NA neurons activity is positively correlated with the forebrain electroencephalograph (EEG) and the behavior index of arousal in cats (Hobson et al., 1975). These relationships provided the methods for monitoring the LC activity in early researches. Historically, our understanding on the LC-NA system started from the wakefulness and arousal, as the pioneer studies found that the LC-NA neurons exhibit different firing rates among the sleep away cycle, as usually there is 3-5Hz of AP firing throughout the waking state depending on the wakefulness, about 1Hz in the NREM sleep and nearly silent in the REM sleep. And this conserved feature was also seen in other mammalian animals (Aston-Jones and Bloom, 1981; Berridge et al., 1993.; Pace-Schott E. F. and Hobson, 2002; Berridge et al., 2012).



In 1981, Aston-Jones and Bloom also revealed that the rat LC-NA neurons did not anticipate the transient of awaking but generally increased their firing rate that preceded the transient for 0.5 to 2 seconds by using the in vivo unit recording, showing the hypothetic role of waking priming. And this argument was supported by studies on cats, too (Aston-Jones and Bloom, 1981; Pace-Schott E. F. and Hobson, 2002). The pharmacological activation of the LC-NA neurons via the AchRs agonists triggered a switch from the REM sleep to the waking state, similar results were obtained by manipulations of the LC-NA neurons by the optogenetics and chemogenetics method in rodents (Berridge and Foote, 1991; Carter et al., 2010; Vazey and Aston-Jones, 2014). In contrast, overall inactivations of rat LC-NA neurons by the infusions of clonidine, a potent  $\alpha_2$  AR agonist, caused an opposite change in the cortical and hippocampal EEG shifting from a desynchronized, high frequency and low amplitude waveform into a slow wave pattern with large amplitude activities (Berridge et al., 1993).

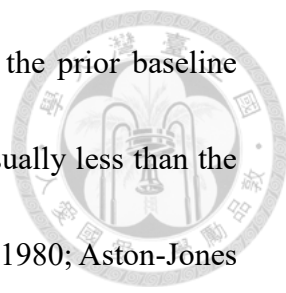
The NA-dependent waking function has been discussed in many wake-promoting regions, for example, the medial septum and the medial preoptic area. The infusion of the  $\beta$  AR agonists in these regions yielded a robust activation of the forebrain EEG pattern and an increase in the waking behavior indices in rats (Berridge and Foote,



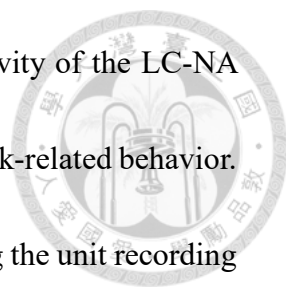
1996a; Berridge et al., 1996b). Studies in rodents demonstrates the interaction between the LC and the preoptic area in regulation of sleep. Neurons in the ventrolateral preoptic area (VLPO), another preoptic region, are characterized as the REM/NREM-on cells that send the GABAergic projections to the LC-NA neurons and receive reciprocal noradrenergic innervations. The bidirectional projection between the wake- and sleep-on cells suggests a dual interaction among the sleep-awake cycle. For instance, the LC-NA neurons receive a dense GABA transmission during sleep and decrease their activity before the REM/NREM-on preoptic neurons begin to increase their firing rate (Steininger et al., 2001; Verret et al., 2006; Zhang et al., 2015). Simply stated, the LC nuclei have been known as a wakefulness and arousal promoting area for decades, and this property was believed to be a casual factor in the regulation of many behaviors by the LC-NA system.

## **2.4 Two Firing Modes of LC**

In addition to the continuous AP firing, Foote, Aston-jones and Bloom revealed that the rat LC-NA neurons exhibited pronounced activation in response to the non-noxious sensory stimuli in the early 1980s. The evoked response was first characterized as the phasic activity and quantified as a burst of AP which displayed a firing rate over



the mean plus triple (or twice) of the standard deviation (SD) of the prior baseline activity, and followed by a silent period with a lower firing rate, usually less than the mean minus twice (or single) of the SD of the baseline (Foote et al., 1980; Aston-Jones and Bloom, 1981). This is the first quantification of the LC phasic activity. The auditory stimulus evoked a phasic activity in the LC-NA neurons were found that underwent rapid habituation throughout the repeated stimuli in rats. This habituation paired with the behavior adaption of startle response, showing the adaptive flexibility of the activity of LC-NA neurons (Hervé-Minvielle and Sara, 1995). The presence of the LC phasic activity may help the individual to focus attention on the conspicuous stimuli or the vigilance alarm (Grant et al., 1988; Aston-Jones et al., 1991). It raised an issue about the influence of the LC phasic activity on the sensory signal processing, which was investigated in many studies on rodents and primates (Florin-Lechner et al., 1996; Waterhouse et al., 1998; Devilbiss and Waterhouse, 2011; Vazey et al., 2018; Waterhouse and Navarra, 2019), and the functional implication of the LC phasic activity will be discussed in Section 4.



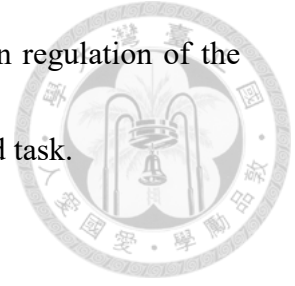
In point of fact, many studies have shown that the phasic activity of the LC-NA neurons has a more complex and specific role in the control of the task-related behavior. Aston-jones and his colleagues performed serious experiments using the unit recording combining the force-choice task in monkeys, and thus, provided a new insight of decisive motivation in response to the salient events. In the force-choice task, monkeys were trained to distinguish two types of visual cues, target and non-target, by operating the levers, a correct choice after the cue of the target earned a drop of juice as a reward, whereas the incorrect attempts or the cue of the non-target resulted in the end of the current trial. They found that the LC-NA neurons displayed a robust phasic activity with the arrival of the visual cues indicating the start of a choice section, while those without the reward delivery lead to no change or a small fluctuation of the AP firing. Surprisingly, the task performance was highly correlated with the accuracy and intensity of the phasic activity in the LC-NA neurons (Aston-Jones et al., 1994; Aston-Jones et al., 1997; Clayton et al., 2004; Rajkowski et al., 2004; Aston-Jones, and Cohen, 2005). Based on these results, they further suggested two distinct firing modes of the LC-NA neurons, the phasic and tonic modes, to describe two different responses of the LC to the uncertainty in the current task. In the phasic mode, the LC-NA neurons

exhibited an obvious phasic activity that was followed by a motor response; since the tonic mode describes a continuous firing of the APs like the prior baseline.



The following evidence indicated that the phasic mode of the LC-NA neurons was dependent on the realization of the choice reliability in the presented task, and was preferentially involved in the motivation of the motor responses rather than the decisive making. First, the phasic activity was not triggered by the delivery of a reward. Second, the expression of the phasic activity was attenuated by a switch of setting logics of the visual cues and restored after the learning of the new logics in several trials. Third, the latency from a visual cue to a phasic activity varied with the task difficulty and showed a higher variation than that from the phasic activity to the onset of a motor response. Fourth, Sara and her colleagues showed similar results obtained from investigations on rodents, indicated a conserved function of the LC throughout the mammalian (Sara and Segal, 1991; Bouret and Sara, 2004; Bouret and Sara, 2005; Sara and Bouret, 2012). Moreover, they also observed the detailed changes in the LC activity corresponding to the learning process. The LC-NA neurons preferentially responded to the conditioned stimuli (a reward) at the beginning of a task, and shifted the excitability to the unconditioned auditory stimuli after tens of trials. Together, these findings delineate a

role of the tonic and phasic firing modes of the LC-NA neurons in regulation of the motor response motivation based on the uncertainty in the presented task.



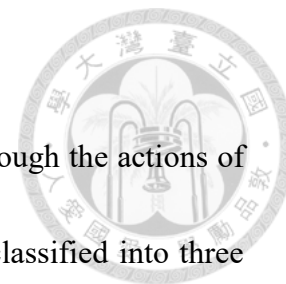
## Section 3



### Effects of NA on Synaptic Transmission

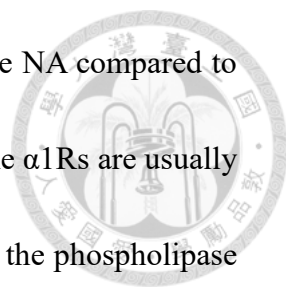
All the functions of the LC-NA neurons are done through the activation of the different ARs among various brain areas. So the investigations of the AR effects serve as a fundamental base for understanding how the LC-NA system affects the different brain functions. This section describes the complex outcome of the NA releasing based on the families of the ARs and the following effects after their activations.

### 3.1 Adrenergic Receptors



The global functions of the LC-NA system are carried out through the actions of the different ARs, which are the G-protein coupled receptor and classified into three families,  $\alpha_1$ ,  $\alpha_2$  and  $\beta$  adrenergic receptors, by the different downstream of the signaling cascades.

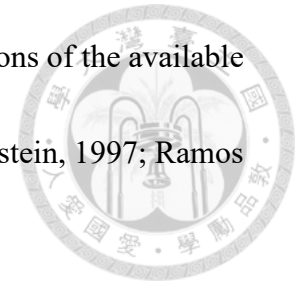
The  $\alpha_2$  adrenergic receptor ( $\alpha_2$ -AR) has the highest affinity for the NA, and three subtypes of  $\alpha_2$ -ARs have been identified, and all of them are coupled with the  $G_{i/o}$  signaling cascade. Generally, the activation of the  $\alpha_2$ -ARs results in an inhibition of adenylate cyclase, leading to a decrease of synaptic or cellular excitabilities through an increase of potassium conductance or a suppression of the voltage-gated calcium channels. The  $\alpha_2$ -ARs subtypes can be distinguished by their different affinities to the various selective agonists and antagonists. For example, clonidine serves as a potent agonist of the  $\alpha_2$ -ARs and has a higher binding activity on the  $\alpha_2A$  subtype; yohimbine acts as an antagonist showing greater affinity on the  $\alpha_2C$  subtype (MacDonald et al., 1997, Ramos and Arnsten, 2006). For the LC-NA system, the  $\alpha_2A$  and  $\alpha_2C$  subtypes expressed presynaptically in the terminals and somatodendritic locations, and all of three subtypes are found in the postsynaptic sites (Lee et al., 1998a; Lee et al., 1998b).



*The*  $\alpha_1$  adrenergic receptor ( $\alpha_1$ -AR) has a lower affinity for the NA compared to the  $\alpha_2$ -AR and can be divided into  $\alpha_1A$ ,  $\alpha_1B$ , and  $\alpha_1D$  receptors. The  $\alpha_1$ Rs are usually coupled to the  $G_q$  protein and thus activate the signaling cascade of the phospholipase C (PLC), leading to a turning on of the PKC pathway and an increase of the intracellular calcium concentration through inositol 1,4,5-triphosphate ( $IP_3$ ), finally resulting with the excitatory effects in the synaptic transmission and cell activity throughout the brain. Likewise,  $\alpha_1$ -AR subtypes can be separated by the specific pharmacology, though they act similarly in response to the NA application (Hieble et al., 1995; Goldstein, 1997; Piascik et al., 2001; Ramos and Arnsten, 2006).

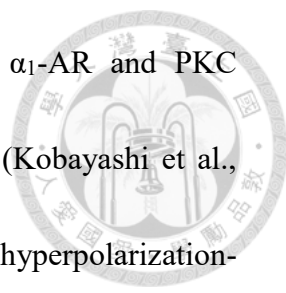
The  $\beta$ -adrenergic receptor ( $\beta$ -AR) is the third group of ARs that has the lowest affinity to the NA. There are three subtypes of  $\beta$ -AR ( $\beta_1$ ,  $\beta_2$ ,  $\beta_3$ ) and all of them can be found in the brain with heterogeneous distribution, for example, the neocortex expresses higher  $\beta_1$ -AR than the other subtypes. Normally, the activation of the  $\beta$ -ARs leads to an elevation of adenylate cyclase activity through the  $G_s$  signaling cascades that raises the intracellular cyclic AMP (cAMP) via activating adenylyl cyclase (AD). The augmented cAMP signaling mainly results in an excitatory effect on the synaptic transmission opposite to the outcome of the  $\alpha_2$ -AR activation, showing a complexity of

the LC-NA system as contrary effects depending on the concentrations of the available extracellular NA (Nicholas et al., 1993; Summers et al., 1995; Goldstein, 1997; Ramos and Arnsten, 2006).



### **3.2 Noradrenergic Effects in Cortex and Hippocampus**

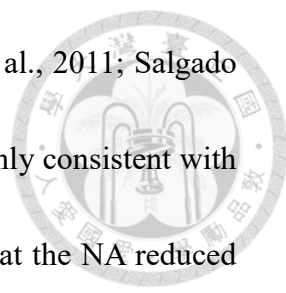
Cerebral cortex and hippocampus express three main families of ARs, the distribution of these ARs and noradrenergic innervations yield a layer- and area-specific noradrenergic modulation through the diversified effects of the NA among the cell types and synaptic sites (Salgado, 2016). For the research of adrenergic receptors, most of early reports used rat brain slice as the experimental material. The pyramidal cells, which exert a principle role of the cortical and hippocampal glutamatergic outputs, typically display regular spiking followed by the accommodation of the APs in response to a depolarized current injection. Studies using in vitro electrophysiology showed variable effects of the NA on the cortical areas, a well-known action is to increase the excitability of the pyramidal cells via the reduction of the calcium dependent potassium conductance. This effect is mediated by the  $\beta$ -ARs and the subsequent enhancement of the intracellular cAMP and PKA activity, attenuating the slower component of the afterhyperpolarization (AHP) (Madison and Nicoll, 1982; Foehring et al., 1989;



McCormick et al.,1991; McCormick et al.,1993). Besides, the  $\alpha_1$ -AR and PKC dependent depolarized effect was reported in the pyramidal cells (Kobayashi et al., 2008). The activation of the  $\beta$ -ARs is also found to enhance the hyperpolarization-activated cyclic nucleotide-gated channels (HCN) mediated inward current, whereas the active  $\alpha_2$ -ARs increase the dendritic tuft excitability by reducing the HCN channels in the apical dendrites of the layer V pyramidal cells in mice (Grzelka et al., 2017; Labarrera et al., 2018). In contrast to the pyramidal cells, the GABAergic INs was revealed to exert the  $\alpha_1$ -AR mediated excitatory response that was resistant to the TTX application. Coupled with the increase of spontaneous IPSP in the pyramidal cells by adding the  $\alpha_1$ -AR and  $\beta$ -ARs agonists, showing an indirect inhibition of the NA via the GABAergic INs, and similar results were also obtained from the CA1 of the hippocampus in rodents (Bergles et al., 1996; Kawaguchi and Shindou, 1998; Madison and Nicoll, 1988 Hillman et al., 2007; Lei et al., 2007; Hillman et al., 2009). Together, the net adrenergic effects on the intrinsic properties of the pyramidal cells resulted in an enhanced excitability that preferentially acts on the cells receiving the trains of synaptic input rather than those cells remaining silent.

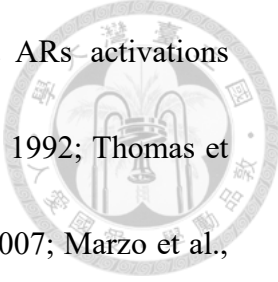
In addition to the cell excitability response to the NA itself, activations of the ARs also bring a conspicuous influence onto the synaptic sites. Many studies have reported that the NA suppressed the glutamatergic transmission in the cortex and hippocampus.

It was shown in rats that activations on both the  $\alpha_1$ -ARs and  $\alpha_2$ -ARs in the hippocampus and cortices caused a postsynaptic suppression of the NMDA or non-NMDA mediated EPSC via the active PLC signaling and the inhibition of the PKA activity, respectively (Law-Tho et al., 1993; Pralong and Magistretti, 1995; Boehm, 1999; Liu et al., 2006; Ji et al., 2008; Dinh et al., 2009; Roychowdhury et al., 2014). Contrary to the suppression of the glutamatergic transmissions, a more complex modulation on the GABAergic synaptic activity by the NA showed an area-specific and a layer-specific regulation across different cortical and hippocampal areas in rats. As aforementioned, the NA enhances the GABAergic transmissions through the direct activation of the inhibitory INs. Moreover, the LC-NA system placed its influence on the cortical and hippocampal GABAergic transmissions as well. In the PFC, the NA releasing decreases the GABAergic transmissions postsynaptically in layers II/III pyramidal cells, but increases those in layer V pyramidal cells by at least partially presynaptic dependent regulations. However, the primary auditory cortex (A1) shows the  $\alpha_1$ -ARs mediated suppression of the GABAergic transmissions postsynaptically in layers II/III pyramidal



cells but remains ineffective in layer V pyramidal cells (Salgado et al., 2011; Salgado et al., 2012; Roychowdhury et al., 2014). These findings were roughly consistent with the antiepileptic property of the LC-NA system. Studies showed that the NA reduced the spontaneous epileptic activity in the hippocampus and cortical areas through the  $\alpha$ -ARs mediated action, furthermore, the lesion of the LC-NA neurons in rats resulted in a self-sustained status of epilepticus in the piriform cortex. (Kokaia et al., 1989; Rutecki et al., 1995; Weinshenker and Szot, 2002; Jurgens et al., 2005; Ghasemia and Mehranfard, 2018).

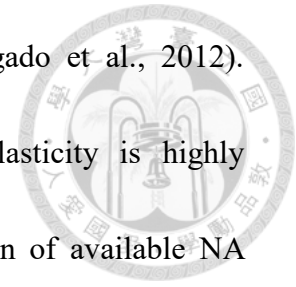
Previous studies on rats and monkeys have shown the LC phasic activity in response to the salient stimuli and cues in the forced choice task, and reflected an action of the phasic NA releasing in the learning functions that led to a better behavior performance (Berridge and Waterhouse, 2003; Bouret and Sara, 2004; Aston-jones and Cohen, 2005). The long term plasticity is required for the noradrenergic modulation of the learning functions through different ARs in the cortex and hippocampus. With regard to this hypothesis, many studies using brain slices from rodents have corroborated that the  $\alpha_1$ -ARs and  $\beta$ -ARs enable the induction of the LTD and LTP in many cortical and hippocampal areas, and showed a bidirectional effect on the plasticity



formation depending on the NA concentration for the different ARs activations (Hopkins and Johnston, 1984; Bröcher et al., 1992; Nowicky et al., 1992; Thomas et al., 1996; Katsuki et al., 1997; Scheiderer et al., 2004; Seol et al., 2007; Marzo et al., 2010; Huang et al., 2012; Laing and Bashir, 2014). The mechanism of the noradrenergic effects on the plasticity has been repeatedly studied, too. The direct depletion of the noradrenergic inputs disabled the long-term potentiation (LTP) induction in the perforant pathway of the rat hippocampus (Stanton and Sarvey, 1985). The  $\alpha_1$ -ARs enabled the NMDA dependent long-term depression (LTD) induction via the PLC pathway induced dephosphorylation and internalization of the AMPA receptors (Kirkwood et al., 1999; Scheiderer et al., 2004). The  $\beta$ -ARs help the induction of the LTP through the PKA activation and an increase of the intracellular calcium, leading to the autophosphorylation of the calmodulin kinase type II (CaMKII) that further raises the functional AMPA receptors (Hu et al., 2007; Havekes et al., 2012). In addition, studies using brain slices from rats examined the spike timing dependent plasticity (STDP) delineate of the detailed influence of the different ARs, as the  $\beta$ -ARs enlarge the magnitude of either the LTD or LTP depending on the timing difference between the stimuli on the pre- and postsynaptic sites. While the  $\alpha_1$ -ARs preferentially induced a stronger LTD when the stimuli on the pre- and postsynaptic sites were set close

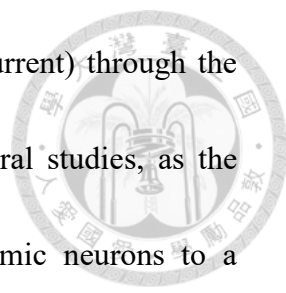
enough regardless of the time sequence (Lin et al., 2003; Salgado et al., 2012).

Collectively, the noradrenergic modulation of the synaptic plasticity is highly dependent on the timing of the NA influx, and the concentration of available NA required for activations of different ARs in the cortical and hippocampal area.



### 3.3 Noradrenergic Effects in Subcortical Area

As in the cortex, the LC-NA system regulates the cell excitability and synaptic transmission through the different ARs in the subcortical areas. Many investigations on the rat thalamus showed that the NA releasing caused a slow depolarization of the thalamic relay neurons and the intrinsic inhibitory INs located in the dorsal lateral geniculate nucleus (LPGN), the perigeniculate reticular nucleus (PGN), and the thalamic reticular nucleus (TRN) via the  $\alpha_1$ -ARs mediated effects. Generally, an activation of the  $\alpha_1$ -ARs leads to a decrease in the leaky potassium conductance, which thus shifts the thalamic neurons from bursting toward the single spike pattern. Similar findings were also reported in the parataenial thalamic nucleus (PTN) and the subthalamic nucleus (STN) (Kayama et al., 1982; Kayama, 1985; McCormick et al., 1991; McCormick and Wang, 1991; McCormick, 1992a; McCormick, 1992b; Arcos et al., 2003). In addition to the  $\alpha_1$ -ARs mediated effects, activations of the  $\beta$ -ARs mediated



an increase of the hyperpolarization-activated cation current ( $I_h$  current) through the cAMP enhancement, and this phenomenon was observed in several studies, as the enhanced  $I_h$  current resulted in a weaker response of the thalamic neurons to a hyperpolarized stimulus, subsequently interfered with the burst firing, and thus, slightly facilitated the single spike firing (McCormick and Prince, 1988; McCormick and Pape, 1990; McCormick, 1992). In conclusion, the NA shifts thalamic activity from the burst mode to the single spike mode which represent the sleep and waking states, therefore echoes the wakefulness promoting role of the LC nuclei.

In the rat midbrain dopaminergic nuclei, the NA application results in the D2-like receptors dependent multisynaptic hyperpolarized effect, coupled with the  $\alpha_1$ -ARs mediated direct depolarization via the decrease of the potassium conductance and the  $\alpha_2$ -ARs mediated decrease of the  $I_h$  current via the PKC pathway (Grenhoff et al., 1995; Inyushin et al., 2010). Besides, the activation of the  $\alpha_1$ -ARs leads to a depolarization and an increase of late AHP in the serotonergic neurons in the dorsal raphe, and results in a higher 5-HT (serotonin) release in rats (Pan et al., 1994; Pudovkina et al., 2003). Together, the pharmacological studies provide lots of evidence of the noradrenergic effects in many brain areas with the distinct affinity of different ARs, hence, this

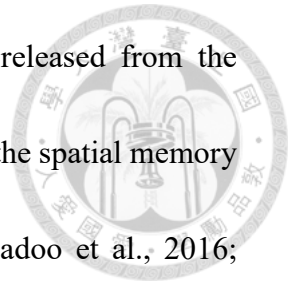
explains the complex and diversified regulations from the LC-NA system through the dynamic activations of the ARs.



### **3.4 Co-release of Dopamine from Noradrenergic Terminals**

According to the synthesis procedure of the catecholamines, the NA is synthesized from the DA under the catalysis of the dopamine  $\beta$  hydroxylase inside the transmitter vesicles. Therefore, it derives a suspicion of the co-release of both the catecholaminergic compounds from the noradrenergic terminals. In regard to this hypothesis, the early evidence in rats came from the studies showing the measurement of the cortical DA and the NA concentration that was well correlated to either the stimulations or suppressions of the LC (Devoto et al., 2001; Kawahara et al., 2001; Devoto et al., 2005). Conversely, these results were often interpreted as an interaction of the noradrenergic and the dopaminergic terminals in certain brain areas as well as the reciprocal connections between the LC and the VTA (Chandler et al., 2014; Xing et al., 2016). However, this interpretation cannot explain the extensive dopaminergic receptors in the specific brain regions containing less dopaminergic innervations, such as parietal, occipital cortices, and the dorsal hippocampus. The emergency of the optogenetic technique allows us to delicately dissect the origins of the different

transmitters. Recent studies in mice have revealed that the DA released from the noradrenergic varicosities in the dorsal hippocampus is involved in the spatial memory and the consolidation of the novelty associated memories (Kempadoo et al., 2016; Takeuchi et al., 2016; Yamasaki and Takeuchi, 2017). These studies provide a new insight of the dopaminergic modulation from the LC-NA system through the dopaminergic receptors with the ARs in response to the extracellular NA concentration (Duszkiewicz et al., 2019 Ranjbar-Slamloo and Fazlali, 2020).



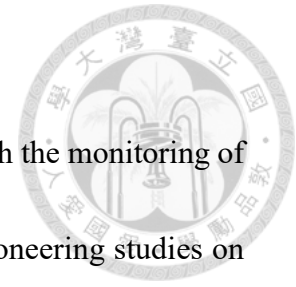
## Section 4



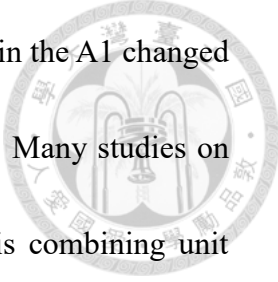
# Functional Implications of LC Discharging Patterns

The LC-NA system was thought to be involved in the sensory processing and the cognitive vigilance, and many studies have proposed models in interpreting the LC-NA neurons's works on them. Among these theories, the most attractive part is the taking turns reloading configurations between the LC-NA system and our brain continuously. It shapes how we allocate our resources when facing the nearly infinite information of the changing world. This section introduces the classical functional implications which build our understanding on the LC-NA system in a systemic level.

## 4.1 Roles of LC-NA System in Sensory Processing

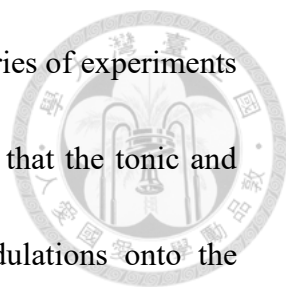


The first glance of the LC phasic activity was disclosed through the monitoring of LC-NA neurons response to the sensory stimuli in the 1980s by pioneering studies on rats (Foote et al., 1980; Aston-Jones and Bloom, 1981). Taken together with the functional interpretations in wakefulness and attention, many studies had established the current understanding of the LC-NA system in modulating the sensory processing and perceptions. In conclusion, the LC-NA system provides a flexible modulation in the cortical and subcortical regions responsible for the sensory information processing, thus, letting the individuals easily adjust their perceptive calculating parameters under the various environmental situations. This state dependent modulation is built on certain abilities of the LC-NA system which can shift its activity rapidly in response to the sensory stimuli as well as the changes in the physiological states. Moreover, the distinct affinity among different ARs makes the noradrenergic innervations capable to provide different regulations by adjusting the releasing behavior of the global projecting noradrenergic terminals (Berridge and Waterhouse, 2003; Waterhouse and Navarra, 2019).



In 1975, Foote and his colleagues showed that the NA infusion in the A1 changed cell responses to stimuli of vocalization in rats (Foote et al., 1975). Many studies on rodents used a similar strategy of the local NA microiontophoresis combining unit recording among cortical and thalamic areas, and monitored the NA effect on the stimuli evoked activities. The NA application resulted in both the excitatory and inhibitory effects, which often displayed an overall decrease of cell activities, but increased the signal to noise ratio of the sensory stimuli evoked response. This enhancement in the signal to noise ratio was due to (1) an unbalanced suppression of cellular responses that reduced the irrelevant noise selectively (2) a specific increase of the evoked activities of the cells expressing better responses, and thus sharpened the receptive field and optimized the sensory processing course as well (Foote et al., 1975; Waterhouse and Woodward, 1980; Rogawski and Aghajanian, 1980; Waterhouse et al., 1990; Armstrong-James and Fox, 1983 McLean and Waterhouse, 1994; George, 1992; Ciombor et al., 1999; Devilbiss and Waterhouse, 2000; Hirata et al., 2006).

Although local applications of the NA revealed its overall effects, the discrepancy of the noradrenergic modulations corresponding to the discharging pattern LC-NA neurons through the NA released from the intact terminals remained less explored. In

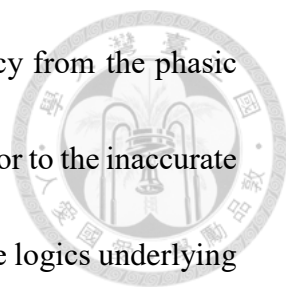


regard to this question, Devilbiss and his colleagues performed a series of experiments on rats using different stimulation protocols of the LC, and found that the tonic and phasic activations of the LC-NA neurons yielded different modulations onto the somatosensory cortex and thalamus. An inverted U relationship (Yerkes Dodson Model) was used to describe that a proper stimulation intensity upon the LC generally enhanced the stimuli sensitivity, whereas those trials with too high or too low stimulations led to a weaker effect (Devilbiss and Waterhouse, 2004; Devilbiss et al., 2006; Escanilla et al., 2010; Devilbiss and Waterhouse, 2011; Devilbiss et al., 2012; Rodenkirch et al., 2019). In contrast, the phasic activation of the LC preferentially facilitated the response evoked by the stronger stimuli or cells expressing a better response. The temporal relationship of the LC phasic activation and stimuli also had an influence on the adrenergic modulation, for example, a proper distance between the LC stimulation and a stimulus brought a larger excitatory response in the S1 followed by a longer inhibitory response in rats (Waterhouse et al., 1998; Bouret and Sara 2002; Motaghi et al., 2006; Escanilla et al., 2010; Devilbiss and Waterhouse, 2011; Linster et al., 2011). Also in rat cortical areas, the new participation of the cells that demonstrated the subthreshold activities but not the APs contributed to the enhancement of the evoked response by the phasic activations of the LC, and this gating effect recruits the silent cells, and therefore

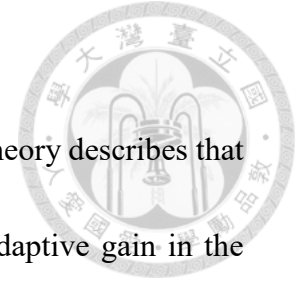
enlarges the processing pool of given stimuli (Waterhouse et al., 1988; Hurley et al., 2004; Vazeya et al., 2019). Collectively, tonic activations of the LC facilitate the sensory detection depending on the level of the LC activity, and regardless of the intensity of the sensory stimuli; the phasic activation of the LC appear in a proper timing selectively augment the response to a stronger stimuli and improve the signal to noise ratio, thus optimizing the discrimination of the sensory stimuli (Berridge and Waterhouse, 2003; Linster et al., 2011; Devilbiss 2019; Waterhouse and Navarra, 2019).

## **4.2 Adaptive Gain Theory**

On the basis of their finding, Aston-jones and Cohen proposed an adaptive gain theory for describing the functional implication of firing patterns of LC-NA neurons on the task performance (Aston-jones and Cohen, 2005). As discussed in Section 2.4, Aston-jones and his colleagues characterized their finding in the forced choice task on monkeys into the tonic mode and phasic mode, which were highly corresponded to the task performance. Their results suggested that the LC phasic activity showed less of a relationship to the decisive weighing of the visual cues and the reward delivery. Based on the following evidence, the adaptive gain theory hypothesized that the LC phasic activity raised the gain of the executive motivation in the decisive system, and thus

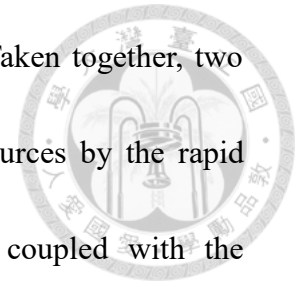


facilitated the motor response. (1) The lower variation of the latency from the phasic activity to the motor movement, (2) The smaller phasic activation prior to the inaccurate choices, (3) The attenuation of the phasic activity by a reversal of the logics underlying the cues for the reward delivery and (4) The restoration of the phasic activity after learning of the new task logics. This theory proposed a putative, multilayer decisive system was to be used in consideration of the task choices following a simple mathematical model, being a drift diffusion model (DDM). Namely, the decision calculating was proceeded through the layers of a decisive system, and the LC phasic activity was triggered when the accumulating evidence promoted the decisive ensemble over the threshold in a given layer. Consequently, this LC phasic activity lifted the gain of the positive assessments among the decisive layers, and the motor layer via the abundant noradrenergic innervations allowed the decisive motivation pass layers rapidly for a fast motor response. Similar to the way of the LC phasic activity affecting sensory functions, the facility of the rapid shifting in firing patterns of LC-NA neurons provided a flexible modulation on the cognitive processing and could be integrated with those functions of sensory processing. Finally, the outcome of choices coupled with the NA release led to an adaptive upgrading of evidence weighing according to the new circumstance therefore shaping the response of LC-NA neurons to a given situation.



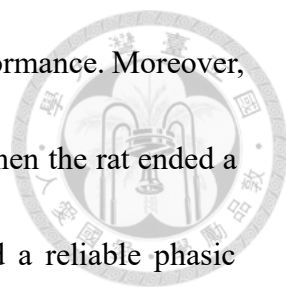
For the tonic mode of the LC-NA neurons, the adaptive gain theory describes that the high tonic activity sustains a persistent enhancement of the adaptive gain in the cognitive system, to facilitate the individuals change in their present behavior to other alternative targets when the current work shows less remunerative. Hence, the LC tonic activity provides advantages in exploring multiple sources of choices that share fairly equal benefits. Whereas the phasic mode of the activity of LC-NA neurons preferentially raises the efficiency of exploiting a known resource via exhibiting a higher gain that is temporally associated with given cognitive vigilances. Again, an inverted U relationship fitting the Yerkes Dodson Model was used to depict the firing mode of LC-NA neuron and the task performance, the low activity of the LC firing represents a less attentive or drowsy state; the high tonic mode of the LC-NA neurons indicated a broader attention to the environment; and the phasic mode usually appears in an intermediate level of the background AP firings, showing that the individual stays in a cognitive concentrating. Subsequently, this hypothesis had been discussed in the following studies on mice, the selectively optical activation and suppression of LC-NA neurons increased the exploring distance and impaired the learning of changes in the attentional set-shifting tasks, respectively (Carter et al., 2010; Howells et al., 2012;

Janitzky et al., 2015; Glennon et al., 2019; Xiang et al., 2019). Taken together, two firing modes of the LC helped to utilize the environmental resources by the rapid behavioral shifts of the exploration- or exploitation-favoring, coupled with the enhanced sensory processing systems of the signal detection or the stimuli discrimination (Devilbiss, 2019; Waterhouse and Navarra, 2019).



### **4.3 Network Reset Theory**

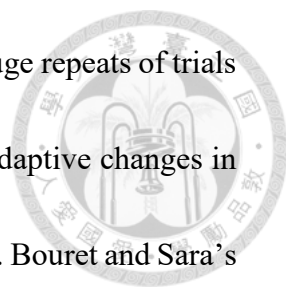
Bouret and Sara proposed a network reset theory for describing how a vigilance induced LC phasic activity promotes the reorganization of the target neural networks. Bouret and Sara published key studies on rats demonstrating the LC activity in the two alternative choice behavior tasks and showed similar results reported in monkeys by Aston-jones and his colleagues (Sara and Segal, 1991; Bouret and Sara, 2004; Bouret and Sara, 2005; Sara and Bouret, 2012). In their experiments, rats were trained to recognize the signal of a light bulb as a sign for the task start, then awaited two possible odor emissions as the conditioned stimuli (CS+ and CS-), the delivery of milk served as a reward (unconditioned stimulus, US) after the CS+ but not CS- odor, and the LC and PFC units were simultaneously recorded through the electrode placement. As Aston-jones and his colleagues reported, Bouret and Sara also found the robust phasic



activation in response to the CS+ stimuli that led to a better task performance. Moreover, the experimental design allowed them to monitor the LC activity when the rat ended a trial then reengaged into the next. Surprisingly, the LC expressed a reliable phasic activity when the light bulb turned throughout the whole task, then followed by the low tonic activity in both the LC and PFC units showing until the emergence of the conditioned stimuli. The difference between these two experimental designs may be due to the inter-trial interval which spared sufficient time pause for the rodents but not the primates to perform a cognitive quit and a re-involvement into the task circumstance. This advantage enabled Bouret and Sara to monitor the details in the LC activity during the learning process among the choice tasks. At the beginning, the LC showed responses to the US but not the CSs, then an increase and decrease of responses to the CS+ stimuli and the US, respectively. Finally, an overall reduction of the LC activity was found after tens of trials, as only a weaker but clearer phasic activity was preserved. The reversal of the conditioned stimuli led to a short repeat of the learning process mentioned above, as usually positive responses appeared after the absence of the US in a few trials after a reversed setting, and the LC phasic activity disappeared after the CS+; which led a response resembling to those presented in the very first trials when the task just began.



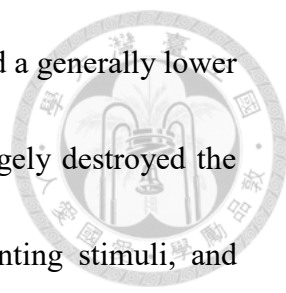
The network reset theory hypothesizes a simplified function of the LC phasic activity in the triggering of the reorganization of the target brain regions, which are usually cognitive, sensory, or motor cortices. The rapid network reset brings fast shifts in the cognitive state that improves the behavior flexibility, and subsequent feedbacks to the LC by afferents from the targets undergoing network reorganizations. Many studies on rodents have shown the role of the LC phasic activity in the memory formation, indicating that a network shift could facilitate the learning of changes in the current task through noradrenergic modulations on the synaptic plasticity and the neural circuits remapping (Tronel et al., 2004; Eschenko and Sara, 2008; Kempadoo et al., 2016; Novitskaya et al., 2016; Takeuchi et al., 2016; Yamasaki and Takeuchi, 2017; Swift et al., 2018; Grella et al., 2019; Zerbi et al., 2019). Therefore, the LC phasic activation promotes the learning process in the current choice, thus raising an advantage by the rapid updating of the valuable environmental events sufficient to trigger such phasic responses. In situations of the forced choice, this updating precisely attenuates the selected unexpectancy by reloading the new data in fewer trials later. Such an updating of conditioning logics appeared at least three times among the task, (1) First trails: the first encounter with an unexpected US; (2) Few trails after a setting reversal:



an unexpected outcome of CSs; (3) Trials after a long task course: huge repeats of trials decreased overall unexpectancy, and all of these updating showed adaptive changes in the LC phasic activity (Sara and Segal, 1991; Bouret and Sara, 2004). Bouret and Sara's network reset theory makes a complementary model to the adaptive gain theory, expands our understanding on the LC phasic activation not only in decisive motivation, but also a general reorganization which is underlying the flexibility of the LC.

#### **4.4 Functional Interpretation of LC Activities in Cognition**

In order to put a further interpretation on their work, Bouret and Sara quoted a concept of the truncated conditioned reflex (TCR) from Kupalov, one of Pavlov's students. The TCR clearly delineates a particular reflex in which the orienting stimuli do not terminate a definite action, but a significant change in the cortical areas (Bouret and Sara, 2012). As the concept, a reorienting was converted from an orienting stimulus in the appearance of the conditioning reinforcement. Phasic responses in the LC after the trail starting cue well fit the concept of the TCR, a signal of the light bulb acted as a reorienting stimulus, then quickly provoked a cognitive shift toward the engagements of a given task. As the adaptive gain theory expected, the quiet period following the reorienting stimuli may be due to the cognitive shift into a particular state with a high



expectancy, and with a high attention to the expected CS stimuli and a generally lower gain to the irrelevant stimuli. Repeated contradictory outcomes largely destroyed the current expectancy, and therefore weakened the CS+ and reorienting stimuli, and caused a higher LC tonic activity that bought a distraction by the high gain to the broad stimuli. In the conclusion of this chapter, the LC phasic activity induces a network shift by either the unexpected salience or the cognitive vigilance, results in an increased gain of motor responses to the given stimuli and an updating of the forthcoming information. Then, the LC “downloads” the new configurations from the brain areas undergoing reorganization as changes in the LC response to the given stimuli. This update-download loop sustained until a decrease in the unexpectancy or vigilant status, the LC tonic activity subsequently raises the gain to a wide range of stimuli for seeking the next valuable event or stimulus. This hypothesis sketches how the LC optimizes the utilizing efficiency of the resources when facing a complex environment, and this concept was further shown in a recent research using a computational model that demonstrated the LC’s response to the dynamic interactions of the choice expectancy and the reward uncertainty (Sales et al., 2019). For the perspective, a more complex model, which comprises not only the outcome uncertainty and prediction error but also

the sensory salience, is required to address how the LC deals with a multi-dimensional situation.



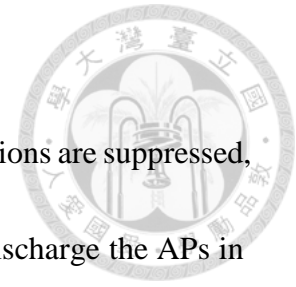
## Section 5



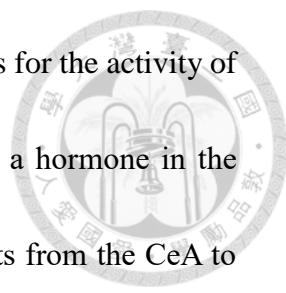
### Local Regulation of the LC Phasic Activity

This section delineates synaptic mechanisms for regulating the activity of LC-NA neurons and show the rationale and hypothesis of our group that the LC local micro-circuit formed by the nearby INs exerts a regulatory function on the firing pattern of LC-NA neurons. Finally, I will briefly review I and my colleagues' findings on the roles of the local micro-circuit in regulating the LC phasic activation.

## 5.1 General Regulations of LC Activity

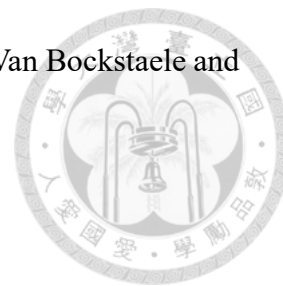


In the in vitro recordings when all of the fast synaptic transmissions are suppressed, it has been demonstrated that the LC-NA neurons spontaneously discharge the APs in a pace maker manner (Williams et al., 1984; de Oliveira et al., 2010). As the tonic discharging at a basal rate is the only activity that remains, it appears that the phasic LC activation would require synaptic drives. Studies on rats have shown that the local infusions of glutamatergic antagonists blocked the LC phasic activations evoked by stimulations of the PFC or the nucleus paragigantocellularis, a brainstem nucleus involved in the sympathetic regulation of the cardiovascular and respiratory functions (Ennis and Aston-Jones, 1988; Ennis et al., 1992; Jodo and Aston-Jones, 1997). On the contrary, studies using the local microiontophoresis of antagonists of the GABA<sub>A</sub> and GABA<sub>B</sub>, or agonists of the muscarinic AChRs into the rat LC, efficiently augmented the LC background activity and significantly decreased the time spent in the REM sleep or the recovery time from anesthesia (Kaur et al., 1997; Gervasoni et al., 1998; Hung et al., 2020). These findings showed the role of the cholinergic and GABAergic transmissions onto the LC tonic activity among the sleep-awake cycle.



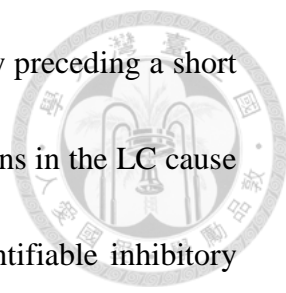
Peptidergic modulations were also reported as potent regulators for the activity of LC-NA neurons. The CRF, a stress-related neural peptide, acts as a hormone in the cardiovascular system (CRH) and a principle transmitter in afferents from the CeA to the LC. Many studies on rodents had shown that the co-action of the amygdala and the LC via reciprocal innervations play a critical role in aversion and defensive behaviors (Valentino et al., 1991; Bouret et al., 2003; Chen and Sara, 2007; Valentino and Van Bockstaele, 2008; McCall et al., 2015; McCall et al., 2017; Uematsu et al., 2017; Wyrofsky et al., 2019). In general, the CRF increases the LC firing rate but suppresses the phasic response evoked by the sensory stimuli. A similar tendency toward the tonic but not the phasic activity was also found in stressful and pathological states of rats and human, hence, echoes to the hypothesis of the inverted U shaped model of the LC tonic-phasic firing (Valentino and Foote, 1987; Valentino and Foote, 1988; Murphy et al., 2011; Elman et al., 2017). Besides, the opioids released in the LC region resulted in a prolonged inhibition onto the LC-NA neurons through an increase of the potassium conductance in postnatal rats (North and Williams, 1985; Travagli et al., 1991). Moreover, studies on rats showed the opposing action of the opioids against that of the CRF on the regulation of stress via the postsynaptic  $\mu$ -opioid receptor on the LC-NA neurons, and the presynaptic  $\kappa$ -opioid receptor on the local glutamatergic terminal

(Valentino and Van Bockstaele, 2001; Van Bockstaele et al., 2010; Van Bockstaele and Valentino, 2013; Wyrofsky et al., 2018).



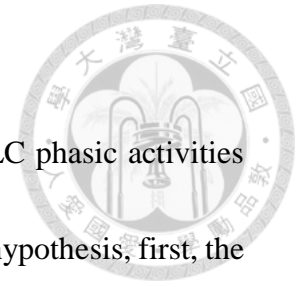
## **5.2 Direct and Indirect Mechanisms Underlying LC Phasic Activity**

Despite the well-known correlations of the tonic and phasic LC activations with the vast behavioral functions, the underlying circuit and cellular mechanisms remain largely unknown. Various approaches were used to evoke the phasic activity in living animals: (1) intact phasic activities triggered by natural stimuli in rodents and monkeys (Aston-Jones and Bloom, 1981; Sara and Segal, 1991; Aston-Jones et al., 1994; Bouret and Sara; 2004 Chen and Sara, 2007; Varazzani et al., 2015; Xiang et al., 2019; Hung et al., 2020); (2) electrical stimulations on regions projecting to the rat LC (Ennis et al., 1992; Jodo and Aston-Jones, 1997; Chen and Sara, 2007); (3) direct activations of LC-NA neurons by using the optogenetic techniques in mice (Carter et al., 2010; Vazey et al., 2018; Hayat et al., 2020) and (4) indirect optical activations of the axon terminals from regions projecting to the mice LC (McCall et al., 2015). It is not surprising that the kinetic differences are shown among the evoked phasic activations through the distinct approaches, as it raises an increasing issue about the contamination caused by the artificial portion of the evoked LC activity. An interesting example in rodents is that



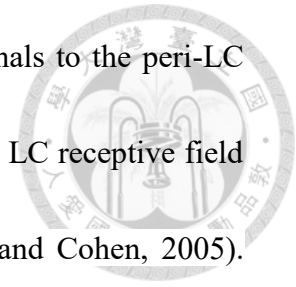
the electrical stimulations on the CeA result in a fast phasic activity preceding a short quiet period, while the selective photo-stimulations on the CeA axons in the LC cause a prolonged response with slower kinetics and a following unidentifiable inhibitory period. Out of this expectation, an electrical foot shock which also mobilizes the CeA neurons leads to both a faster and slower response preceding a longer inhibition (Bouret et al., 2003; Chen and Sara, 2007; McCall et al., 2015). This discrepancy may be due to the different population of activated LC-NA neurons; the involvement of the divergent effect from the other brain regions, or the differential disturbance of a hypothetical local circuit that integrates synaptic inputs onto LC-NA neurons. On the other hand, for those vigilance triggered phasic activities to optimize the task performance by gain modulations as proposed by Aston-Jones and Cohen (2005), as well as Bouret and Sara (2005, 2012), a part of the synaptic drives should originate from the higher cognitive cortical areas. The top-down cortical inputs could directly drive the phasic LC activation or indirectly through a local neural circuit that integrates inputs from the cortex as well as other brain regions. However, the discrepancy underlying the proposed mechanisms of the LC phasic activity evoked by various approaches is still unclear, including the direct and indirect portion of the synaptic drive to the LC phasic activation.

### 5.3 Possible Role of Local Circuit



Our group aims to investigate the indirect regulation of the LC phasic activities exerted by the local circuit. There is some evidence supporting our hypothesis, first, the study on rats published by Bouret and Sara (2004) showed that the lower tonic firing of the LC-NA unit significantly coincided with a quiet unit activity of the prelimbic cortex, one of the cognitive area, the vigilance of a trail start was able to induce LC phasic response but not the similar excitatory pattern of the same cortical unit. Theoretically, all of the goal-directed information to the LC should originate from the cognitive cortex, hence, this finding indicated that there is more than a pure, direct source of the cortical drive in the formation of LC phasic activity. Second, Aston-jones and his colleagues revealed a population of GABAergic INs which was located in the pericerular dendritic zone (peri-LC) and projecting to the rat LC-NA neurons. Breton-Provenche and Sur further found the GABAergic neurons near the mice LC responded to the auditory stimuli and had an ability to attenuate the evoked LC phasic activity (Aston-Jones et al., 2004; Breton-Provenche and Sur, 2019). Third, it has been shown that the cortical areas, including the anterior cingulate cortex (ACC), and the orbitofrontal cortex (OFC), which play crucial roles in the evaluation of the reward and the cost of the stimuli, respectively (Schultz et al., 2000; O’Doherty et al., 2002; Ito et al., 2003;

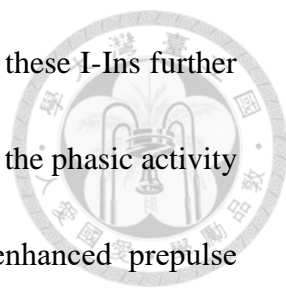
Roesch and Olson, 2004; Sugrue et al., 2004), send axonal terminals to the peri-LC where LC-NA neurons yield dendritic arborizations and the located LC receptive field (Shipley et al., 1996; Swanson and Hartman, 1975; Aston-Jones and Cohen, 2005).



These observations suggest that the OFC and ACC may have concomitant projections onto the LC-NA neurons and the GABAergic INs. Fourth, as the LC phasic activity can be triggered by the activation of one of many brain areas, it is reasonable to have a population of local interneurons for integrating the information across parallel sources of the LC activity. Moreover, the differential activation of the local neurons near the LC in states of stress, fear conditioning, and sleep, strongly indicates a broad role of local interneurons and possible functional divisions for integrating various afferents (Mallick et al., 2001; Ishida et al., 2002; McDevitt et al., 2009; Yang et al., 2016). Fifth, an example of the INs regulating the burst response of the principle neuron was reported in the mice VTA, another catecholaminergic nucleus. The VTA dopaminergic (VTA-DA) neuron responds with a burst to the reward appearance and is thought to facilitate the learning of conditioning behavior by comparing the expected and actual reward. This reinforcement learning system in the VTA continuously reports the prediction error as a stronger burst response for the next information updating, while the expected reward suppresses of VTA dopaminergic neurons (Montague et al., 2004). The study

of Eshel and his colleagues suggested that the VTA GABAergic neurons take the responsibility for inhibiting the burst response of VTA-DA neurons when the reward fits the expectations, and the suppressing of VTA GABAergic neurons impaired the learning process when a new reward appeared (Eshel et al., 2015). Based on the above arguments, I and my colleagues propose a group of local INs which integrate afferents to the LC and exert the regulations on the LC phasic activity.

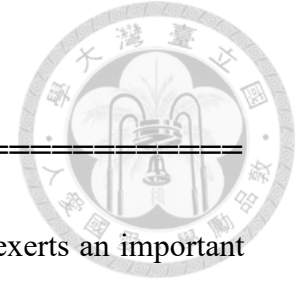
In this thesis, our group reports that under the in vitro condition the LC-NA neurons discharge the spontaneous phasic-like activity (sPLA) which shows a high similarity to those recorded in living animals and is induced by the spontaneously large EPSC (large sEPSC), this finding indicates an active local circuit sufficient to drive and regulate the sPLAs. The sPLA was named after the similar profiles compared to the intact phasic activation in living animal and the possible discrepancy between it and the natural LC phasic activity. Next, I and my colleagues identify a group of inhibitory interneurons that are located in the peri-LC (peri-LC I-INs) and exert the feed-forward inhibition of LC-NA neurons to modulate the phasic activity. Features in morphology and electrophysiology suggest an active inhibitory modulation of the LC-NA neurons from the peri-LC I-INs. The evidence of functional connections from the ventral OFC



(vOFC), medial OFC (mOFC), and the prelimbic cortex (PrL) onto these I-Ins further supports our speculation of an integrative role of the interneurons to the phasic activity driving afferents. Finally, the inhibition of the peri-LC I-Ins enhanced prepulse inhibition (PPI) of the startle behavior, suggests that the peri-LC I-Ins are involved in a sensorimotor gating functions through regulating the LC phasic activity. These features support a role of the identified peri-LC I-Ins in integrating the top-down cortical signal onto the LC-NA neurons and gating their output with the phasic activation. In addition, I and my colleagues also found that the local excitatory interneurons (E-Ins) send synaptic contacts onto the LC-NA neurons, and identified a group of E-Ins with the capability to intrinsically express burst firing as a potent candidate of the origin of the sPLA. The reconstructed morphology of the bursty E-Ins display some close appositions of bouton-like swelling onto the local large fusiform cells supposed as the LC-NA neurons, and thus provides indirect evidence of the direct functional connection. Our preliminary results using the GCaMP6s calcium imaging on bursty E-Ins show a positive correlation to the sPLA generation. Recently, works of our group on the role of the peri-LC I-Ins in regulating the LC phasic activities has been published, the rest of this thesis are the unpublished results (Kuo et al., 2020).

# Specific Aims

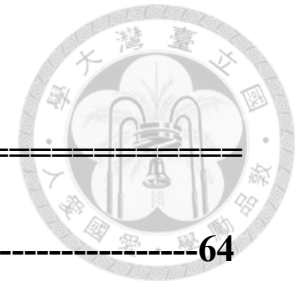
---



The phasic activation of the LC-NA neurons has been found that exerts an important role in the physiology and behavior. It helps an individual to allocate the brain resource of attention properly and thus facilitate the processing or realizing of valuable or unexpected events. However, the detailed cellular mechanism underlying the LC phasic activation remains largely unknown. With this regard, our group proposed an indirect origin and regulation of the LC phasic activity. In this thesis, I and my colleagues plan (1) to define the functional interneuron pool and local circuit of LC nuclei using brain slice in vitro recordings and viral-induced WGA tracing techniques; (2) to characterize the detailed mechanism of peri-LC I-INs in regulation of phasic activations of LC-NA neurons in brain slices; (3) to find the functional role of these peri-LC I-INs on the intact phasic activity of LC-NA neurons in living animals and (4) to investigate the role LC E-INs in regulation of phasic burst activation of principle neurons in brain slice. Together, the goal of my research aims to reveal the role of local interneurons in the regulating of phasic activity of LC-NA neurons.

---

# Materials and Methods



---

<b>1. Animal</b>	<b>64</b>
<b>2. Viral Vector and Stereotaxic Surgery</b>	<b>64</b>
<b>3. Preparation of Brain Slices</b>	<b>66</b>
<b>4. Electrophysiology</b>	<b>67</b>
<b>5. <i>Post-hoc</i> Staining of Recorded Slices</b>	<b>72</b>
<b>6. Genetic viral WGA tracing</b>	<b>73</b>
<b>7. IHC for WGA tracing and imaging data analysis</b>	<b>75</b>
<b>8. Behavioral tasks: startle response, PPI and open field</b>	<b>79</b>
<b>9. Calcoim Imaging</b>	<b>83</b>
<b>10. Statistical analysis</b>	<b>84</b>

---

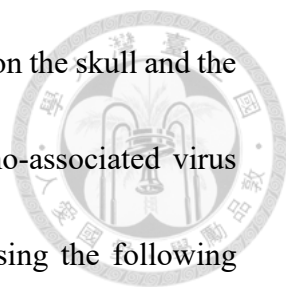
## 1. Animals



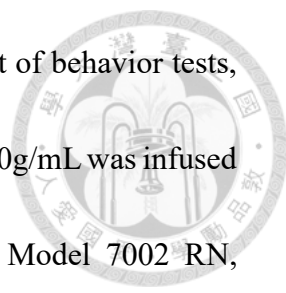
All animal experiments were approved by the Institutional Animal Care and Use Committees of the NTU & CSMU. Every effort was made to minimize the number of animals used and their suffering. The information on the mouse lines used in this study is as listed in Table 1. Animals were housed and bred in a temperature-controlled vivarium under a light-dark cycle of 12 hr, with food and water available *ad libitum*. Male and female mice were used for electrophysiological and tracing experiments; only male mice were used for behavioral experiments. Numbers in the Results section and the Figure Legends describe the number of cells recorded in the electrophysiological experiments and the number of animals used in the tracing and behavioral experiments. The usage of mouse lines is as shown in Table 1, and the number of animals and brain slices used is as detailed in Table 2.

## 2. Viral Vector and Stereotaxic Surgery

Mice aged 4-12 weeks were deeply anesthetized, as indicated by the absence of the hind-paw withdraw reflex, with an intraperitoneal (IP) injection of a mixture of ketamine (75 mg/kg) and xylazine hydrochloride (15 mg/kg); supplementary doses of the anesthetics were administered as and when necessary. The animals were then



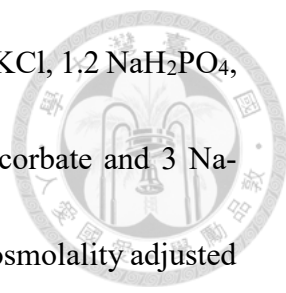
mounted in a stereotaxic apparatus, small craniotomies were drilled on the skull and the dura was reflected carefully. A glass pipette loaded with the adeno-associated virus (AAV) was then slowly advanced to the brain areas of interest using the following coordinates (in mm), LC: 0.8 caudal, 0.9 lateral, and 2.9 dorsal to the lambda; OFC and PrL: 2.5 rostral, 0.3-1.2 lateral, and 1.7-2.2 dorsal to the bregma; secondary motor cortex (M2): 2.5 rostral, 1.2 lateral, and 1.7 dorsal to the bregma. The tip of the glass pipette was beveled to an angle of  $\sim 40^\circ$  with a tip opening of 60-80  $\mu\text{m}$  using a microelectrode beveler (BV-10, Sutter Instrument, Novato CA, USA), and was connected to a 2.0  $\mu\text{L}$  Hamilton glass syringe (Neuros Model 7002 KH, Hamilton, Reno, NV, USA). The AAV was manually delivered at a rate of  $\sim 5$  nL/min, a short pause of 10 minutes was held just before and after the delivery of the AAVs. For diminishing the AAV's leakage, the glass pipette then slowly withdrew in the rate of 300-500  $\mu\text{m}/\text{min}$ . Information on the AAVs used, the infusion volume and the survival time after the AAV infusion are as summarized in Table 3. The AAV infusion was made unilaterally to the LC and previously described cortical areas, unless otherwise specified. For the infusion of 6-OHDA, a dose of 10 $\mu\text{g}/\mu\text{l}$  6-OHDA was dissolved in 0.2% ascorbic acid in saline and was delivered to the LC bilaterally with a total volume of 800-1000nL. In consideration of the large amount, the injection was done at a higher rate but costed



more time than those AAV infusions. For lesions of the LC in a part of behavior tests, 800-1000nL of 6-hydroxydopamine (6-OHDA) in concentration of 10g/mL was infused into the right LC via a 5.0  $\mu$ L Hamilton glass syringe (Neuros Model 7002 RN, Hamilton, Reno, NV, USA) in a rate of  $\sim$ 50 nL/min. The mice received 6-OHDA infusions were allowed to recover at least 2 weeks for the completing of lesion process.

### **3. Preparation of Brain Slices**

Mice aged 8-16 weeks were deeply anesthetized via the IP injections of urethane (1.3 g/1 kg) and were perfused through their cardiovascular system with 5-10 ml of ice-cold slicing-aCSF (artificial cerebrospinal fluid) that consisted of the following (in mM): 92 N-methyl-D-glucose (NMDG), 2.5 KCl, 1.2 NaH<sub>2</sub>PO<sub>4</sub>, 10 MgSO<sub>4</sub>, 0.5 CaCl<sub>2</sub>, 20 HEPES, 30 NaHCO<sub>3</sub>, 25 glucose, 5 Na-ascorbate and 3 Na-pyruvate, oxygenated with 95% O<sub>2</sub> and 5% CO<sub>2</sub>, pH 7.35-7.4, and osmolality adjusted to 315-320 mOsm with sucrose. The brain was rapidly dissected after perfusion, and the brainstem was then blocked and embedded in 2% agarose in saline. Coronal brain slices of 350  $\mu$ m thickness were cut using a vibratome (Leica VT1000 S, Leica Biosystems, Nussloch, Germany), and the slices that comprised of the LC were collected and incubated with slicing-aCSF at 32°C for 30 to 60 minutes. The slices were then incubated with the



holding-aCSF that consisted of the following (in mM): 92 NaCl, 2.5 KCl, 1.2 NaH<sub>2</sub>PO<sub>4</sub>, 2 MgSO<sub>4</sub>, 2 CaCl<sub>2</sub>, 20 HEPES, 30 NaHCO<sub>3</sub>, 25 glucose, 5 Na-ascorbate and 3 Na-pyruvate, oxygenated with 95% O<sub>2</sub> and 5% CO<sub>2</sub>, pH 7.35-7.4, and osmolality adjusted to 310-315 mOsm with sucrose. It should be noted that the Na-ascorbate and Na-pyruvate mentioned above must be freshly prepared before the adjusting of pH value.

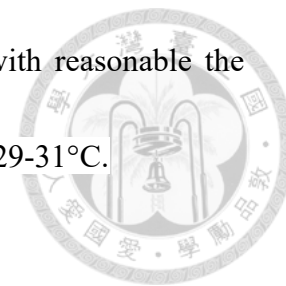
#### **4. Electrophysiology**

The slices were then transferred to a recording chamber mounted on an upright microscope equipped with the Nomarski and epifluorescent optic systems (BX51WI, Olympus Optical Co., Ltd, Tokyo, Japan), and an ORCA-R2 camera (Hamamatsu Photonics, Shizuoka, Japan). The slices were continuously perfused with regular aCSF that contained the following (in mM): 119 NaCl, 2.5 KCl, 1 NaH<sub>2</sub>PO<sub>4</sub>, 1.3 MgSO<sub>4</sub>, 2.5 CaCl<sub>2</sub>, 26.2 NaHCO<sub>3</sub>, and 11 glucose, oxygenated with 95% O<sub>2</sub> and 5% CO<sub>2</sub>, pH 7.35-7.4, and osmolality 305-310 mOsm. To record LC-NA neurons, neurons located in the LC-proper where the cell bodies of LC-NA neurons were tightly packed (Swanson 1975; Shipley et al., 1996), were selected for recording. To record the peri-LC I-INs and the E-INs, neurons located near the LC-proper, especially in the medial part of the peri-LC and expressing fluorescent proteins were recorded. The recordings were made under

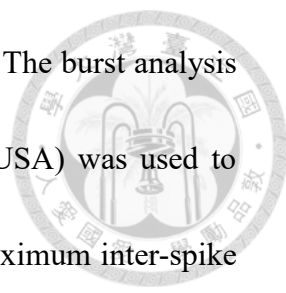


visual guidance with a glass pipette that was pulled from a borosilicate glass capillary (GC150F-10, Warner Instruments, Hamden, CT, USA) and had a tip resistance of 10-15 M $\Omega$  when filled with pipette solutions. For the current (I)-clamp recording, the patch pipettes were filled with a low Cl<sup>-</sup> solution that consisted of the following (in mM): 131 K-gluconate, 2 KCl, 10 HEPES, 2 EGTA, 8 NaCl, 2 ATP, and 0.3 GTP, pH 7.2-7.3, and osmolality 300-305 mOsm. Data were only accepted if the V<sub>m</sub> of the recorded cell was at least -40 mV and the APs were able to overshoot 0 mV or have an amplitude of 40mV. For the voltage (V)-clamp recordings, the pipette solution contained the same ingredients as the solution used for I-clamp recordings with the exception of 131 K-gluconate replaced with 32.5 K-gluconate and 116.5 KCl to make the Cl<sup>-</sup> reversal potential at ~ 0 mV. The V<sub>m</sub> was clamped at -70 mV unless otherwise specified, and the serial resistance was constantly monitored throughout the recording. The data were excluded if the serial resistance varied by greater than 20% of the original value, which was typically less than 20 M $\Omega$ . All recordings were performed at 29-31°C using a Multiclamp 700B amplifier (Molecular Device, San Jose, CA, USA), and the signals were low-pass filtered at 2 kHz. The signal was digitized at 10 kHz using the Micro 1401 interface running Signal and Spike2 (Cambridge Electronic Design, Cambridge, UK). The recording temperature was chosen because our pioneer experiments

demonstrated that the chance of obtaining the LC-NA neurons with reasonable the sPLA was considerably lower at room temperature compared with 29-31°C.



In the optogenetic experiments, the peri-LC I-INs were photostimulated by light pulses (470 nm, duration: 2 ms, intensity: 10 mW/cm<sup>2</sup>) generated by OptoLED Light Source (Cairn Research, Faversham, Kent, UK) and delivered through the epifluorescent light path and the objective (40x water immersion lens, LUMPLFLN-40xW, Olympus, Tokyo, Japan) of the microscope. The LED OptoLED Light Source was controlled by a Master-8 stimulator (A.M.P.I., Jerusalem, Israel) for delivery of a single light pulse every 10-s or a train that consisted of pulses at a different frequency every 40-s. In electrical stimulation experiments, electrical pulses (duration: 20-60  $\mu$ s; intensity: 50-150  $\mu$ A) were generated by an isolated constant current stimulator (DS3, Digitimer Ltd, WGC, Herts, UK) and delivered through a bipolar tungsten electrode (FHC, Inc., Bowdoin, ME, USA) placed in the medial part of the peri-LC. The constant current stimulator was controlled by a Master-8 stimulator for the delivery of a paired-pulse (interval 50 ms) every 20-s in the V-clamp recording or a train that consisted of 10 pulses at 50 Hz every 40-s in the I-clamp recording. All the electrophysiological data were measured and analyzed using the Signal and Spike2 softwares (Cambridge



Electronic Design, Cambridge, UK) with the following exceptions. The burst analysis function of the NeuroExplorer software (Nex technologies, CO, USA) was used to detect the sPLA in LC-NA neurons (Figs. 1-4; 17-20), with the maximum inter-spike interval to start and end a burst set to 200 ms, the minimum inter-burst interval set to 400 ms, the minimum duration of a burst set to 200 ms, and the minimum number of consecutive spike set to three spikes. I and my colleagues then manually examined each detected burst to confirm as to whether it could fulfill the criteria modified from those used for the detection of the phasic activity in the previous in vivo studies (Aston-Jones and Bloom, 1981; Bouret et al., 2003). A detected burst was accepted as a sPLA, only if it passed the criteria. Namely, a sPLA starts when the instant frequency between two consecutive spikes was increased beyond a rolling threshold calculated as being 2 standard deviation (SD) above the baseline firing rate over the last 20-s. If there was a sPLA that preceded the one detected in the 20-s period of the baseline firing, this sPLA was removed from the calculation of the mean and SD of the baseline firing. The spontaneous excitatory synaptic current (sEPSC) was analyzed using the Mini Analysis (Synaptosoft, Inc., Fort Lee, NJ, USA). To detect the large sEPSC in the LC-NA neurons (Figs. 1F & G), the amplitude threshold was set to 5 times of the root mean square (RMS) noise level, and the event area was set to 500 times of the RMS noise

cross time (pA×ms).

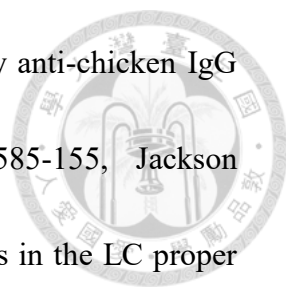


Both hemispheres were used for the brain slice preparation in the experiments as shown in Figs. 1-4 & 20. To selectively stimulate peri-LC I-INs using the optogenetic method (Figs. 9-14), the brain slices were prepared from the right hemisphere of the vesicular GABA transporter (Vgat)<sup>Cre</sup> mice infused with the AAV stereotypic 2 (AAV2) encoding a double-flanked inverse orientation (DIO) of channelrhodopsin 2 (ChR2) tagged with the enhanced yellow fluorescent proteins (eYFP) into the right LC (Tables 1 & 3). To selectively inhibit peri-LC I-INs using the chemogenetic method, the designer receptors exclusively activated by the designer drugs (DREADD) (Figs. 17-19), AAV2 encoding DIO of the hM4Di receptor (hM4DiR) tagged with mCherry was used (Table 3). To selectively target the LC E-INs using the optogenetics and calcium imaging techniques, an AAV2 encoding DIO of ChR2-eYFP, an AAV2-DIO-mcherry as well as an AAV5 encoding DIO of GCaMP6s was bilaterally induced to the LC of Vglut2(vesicular glutamate transporter)<sup>Cre</sup> mice (Figs. 31-37; Table 1, 3).

## 5. *Post-hoc* Staining of Recorded Slices



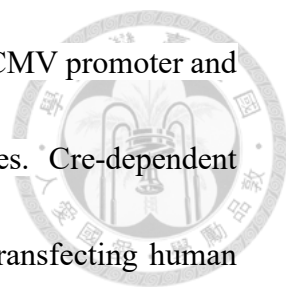
For the *post-hoc* validation of the AAV2 transfection pattern after the electrophysiological experiments, the slices were fixed with 4% paraformaldehyde immediately after the recording in the phosphate buffer (PB) at 4°C overnight. Following several brief rinses with PB followed by the phosphate buffer saline (PBS; 0.9% NaCl in 0.01 M PB), the slices were subjected to the following incubation processes without further sectioning. The slices were incubated with 0.3% sodium borohydride in PB for 15 mins for antigen retrieval and then in 2% bovine serum albumin (BSA) in PBST (0.3% Triton X-100 in PBS) for 1 hour to block the nonspecific reactions. For the optogenetic experiments, they were then incubated with the primary antibody cocktail that contained the rabbit anti-TH (dilution 1:2000; Cat # AB152, Merck Millipore) and chicken anti-GFP (dilution 1:2000; Cat. # ab205402, Abcam, Cambridge, UK) antibodies in PBST at 4°C for 2-3 days, followed by incubation with the secondary antibody cocktail that contained goat anti-rabbit IgG conjugated Dylight 405 (dilution 1:200; Cat # 20020, Biotium, Fremont, CA, USA) and goat anti-chicken IgG conjugated CF 488 in PBST at 4°C overnight. For the DREADD experiments, the primary antibody cocktail contained rabbit anti-TH and chicken anti-mcherry (dilution 1:200; Cat # ab205402, Abcam) antibodies, and the secondary antibody cocktail



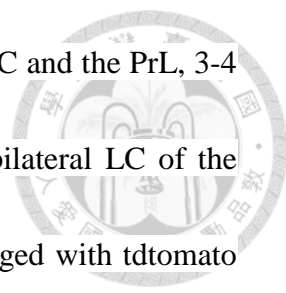
contained goat anti-rabbit IgG conjugated Dylight 405 and donkey anti-chicken IgG conjugated Alexa Fluor 594 (dilution 1:200; Cat # 703-585-155, Jackson ImmunoResearch). The *post hoc* validation of the recorded neurons in the LC proper were LC-NA neurons, the slices were fixed after recording as previously described and were subjected to the biocytin histochemistry and immunohistochemistry procedures. The slices were incubated in PBST containing the rabbit anti-TH primary antibody, followed by incubation with the goat anti-rabbit IgG conjugated Dylight 405 and streptavidin conjugated Alexa Fluor 647 (dilution 1:200; Cat # 016-600-084, Jackson ImmunoResearch) overnight at 4°C. For the previously described processes, the sections were intensely washed with PBST for at least three times of 10-minute wash between the incubation steps. All incubations occurred at room temperature, unless otherwise specified. The slices on the glass slide were examined with a Zeiss LSM 780 confocal microscopic system (Carl Zeiss, Oberkochen, Germany).

## **6. Genetic viral WGA tracing**

For the production of the Cre-dependent AAV vector carries a DIO of wheat germ agglutinin (WGA) gene, I and my colleagues chose the truncated WGA cDNA generously provided by Yoshihara et al., (1999). The truncated WGA was inserted into



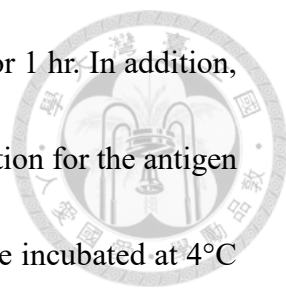
an AAV2 backbone plasmid in reverse orientation relative to the 5' CMV promoter and was flanked by the oppositely oriented loxP and lox2272 sites. Cre-dependent expression of the new DIO-WGA plasmid was tested by the co-transfecting human embryonic kidney (HEK-293) cells with the DIO-WGA plasmid using the lipotransfection (Lipofectamine 2000 Transfection Reagent, Thermo Fisher Scientific, Waltham MA, USA) and an AAV vector carrying Cre recombinase and green fluorescent protein (GFP) (Vector Core, UNC). The transfected HEK-293 cells were stained with anti-WGA antibody (Fig. 8). After confirming that the HEK-293 cells could successfully express the transfected WGA in a Cre-dependent manner, the DIO-WGA plasmid was packaged in the AAV2 (Vector Core, Techcomm Platform, College of Life Science, NTU). The AAV2-DIO-WGA was then used to locate local I-INs making functional connections with LC-NA neurons (Figs. 5-8). To this end, the AAV2 was infused into the left LC, the offspring of TH<sup>Cre</sup> mice and the glutamic acid decarboxylase 67 (GAD)<sup>GFP</sup> mice (Tsunekawa et al., 2005; Tables 1 & 2), referred to as TH<sup>Cre</sup>×GAD<sup>GFP</sup> mice. For the control comparison, the AAV2 encoding DIO of the eYFP (Table 3), which is well known not to undergo the transneuronal (TransN) transportation, was infused into the left LC of TH<sup>Cre</sup>×GAD<sup>GFP</sup> mice (Fig. 6). In addition, the AAV2-DIO-WGA was infused into the left LC of the wild type (WT) mice (Fig. 6). To examine



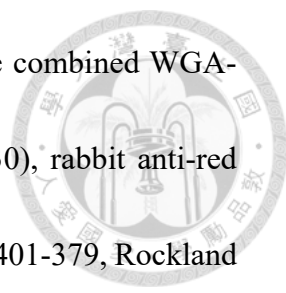
whether peri-LC I-INs received the axonal projections from the OFC and the PrL, 3-4 weeks after the AAV2-DIO-WGA injection made to the left or bilateral LC of the  $TH^{Cre} \times GAD^{GFP}$  mice, the AAV9s that encodes the ChrimsonR tagged with tdTomato (ChR1R-tdT) was injected into the left OFC/PrL for the anterograde tracing (Figs. 27-28 & 30). In another series of experiments aiming to confirm that fibers from the OFC and PrL made functional contacts with the I-INs, the AAV9 encodes GFP sequence was injected into the left OFC/PrL of  $TH^{Cre}$  mice for anterograde tracing and further IHC of synaptic markers (Fig. 29).

## **7. IHC for WGA tracing and imaging data analysis**

Following the AAV injection, mice were deeply anesthetized with urethane (1.3 g/kg) and then perfused via the cardiovascular system with 4% paraformaldehyde in 0.1 M PB. The brain was dissected and postfixed overnight at 4°C with the same fixative. The brain was then soaked in 30% sucrose in 0.05 M PB at 4°C for cryoprotection. After sinking in the sucrose solution, the brain was cut into sections of 50  $\mu$ m thickness using a freezing microtome. Sections that comprised of the brain regions of interest were collected and briefly rinsed with PB followed by PBS. The sections were incubated with a solution that consisted of 10% normal donkey serum



(NDS) and 0.1% BSA in PBST to block the nonspecific reactions for 1 hr. In addition, 0.05% thimerosal and 0.01% sodium azide were added into the solution for the antigen retrieval. For the IHC of WGA-tracing (Figs. 5-8), the sections were incubated at 4°C overnight in the primary antibody cocktail that contained goat anti-WGA (dilution 1:200, Cat. # AS2024, Vector Laboratories INC, Burlingame, CA, USA), mouse anti-TH (dilution 1:500; Cat # MAB318, Merck Millipore, Burlington, MA, USA), and the chicken anti-GFP antibodies in PBST, followed by incubation for 2 hr with the secondary antibody cocktail that contained donkey anti-goat IgG conjugated Alexa Fluor 647 (dilution 1:200; Cat. # 705-605-147, Jackson ImmunoResearch, West Grove, PA, USA), donkey anti-mouse IgG conjugated Dylight 405 (dilution 1:200; Cat # 715-475-150, Jackson ImmunoResearch) and donkey anti-chicken IgG conjugated Alexa Fluor 488 (dilution 1:200; Cat # 703-545-155, Jackson ImmunoResearch) in PBST. For the Cre control experiment (Fig. 6), the primary antibody cocktail contained chicken anti-GFP and mouse anti-TH antibodies, and the secondary antibody cocktail contained donkey anti-chicken IgG conjugated Alexa Fluor 488 and donkey anti-mouse IgG conjugated Dylight 405. For the control experiment of the AAV2-DIO-WGA (Fig. 6), the primary antibody cocktail contained goat anti-WGA and mouse anti-TH antibodies, and the secondary antibody cocktail contained donkey anti-goat IgG conjugated Alexa



Fluor and donkey anti-mouse IgG conjugated Dylight 405. For the combined WGA-tracing and anterograde viral tracing experiment (Figs. 27-28 & 30), rabbit anti-red fluorescent protein (tdtomato) antibody (dilution 1:2000; Cat # 600-401-379, Rockland Immunochemicals, Limerick, PA, USA) was added into the primary antibody cocktail and donkey anti-rabbit IgG conjugated Rhodamine Red-X (dilution 1:200; Cat # 711-295-152, Jackson ImmunoResearch) was added into the secondary antibody cocktail. For the experiments aiming to confirm the axons from the OFC/PrL made functional contacts on the WGA-ir neurons (Fig. 29), the primary antibody cocktail contained goat anti-WGA, chicken anti-GFP, and mouse anti-synaptophysin (dilution: 1:750; Cat # 1-101-001, Synaptic System, Gottingen, Germany) antibodies; the secondary antibody cocktail contained donkey anti-goat IgG conjugated Alexa Fluor, donkey anti-chicken IgG conjugated Alexa Fluor 488, and donkey anti-mouse IgG conjugated Alexa Fluor 568 (dilution: 1:200; Cat # A10037, Thermo Fisher, Waltham, MA, USA). I and my colleagues ensured that the excitation and emission spectrums of the selected fluorescence markers conjugated to the secondary antibodies were well separated, so that the signal interference among the markers was limited. For the previously described processes, the sections were intensely washed with PBST for at least three times of 10-minute wash between the incubation steps. All incubations occurred at room

temperature, unless otherwise specified. The sections were then mounted on glass slides and coverslipped with DPX mounting medium.



For the cell number counting as shown in Figs. 6-7, three sections cut through the rostral, middle, and caudal LC-proper, corresponding approximately to Bregma -5.34, -5.52, and -5.68, were subjected to analysis. In each section, 40x tiled, z-stack images that comprised of seven scanning planes with an inter-plane interval of 0.5-1  $\mu\text{m}$  were obtained, converted to maximum intensity projection images, and exported in different fluorescent channels separately using the Zen 2014 Software (Carl Zeiss, Oberkochen, Germany). The brightness and contrast of the images were modified, and the background noise was subsequently subtracted using the ImageJ Software (National Institutes of Health, Bethesda, MD, USA). To determine the background noise, the three regions of interest (ROIs) that did not cover the LC or the peri-LC were defined, and the mean and the SD of the mean pixel intensity in the 3 ROIs were calculated; the background noise was taken as the mean plus twice the standard deviation. After the subtraction, the aggregation of the remaining pixels into a recognizable soma structure was accepted as a neuron showing the immunoreactivity (refer to arrows & arrowheads in Fig. 5), and their number throughout the z-stack image of a section was counted. The

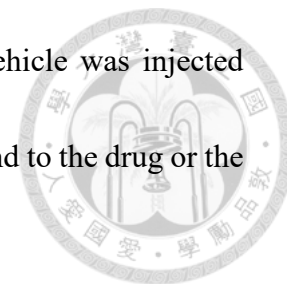
numbers counted from the 3 sections were summed up for an animal (Figs. 6-7).



## **8. Behavioral tasks: startle response, PPI and open field**

To examine the potential role of peri-LC I-INs in the control of behaviors (Fig. 7), male *Vgat<sup>Cre</sup>* mice aged 4-8 weeks and 15-20 g in weight were used. The animals were randomly grouped into the DREADD and control groups; the number of animals in each group was roughly equal. The DREADD group received a bilateral injection of the AAV2-DIO-hM4DiR-mCherry into the LC, and the control group received the AAV2-DIO-mCherry injection. Four weeks after the AAV2 injection, animals were randomly assigned to receive an IP injection of CNO (1 mg/kg; Tocris Bioscience, Bristol, UK) or vehicle (2% DMSO in 0.9% saline) 30 minutes before the first behavior test. After one week, the same injection protocols were repeated for the second behavioral test, and whether an animal received the CNO or the vehicle injection depended on the first test. For animals that received the CNO injection in the first test, the vehicle was administered in the second test, and *vice versa*. In a subset of the experiment, the open field test was performed two days after the startle reflex and PPI. Again, animals were randomly assigned to receive an IP injection of the CNO or vehicle 30 minutes before the first behavior test. After one week, the same injection protocols

were repeated for the second behavioral test, and the CNO or vehicle was injected depending on the first test. The same experimenter who was not blind to the drug or the animal group conducted all behavioral tests.



The acoustic startle task and PPI were performed in a sound-attenuating ventilated cabinet with startle (acoustic) stimuli produced by a high-frequency loudspeaker (Panlab, Harvard Apparatus, Spain). The analogical signal of the vibration generated by the whole-body startle response to the acoustic pulse was converted and digitized with a high-sensitivity weight transducer system and analyzed with the PACKWINCSST software (Panlab, Harvard Apparatus, Spain). To begin the test, animals were first placed in a nonrestrictive transparent cylinder inside the cabinet, and 60-dB background white noise was continuously applied throughout the entire test session. The test session started with a 10-minute exploration stage followed by a 5-minute basal stage that consisted of 10 Pulse-Alone trials; an acoustic pulse (120 dB, 8 kHz, 40 ms bursts) was delivered every 30-s in each trial. Following the basal stage, there was a 20-minute test stage that consisted of 40 trials delivered every 30-s. The 40 trials consisted of 10 Pulse-Alone trials, 10 Prepulse-Alone trials, 10 No-Stimulus trials, and 10 Prepulse- Pulse trials, and were delivered in the pseudorandom order. In each

Prepulse-Alone trial, an acoustic prepulse (80 dB, 8 kHz, 20 ms noises) was delivered.

In each Prepulse-Pulse trial, the prepulse and pulse pair was delivered with the prepulse

leading the pulse by 100 ms. Finally, the test session ended with a 2-minute ensure stage

that consisted of 4 Prepulse-Alone trials. In each trial, the startle response was recorded

over a 100-ms period that started immediately at the onset of the 120-dB pulse. The

baseline of the startle response was measured by averaging the magnitudes of the startle

response to the 10 Pulse-Alone trials in the test stage. PPI was calculated using the

following equation:

$$\text{PPI (\%)} = [(\text{SR} - \text{PreSR}) / \text{PreSR}] \times 100\%,$$

where the SR is the baseline of the startle response, and the PreSR is the average from

the 10 Prepulse-Pulse trials of the startle response to the 120-dB pulse in the test stage.

For the open field test, the animals were placed separately into a no-lid chamber (49 cm

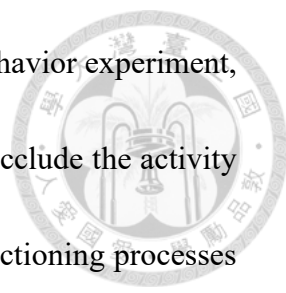
in length x 49 cm in width x 49 cm in height) composed of white high density and

nonporous plastic with a camera recording from above. The travel distance of the total

30 minutes of free exploration of the mice was tracked using the ANY-maze software

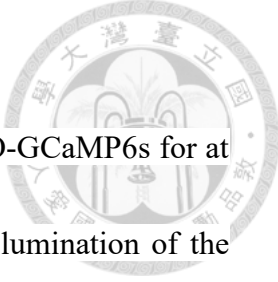
(Stoelting Co., IL, USA). In addition, the incidence of the rearing behavior and the

duration of the grooming behavior were counted based on the video.



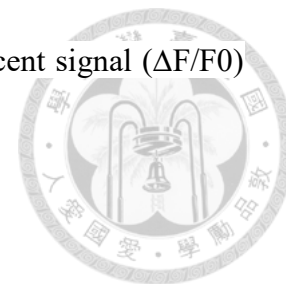
For the *post hoc* validation of the AAV2 injection site in the behavior experiment, the sections were incubated in 3% H<sub>2</sub>O<sub>2</sub> in PBS for 10 minutes to occlude the activity of the endogenous peroxidase, following the same perfusion and sectioning processes previously described. The sections were then incubated in 2% BSA in PBST for 1 hr to block the nonspecific reactions; they were then incubated with chicken anti-mCherry primary antibody, in PBST at 4°C overnight, followed by incubation with the biotinylated goat anti-chicken IgG (dilution: 1:200; Cat # BA-9010, Vector Laboratories INC) in PBST for 2 hrs. The sections were then reacted with avidin-biotin horseradish peroxidase complex (dilution: 1:200; Cat # PK6010, Vector Laboratories INC) in PBST for 2 hrs and visualized with 0.025% 3,3'-diaminobenzidine (DAB) and 0.01% H<sub>2</sub>O<sub>2</sub> in PB. Finally, they were mounted on the slides, counter stained with the Nissl method to provide the background cytoarchitecture and coverslipped with DPX. The results of staining were then observed under an Olympus BX50 microscope (Olympus, Tokyo, Japan) and images acquired. Again, the sections or slices were intensely washed with PBST for at least three times of 10-minute wash between the incubation steps; all incubations occurred at room temperature, unless otherwise specified.

## 9. Calcium Imaging



Slices were cut from  $Vglut2^{cre}$  mice and received the AAV5-DIO-GCaMP6s for at least 6 weeks in the calcium imaging experiments. A continuous illumination of the blue light in a proper intensity ( $\sim 1-5 \times 10 \text{ mW/cm}^2$ ) was dependent on the GCaMP6s expression. Videos of the GFP fluorescence was recorded by an ORCA-R2 or ORCA-Flash 4.0 V2 cameras (Hamamatsu Photonics, Shizuoka, Japan) under the pulse triggering of a Master-8 stimulator with 35ms as the exposure time at 20 fps. The videos typically lasted 100-300-s and the recording field was usually located in the peri-LC regions depending on the expression pattern of the GCaMP6s. For analysis of the calcium imaging, videos were processed into stacks of images, then the fluorescent signal was calculated as  $\Delta F/F_0$  for each pixel, the  $F_0$  denotes the mean fluorescence and the  $\Delta F$  was calculated as  $F(t) - F_0$ . The burst firing E-INs were classified by the presence of the obvious EPSP-like activities fluctuations which typically lasted for 10-s, while the rest of cells with persistent fluorescence were considered as tonic E-INs. For detecting the activity corresponding to the bursts, many ROIs containing the  $GFP^+$  soma or dendrite were manually enclosed and the trace of the mean fluorescence was plotted. Instantaneous changes of the fluorescence,  $d(\Delta F/F_0)$ , were calculated, and a burst related activity was identified by a  $d(\Delta F/F_0)$  greater than the mean plus twice that

of the SD of the overall  $d$  ( $\Delta F/F_0$ )s and the raising of this fluorescent signal ( $\Delta F/F_0$ ) lasted for at least 0.25-s (5 data points).

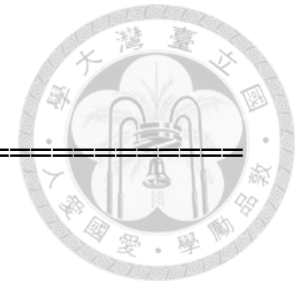


## 10. Statistical analysis

For statistical comparisons, the normality of the data was first tested using the Shapiro-Wilk test. For both compared groups showing normal distributions, Student's t test, the paired t test, or one-way ANOVA were used; otherwise, the non-parametric paired Wilcoxon-sign rank test, Mann-Whitney test and the Kruskal-wallis test were used. The paired t test and the non-parametric paired Wilcoxon-sign rank test were used for comparison of data collected before and after the drug application from an individual neuron or mouse; Student's t test and Mann-Whitney test were used for the two independent groups. one-way ANOVA and Kruskal-wallis test were used in the comparisons among three or more groups. For the statistical comparison in Table 4, the Kruskal-wallis test and post hoc Dunn-bonferroni test were used. All statistics were performed using the Originpro 8 software (OriginLab, MA, USA) as well as Microsoft Excel (Microsoft Corp., Redmond, WA). All data are presented as the mean  $\pm$ SE. In the figures, "ns" denotes not statistically significant, \* denotes  $p < 0.05$ , \*\* denotes  $p < 0.01$ , and \*\*\* denotes  $p < 0.005$ .

# RESULTS

---



## Section 1: Identification of LC Local Circuit

1.1 Recording of LC-NA Neurons in Brain Slices-----	88
1.2 Discovery of sPLA Showing Synaptic Origin and Regulation-----	89
1.3 Localization of I-INs Making Contacts with LC-NA Neurons-----	91
Figures-----	95

## Section 2: Role of peri-LC I-IN in Regulation of sPLA

2.1 Synaptic Transmission from peri-LC I-INs to LC-NA Neurons-----	117
2.2 Suppression of peri-LC I-INs with hM4DiR DREADD Enhanced sPLA in LC-NA Neurons-----	122
2.3 Electrical Stimulation Recruits peri-LC I-INs to Exert a Feedforward Inhibition-----	125
Figures-----	127

---



---

---

### **Section 3: Functional Implications of peri-LC I-IN**

<b>3.1 Inhibition of peri-LC I-INS Enhances Prepulse Inhibition-----</b>	<b>168</b>
<b>3.2 Peri-LC I-INS Receive Axonal Contacts from the OFC and PrL-----</b>	<b>170</b>
<b>Figures-----</b>	<b>174</b>

### **Section 4: Positive Evidence of LC E-INS in Regulation of LC Phasic Activation**

<b>4.1 Excitatory Connection from LC E-INS onto LC-NA Neurons-----</b>	<b>199</b>
<b>4.2 Spontaneous Activity of LC E-INS-----</b>	<b>201</b>
<b>4.3 Preliminary but Positive Evidence of burst E-IN in Driving sPLA in LC-NA Neurons-----</b>	<b>204</b>
<b>Figures-----</b>	<b>208</b>

---

---

# Section 1



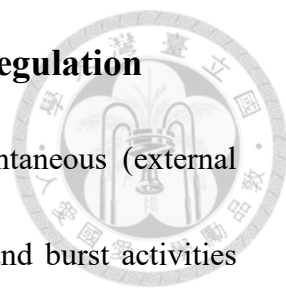
## Identification of LC Local Circuit

This section shows the data from brain slice in vitro recordings to support the presence of a conceptual, local circuit forming functional contacts onto the LC-NA neurons, also the discovery of the sPLAs. Results from works of viral WGA tracing further identify the interneuron population and indicate as to whether they are inhibitory or supposed excitatory cells. Our efforts serve as the first systematic identification of the LC local circuit and the sPLAs in brain slice in vitro recordings.

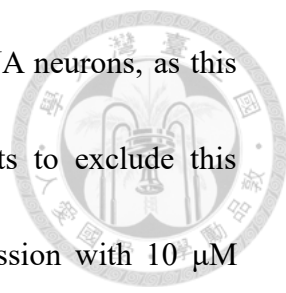
## 1.1 Recording of LC-NA Neurons in Brain Slices

By using a Nomarski microscopy video, the LC-proper was identified as a transparent and kidney-shaped area located beneath the 4th ventricle and medial to the superior cerebellar peduncle (Fig. 1A1). At high magnification, numerous large neurons with a soma diameter of  $\sim 30 \mu\text{m}$  were identified for recording (Fig. 1A2). I filled the recorded neurons with biocytin to confirm that these cells were immunoreactive (ir) with the anti-TH antibody (Fig. 1B). In I-clamp recordings, these TH-ir neurons were able to fire APs at usually 1-1.5 Hz without additional stimulation (Table. 4). Upon injection of the depolarizing current pulses, the TH-ir neurons exhibited a delay in the firing of AP, the duration of which depended on the  $V_m$  responding to the hyperpolarizing current prepulse (Fig. 1C, D). All of these features are consistent with our previous observations made in rats (Wang et al., 2015; Wu et al., 2020), and I and my colleagues hypothesized that the recorded TH-ir neurons were LC-NA neurons. As all of the recorded LC-NA neurons exhibited the above-described physiological properties, and I and my colleagues used these physiological criteria for the identification of LC-NA neurons and discontinued the histological practice after this series of experiments.

## 1.2 Discovery of sPLA Showing Synaptic Origin and Regulation

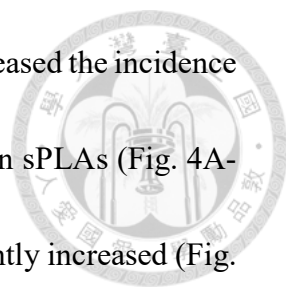


When the slices were perfused with regular aCSF, the spontaneous (external stimulation-independent) APs consisted of the background tonic and burst activities (Fig. 2A). I and my colleagues refer to the burst activity as the sPLA hereafter, as it was frequently followed by a long-period inhibition of the tonic activity, a characteristic that resembles the phasic activation-pause profile observed in animal studies (Bouret and Sara, 2004; Clayton et al., 2004; Bari and Aston-Jones, 2013; Marzo et al., 2013). As the naturally occurred phasic activation of LC-NA neurons shown by previous studies, the sPLA shows its high similarity but varies largely in the intensity and incidence among the recorded cells. I propose that the sPLA is produced by local interneurons, and this LC local circuit can be able to generate phasic activation in living animal. Moreover, the variable intensity and incidence of sPLAs suggest the local circuit is able to scale its output for a delicate regulation of phasic activation of LC-NA neurons. And this ability is controlled by far innervations from other brain regions, the local circuit in brain slice remains its phasic-driven ability but lost most of external control. This argument can explain the occurrence of some large sPLA overing the normal scale of phasic activation in living animal.



However, the sPLA may be purely intrinsic property of LC-NA neurons, as this consideration, I performed a series of pharmacology experiments to exclude this possibility. As I expected, blockade of the glutamatergic transmission with 10  $\mu\text{M}$  DNQX, an AMPA receptor antagonist, plus 50  $\mu\text{M}$  AP5, an NMDA receptor antagonist, completely abolished the sPLA, without affecting the background tonic rate (Fig. 2; Table 4). Interestingly, in the LC-NA neurons that exhibited a high incidence of the sPLA, I typically observed the copious spontaneous synaptic activity with large amplitudes and long durations up to seconds when the recordings were switched to V-clamp mode (Fig. 3A, B). The large synaptic activity was blocked by the bath application of 10  $\mu\text{M}$  DNOX plus 50  $\mu\text{M}$  AP5, indicating that the activity was EPSC mediated via AMPA and NMDA receptors (Fig. 3C, D). As per features observed, I and my colleagues refer to the large synaptic activity as the large sEPSC showing significant charge transfer when compared to the general fast EPSC. Analysis over fifteen LC-NA neurons revealed a quite strong correlation between the incidences of the sPLA and the large sEPSC (Fig. 3E), suggesting that the sPLA could be driven by the large sEPSC.

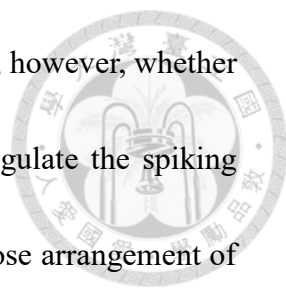
In contrast to the application of DNQX plus AP5, the bath application of 10  $\mu\text{M}$  bicuculline methochloride (BM), a GABA<sub>A</sub> receptor (GABA<sub>A</sub>R) antagonist, plus 1  $\mu\text{M}$



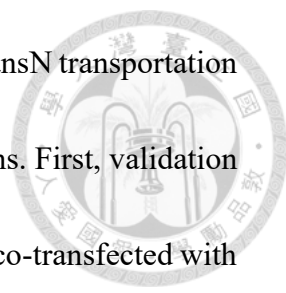
strychnine (Stry), a glycine receptor (GlyR) antagonist, robustly increased the incidence of the sPLA without altering the AP number and the mean AP rate in sPLAs (Fig. 4A-B, D-F; Table 4), while the background tonic rate was also significantly increased (Fig. 4G; Table 4). Furthermore, the background tonic activity under the BM and Stry application into the bath often exhibits corpious fluctuations of a firing rate resembling the subthreshold sPLA, indicating that the increase of the large sEPSCs incidence comprised many smaller events (Fig. 4C). This observation may explain why the application of BM plus Stry doesn't change the spike number within sPLAs. Given that the somata of the long-range input to the LC were not preserved in brain slices, and it is unlikely that the remaining axonal terminals could spontaneously generate APs, these observations suggest the existence of local E-INs to drive the sPLA in LC-NA neurons and I-INs to modulate the sPLA. Our group is the first team to discover this spontaneous event in brain slice.

### **1.3 Localization of I-INs Making Contacts with LC-NA Neurons**

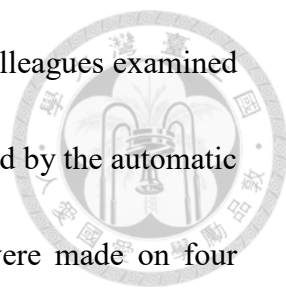
After the discovery of putative LC local circuit that is able to generate and modulate the sPLA, I and my colleagues aimed to localize the I-INs given that the previous studies have provided evidence for the existence of I-INs in the LC (Aston-



Jones et al., 2004; Jin et al., 2016; Breton-Provenche and Sur, 2019); however, whether I-INs could control the synaptic inputs to LC-NA neurons and regulate the spiking pattern of LC-NA neurons remains unknown. With regard of the close arrangement of the brainstem nuclei settling dendritic fields and the interneuron interface in an overlapping manner, a selective identification of LC-IN population shows it was necessary. To this end, I and my colleagues produced an AAV2 encoding a DIO of WGA, a widely used Trans-neuronal (TransN) tracer (Gerfen et al., 1982; Porter et al., 1985). The AAV2 was infused into the left LC of TH<sup>Cre</sup>×GAD<sup>GFP</sup> mice to enable the selective expression of the WGA in LC-NA neurons (Fig. 5A). When I and my colleagues examined the sections cut through the pontine area and stained with IHC using the antibodies against the WGA and TH, I and my colleagues observed numerous neurons in the LC exhibiting WGA-ir and TH-ir. Moreover, neurons that exhibited WGA-ir but not TH-ir were also noted (Fig. 5B-D). Some of WGA<sup>+</sup>/TH<sup>-</sup> cells were GABAergic as they also expressed GFP (Fig. 5E). An analysis of 4 mice showed that the WGA<sup>+</sup>/TH<sup>-</sup> neurons accounted for 28.4±2.5% of the WGA-ir neurons (Fig. 7A, B) and were mainly located in the medial part of the peri-LC (Fig. 7C). Of the TH<sup>-</sup>/WGA<sup>+</sup> neurons, 20.7±1.5% were GABAergic in a scattered distribution (Fig. 7A-C).



I and my colleagues reasoned that the results were due to the TransN transportation of the WGA from transfected LC-NA neurons to TH<sup>-</sup>/WGA<sup>+</sup> neurons. First, validation with the IHC using anti-WGA antibodies showed that all HEK cells co-transfected with the WGA plasmid and viral Cre insertion expressed the WGA with granule-like structures aggregating in the cytoplasm (Fig. 8), which was consistent with the WGA-ir profile reported in a previous study (Yoshihara et al., 1999). Second, the catecholaminergic neurons other than LC-NA neurons were not present in the dorsal pons. Finally, leaky Cre expression in neurons that were not catecholaminergic was minimal in TH<sup>Cre</sup> mice. When eYFP, which cannot undergo TransN transportation, replaced WGA as the transgene, a significantly reduced number of TH<sup>-</sup>/eYFP<sup>+</sup> neurons were observed (Fig. 6A). The infusion of the AAV2-DIO-eYFP into the left LC of the TH<sup>Cre</sup> mouse resulted in only  $7.6 \pm 0.4\%$  of eYFP<sup>+</sup>/TH<sup>-</sup> neurons ( $n = 5$  mice), which was significantly lower than that of the WGA<sup>+</sup>/TH<sup>-</sup> portion ( $p < 0.005$ ; Student's *t* test; Fig. 7B). I and my colleagues also examined the transfection rate, which was defined as the percentage of TH-ir neurons expressing the WGA-ir or eYFP-ir signals in the TH<sup>Cre</sup> mice injected with the AAV2-DIO-WGA or the AAV2-DIO-eYFP, respectively, and observed no significant difference between the two AAV2s ( $p = 0.178$ ; Mann-Whiney test). The transfection rates were  $73.0 \pm 7.6\%$  for the AAV2-DIO-WGA and



87.1±9.6% for the AAV2-DIO-eYFP (Fig. 6B). Finally, I and my colleagues examined the possibility of the Cre-independent expression of the WGA caused by the automatic flipping of the AAV2 introduced DIO sequence. Examinations were made on four hemispheres from two WT mice that received the bilateral infusion of the AAV2-DIO-WGA into the LC. In all cases, none of the WGA-ir neuron was observed in sections that cut through the LC and the peri-LC region (Fig. 6C); accordingly, the leaky WGA expression in non-Cre cells was minimal. Together, these observations showed that the labeled TH<sup>-</sup>/WGA<sup>+</sup>/GFP<sup>+</sup> neurons were local I-INs mainly in the medial part of the peri-LC and could make functional contacts with LC-NA neurons. Hereafter I and my colleagues refer to the identified cells as peri-LC I-INs by their location and synaptic contacts onto LC-NA neurons.

# Figures

---



## Section 1: Identification of LC Local Circuit

<b>Figure 1. Recording of LC-NA neurons</b> -----	<b>96</b>
<b>Figure 2. Glutamatergic regulation of sPLA in brain slices</b> -----	<b>98</b>
<b>Figure 3. Large sEPSC underlying sPLAs</b> -----	<b>101</b>
<b>Figure 4. Blockade of GABAergic and glycinergic transmission enhances sPLA</b> -----	<b>104</b>
<b>Figure 5. Localization of I-INs making functional connections with LC-NA neurons by viral-genetic WGA tracing</b> -----	<b>107</b>
<b>Figure 6. Control experiments for confirmation of results from viral-genetic WGA tracing</b> -----	<b>110</b>
<b>Figure 7. Quantitative analysis of viral-genetic WGA-tracing</b> -----	<b>112</b>
<b>Figure 8. Validation of WGA plasmid</b> -----	<b>114</b>

---

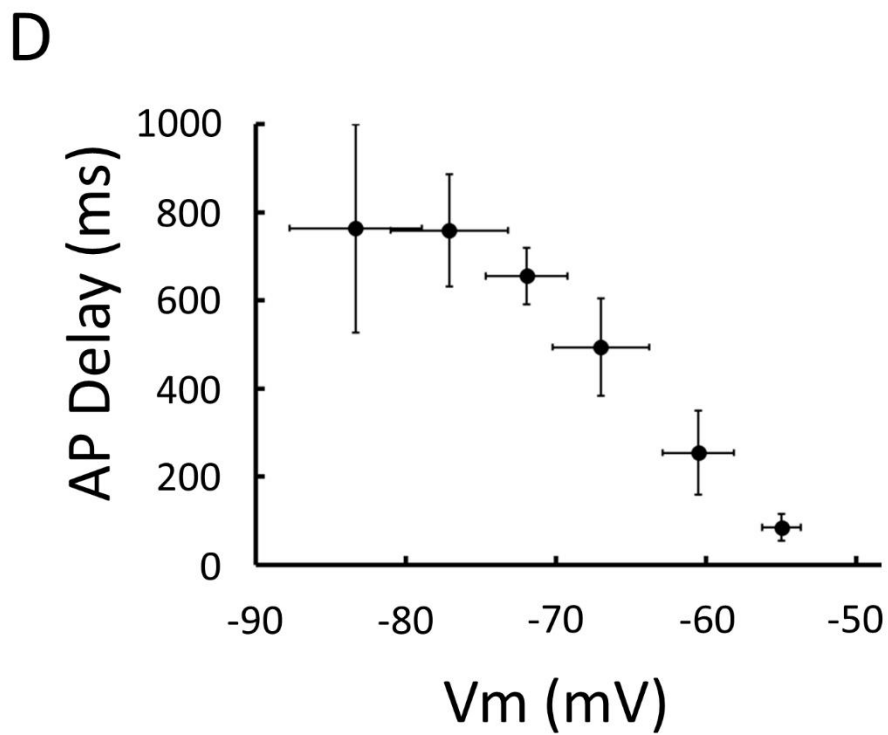
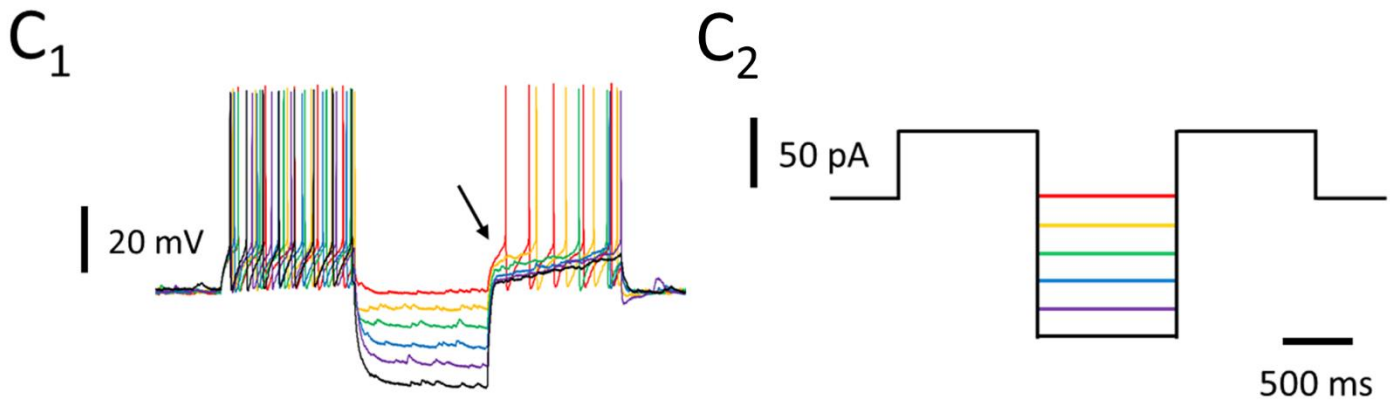
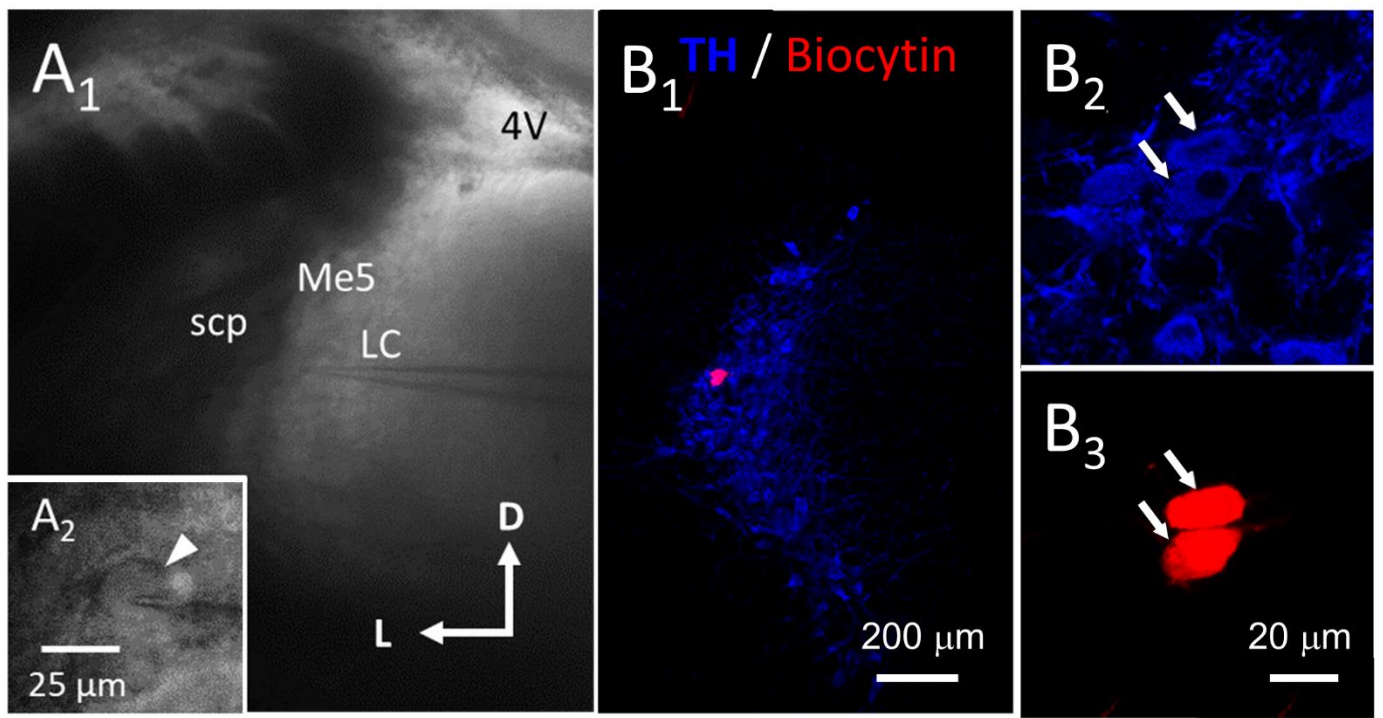
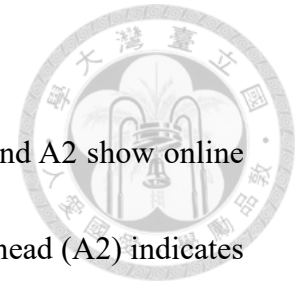


Figure 1

## Figure 1. Recordings of LC-NA neurons



**A**, Identification of LC-NA neurons for whole-cell recording. A1 and A2 show online DIC images of a brainstem slice that comprised the LC. The arrowhead (A2) indicates a LC-NA neuron under whole-cell recording. **B**, Validation of recorded LC-NA neurons by *post hoc* IHC of TH and biocytin. B1 presents a merged fluorescence image of *post hoc* IHC using anti-TH antibodies (blue) and biocytin histochemistry (red). B2 shows the anti-TH stain and B3 shows biocytin histochemistry from the same experiment at high magnification. Note that two neurons marked by arrows were recorded and filled with biocytin, and both showed TH-ir. Abbreviations: Me5, mesencephalic trigeminal nucleus; scp, superior cerebellar peduncle; D, dorsal; L, lateral. **C**, Electrophysiology property of LC-NA neurons showing the delay of firing onset after a hyperpolarized pulse. C1 demonstrates a representative I-clamp recording from a TH-ir neuron. Note that traces show the delay of AP onset in a hyperpolarization dependent manner, and the arrow indicates the delayed onset of AP firing. C2 shows a current injection protocol. **D**, A quantitative plot of summarized results from 4 cells. The delayed onset of AP firing shows a negative relationship to the decreases in hyperpolarized pulses.

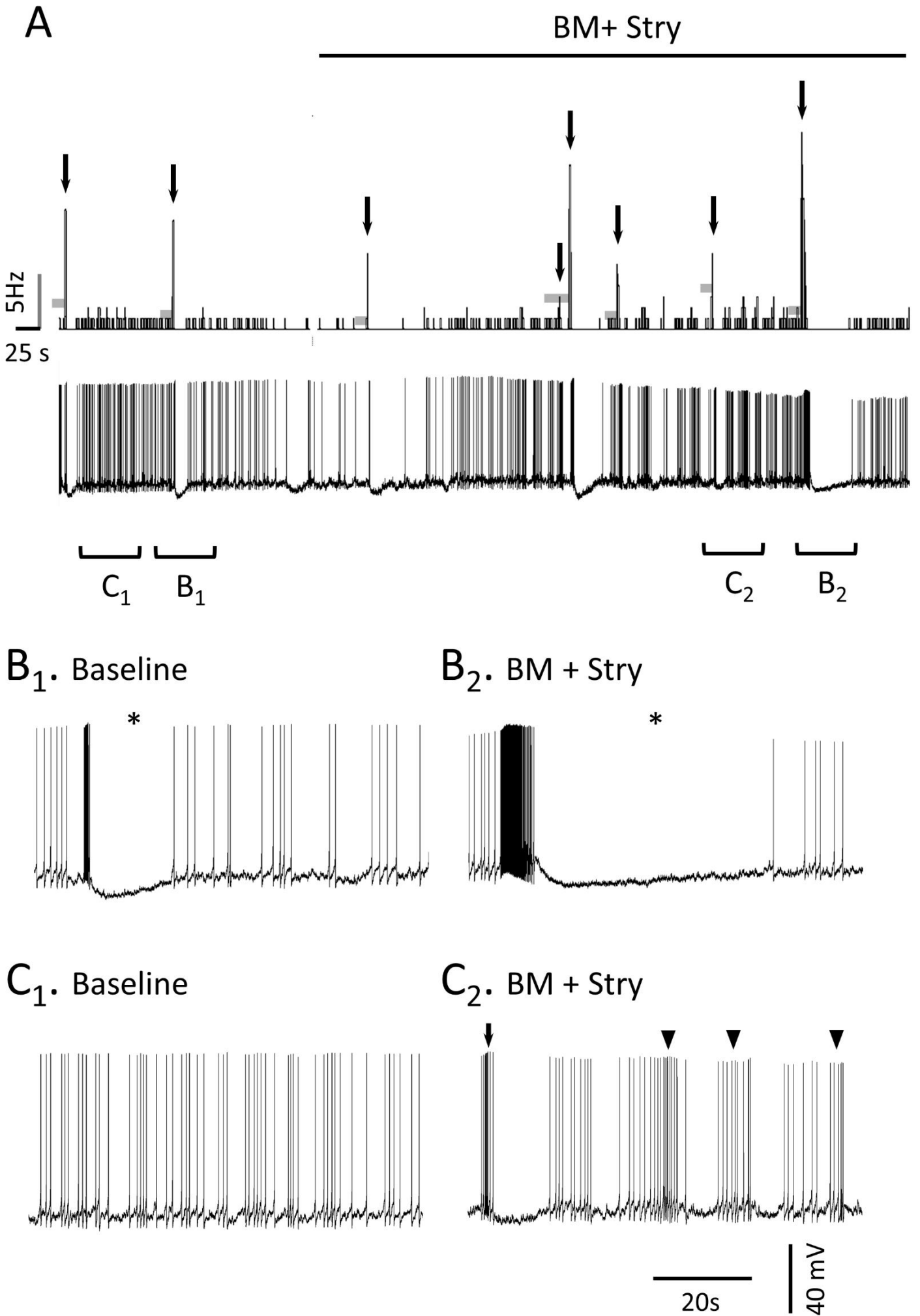


Figure 4

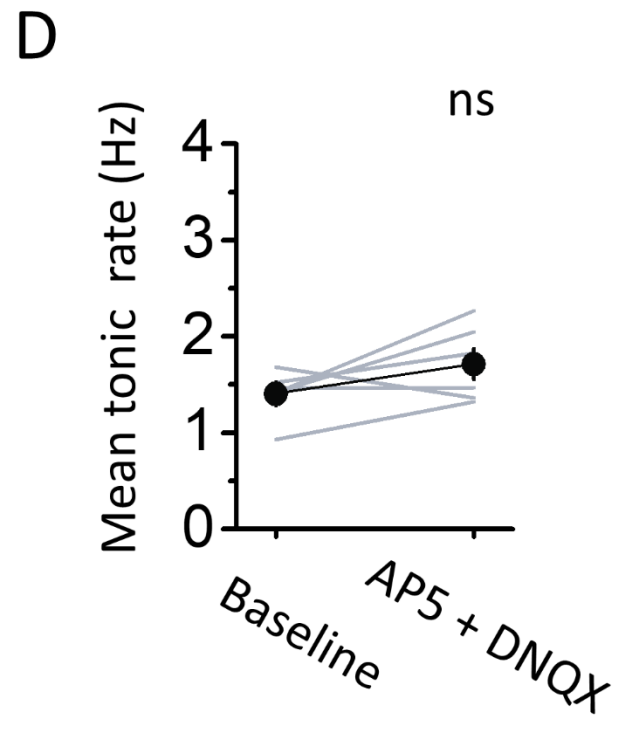
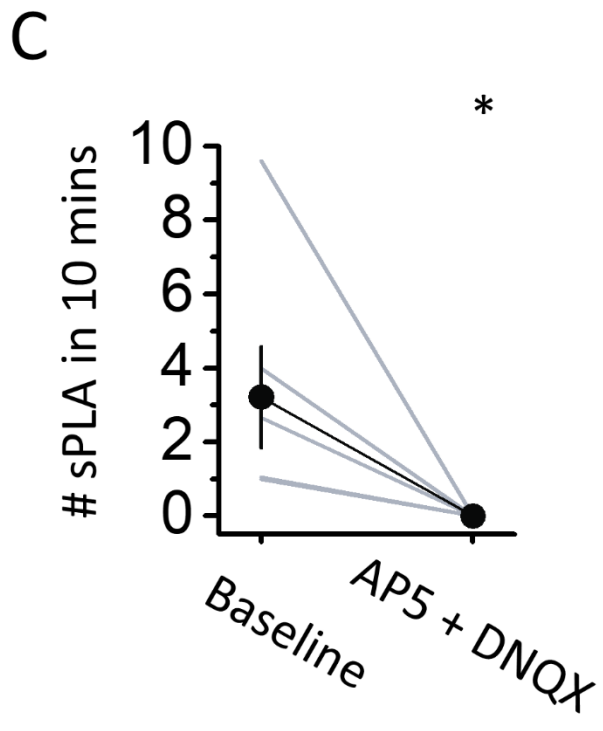
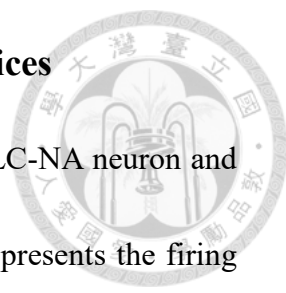


Figure 2

## Figure 2. Glutamatergic regulation of sPLA in brain slices



**A**, A representative recording reveal the spontaneous activity in a LC-NA neuron and the effects of DNQX+AP5 application on it. The upper histogram presents the firing rate of recorded neuron (bin = 1 s), lines beneath the histogram represent the standard for each of detected sPLA marked by arrows above the histogram; and the lower trace show a representative recording underlying the upper histogram. **B**, Two episodes of the recording shown in A. B1 and B2 display the episode before and after the DNQX+AP5 application, respectively. The asterisks in B1 indicates the long inhibition period following the burst activities. **D & E**, Summarized plots show effects of DNQX+AP5 application on sPLA incidence (D) and the background tonic rate (E). Each line in the plots shows the results of an individual experiment, and the circles (mean) + capped vertical lines (SEM) present the averaged results. Also see Table 4 for statistical information. All of results were gathered in brain slices from naïve *vgat<sup>cre</sup>* mice not receiving any treatment or AAV infusion.

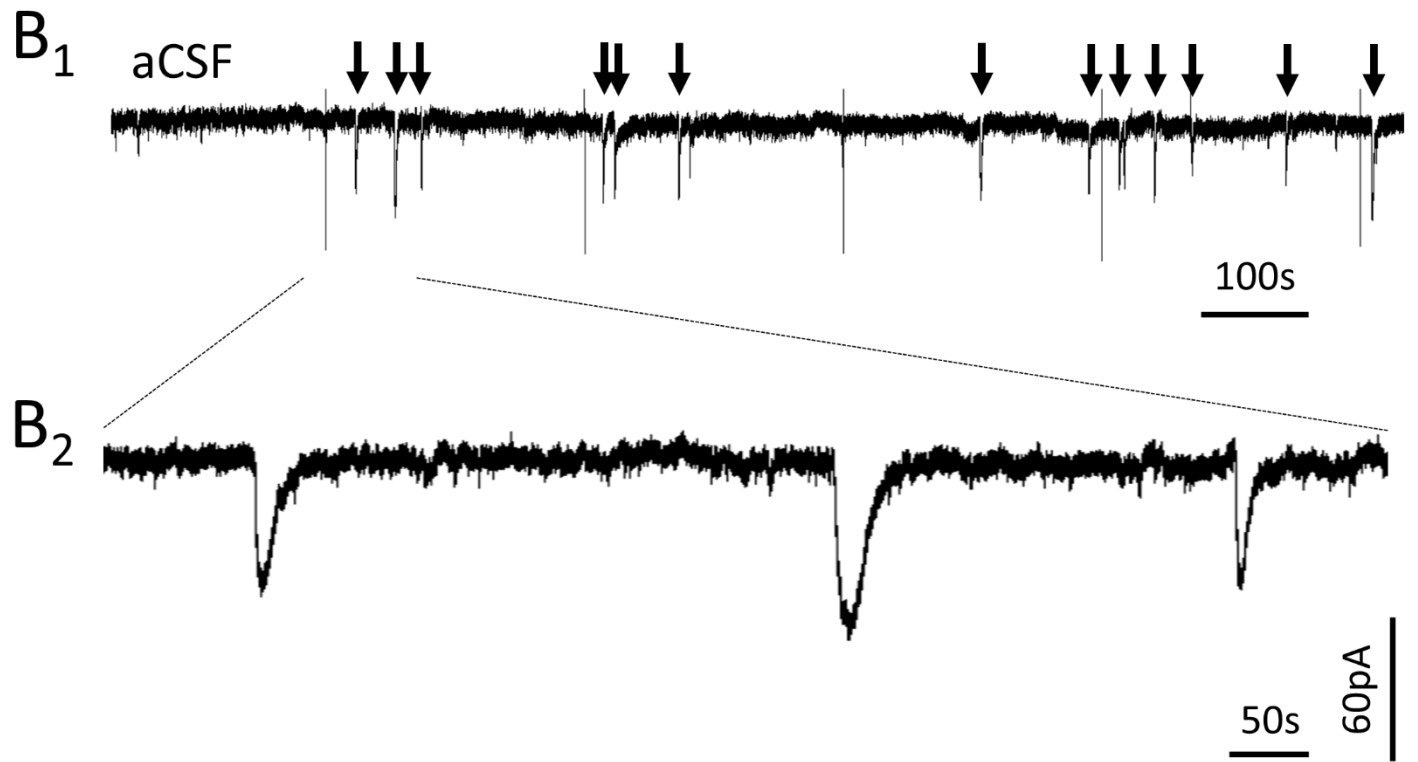
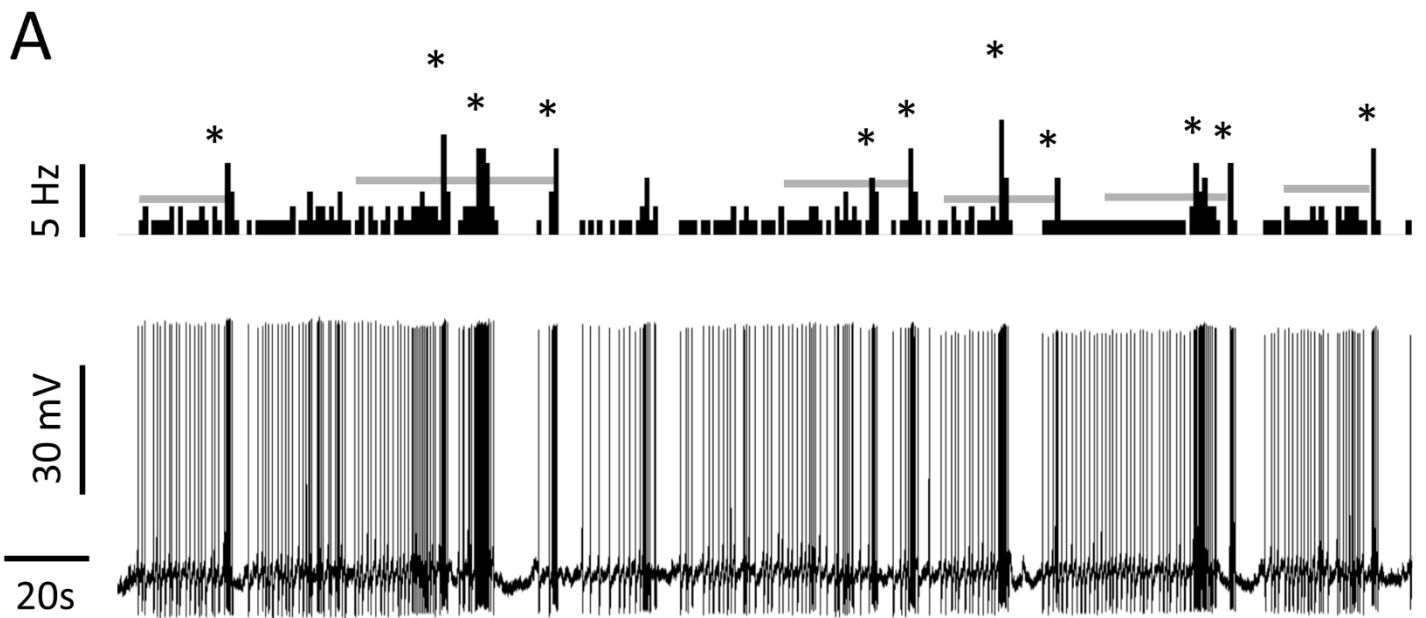
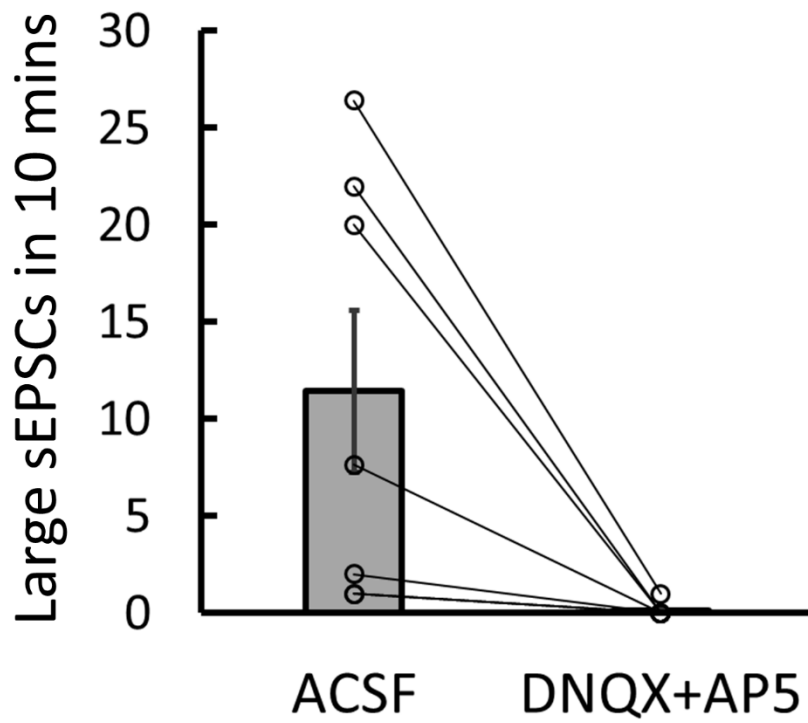


Figure 3

D



E

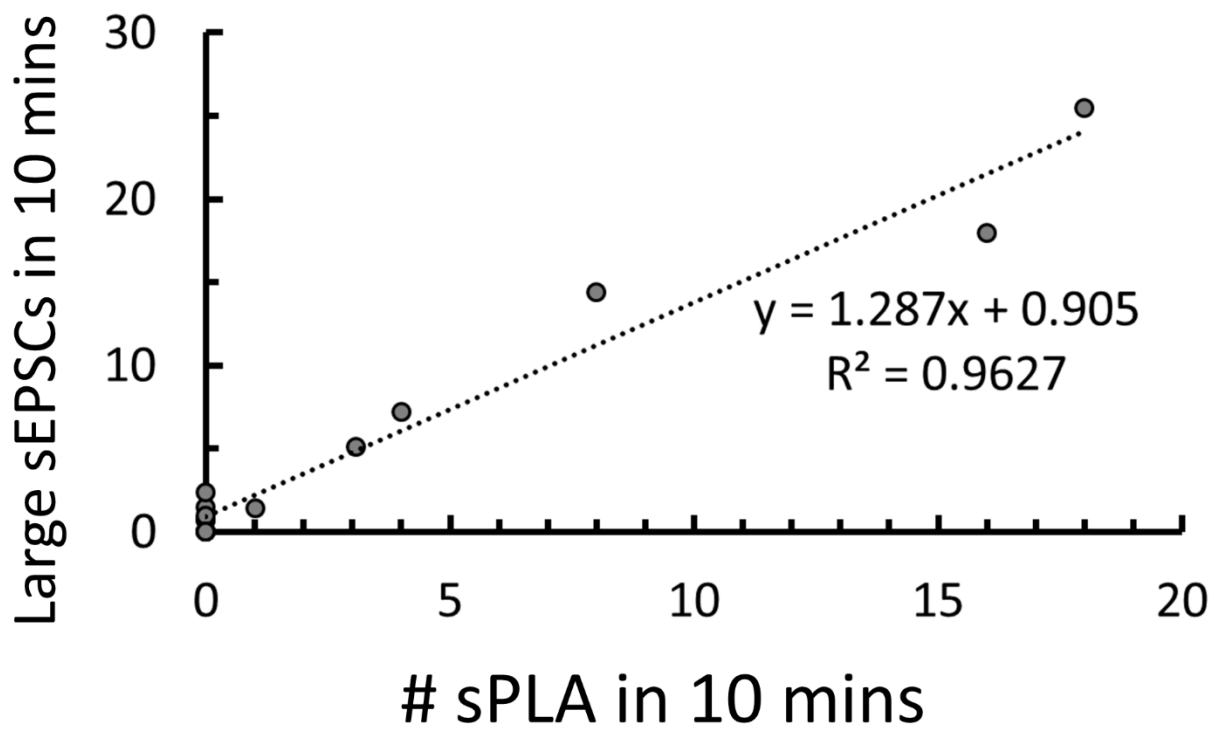


Figure 3

### Figure 3. Large sEPSC underlying sPLAs



**A**, A representative recording from a LC-NA neuron that shows the high incidence of sPLA and large sEPSCs in I-clamp and V-clamp recordings. The upper histogram shows firing rate (bin = 1 s), and bottom trace presents raw data in the I-clamp recording. The horizontal dashed lines represent the standard for each of detected sPLA marked by the asterisks. **B**, Large sEPSCs shown in the LC-NA neuron with high incidence of sPLA. **B1**, A trace shows raw data of the V-clamp recording of the same neuron shown in **A**. Note the large sEPSCs marked by the arrows and show a incidence slightly higher than the sPLA. **B2** demonstrates an episode comprises three large sEPSC (as indicated by the dashed lines) of the recording presented on a faster time scale. **C**, A trace shows the complete blockade of large sEPSCs by the DNQX+AP5 application in the same recording. **D**, Quantitative plot shows the complete suppression of large sEPSCs before and after DNQX+AP5 application. **E**, Summarized results from 15 LC-NA neurons reveals a strong correlation of sPLA incidences and large EPSCs. Note that about 20% of large sEPSC cannot trigger to a detected sPLA successfully. All of results were gathered in brain slices from naïve *vgat<sup>cre</sup>* mice not receiving any treatment or AAV infusion.

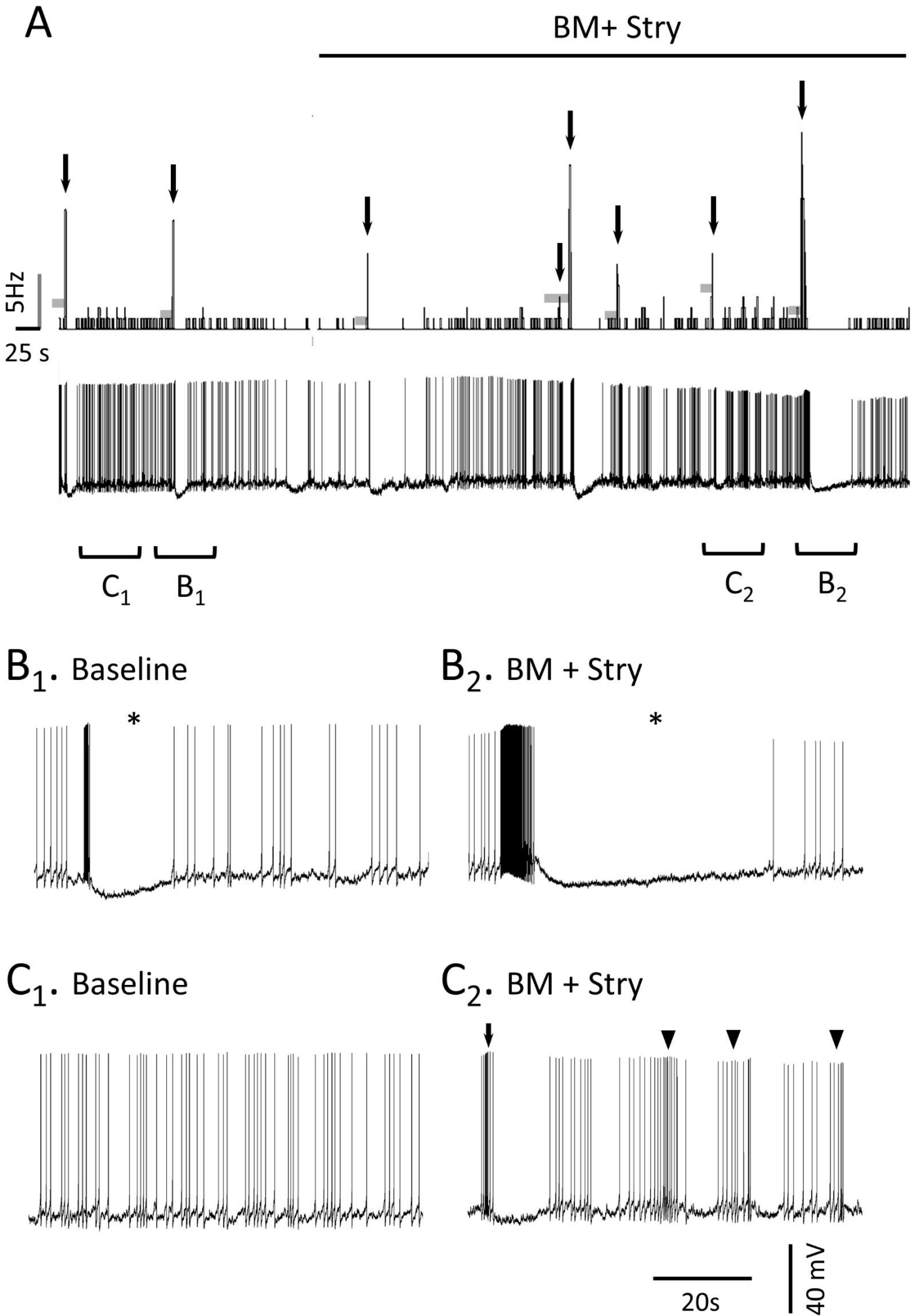
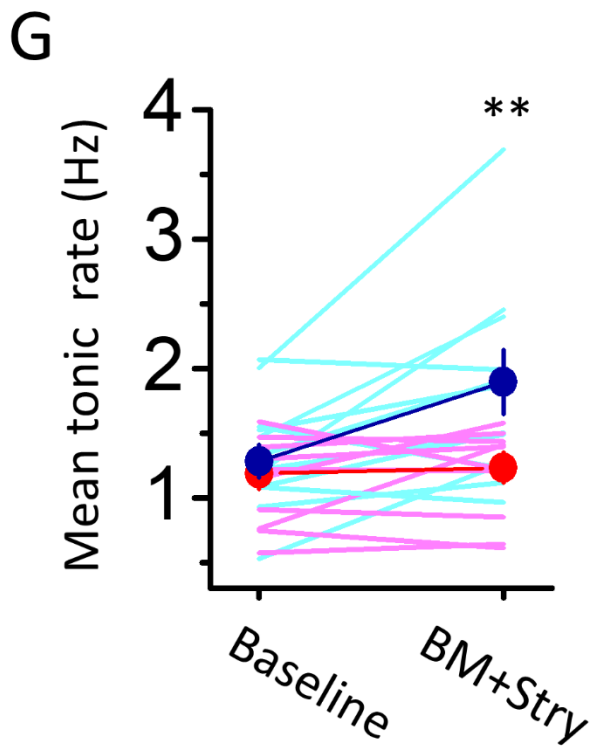
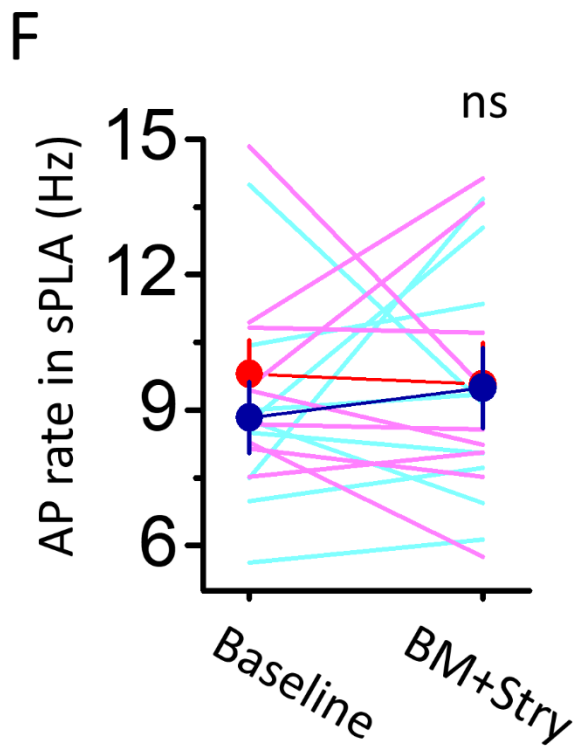
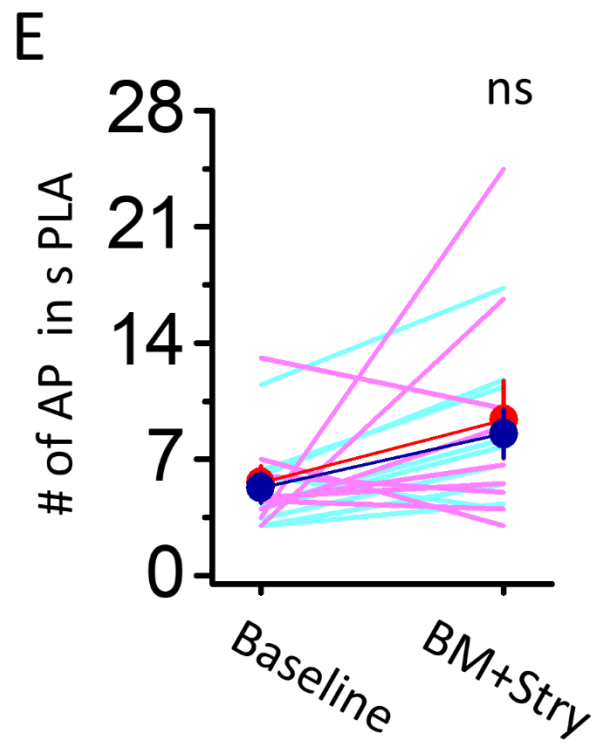
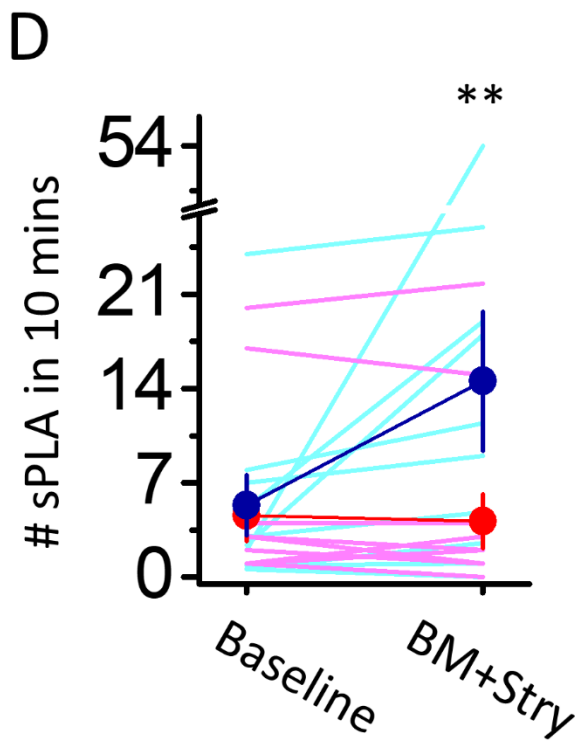


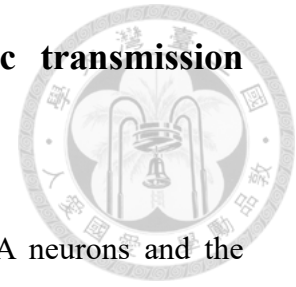
Figure 4



BM + Stry: — / ● ; Vehicle: — / ●

Figure 4

## Figure 4. Blockade of GABAergic and glycinergic transmission enhances sPLA



**A**, Representative recordings show spontaneous APs in a LC-NA neurons and the effects of BM+Stry application on the activity. The data are presented in the same way as shown in Fig. 2A. Note the BM+Stry application lead to a dramatic increase of sPLAs that distort the regularity of background tonic firings. **B**, Example traces of two episodes represent sPLAs before (B1) and after (B2) the BM+Stry application. **C**, Example traces of two episodes without detected sPLAs before (C1) and after (C2) BM+Stry application. Note many sPLA-like events which cannot fulfill the detection criteria appear under BM+Stry application. **D-G**, Summarized plots show effects of BM+Stry (cyan/blue) and vehicle (magenta/red) application on the incidence (D), AP number (E) and mean AP rate (F) in the sPLA as well as the background tonic rate (G). Each line in the plots shows the result of an individual experiment, and the circles (mean) + capped vertical lines (SEM) show the averaged results. Also see Table 4 for statistical information. All of results were gathered in brain slices from naïve *vgat<sup>cre</sup>* mice not receiving any treatment or AAV infusion.

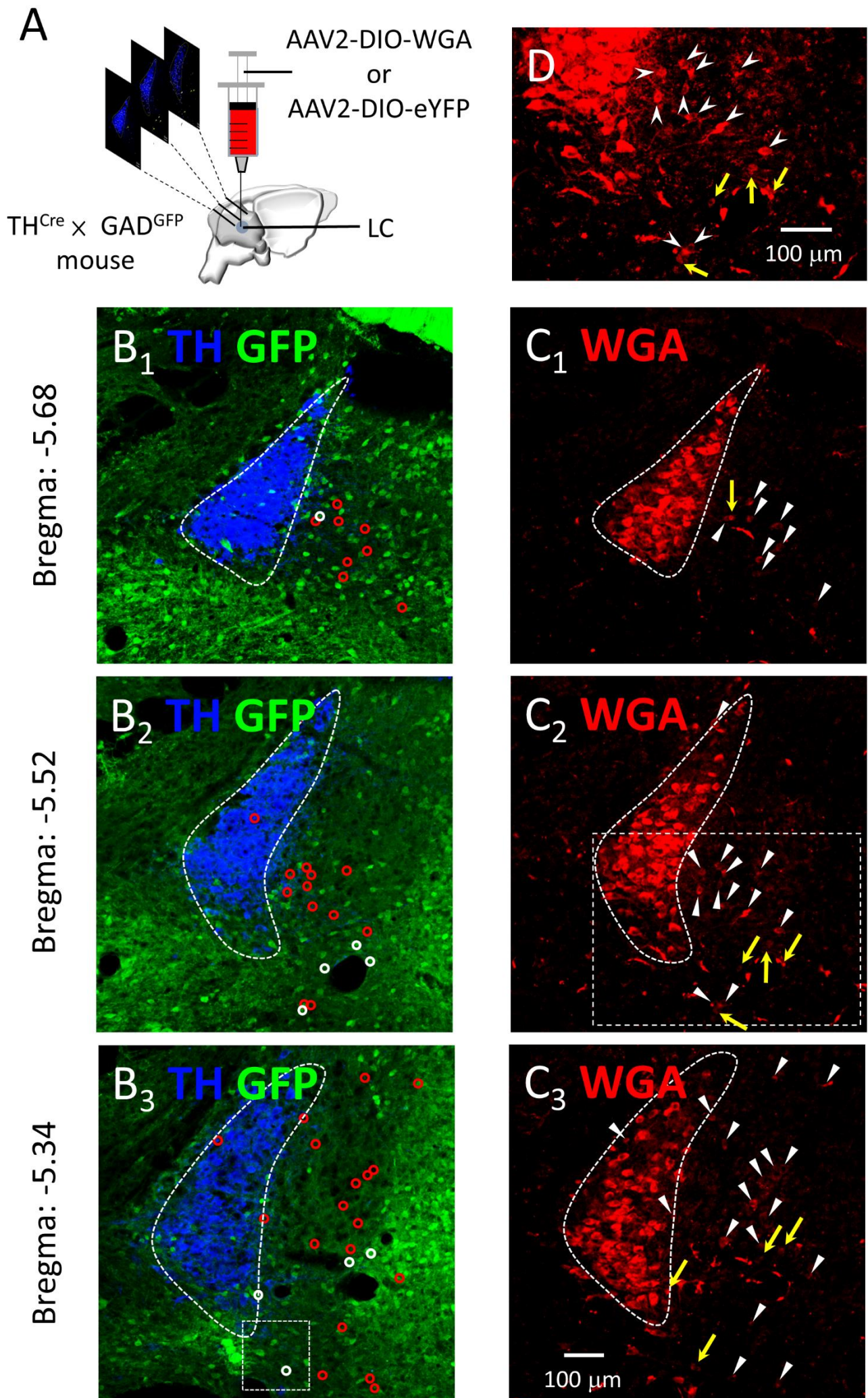


Figure 5

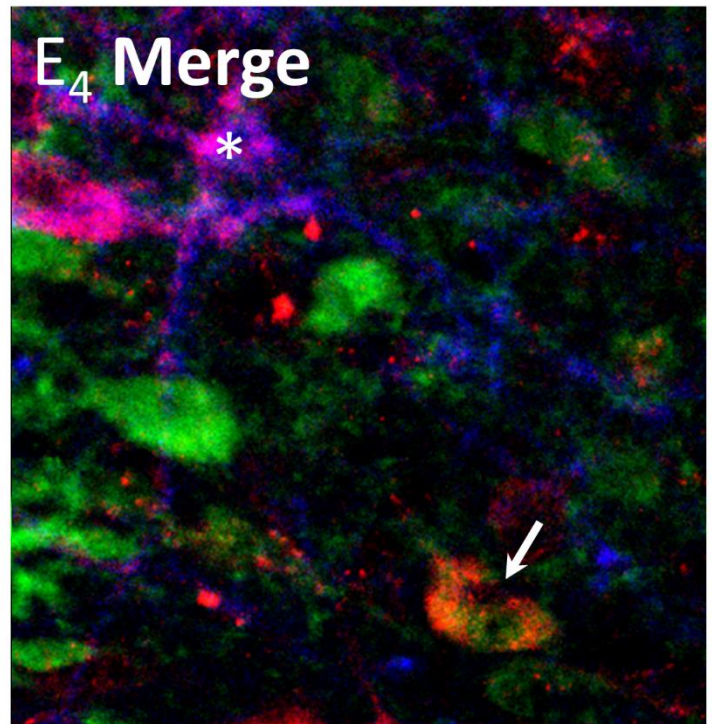
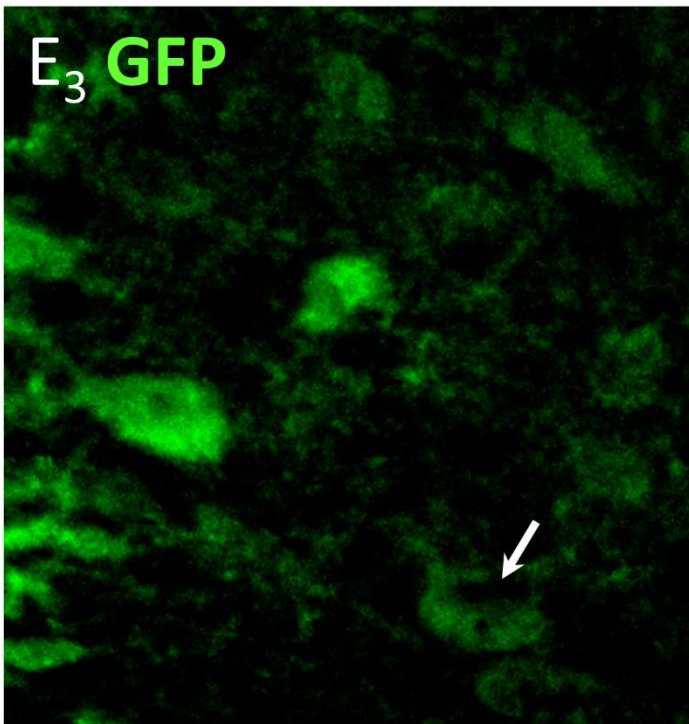
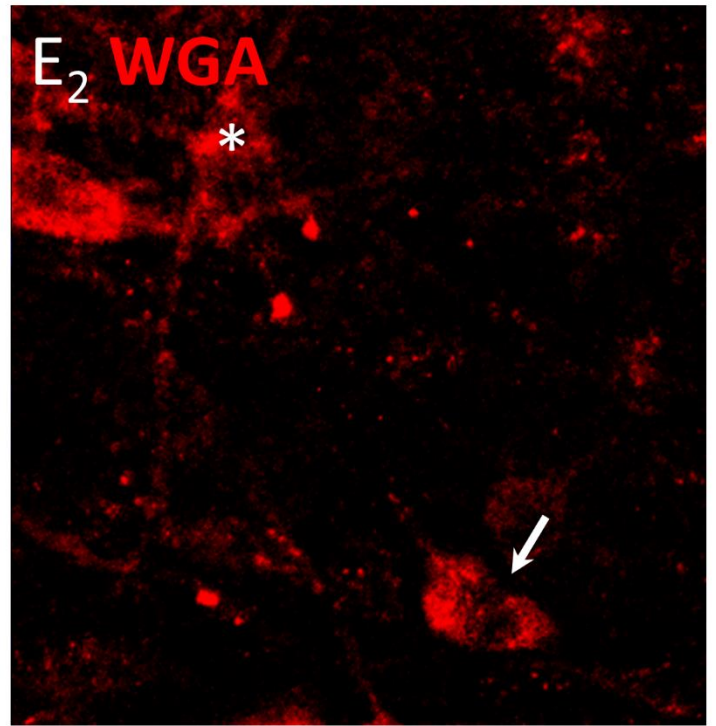
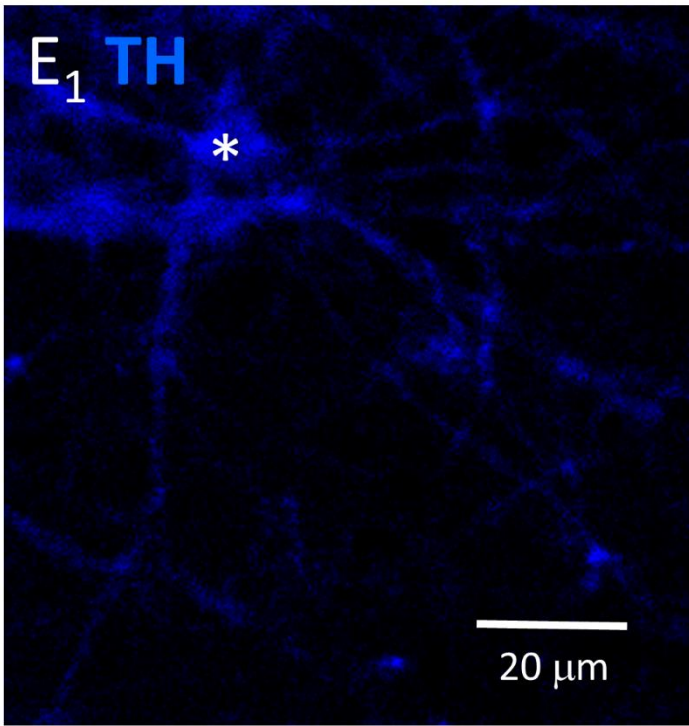
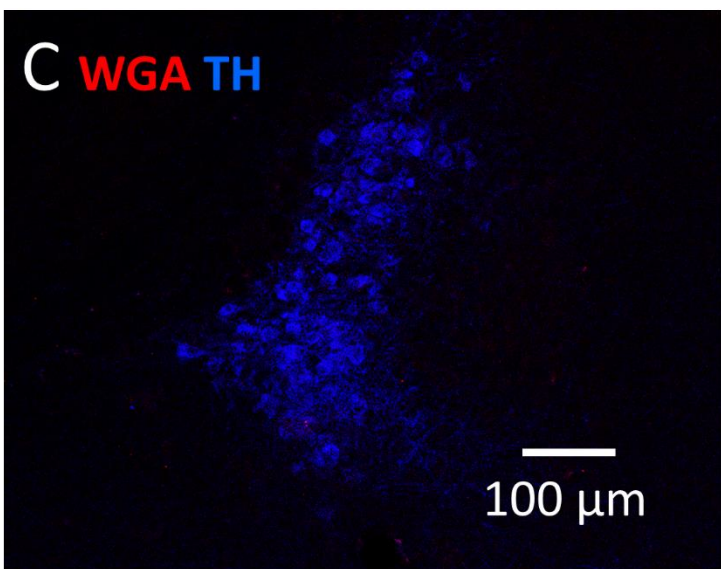
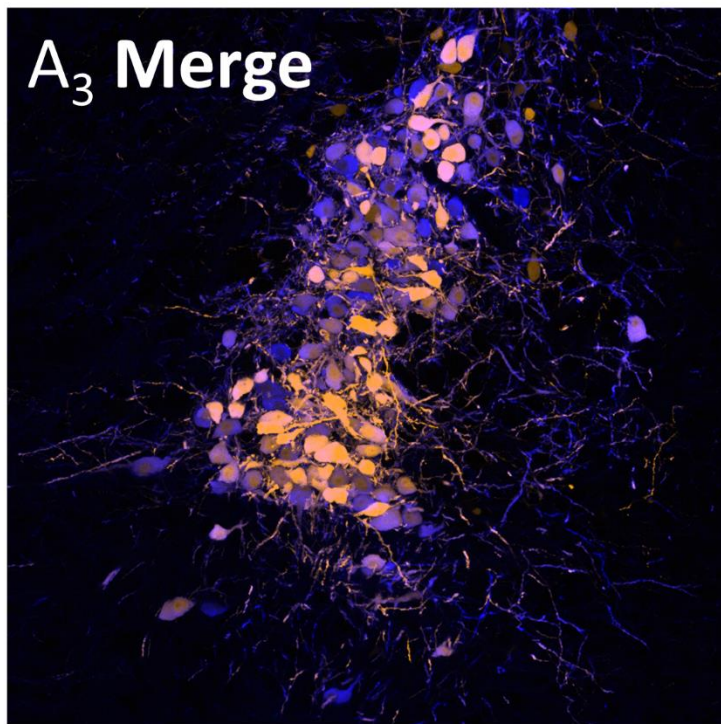
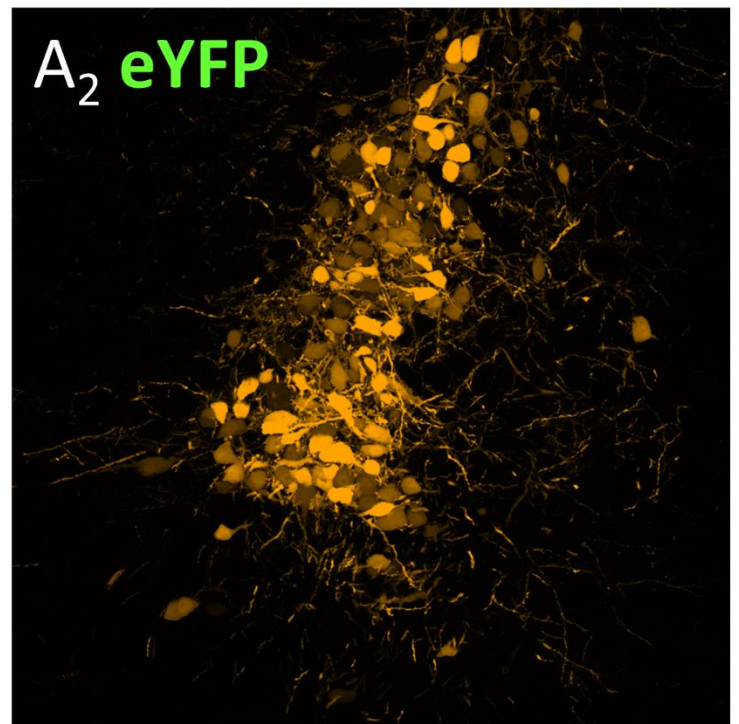
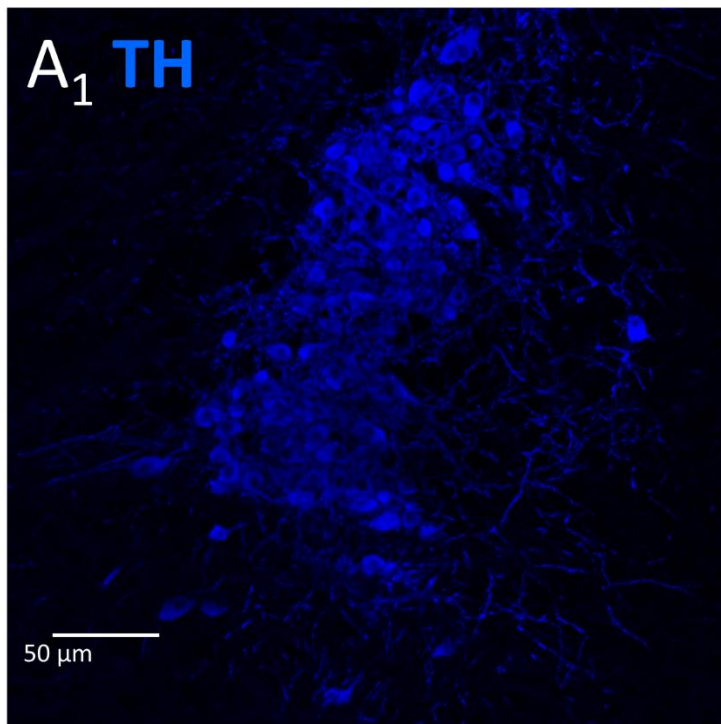


Figure 5

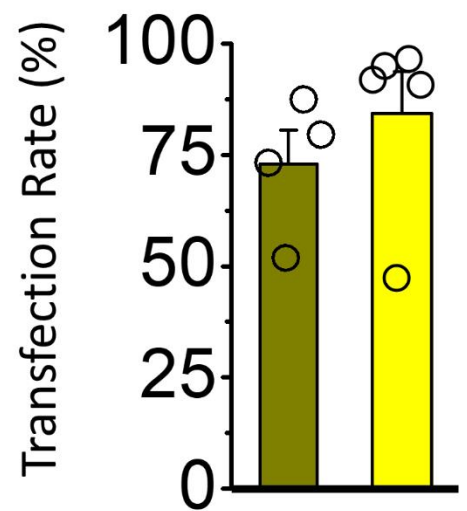
## Figure 5. Localization of I-INs making functional connections with LC-NA neurons by viral-genetic WGA tracing



*A*, A schematic diagram illustrates the experimental arrangements. TH<sup>cre</sup> :: GADGFP mice with infusion of AAV2-DIO-WGA into the left LC were used. ***B & C***, Representative images show IHC results of 3 sections cut through the rostral (B1, C1), middle (B2, C2) and caudal LC (B3, C3) at low magnification. B shows merged image of TH and GFP and C shows WGA. The red and white circles in B and the arrows (yellow) and arrowheads (white) in C mark some examples of the same TH-/WGA+ neurons in the medial part of the peri-LC. The neurons marked by the white circles and yellow arrows were also GFP<sup>+</sup> neurons. *D*, An image presents the dashed-square in C2 in a higher magnification. *E*, A representative example shows a TH<sup>-</sup>/WGA<sup>+</sup>/GFP<sup>+</sup> neuron at high magnification. The asterisk marks a LC-NA neuron (TH<sup>+</sup>/WGA<sup>+</sup>/GFP<sup>-</sup>); the arrow indicates a LC I-IN (TH<sup>-</sup>/WGA<sup>+</sup>/GFP<sup>+</sup>). The field is the enlargement of the dashed-square shown in B3. The experiments were performed with Mr. Jung-Chien Hsieh and Ms. Yu-Shan Kuo, and some of the presented data also formed a part of Mr. Jung-Chien Hsieh's Master thesis (National Taiwan University).



**B**

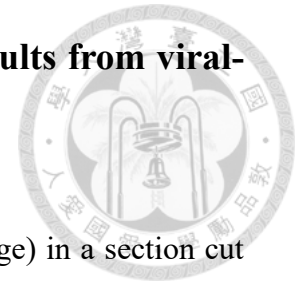


■ (TH<sup>+</sup>+WGA<sup>+</sup>)/TH<sup>+</sup>

■ (TH<sup>+</sup>+eYFP<sup>+</sup>)/TH<sup>+</sup>

Figure 6

## Figure 6. Control experiments for confirmation of results from viral-genetic WGA tracing



**A**, Representative images show IHC of TH (blue) and eYFP (orange) in a section cut through the middle LC of a TH<sup>Cre</sup> × GADGFP mouse that received AAV2-DIO-eYFP infusions into the LC. A1, A2 and A3 show the TH-ir, eYFP-ir and merge images. **B**, A plot of summarized results from 4 cases of WGA tracing and 5 cases of genetic leakage estimation by the eYFP expression. Each circle in the plots shows results from an animal, and the bar (mean) + capped vertical lines (SEM) represent the summarized results. **C**, Representative images show IHC of TH and WGA in section cut through the middle LC of a WT mouse that received an AAV2-DIO-WGA infusion into the LC. Note that none of WGA<sup>+</sup> cell was found in this series of control experiments. The experiments were performed with Mr. Jung-Chien Hsieh, and some of the presented data also formed a part of Mr. Jung-Chien Hsieh's Master thesis (National Taiwan University).

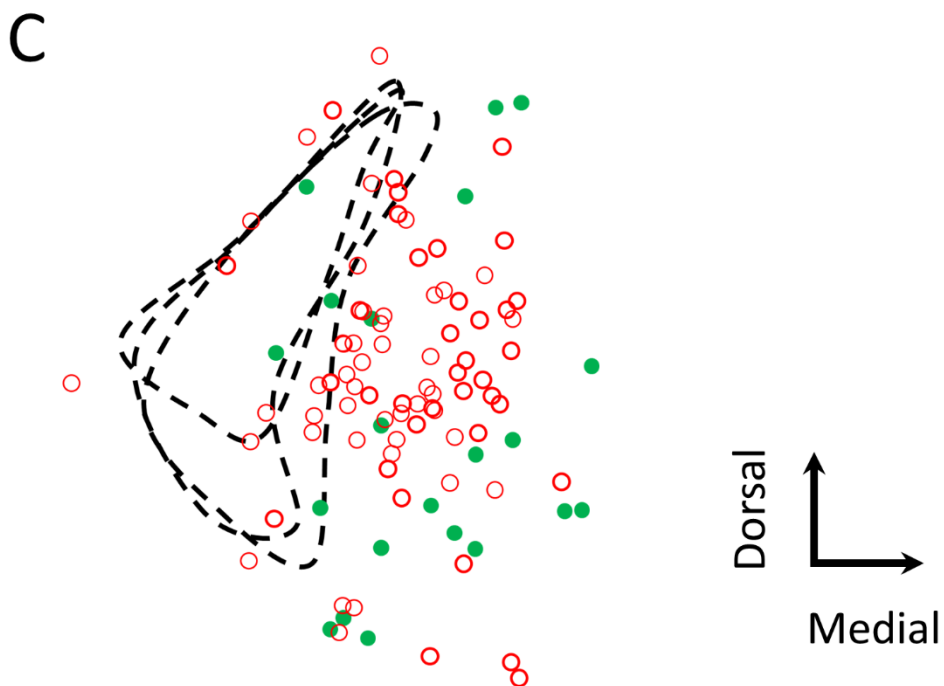
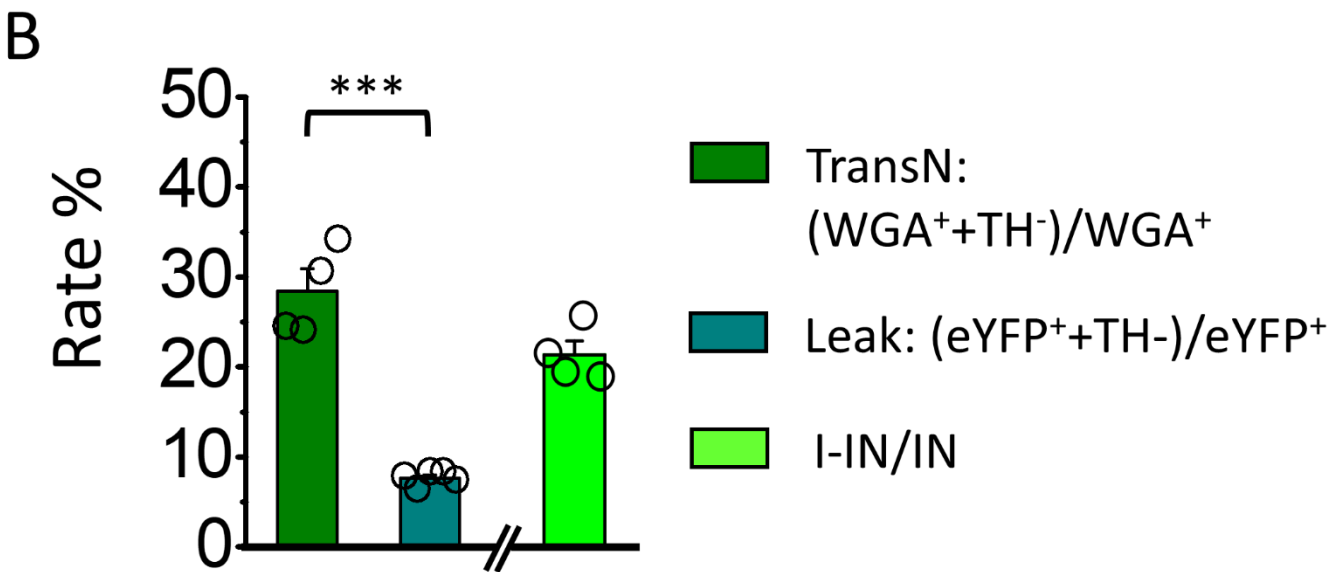
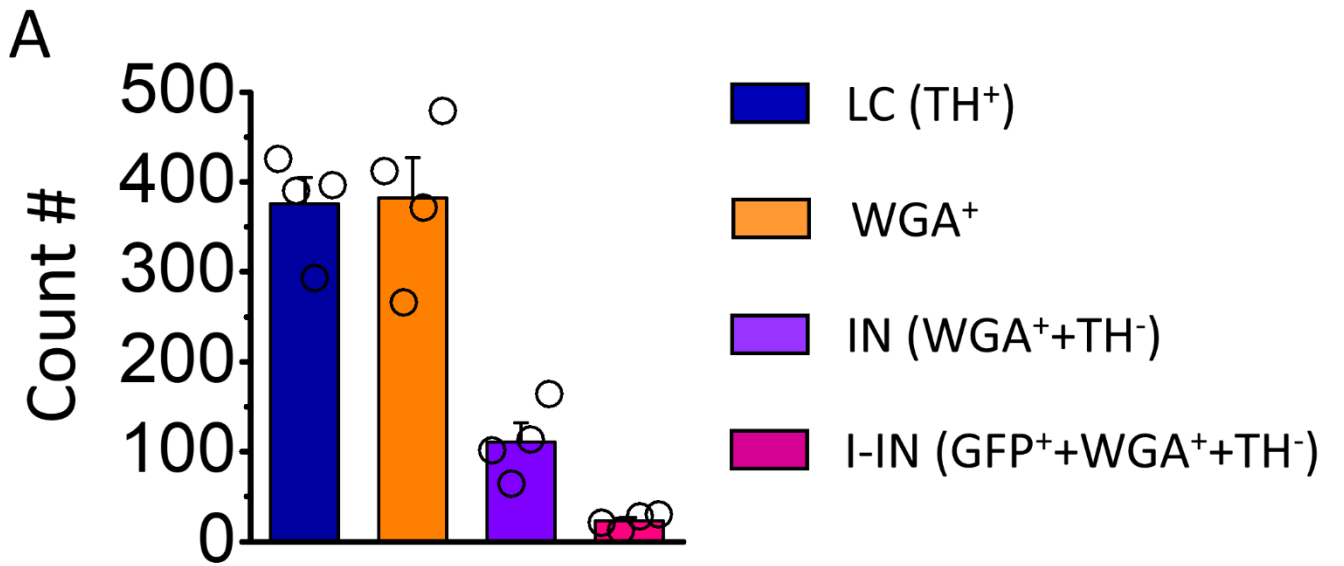
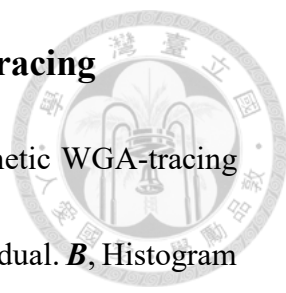


Figure 7

## Figure 7. Quantitative analysis of viral-genetic WGA-tracing



**A**, Histogram plots summarize results of cell counting in viral-genetic WGA-tracing experiments from 4 mice with different IHC profiles in each of individual. **B**, Histogram plots summarize proportions of cell types in viral-genetic WGA-tracing experiments from 4 mice with different IHC profiles in an animal. In A and B, each circle in the plots presents the total number (A) and percentage (B) of neurons in an animal. Note that the proportion of cells receiving WGA molecules transneuronally is significantly higher than those counted in the genetic leakage control experiments. The bar (mean) + capped vertical lines (SEM) show the averaged results. Cell counting was performed for the three (rostral, middle, and caudal) sections containing LC-proper indicated in Fig. 5B.

**C**, Camera lucida drawing shows the locations of all TH<sup>-</sup>/WGA<sup>+</sup> neurons (red circles) and TH<sup>-</sup>/WGA<sup>+</sup>/GFP<sup>+</sup> neurons (filled-green circles) in one mouse. Data in C are obtained from the 3 sections shown in Fig. 5B & C. The experiments were performed with Mr. Jung-Chien Hsieh and Ms. Yu-Shan Kuo, and some of the presented data also formed a part of Mr. Jung-Chien Hsieh's Master thesis (National Taiwan University).

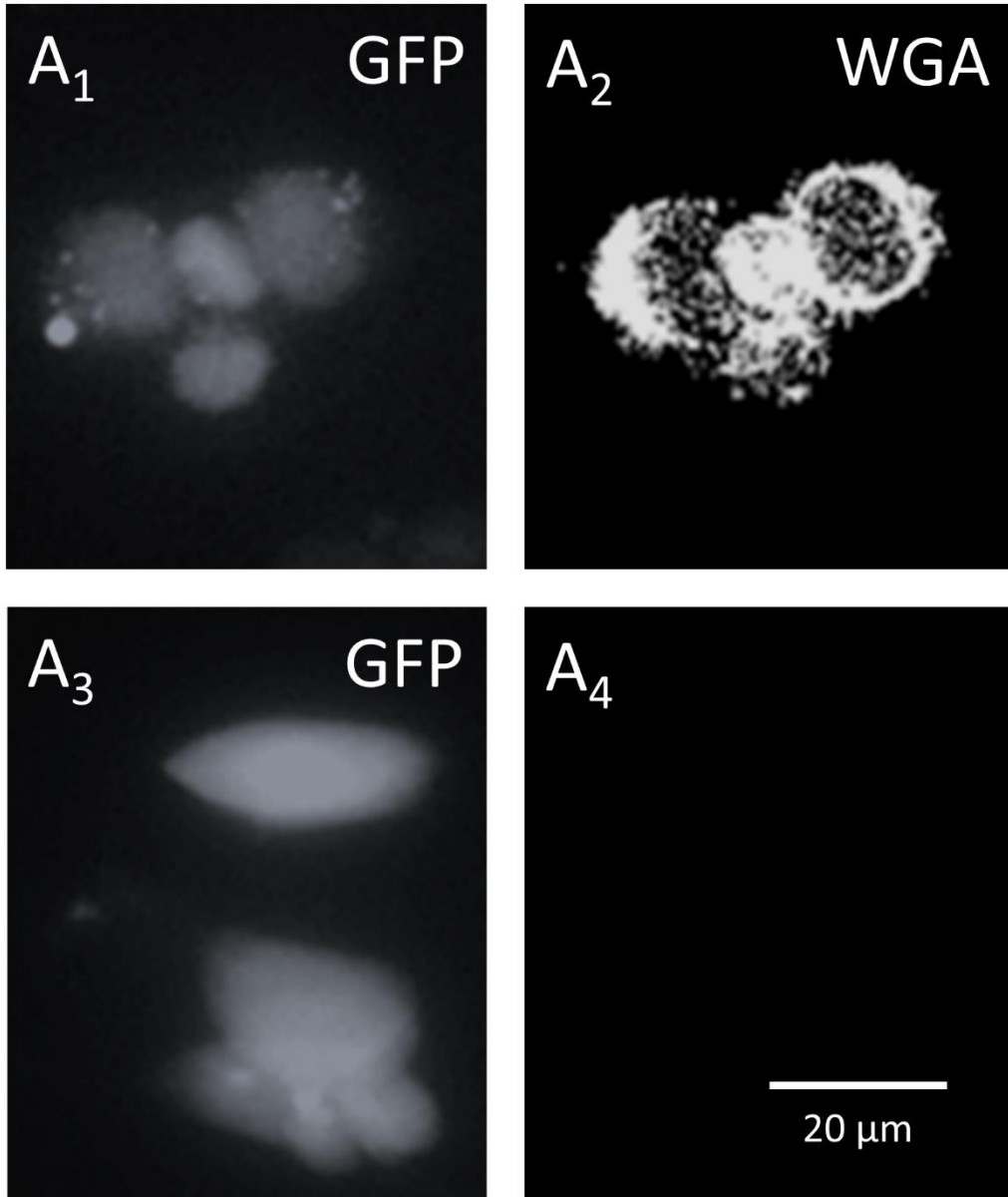
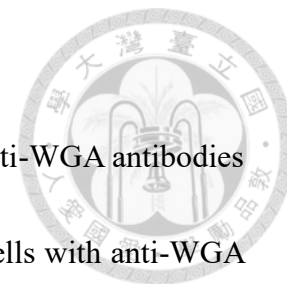


Figure 8

## Figure 8. Validation of WGA plasmid



A, Tests of the efficiency of the WGA plasmid and specificity of anti-WGA antibodies in the HEK-293 cell-line. A1 and A2 show staining of HEK-293 cells with anti-WGA antibodies (blue). Cells were transfected with AAV2-CMV-Cre-GFP (green) and a DIO-WGA plasmid using lipotransfection. Note cells that expressed Cre and GFP (A1) showed aggregation of granule-like WGA-ir structures in the cytoplasm (A2). A3 and A4 show control experiment results repeated as described in A1 and A2 but anti-WGA antibodies were omitted during IHC processes. As indicated, cells that expressed Cre and GFP did not show immunoreactivity. The experiments were performed with Mr. Jung-Chien Hsieh, and the presented data also formed a part of Mr. Jung-Chien Hsieh's Master thesis (National Taiwan University).

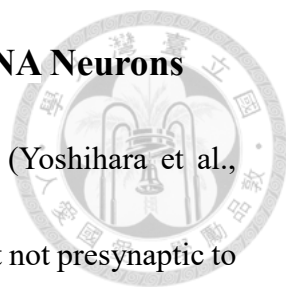
## Section 2



# Role of peri-LC I-IN in Regulation of sPLA

The data from the sPLA recording show the presence of the local circuit. In this section I focus the investigation upon the peri-LC I-INs in brain slices. In vitro experiments combining multiple techniques for manipulating the neural activity reveal that the peri-LC I-INs exert a potent role in regulation of LC phasic activations.

## 2.1 Synaptic Transmission from peri-LC I-INs to LC-NA Neurons

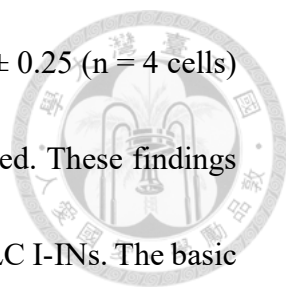


The WGA transportation is both retrograde and anterograde (Yoshihara et al., 1999); therefore, the labeled peri-LC I-INs could be postsynaptic but not presynaptic to LC-NA neurons. To verify the issue, I examined as to whether the selective activation of peri-LC I-INs using an optogenetic method could evoke inhibitory postsynaptic currents (IPSC) in LC-NA neurons. Brain slices comprising the LC were prepared from *Vgat<sup>Cre</sup>* mice infused with the AAV2-DIO-ChR2-eYFP into the right LC. I first confirmed that the ChR2-eYFP expression was restricted in the LC and peri-LC, corresponding to Bregma -4.7 to -5.9 of the Allen Brain Atlas, by examining sections that cut through whole brain; the boundary was within the brainstem block used for the slice preparation (Fig. 9A). *Post hoc* IHC staining of TH and eYFP was performed to validate the ChR2-eYFP expression pattern in the slices used in electrophysiology experiments (Fig. 9C), and the expression of eYFP also let me to record the peri-LC I-INs selectively (Fig. 9B). I also examined the possibility of the Cre-independent expression of Chr2-eYFP as the genetic leakage. The AAV2-DIO-Chr2-eYFP was bilaterally infused into the LC of two WT mice. In three of the four hemispheres, cells expressing ChR2-eYFP were not identified in sections that cut through the LC and peri-LC (Fig. 9D), and only one cell expressing ChR2-eYFP was observed in the LC area of

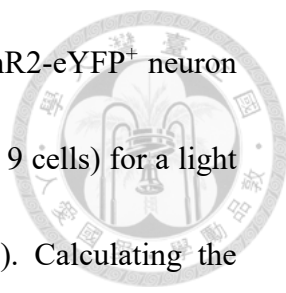
the remaining hemisphere. These results showed the rare Cre-independent leaky Chr2-eYFP expression in non-Cre cells.



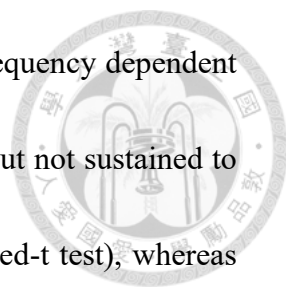
I began the electrophysiological recording by obtaining the I-clamp recording from neurons expressing Chr2-eYFP (Fig. 10A), which represent presumed I-INs, in the medial part of the peri-LC in *Vgat<sup>Cre</sup>* mice receiving the AAV2-DIO-ChR2-eYFP infusion in the right LC. The recorded I-INs expressed functional ChR2 because they could fire an AP in response to the photostimulation with a blue light pulse (470 nm, intensity: 10 mW/mm<sup>2</sup>, pulse duration: 2 ms) (Fig. 10B). In the V-clamp recording from LC-NA neurons in the presence of a high intracellular Cl<sup>-</sup> (Cl<sup>-</sup> reversal potential ~ 0mV), I found that the photostimulation could evoke inward currents which were supposed to be the IPSCs from contacts formed by these I-INs. The currents were partially reduced by the Stry or BM application and were subsequently suppressed when the two drugs were applied simultaneously (Fig. 10B). These results showed that the current was IPSC mediated by both GABA<sub>A</sub>Rs and GlyRs showing no significant difference in the detailed properties of the synaptic transmission, including the amplitude, charge transfer, rising time, and delay time constant (Fig. 11, Table 5). The paired pulse of the light illumination was 0.44± 0.08 (n = 17 cells) in normal aCSF; 0.57± 0.16 (n = 7 cells)



in presence of Stry, supposed as GABA<sub>A</sub>R's contribution; and  $0.39 \pm 0.25$  ( $n = 4$  cells) in the trace supposed to be conducted by GlyRs when BM was added. These findings also raise an issue of co-releasing of GABA and glycine in the peri-LC I-INS. The basic properties of synaptic transmissions are also characterized, and the detailed results are shown in Table 5. Moreover, I found that the IPSC induction was dependent on the territory and efficiency of AAV2 transfection. Forty-two experiments were performed to test the responses of LC-NA neurons to photostimulation. In 34 experiments, the photostimulation could evoke IPSC in the V-clamp recording or inhibit spontaneous APs in the I-clamp recording. For the remaining eight experiments, LC-NA neuron responses were not observed in the V-clamp recording or the I-clamp recording. I superimposed the camera lucida drawing of the *post hoc* IHC profiles for the 34 and 8 experiments (2 sections, usually a rostral slice and a caudal slice from one mouse for each experiment) and for comparing the two cases. The results indicated that photostimulation triggered LC-NA neuron responses only if the AAV2 transfection covered the LC-proper and peri-LC; photostimulation did not evoke a response if the AAV2 transfection failed to cover these regions (Fig. 12).

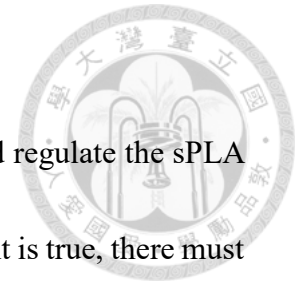


The latency from a light pulse onset to the AP peak of the ChR2-eYFP<sup>+</sup> neuron was  $2.08 \pm 0.22$  ms ( $n = 10$  cells) compared with  $3.09 \pm 0.16$  ms ( $n = 9$  cells) for a light pulse onset to the IPSC onset in LC-NA neurons (Fig. 10B, C). Calculating the difference yielded a synaptic delay of 1.01 ms, demonstrating that the transmission was monosynaptic. This conclusion was further supported by the experiments that showed IPSCs could be evoked when 1  $\mu$ M tetrodotoxin (TTX), a voltage-gated Na<sup>+</sup> channel blocker, and 200  $\mu$ M 4-AP, a voltage-gated K<sup>+</sup> channel blocker, were added into the aCSF to inhibit AP conduction and enhance membrane depolarization at the local axonal terminal, respectively (Fig. 10D). In the presence of TTX plus 4AP, cation channels for the terminal depolarization and calcium influx were mainly ChR2 itself, and the longer latency of IPSCs reflected the slower kinetics of ChR2 channels. Consistent with the previously described V-clamp recording, the delivery of a train of the light pulse at 10 Hz for 12 s significantly reduced the spontaneous APs in LC-NA neurons in the I-clamp recording, and the effect was blocked by the application of BM plus Stry (Fig. 13). Photostimulation repressed the spontaneous APs to  $52.5 \pm 4.8\%$  of baseline before the BM+Stry application ( $n = 10$  cells;  $p < 0.05$ , paired *t*-test); there was no effect of photostimulation on spontaneous APs after the BM+Stry application ( $102.4 \pm 4.2\%$  of the baseline; ns, paired *t*-test). 12-s of illuminations in different

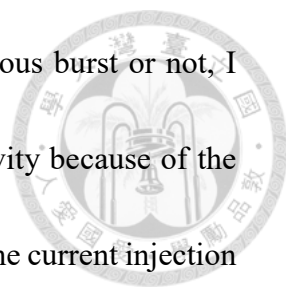


frequencies of light pulses showed the repression capability in a frequency dependent manner, a train of illumination at 5Hz caused a smaller inhibition but not sustained to the end of the illumination ( $60.6 \pm 7.2\%$ ,  $n = 10$  cells;  $p > 0.05$ , paired-t test), whereas the trains at 2Hz led to a light and undetectable change in the firing rate ( $77.0 \pm 6.2\%$ ,  $n = 10$  cells;  $p > 0.05$ , paired-t test), the most efficient repression was the train of pulses at 10Hz because trains at 20Hz ( $n = 10$  cells;  $p < 0.01$ , paired-t test) yielded a smaller repression than that in 10Hz (Fig. 14A, B). This finding may be due to the depletion of the synaptic vesicle or poor kinetics of the ChR2 protein conformational changes under a high frequency stimulation. The data obtained in the V-clamp configuration also showed a frequency dependent inhibition of the spontaneous firing as that observed under I-Clamp (Figs. 14C, D). Taken together, the optogenetic experiment results were consistent with those of the viral-genetic WGA tracing and provided functional evidence for monosynaptic connections from peri-LC I-INs onto LC-NA neurons with the transmission mediated by GABA<sub>A</sub>Rs and GlyRs.

## 2.2 Characterization basic properties of peri-LC I-INs

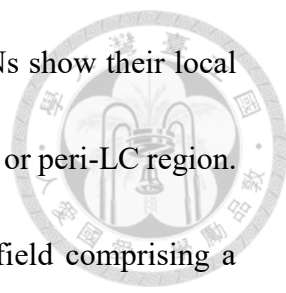


I and my colleagues hypothesized that the peri-LC I-INs could regulate the sPLA by their functional contacts on the principle neurons. If our argument is true, there must be a population of peri-LC I-INs exhibiting spontaneous firings in brain slices. Therefore, I selectively record the peri-LC I-INs under the guidance of fluorescent signals by using GADGFP mice or *vgat<sup>cre</sup>* mice with infusions of AAV2-DIO-ChR2-eYFP into the LC. (Fig. 15A). According to the response of positive current injections, cells are divided into two main populations, the regular (53%, 26/49 cells) and delay groups (45%, 22/49 cells), and only one case with irregular firing in response to the current injection (2% 1/49 cells) (Fig. 15B, C). Moreover, I also found the spontaneous burst activity under the cell-attachment recording, and these burst firings were likely correlated to the modulation on the sPLA. And these burst activities may cause by the local projection from E-INs onto I-INs. In this regard, the recorded peri-LC I-INs were further divided into groups by not only the response to current injections but also the expressing of spontaneous activities and bursts. It was about 82% (33/40) of recorded cells exhibited spontaneous activity under the cell attachment configuration (20/25 cells); 44% of recorded cells exhibited spontaneous bursts in the background AP firings (11/25 cells) and 36% of recorded cells expressed regular, continuous AP firings (9/25



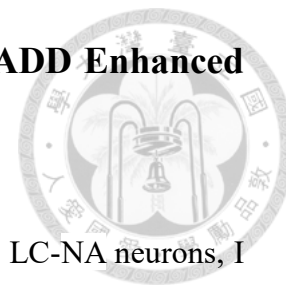
cells) (Fig. 15D, E). For the recorded cells expressing of spontaneous burst or not, I cannot rule out that the tonic population of I-INs lacked burst activity because of the cut of neurophil or microcircuit. So the firing pattern in response to the current injection should be used as a more reliable way for the classification of peri-LC I-INs. Besides, I also noticed that the corpious burst activity of I-INs was not followed by a quieter period as phasic activations in LC-NA neurons, this may due to the different cell membrane properties among principle neurons and INs. The findings also raise an interesting issue as to whether the burst and post-burst activity contribute to the silent period of phasic activations in LC-NA neurons.

Post hoc validation of the recorded slices revealed locations of the recorded I-INs by IHC of the biocytin introduced by glass pipette. All of recorded I-INs were located in the LC proper or peri-LC region indicated by the WGA tracing experiments (Fig. 7C; 16A). After the acquisition of fluorescent images, the slices were re-stained by the DAB immune-precipitation targeting the biocytin. The neurophil arborization of recorded cells was enhanced by DAB stain and reconstructed by camera lucida drawings (Fig. 16B). Many of peri-LC I-INs send an axon with simple structure and formed bouton-like, swollen structures, which were supposed to be varicosities from these I-INs (Fig.



16C). The superimposed images of the reconstructed peri-LC I-INs show their local projection profiles, and most of axons were located in the LC proper or peri-LC region. Interestingly, many of the reconstructed axon cover a restricted field comprising a small part of the LC region, this feature supports a speculation that LC-NA neurons with different locations do not share the same population of peri-LC I-INs (Fig. 16D). Besides, few of reconstructed axons formed branches to the near areas like the parabrachial nucleus or the pontine central grey. The inter-nucleus projection suggests that some of peri-LC I-INs exert a multiple role in regulation of more than one nucleus. As the close and compact arrangement of brainstem nuclei, my data demonstrate that there may be a misunderstanding of the territory of IN pools for each nucleus. Collectively, my results show the spontaneous tonic and burst activity of peri-LC I-INs and the local projection of their axons. And thus provide a theoretical base for the modulation of sPLAs by peri-LC I-INs.

### 2.3 Suppression of peri-LC I-INs with hM4DiR DREADD Enhanced sPLA in LC-NA Neurons



As the blockade of GABA<sub>A</sub>Rs and GlyRs increased sPLAs in LC-NA neurons, I examined whether peri-LC I-INs were involved in the regulation of sPLA using a chemogenetic DREADD method. With regard to the low possibility of the spontaneous AP firing at those axonal terminals from far afferents remaining in the brain slice, peri-LC I-INs were suggested to provide the GABAergic and glycinergic transmission. Brain slices comprising the LC were prepared from Vgat<sup>Cre</sup> mice receiving the AAV2-DIO-hM4DiR-mCherry infusion into the right LC (Figs. 17A, C). Again, the possibility of high levels of Cre-independent expression of hM4DiR-mCherry in non-Cre cells was excluded as the bilateral AAV2-DIO-hM4DiR-mCherry infusion into the LC of two WT mice resulted in an average of 1.75 (range: 0 – 4) cells that expressed hM4DiR-mCherry in the LC and peri-LC per hemisphere (Fig. 17B). I obtained the I-clamp recording from the neurons expressing hM4DiR-mCherry, which represented the presumed peri-LC I-INs, and found that recorded peri-LC I-INs exhibited spontaneous APs (n = 3 cells from three slices and three mice). The application of clozapine-N-oxide (CNO), a synthetic agonist for hM4DiR, inhibited the activity in a dose-dependent manner with 20  $\mu$ M CNO producing an average of 86.5% (range: 61.7% – 99.4%)

reduction in the spontaneous AP frequency. These results confirmed the functional expression of hM4DiRs in peri-LC I-INs (Fig. 18A-C).

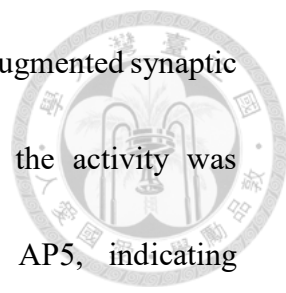


As expected, I then recorded LC-NA neurons and found the application of the 20 $\mu$ M CNO yielded approximately the same effects on the sPLA as the BM plus Stry (Figs. 4A; 18D; Table 4). Specifically, the CNO application significantly increased the incidence of the sPLA (Figs. 18D, E; 19A), but had no effect on the AP number and the mean frequency in a sPLA (Fig. 19B, C; Table 4). In contrast to the pharmacological studies (Fig. 4), the CNO application did not significantly affect the background tonic rate (Fig. 18D; 19D; Table 4). The discrepancy could be due to the more specific inhibition of peri-LC I-INs by the hM4DiR DREADD compared with the pharmacological method. Again, I routinely used the *post hoc* IHC for validation of the hM4DiR-mCherry expression pattern, which was very similar to the optogenetic pattern (*cf.* Fig. 12 and Fig. 17C). The effect of the CNO application on sPLA was not observed when the control AAV2-DIO-mCherry was used instead of the DREADD AAVs (Table 4). To echo our previous finding of the GABA<sub>B</sub> receptor mediated tonic inhibition on rat LC-NA neurons (Wang et al., 2015), I also performed the same I-clamp experiment using 20  $\mu$ M CGP54626, a potent antagonist of the GABA<sub>B</sub>

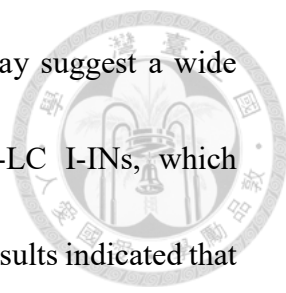
receptor, replacing BM plus Stry or CNO applications. The results showed an increase of the background activity as the only significant change I found, indicated the reduced influence of GABA<sub>B</sub> receptors in the regulation of sPLAs (Fig. 20). The statistical information is shown in Table 4. Collectively, these observations show that peri-LC I-INs were involved in the sPLA regulation but not the background tonic rate of LC-NA neurons.

## **2.4 Electrical Stimulation Recruits peri-LC I-INs to Exert a Feedforward Inhibition**

To gain further insight into how peri-LC I-INs regulated the sPLA, I tested the effects of inhibiting peri-LC I-INs by the hM4DiR DREADD on the excitatory transmissions onto LC-NA neurons. Considering with the spontaneous bursts of peri-LC I-INs, I hypothesized that these I-INs provided a feedforward inhibition to counteract the large EPSPs in a precisely temperospatial manner. The experimental design was the same as that previously described in Fig. 18 with the exception that a bipolar stimulating electrode was positioned in the medial part of the peri-LC for electrical stimulations. LC-NA neurons were subject to V-clamp recordings (holding V<sub>m</sub>: -50 mV), and the patch pipettes were filled with low Cl<sup>-</sup> internal solution to obtain

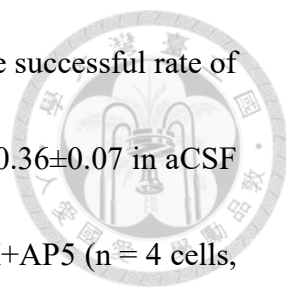


a Cl<sup>-</sup> reversal potential of ~65 mV (Fig. 21A). The CNO application augmented synaptic currents in LC-NA neurons evoked via electrical stimulations; the activity was dramatically blocked by further application of DNQX plus AP5, indicating glutamatergic EPSCs (Fig. 21B). Subtracting the activity recorded in CNO from that in aCSF indicated an outward CNO sensitive current ( $I_{\text{CNO}}$ ) (Fig. 21B). The latency of the electrical pulse onset to the  $I_{\text{CNO}}$  onset was significantly longer (1.654-fold) compared with the EPSC onset (EPSC latency:  $2.43 \pm 0.26$  ms,  $I_{\text{CNO}}$  latency:  $4.02 \pm 0.26$  ms,  $n = 6$  cells;  $p < 0.001$ , *paired-t test*) (Fig. 21C), which suggested that the EPSC was monosynaptic and the  $I_{\text{CNO}}$  was bisynaptic. I repeated the same experiments with the substitution of BM plus Stry application for CNO application using slices prepared from  $V\text{gat}^{\text{Cre}}$  mice receiving no AAV2 injection (Fig. 21D). Subtracting the activity recorded for BM plus Stry application from that in aCSF indicated an outward IPSC that exhibited a significantly longer latency (1.646-fold) as compared with the EPSC (EPSC latency:  $1.98 \pm 0.20$  ms, IPSC latency:  $3.26 \pm 0.39$  ms,  $n = 8$  cells;  $p < 0.0005$ , *paired-t test*) (Fig. 21E), a result that was highly compatible with the DREADD experimental results. In addition, the IPSC and  $I_{\text{CNO}}$  exhibited a similar dynamic (Fig. 21F); there was no difference in the 20-80% rise time (RT) or the half width (HW) between the IPSC (RT:  $2.7 \pm 0.6$  ms; HW:  $8.5 \pm 1.5$  ms) and the  $I_{\text{CNO}}$  (RT:  $1.9 \pm 0.5$  ms;



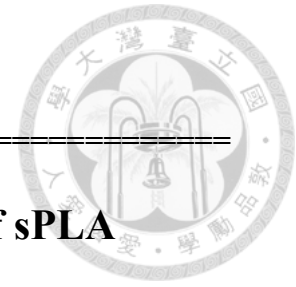
HW:  $8.4 \pm 2.7$  ms) (ns, *Mann-Whitney test*). The high variations may suggest a wide distribution of contact sites on the LC-NA neurons from peri-LC I-INs, which diversified the dynamics of the IPSC and  $I_{CNO}$ . Conceptually, these results indicated that the  $I_{CNO}$  was the IPSC of peri-LC I-INs onto LC-NA neurons and showed that the focal electrical stimulation to the LC activated excitatory inputs that not only directly excited LC-NA neurons, but also peri-LC I-INs to exert a feedforward inhibition onto LC-NA neurons.

To test whether the feedforward inhibition was involved in the regulation of the phasic activity of LC-NA neurons, I obtained an I-clamp recording and stimulated an LC-NA neuron with a train that consisted of 10 electrical pulses at 50 Hz. The intensity of the electrical pulse was adjusted so that the trial-to-trial success in the induction of a phasic activity approximately occurred at a rate of 30-50%. Phasic activity was defined by at least three APs that were evoked with a spiking rate greater than 5 Hz, which was modified from the standard for detecting the sPLA. Interestingly, the evoked phasic was also followed by a lasting inhibition of the background activity (Fig. 22A), which resembled the phasic activation-pause profile of LC-NA neuron activity observed in the animal studies (Bouret and Sara, 2004; Clayton et al., 2004; Bari and Aston-Jones, 2013;



Marzo et al., 2013). The CNO application significantly increased the successful rate of the phasic activity (Figs. 22B-D). The rates of phasic activity were  $0.36 \pm 0.07$  in aCSF (n = 8 cells),  $0.60 \pm 0.11$  in CNO (n = 8 cells) and 0 in CNO+DNQX+AP5 (n = 4 cells, lost recording in 4 cells). A significant difference was noted between the aCSF and the CNO ( $p < 0.001$ , *paired-t test*). Similar results were obtained with the pharmacological tools (Fig. 18E). The incidence of phasic activity was  $0.49 \pm 0.08$  in aCSF (n = 8 cells),  $0.87 \pm 0.05$  in BM+Stry application (n = 8 cells), and 0 in BM+Stry+DNQX+AP5 application (n = 5 cells, lost recording in 3 cells). A significant difference was noted between the aCSF and the BM+Stry application ( $p < 0.005$ , *paired-t test*). Together, these results demonstrate that the feedforward inhibition of LC-NA neurons by peri-LC I-INs could gate the phasic activity.

# Figures



---

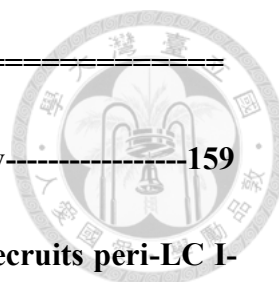
---

## Section 2: Role of peri-LC I-IN in Regulation of sPLA

Figure 9. Design of optogenetics experiment-----	133
Figure 10. Functional connection from peri-LC I-INs onto LC-NA neurons -- -----	135
Figure 11. Characterization of transmission property from peri-LC I-INs onto LC-NA neurons-----	137
Figure 12. ChR2-eYFP expression profiles -----	139
Figure 13. Prolonged inhibition of LC-NA neuron by long lasting stimulation of peri-LC I-INs -----	141
Figure 14. Frequency dependent inhibition from peri-LC I-INs-----	143
Figure 15. Characterization of basic properties of peri-LC I-INs-----	146
Figure 16. Morphology reconstruction of recorded peri-LC I-INs-----	149
Figure 17. Experimental design of hM4DiR DREADD on brain slice -----	152
Figure 18. Inhibition of peri-LC I-INs with hM4DiR DREADD enhanced sPLA in LC-NA neurons-----	154
Figure 19. Summarized results of hM4DiR DREADD experiment-----	157

---

---



---

**Figure 20. Summarized results of CGP54626 pharmacology-----159**

**Figure 21. Electrical stimulation of glutamatergic inputs recruits peri-LC I-  
INs that exert a feedforward inhibition-----161**

**Figure 22. Evoked phasic activations are regulated by peri-LC I-INs-----164**

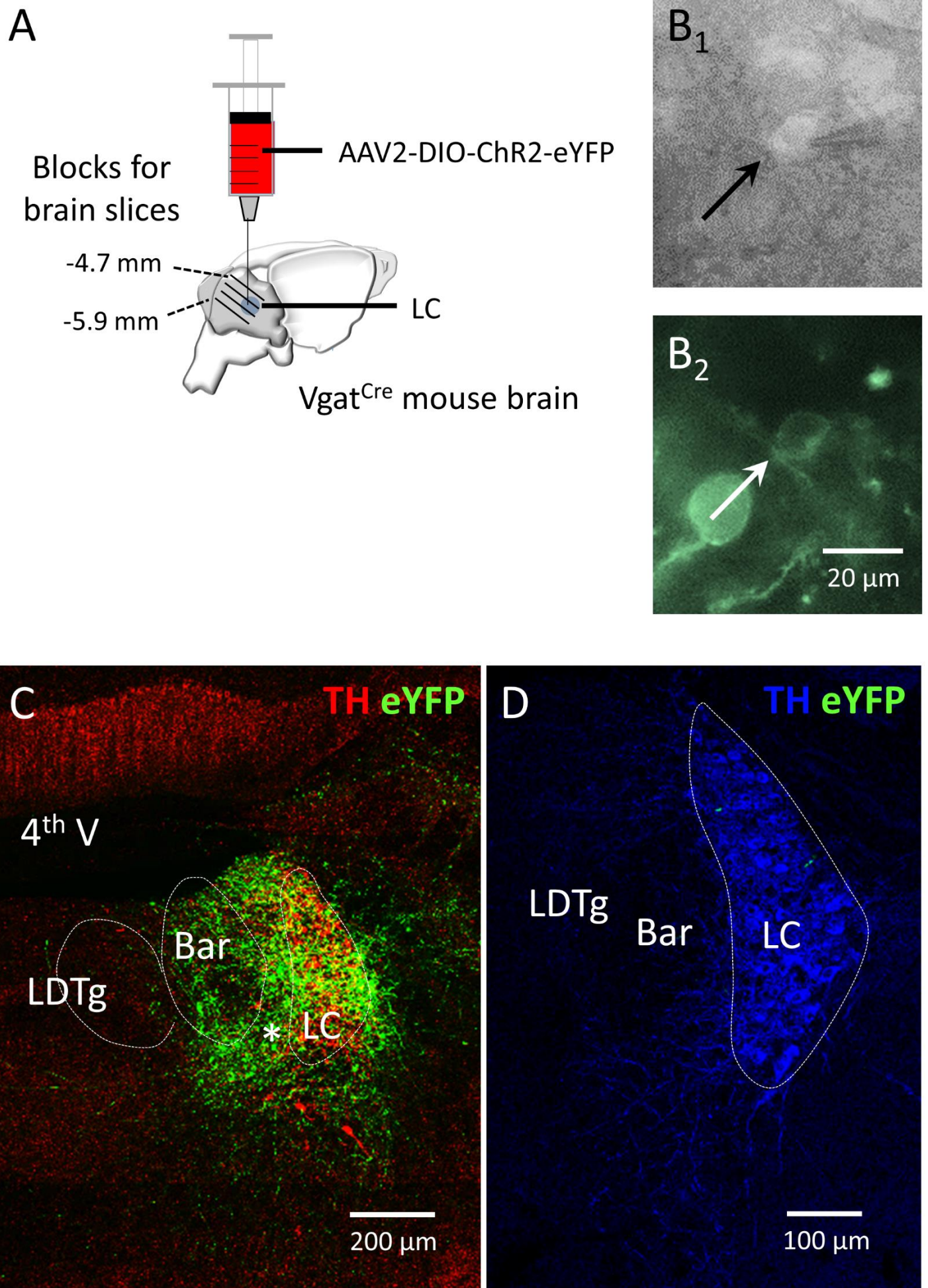
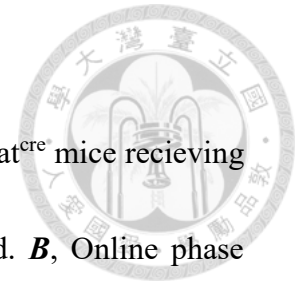


Figure 9

## Figure 9. Design of optogenetics experiment

**A**, Schematic diagram shows the usage of animal and AAV. The *vgat<sup>cre</sup>* mice receiving infusions of AAV2-DIO-ChR2-eYFP into the right LC were used. **B**, Online phase contrast (B1) and fluorescent images (B2) show a recording from a Chr2-eYFP<sup>+</sup> neuron in the medial part of the peri-LC. **C**, A representative fluorescent image shows post hoc IHC that validates ChR2-eYFP expression in the LC-proper and peri-LC region. The asterisk marks the gap between the LC and Bar, where numerous ChR2-eYFP<sup>+</sup> neurons were located. **D**, A representative fluorescent image shows IHC of TH and eYFP in a section cut through the middle LC of a WT mouse that received AAV2-DIO-Chr2-eYFP infusion into the LC. None of ChR2-eYFP expressing cell was observed throughout 4 hemispheres from 2 mice.



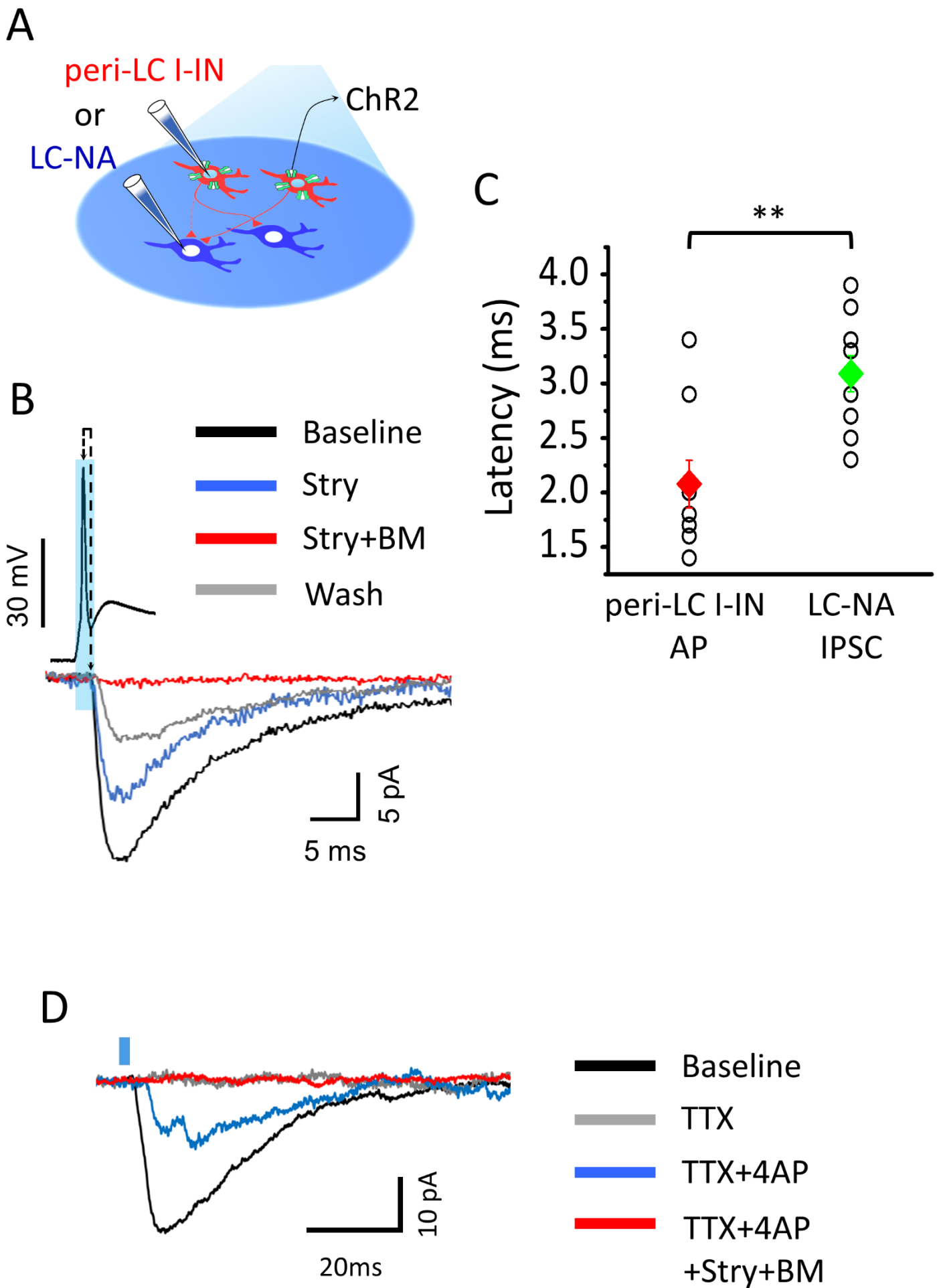
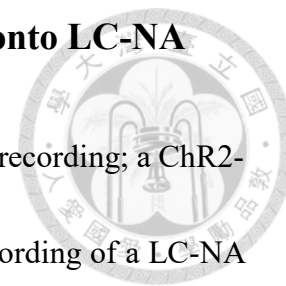


Figure 10

**Figure 10. Functional connection from peri-LC I-INs onto LC-NA neurons**



**A**, Schematic diagram shows the experimental arrangements of the recording; a ChR2-eYFP<sup>+</sup> (presumed peri-LC I-IN) was first recorded followed by recording of a LC-NA neuron. The *vgat<sup>cre</sup>* mice receiving infusions of AAV2-DIO-ChR2-eYFP into the right LC were used. **B**, Photostimulation of the slice, as indicated by the blue rectangle, evoked IPSCs in the LC-NA neuron. The upper trace shows an evoked AP in the peri-LC I-IN and the bottom trace shows IPSCs in a LC-NA neuron. The activities were aligned to the onset of the light pulse. **C**, Plot shows summarized results of the AP latency in peri-LC I-INs and the IPSC latency in LC-NA neurons. Each circle in the plots presents result from a neuron, the diamond (mean) + capped vertical lines (SEM) show the averaged results. **D**, Representative V-clamp recordings show that the IPSCs evoked in an LC-NA neuron by the photostimulation (black trace) were blocked by TTX application (gray trace) and later restored following TTX+4-AP application (blue trace); subsequent application of TTX+4-AP+BM+Sry blocked the IPSCs (red trace). The same results were repeated in 3 additional experiments.

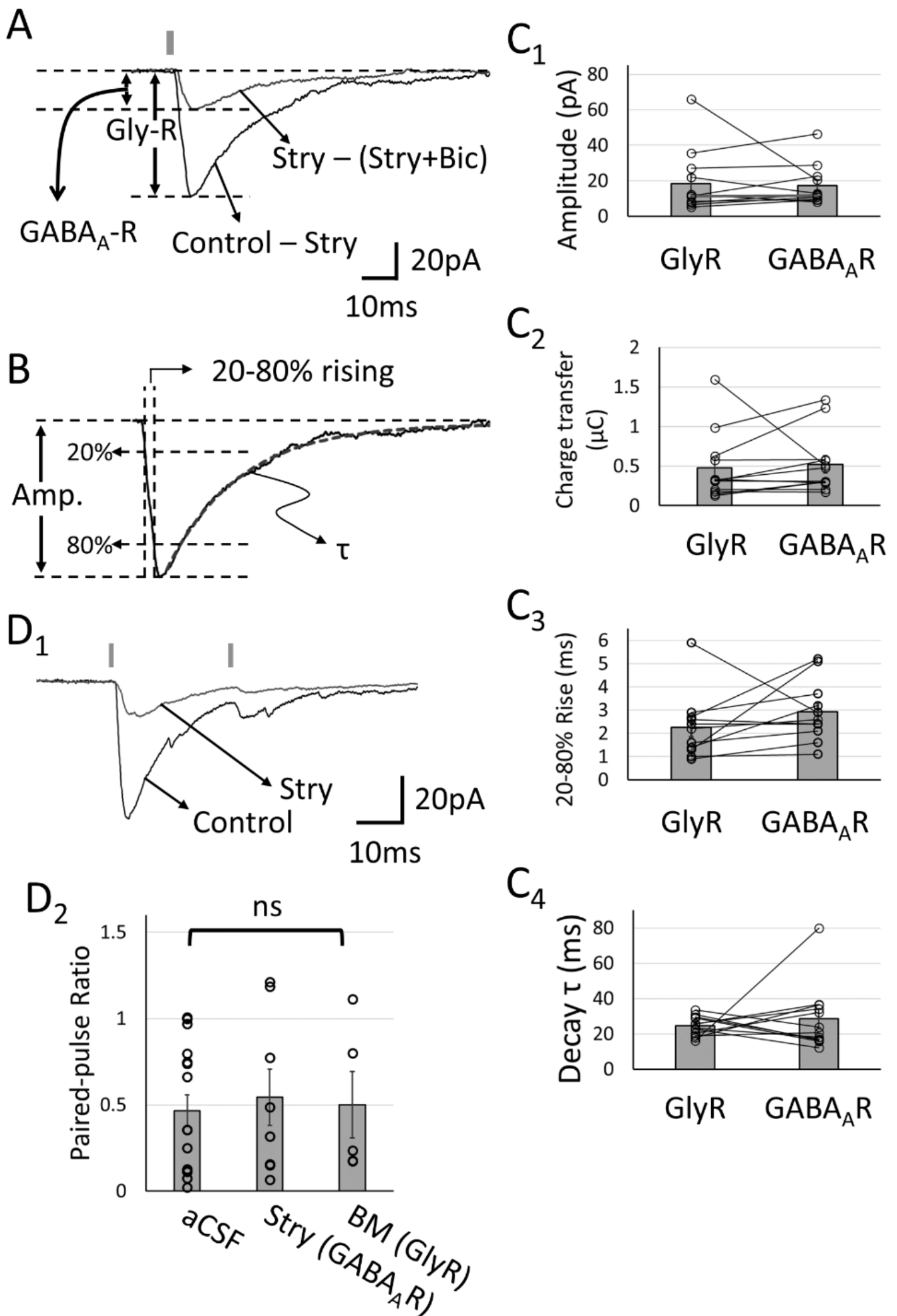
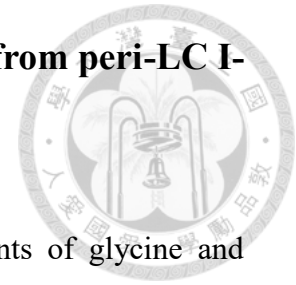


Figure 11

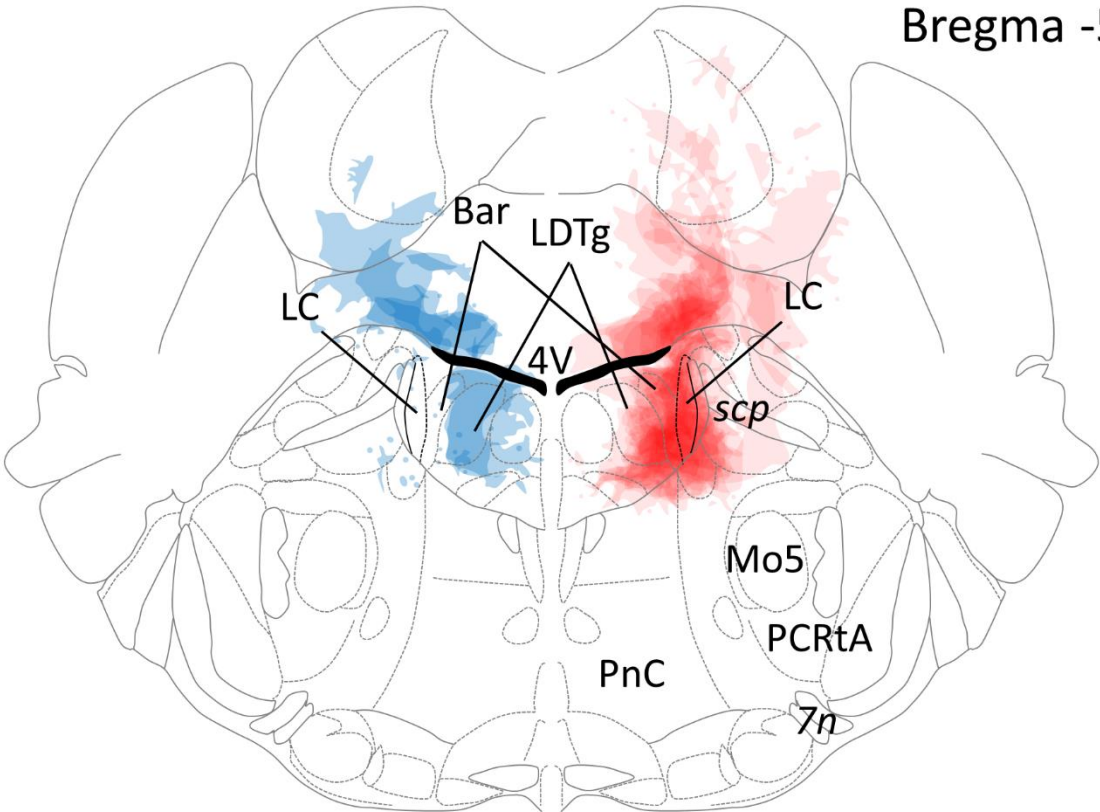
## Figure 11. Characterization of transmission property from peri-LC I-INs onto LC-NA neurons



**A**, An example of V-clamp recordings shows isolated components of glycine and GABA<sub>A</sub> receptors by pharmacology experiment. The trace is obtained from results in Fig. 10B. **B**, Normalized traces display IPSCs mediated by glycine and GABA<sub>A</sub> receptors from the same recording. Calculations of 20-80% rising time and decay time constant are also marked. **C**, Plots summarize transmission properties of synapses from peri-LC I-INs onto LC-NA neurons. **D**, A representative recording (D1) and statistics plot (D2) show a paired pulse depression among IPSC components. In C & D, each circle in the plots presents data gathered from a neuron, the bar (mean) + capped vertical lines (SEM) show the averaged results. Table 5 provided detailed statistical information.

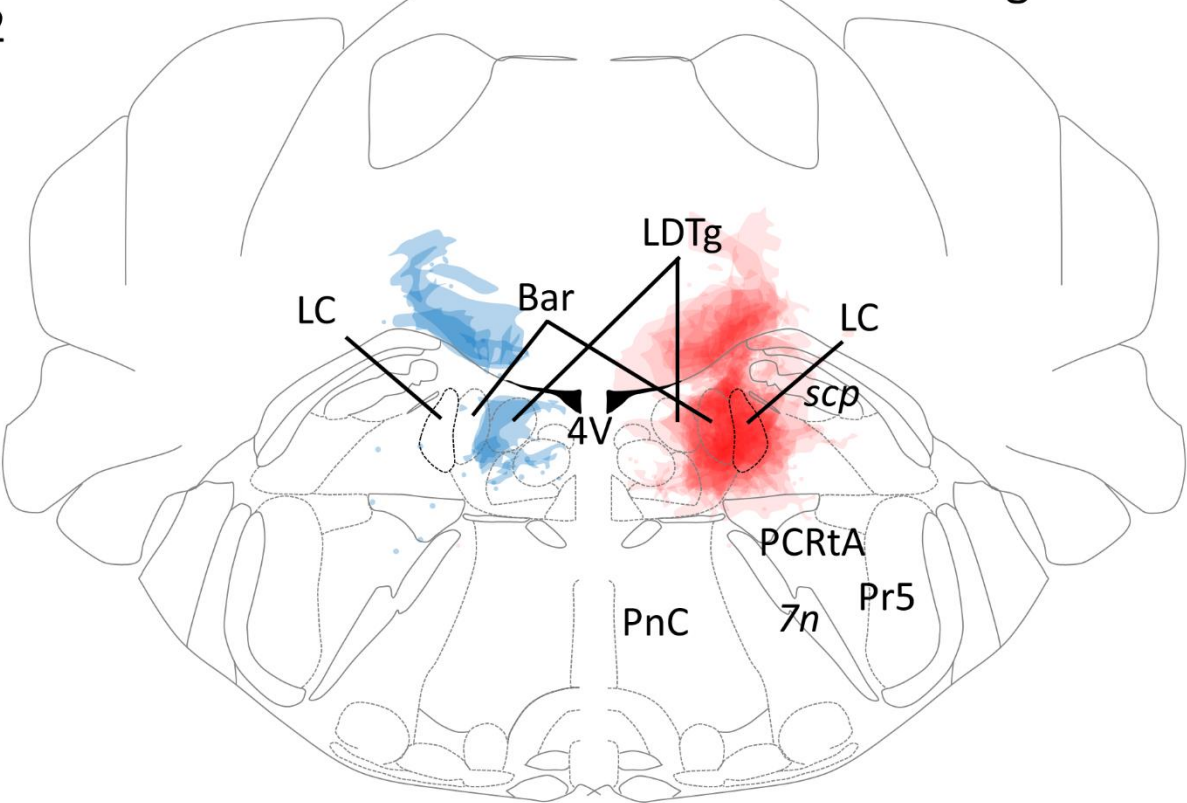
A<sub>1</sub>

Bregma -5.3 mm



A<sub>2</sub>

Bregma -5.6 mm

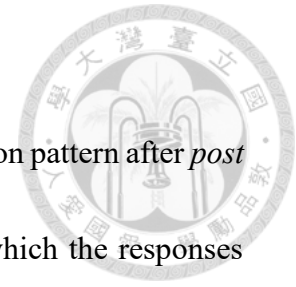


1 mm



Figure 12

## Figure 12. Chr2-eYFP expression profiles



A, Superimposed camera lucida drawing of the Chr2-eYFP expression pattern after *post hoc* validation. The data were collected from 34 experiments in which the responses were evoked in LC-NA neurons (right) and 8 experiments in which no responses were evoked (left). The colors show the trajectory of Chr2-eYFP expression; the denser the color in a region, the more often Chr2-eYFP expression covers that region in the slice. Two slices were collected in each experiment, and Chr2-eYFP expression was examined for both slices regardless of whether the neuron was recorded in the rostral (upper) and/or caudal slice (bottom). Abbreviations: 7n, facial nerve; Bar: Barrington Nucleus; LDTg: laterodorsal tegmental nucleus; Mo5, motor trigeminal nucleus; PCRtA, parvicellular reticular nucleus, alpha; PnC, Nucleus reticularis pontis caudalis; Pr5, principal sensory trigeminal nucleus; scp, superior cerebellar peduncle.

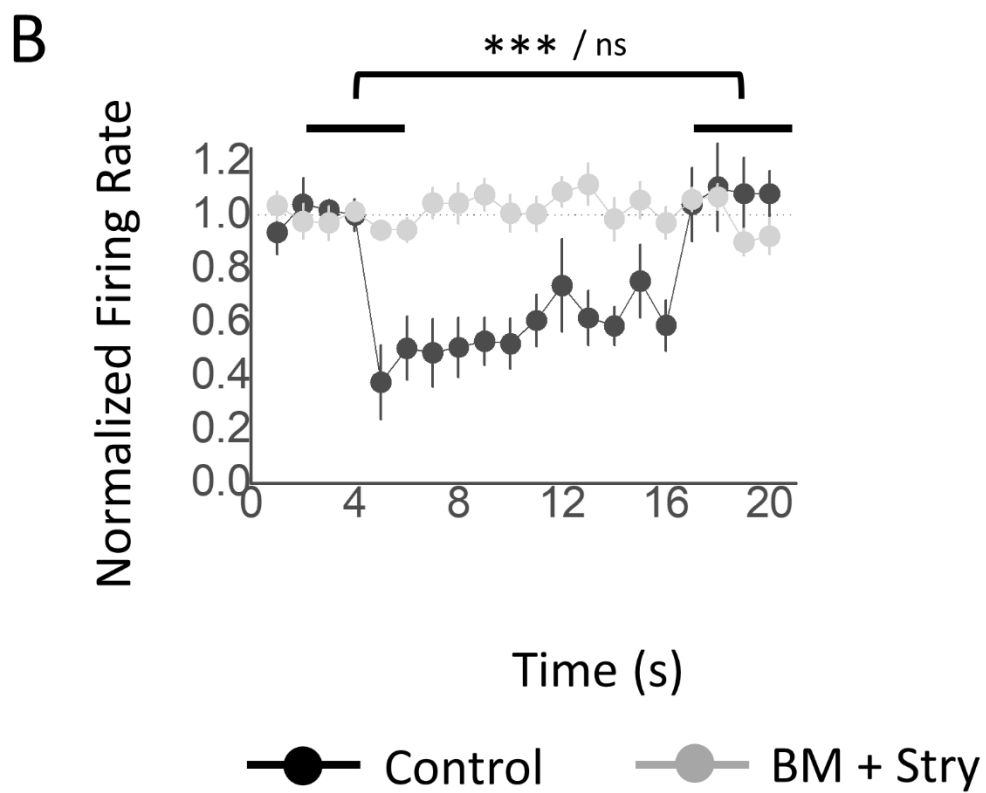
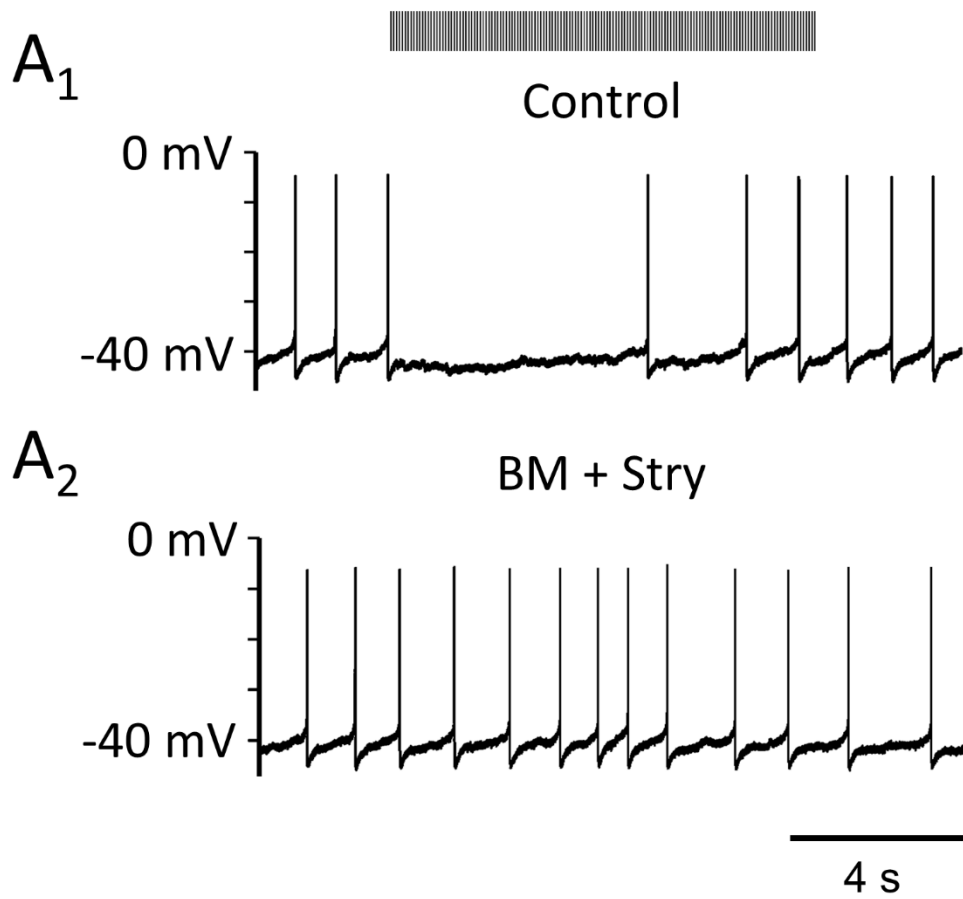
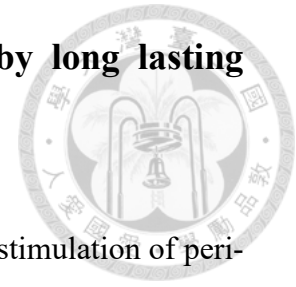


Figure 13

**Figure 13. Prolonged inhibition of LC-NA neuron by long lasting stimulation of peri-LC I-INs**



*A*, A representative I-clamp recording shows the effect of the photostimulation of peri-LC I-INs on spontaneous APs in a LC-NA neuron before (*A1*) and after BM+Stry application (*A2*). Note the adding of BM+Stry completely abolishes the prolonged inhibition on a LC-NA neuron. *B*, A plot shows summarized results. Black and grey circles denote data collected before and after BM+Stry application, respectively. Each filled circle denotes the mean in a given time segment; capped vertical lines denote the SE. Blue bars on the top indicate timing of photostimulation and are applied to both traces and the plot.

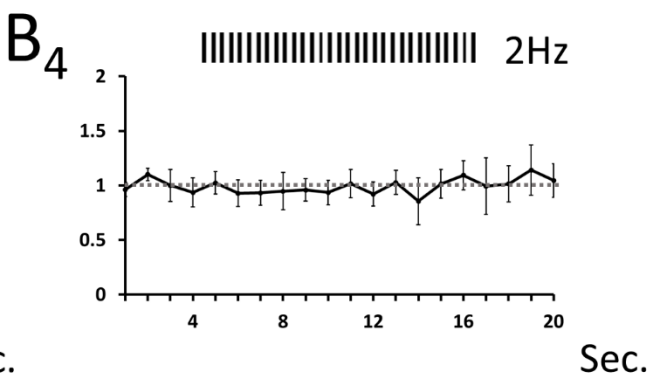
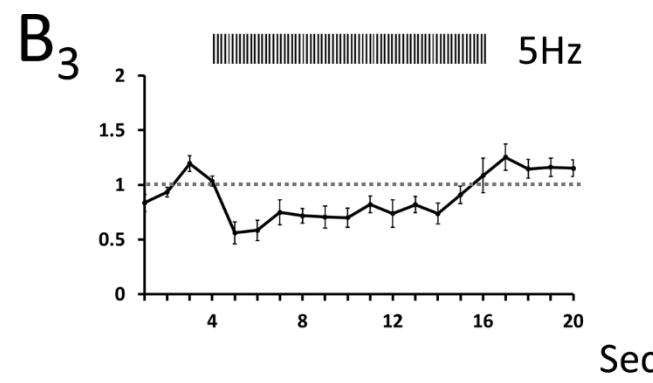
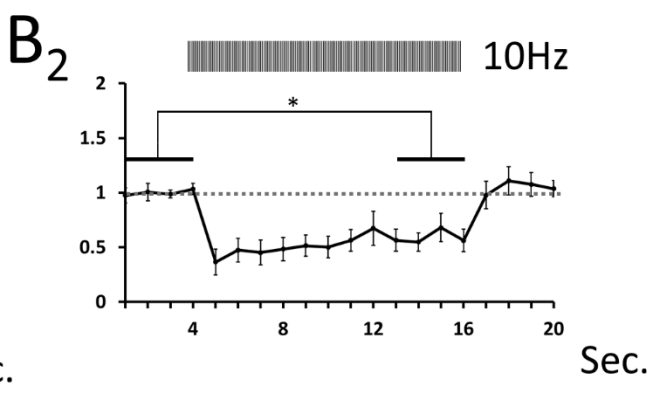
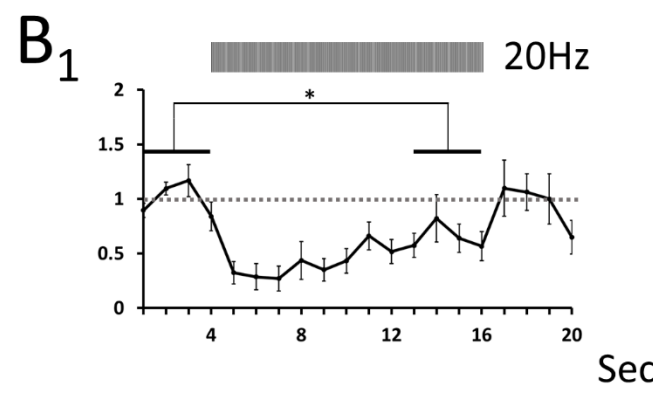
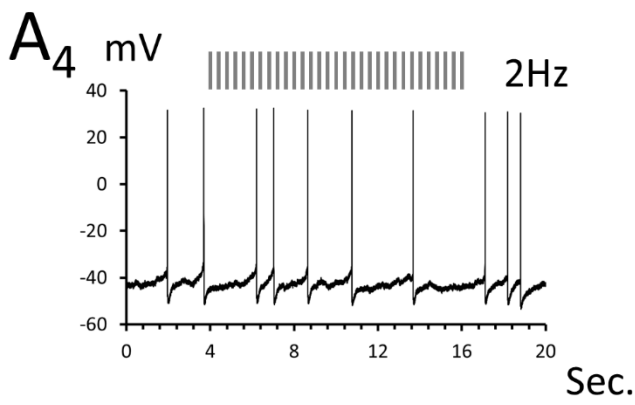
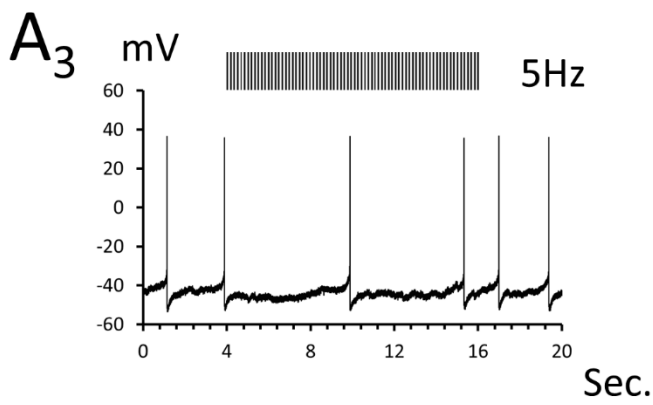
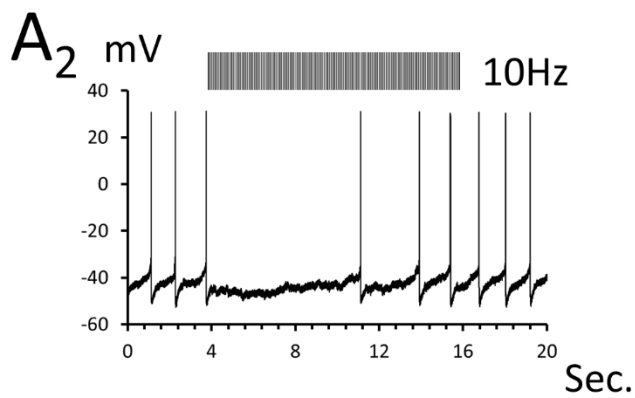
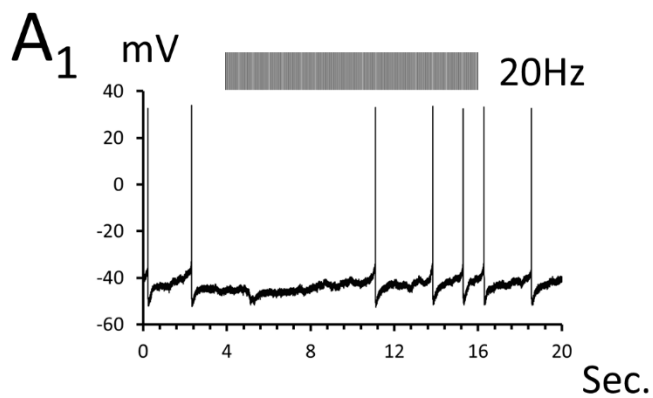


Figure 14

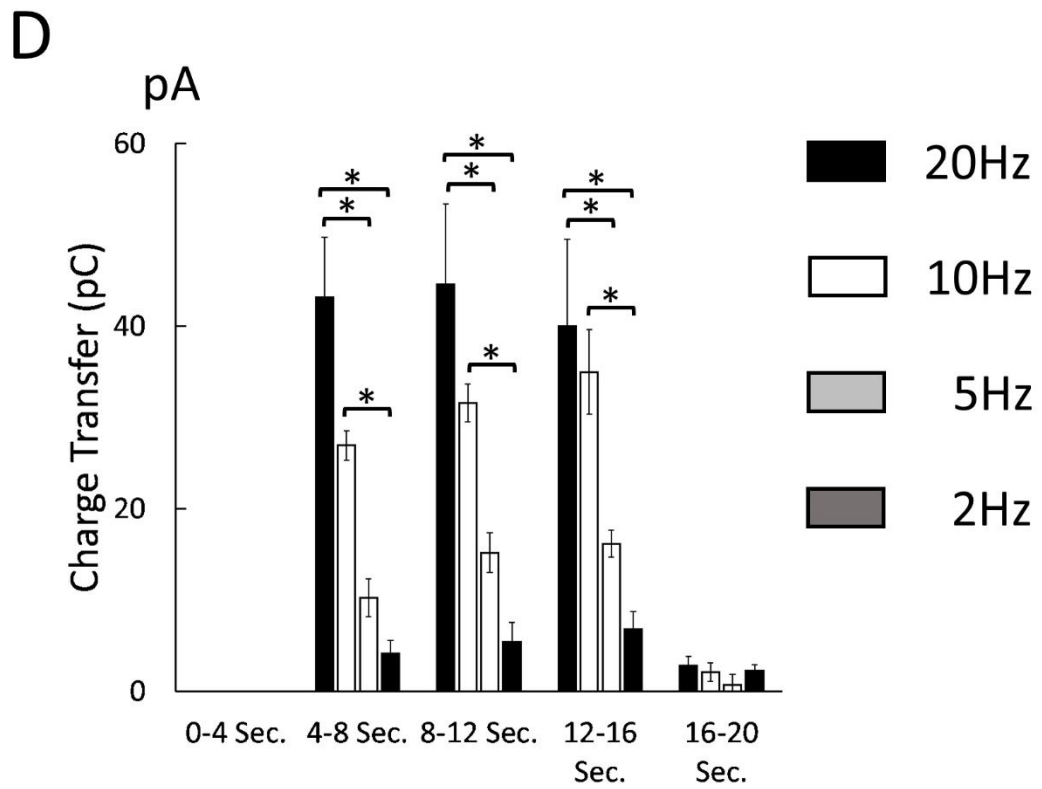
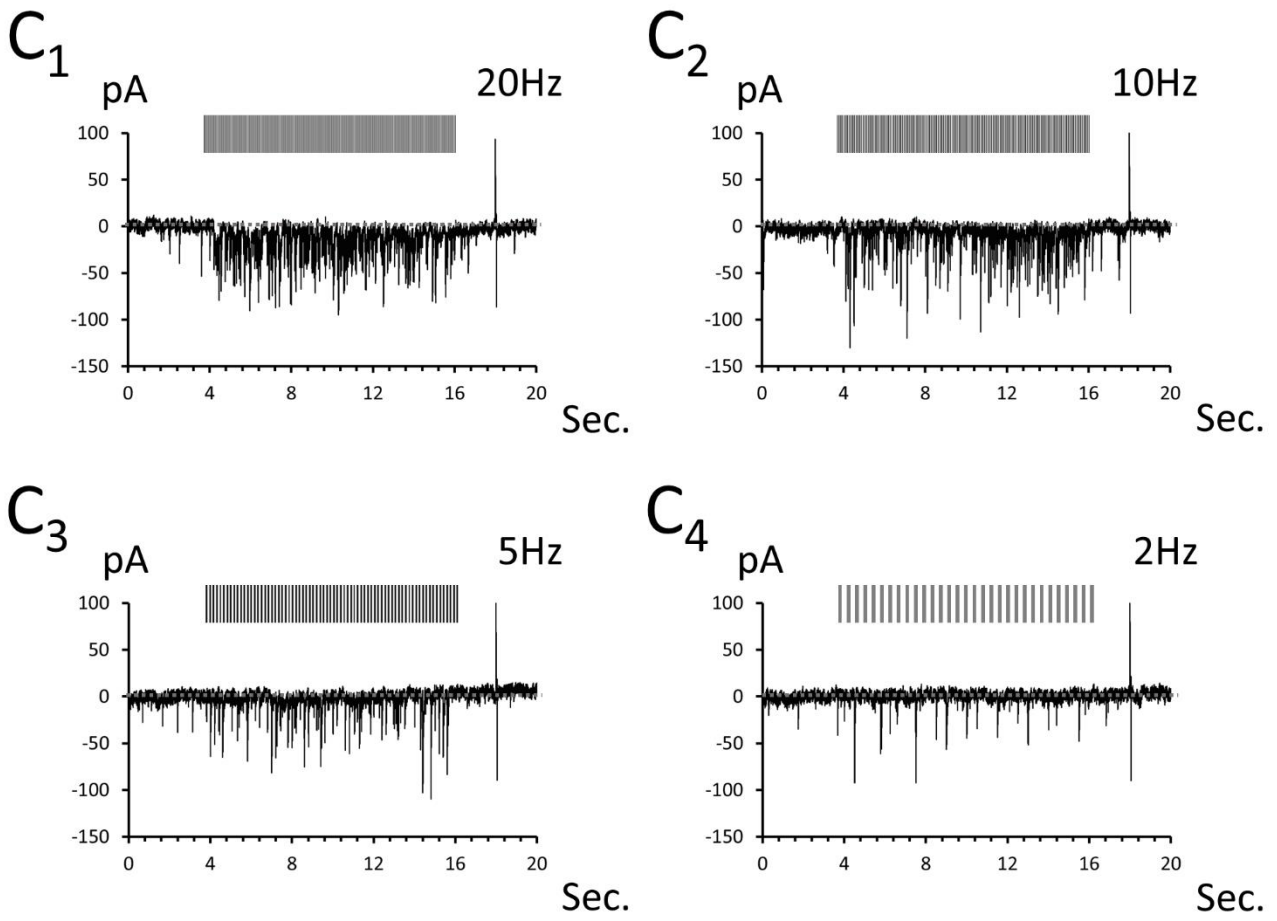


Figure 14

## Figure 14. Frequency dependent inhibition from onto peri-LC I-INs

**A**, Representative recordings demonstrating a frequency dependent inhibition of peri-LC I-INs receiving trains of optical stimulation. Traces show that 12 s trains of light pulses at 20 Hz (A1), 10 Hz (A2), 5 Hz (A3) and 2 Hz (A4) yield different inhibitory effects on a LC-NA neuron. **B**, Plots summarize results from 10 cells receiving long lasting stimulations at 20 Hz (B1), 10 Hz (B2), 5 Hz (B3) and 2 Hz (B4). Traces denotes the mean firing rate throughout the frame; capped vertical lines denote the SE. Blue bars on the top indicate timing of photostimulation and are applied to both traces and the plot. Note only results from stimulations at 20, 10 Hz but not 5, 2 Hz show the significant inhibition in firing rate of LC-NA neurons (paired t test,  $p > 0.05$  in 5, 2 Hz;  $p < 0.05$  in othes) **C**, Representative recordings show the similar experiments under V-clamp configuration in a LC-NA neuron. Note the frequency dependent manner of the IPSC summation. **D**, A plot summarizes the results from 4 cells, note the stronger IPSCs in trials with prolonged light stimulations at 20 or 10 Hz.

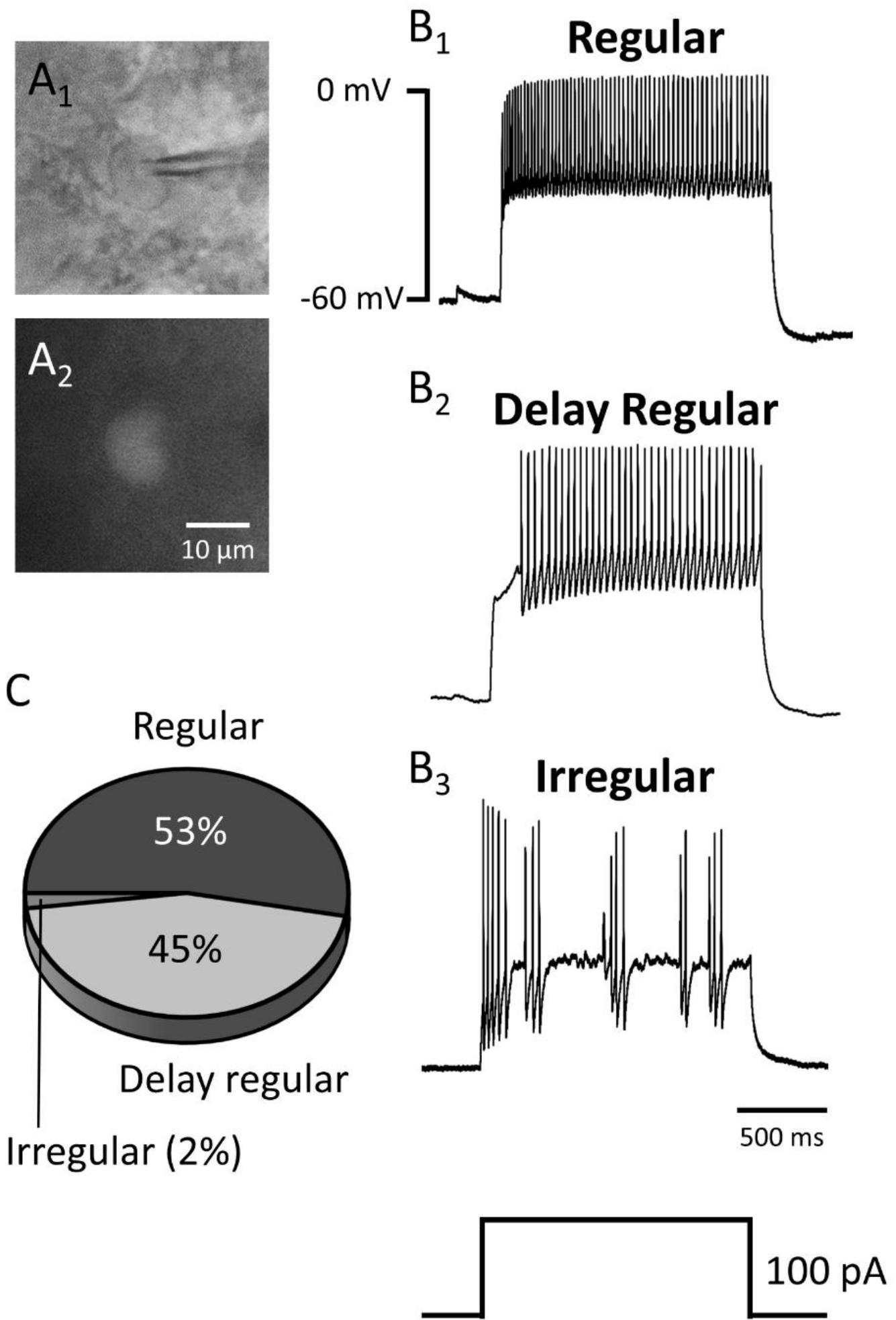


Figure 15

D

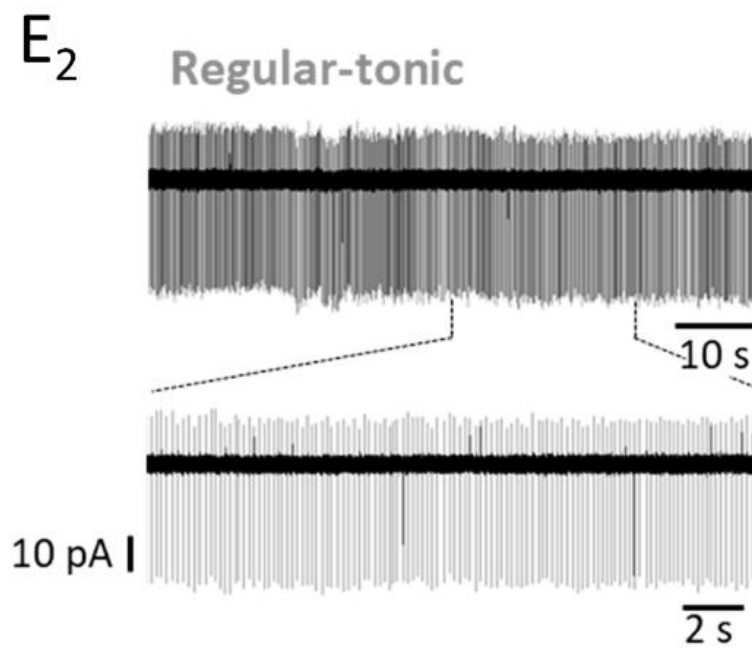
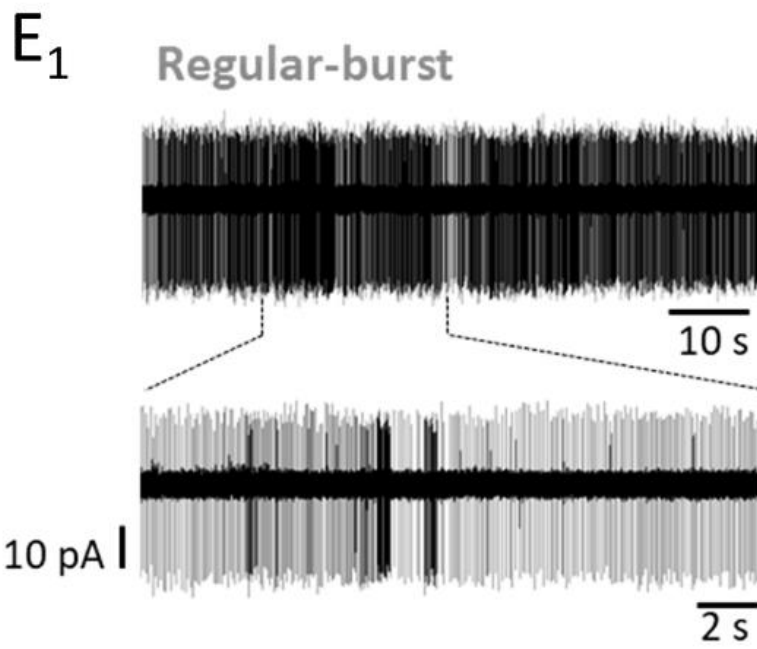
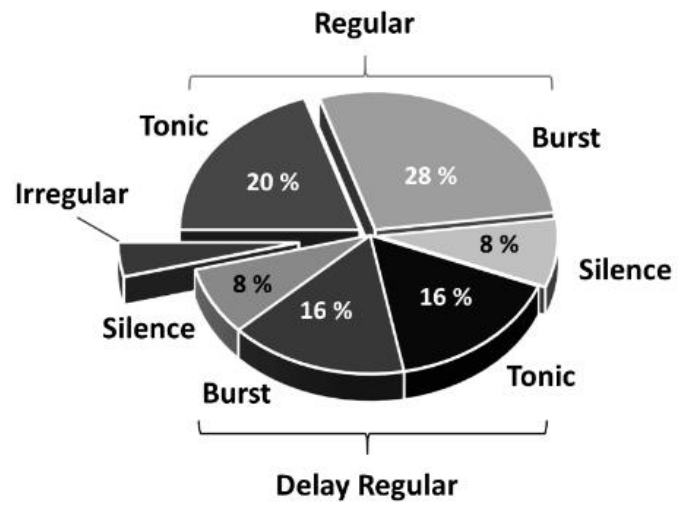


Figure 15

## Figure 15. Characterization of basic properties of peri-LC I-INs

*A*, Online phase contrast (*A1*) and fluorescent images (*A2*) show a recording from a GADGFP<sup>+</sup> neuron in the medial part of the peri-LC. The GADGFP mice and *vgat*<sup>cre</sup> mice receiving infusions of AAV2-DIO-ChR2-eYFP into the right LC were used. *B*, Representative I-clamp recordings shows examples of three I-IN populations which exhibit different firing patterns in response to a 100 pA current injection. *C*, A pi-plot illustrates the proportion of neurons belonging to regular, delay regular or irregular population. *D*, A pi-plot shows a detailed composition of peri-LC I-INs populations in regard to both the firing pattern and the spontaneous burst activity. *E*, Representative cell-attachment recordings demonstrate two episodes from a regular burst (*E1*) and a regular tonic (*E2*) peri-LC I-IN. Note the lack of post-burst silence in the recorded peri-LC I-IN.

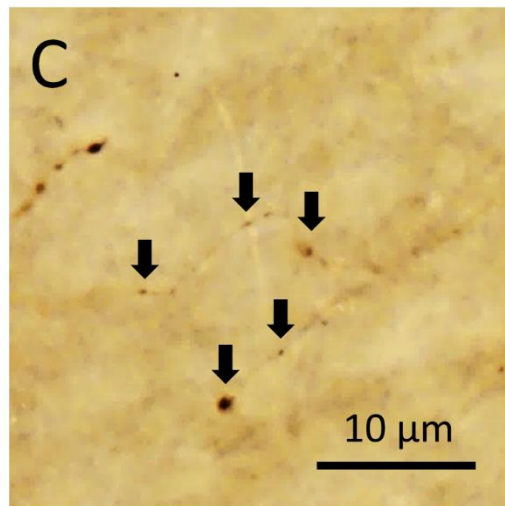
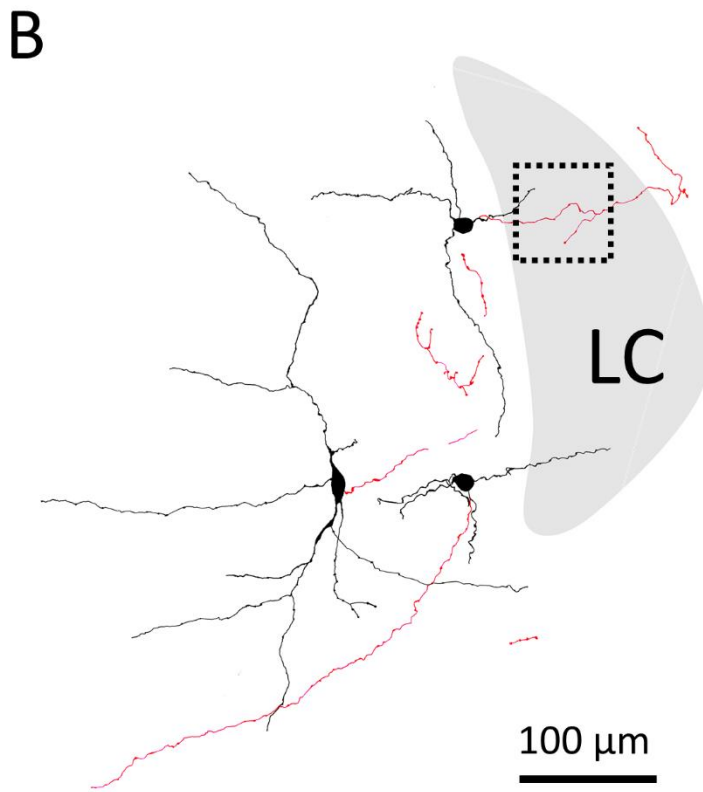
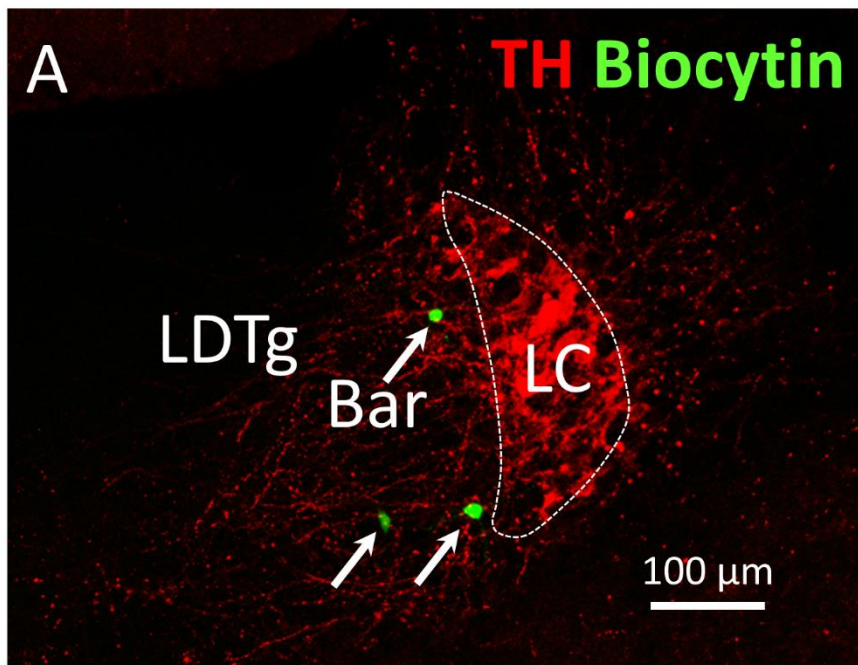


Figure 16

D

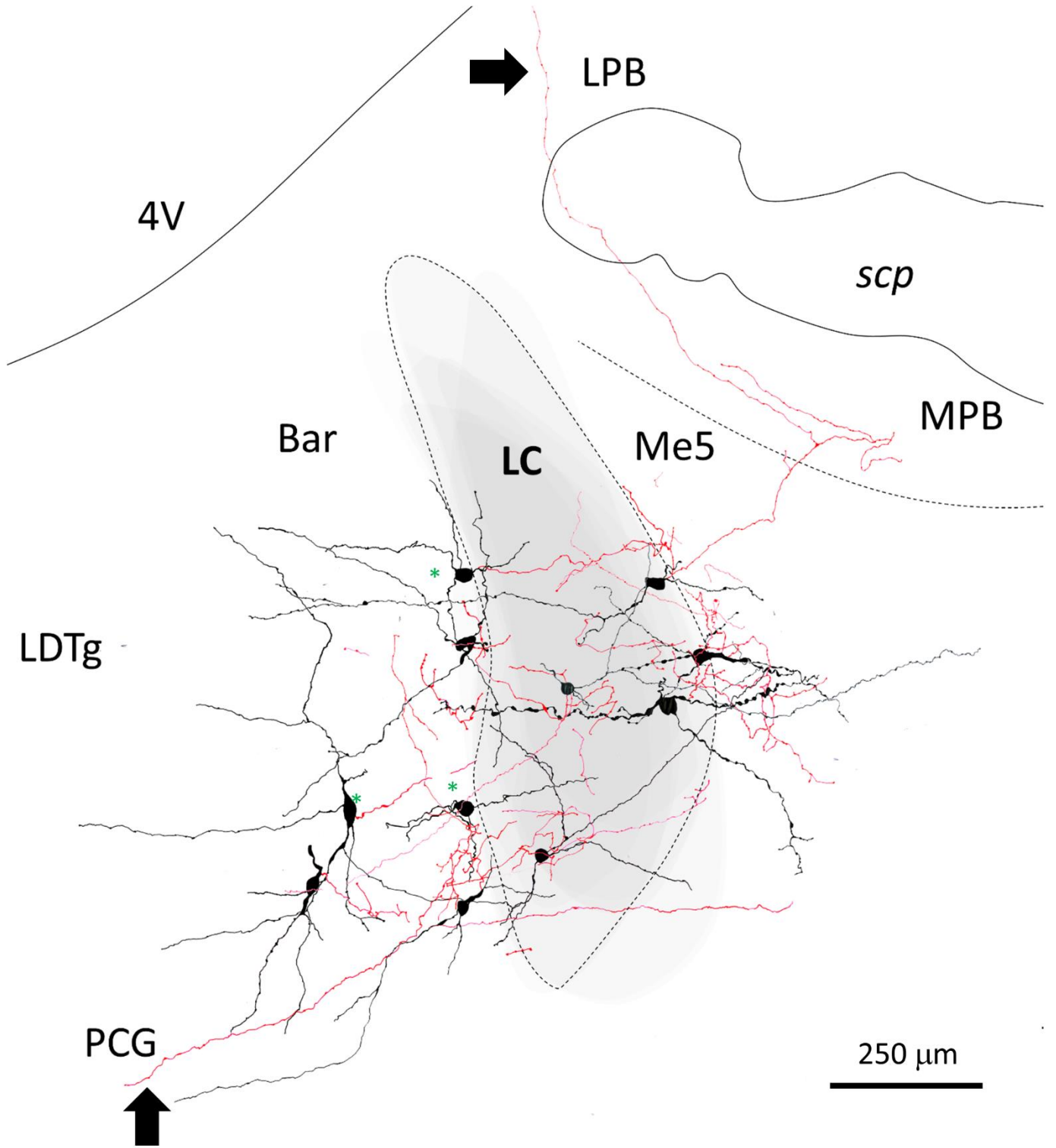
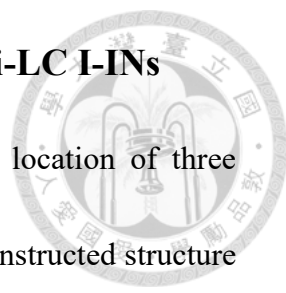
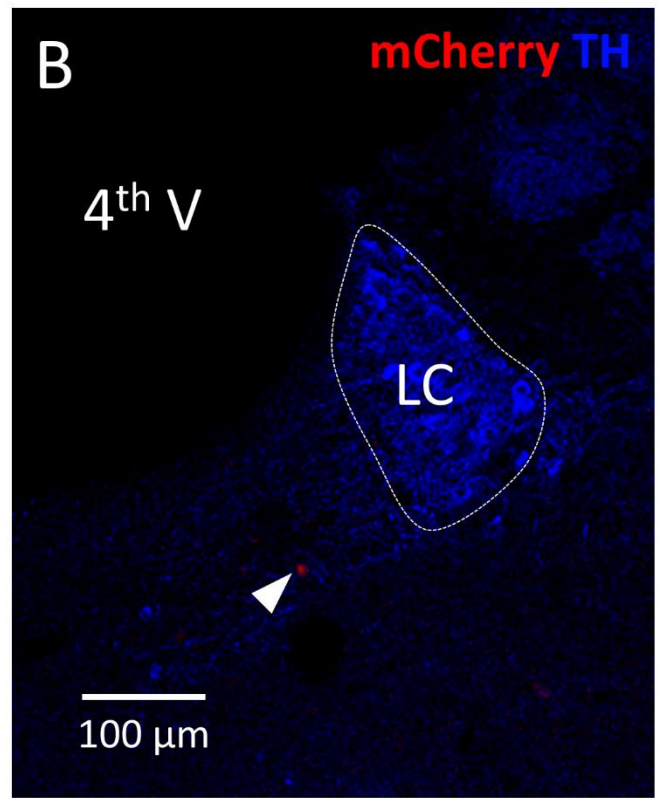
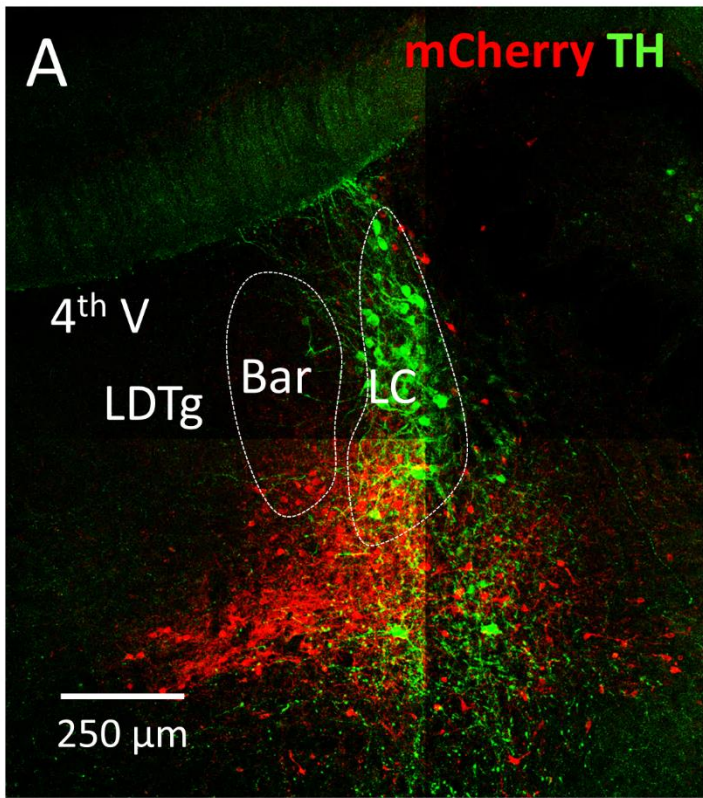


Figure 16

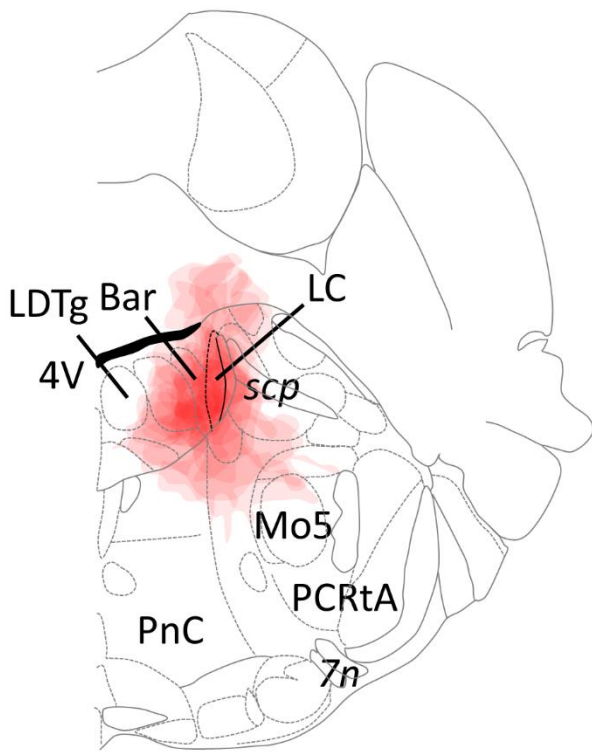
## Figure 16. Morphology reconstruction of recorded peri-LC I-INs



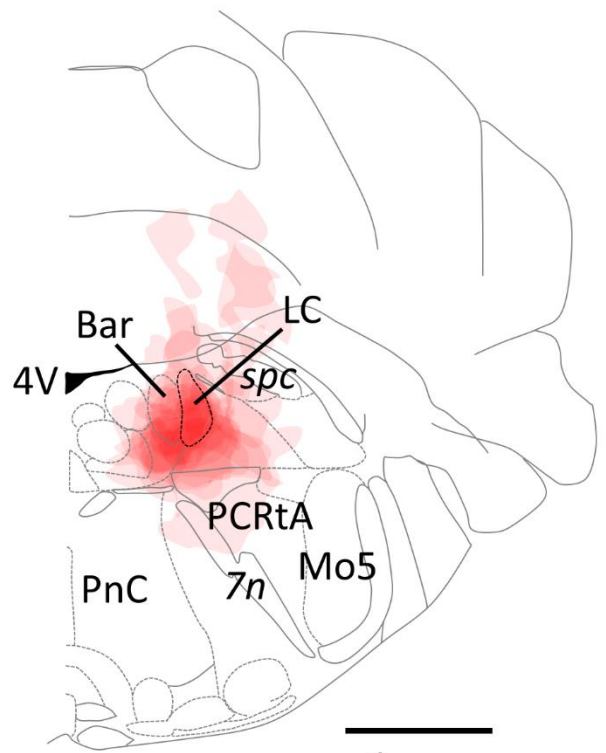
*A*, An immunofluorescent image of TH and biocytin shows the location of three recorded peri-LC I-INs. *B*, A camera lucida drawing shows the reconstructed structure of three recorded neurons shown in *A*. The territory of the LC proper is defined by the IHC of TH. *C*, An image from light microscopy of the dashed zone in *B* in a higher magnification, arrows indicate the bouton-like structure along the axon process. *D*, A superimposed image of camera lucida drawings from 11 reconstructed neurons displays the local axonal projection near the LC proper and the peri-LC region. Note the axonal branches travel toward the parabrachial nucleus and the pontine central grey (arrows).



**C<sub>1</sub>** Bregma -5.3 mm



**C<sub>2</sub>** Bregma -5.6 mm



1  24 (Slices)

Figure 17

## Figure 17. Experimental design of hM4DiR DREADD on brain slice

**A**, A representative image shows post hoc IHC that validates the hM4DiR-mCherry expression profile similar to those in optogenetics experiments. The *vgat<sup>cre</sup>* mice receiving infusions of AAV2-DIO-hM4Di-mcherry into the right LC were used. **B**, A representative fluorescent image shows IHC of TH and mCherry in a section cut through the LC of a WT mouse that received an AAV2-DIO-hM4DiR-mCherry infusion into the LC. Note that there was no expression of hM4DiR-mCherry. **C**, An overlay of camera lucida drawings summarizes the AAV2 expression profile from 24 experiments in this series of studies. The same expression of color density shown in Fig. 12 is used to indicate the frequency of hM4DiR-mCherry expression covering a region in the slice.

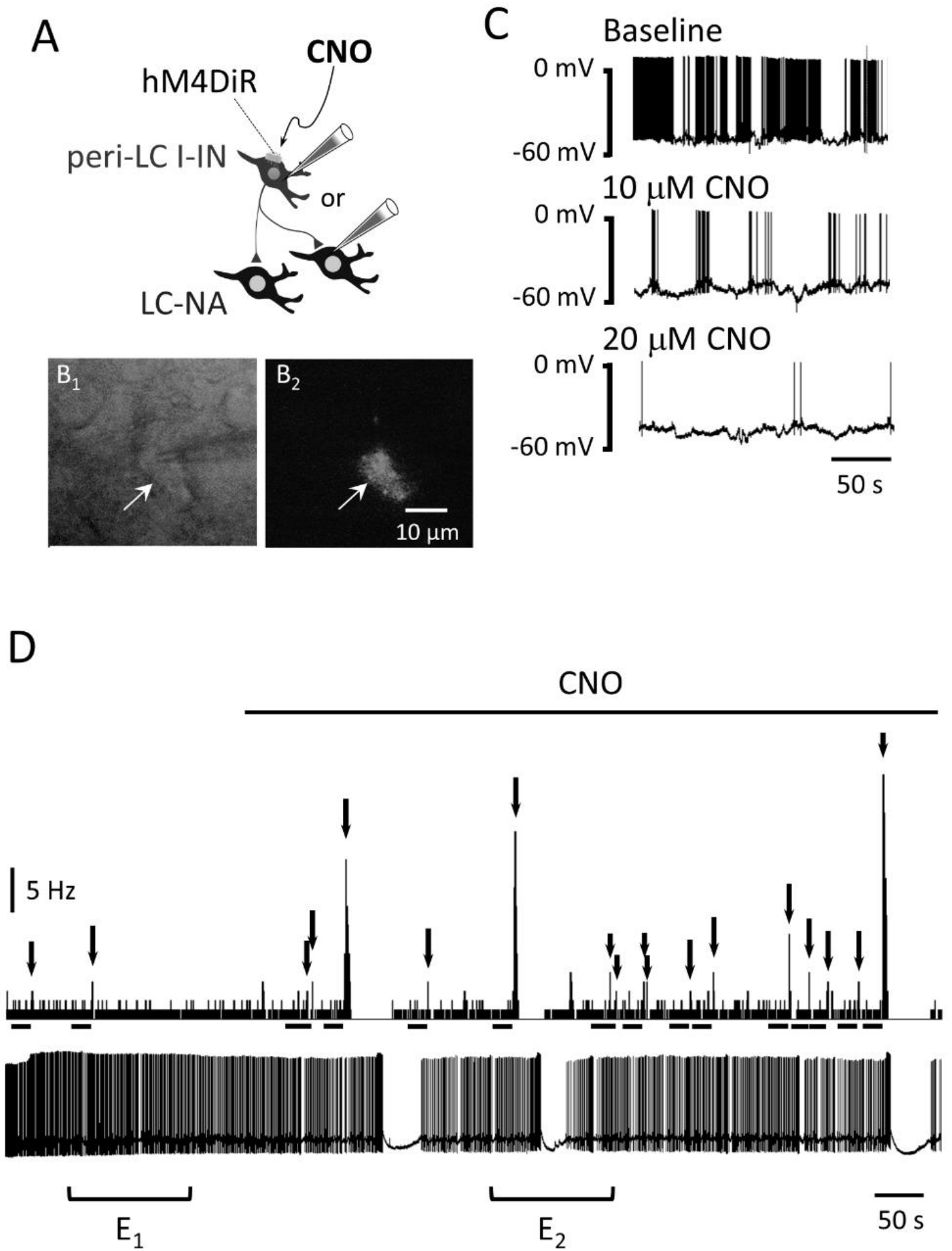
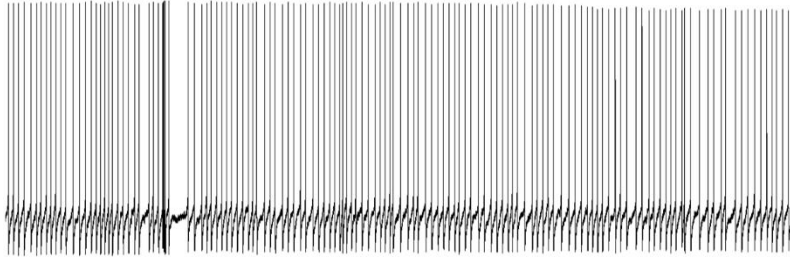


Figure 18

E<sub>1</sub>. Baseline



E<sub>2</sub>. CNO

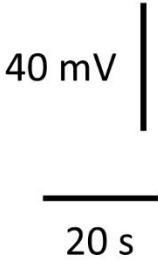
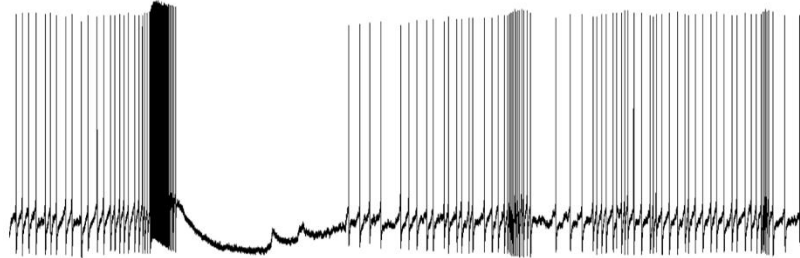


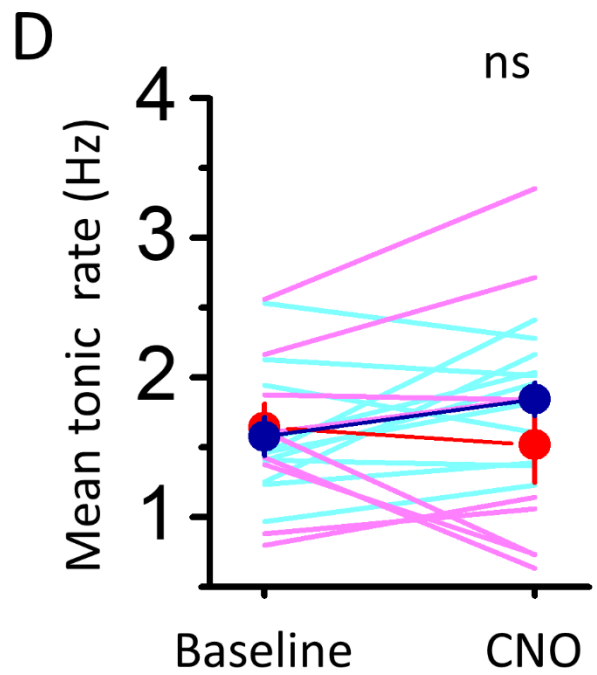
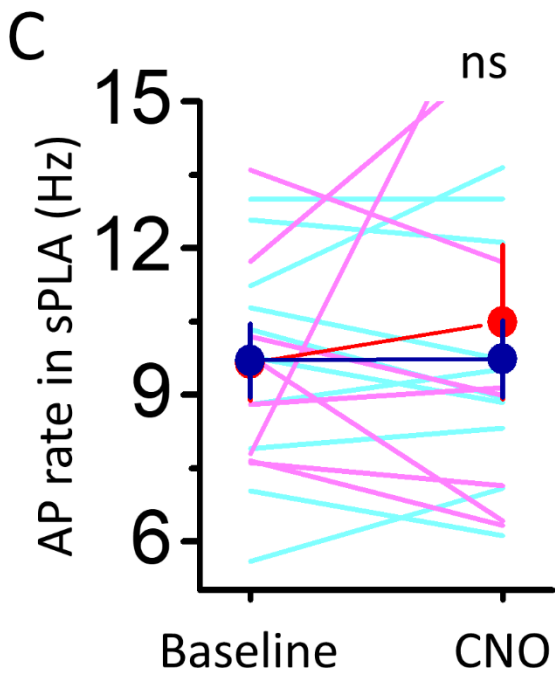
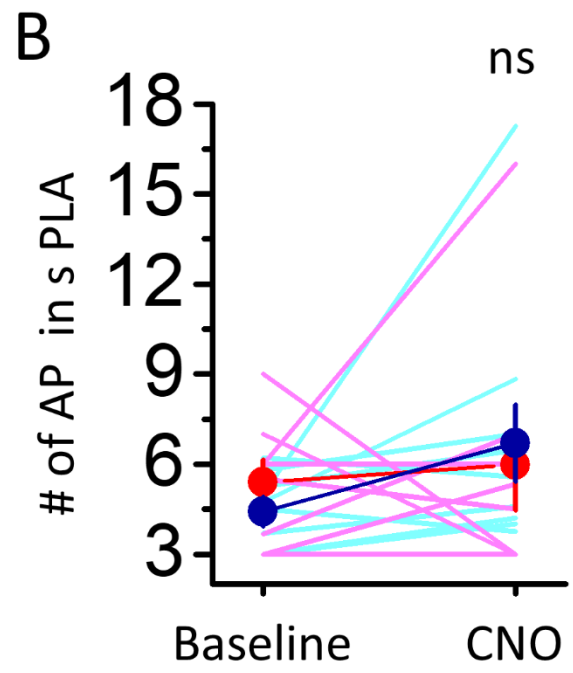
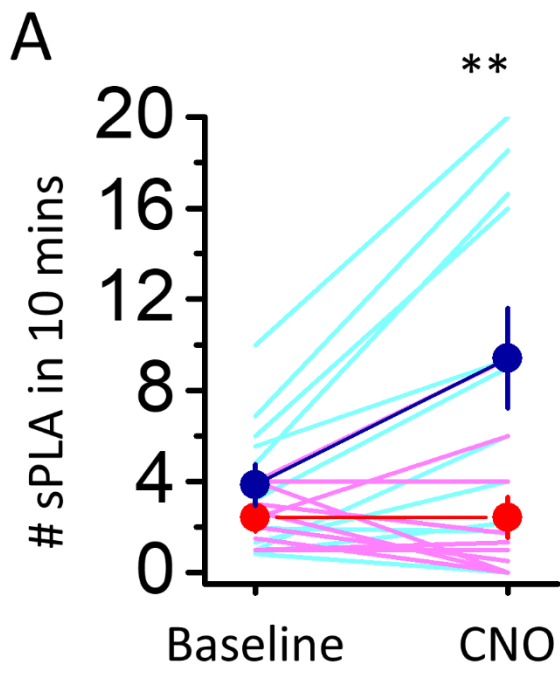
Figure 18

## Figure 18. Inhibition of peri-LC I-INs with hM4DiR DREADD

### enhanced sPLA in LC-NA neurons



*A*, The schematic diagram shows experimental arrangements. The  $vgat^{cre}$  mice receiving infusions of AAV2-DIO-hM4Di-mcherry into the right LC were used. *B*, Online phase contrast (B1) and fluorescent (B2) images show a representative recording from an hM4DiR-mCherry<sup>+</sup> neuron in the medial part of the peri-LC (refer to arrows). *C*, A representative recording shows spontaneous APs recorded from an hM4DiR-mCherry<sup>+</sup> neuron and CNO application repressing the activity in a dose-dependent manner. *D*, A representative recording from a LC-NA neuron shows CNO application enhanced sPLA. The top histogram shows firing rate; the horizontal dashed lines show the standard for the detected sPLA marked by arrows and the bottom trace shows the representative recording. Note that the distortion in LC tonic activity led by CNO application is highly similar to the BM+Stry application. *E*, Two examples of recording episodes before (E1) and after (E2) CNO application. Note the stronger burst and post-burst silence of the sPLA in presence of CNO.

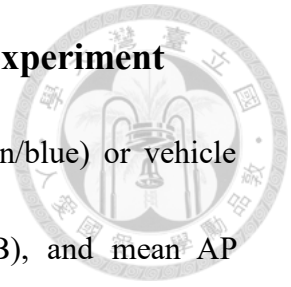


AAV2-hM4Di-mCherry: — / ● ; AAV2-mCherry : — / ●

Figure 19

## Figure 19. Summarized results of hM4DiR DREADD experiment

*A-D*, Plots show summarized results of the effects of CNO (cyan/blue) or vehicle (magenta/red) application on the incidence (A), AP number (B), and mean AP frequency (C) of sPLA as well as the background tonic rate (D). For plots in A-D, each light shows the result of an individual experiment, and the circles (mean) + capped vertical lines (SEM) show the averaged results. Also see Table 4 for statistical information.



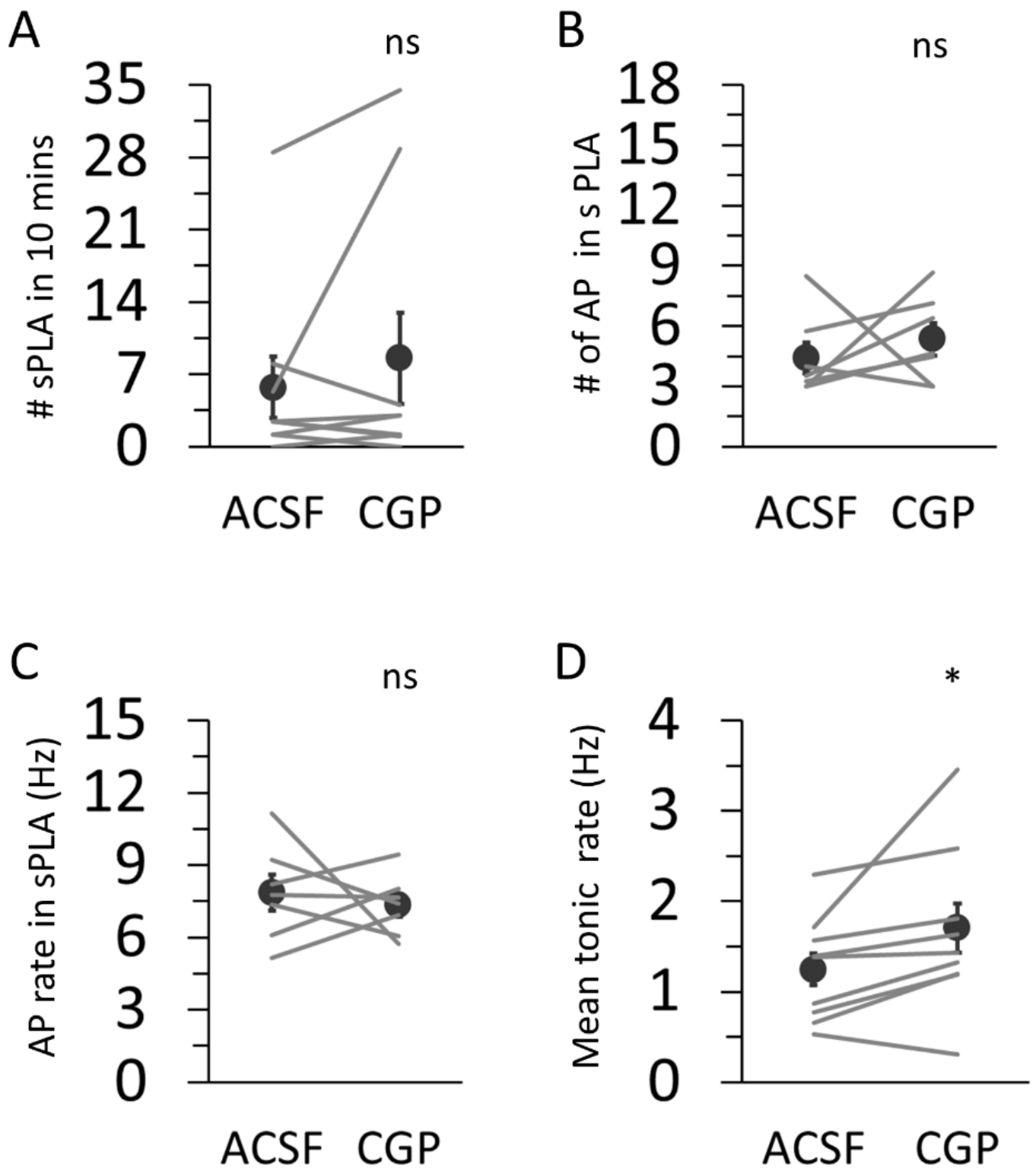
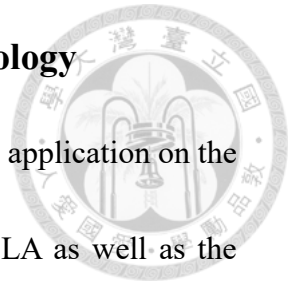


Figure 20

## Figure 20. Summarized results of CGP54626 pharmacology

*A-D*, Plots show summarized results of the effects of the CGP54626 application on the incidence (A), AP number (B), and mean AP frequency (C) of sPLA as well as the background tonic rate (D). For plots in A-D, each light shows the result of an individual experiment, and the circles (mean) + capped vertical lines (SEM) show the averaged results. Also see Table 4 for statistical information. All results were gathered in brain slices from naïve *vgatcre* mice not receiving any treatment and AAV infusion.



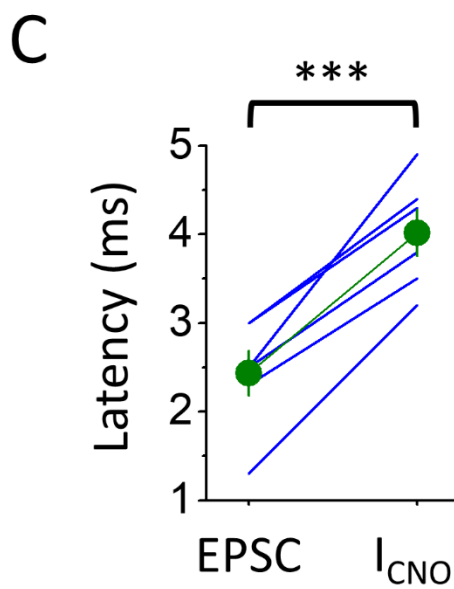
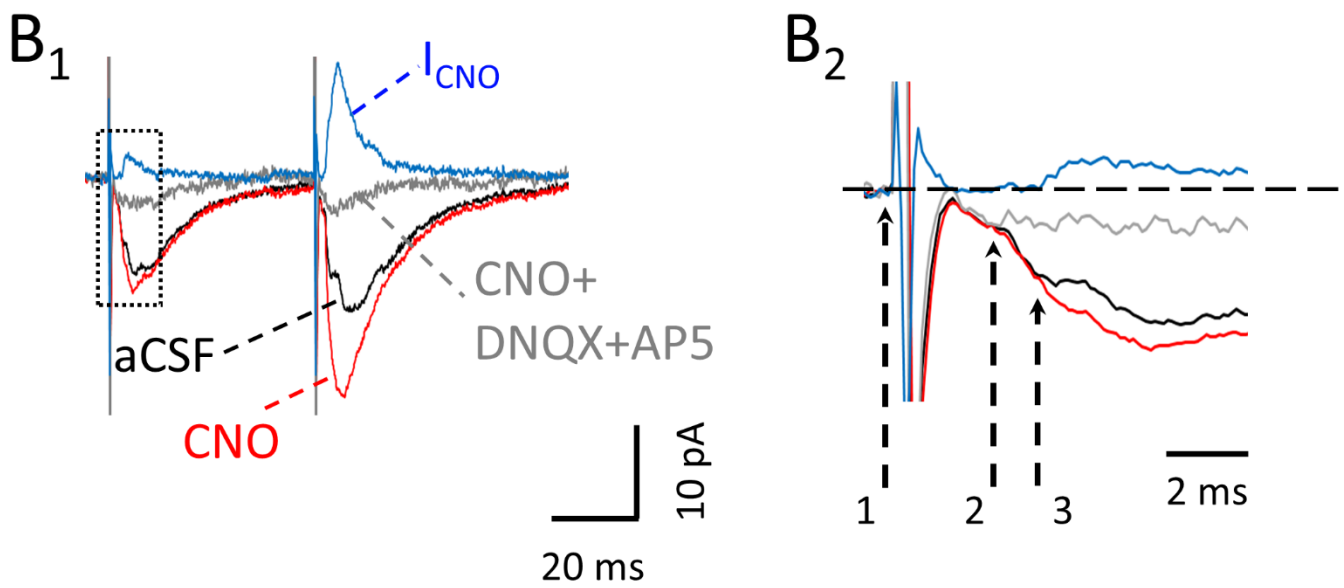
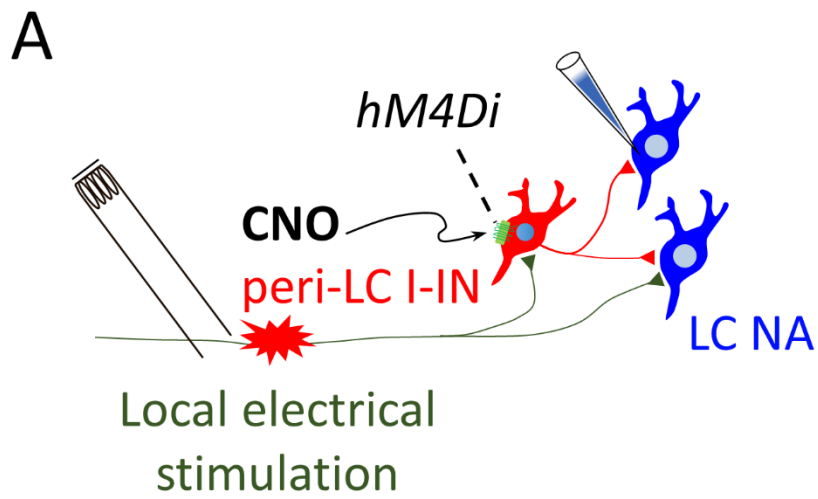


Figure 21

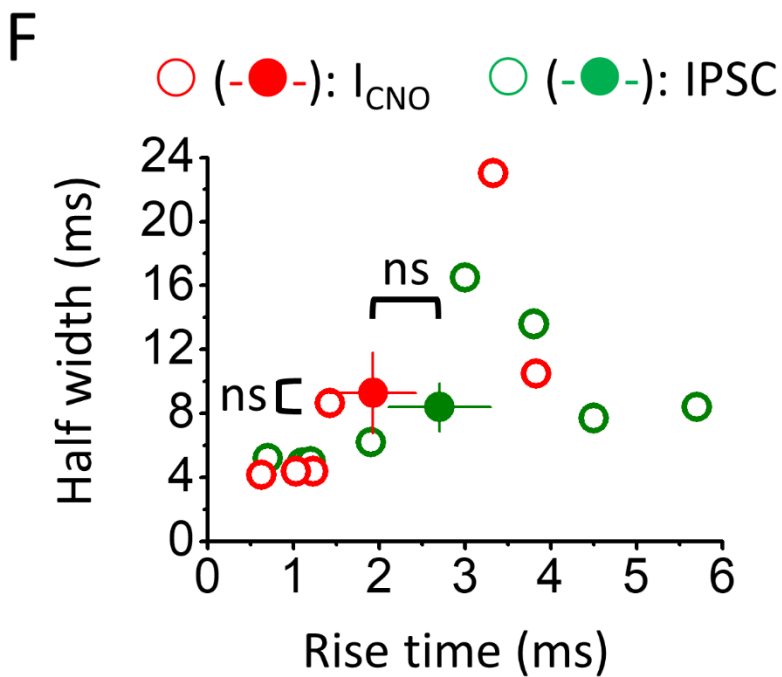
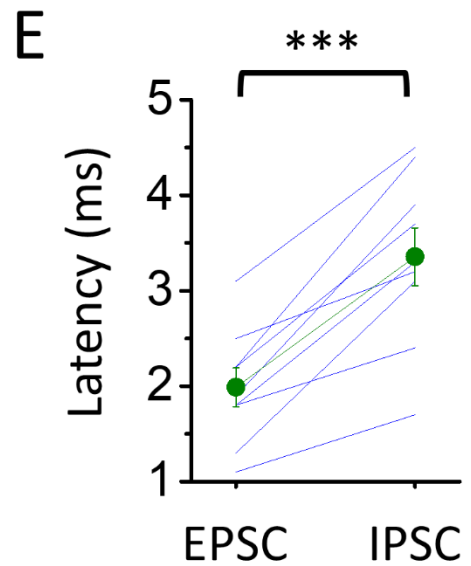
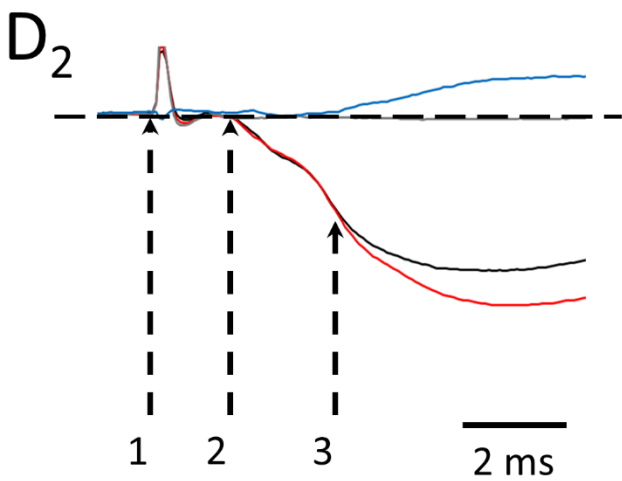
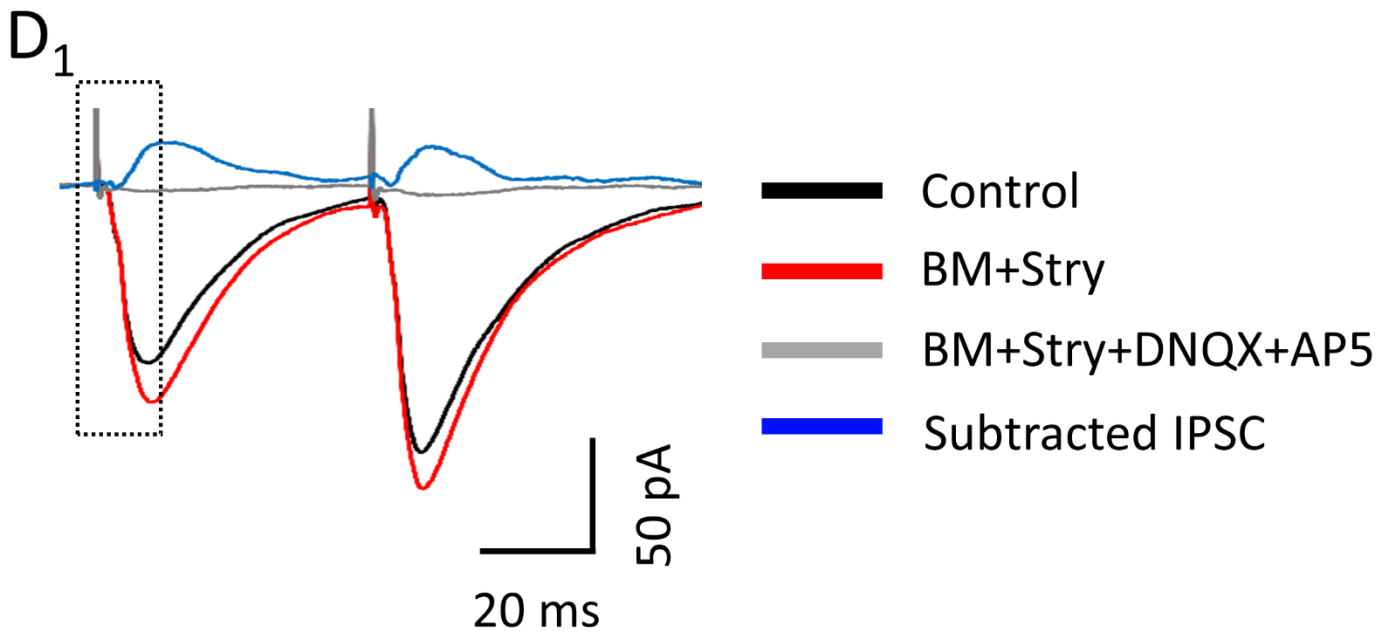


Figure 21

**Figure 21. Electrical stimulation of glutamatergic inputs recruits peri-LC I-INs that exert a feedforward inhibition**



**A**, Schematic diagram shows experimental arrangements. The  $vgat^{cre}$  mice receiving infusions of AAV2-DIO-hM4Di-mcherry into the right LC were used. **B & D**, Representative V-clamp recording shows synaptic currents evoked in a LC-NA neuron upon local electrical stimulation with a paired-pulse. B1 & D1 show superimposed responses from LC-NA neurons in aCSF (black trace), CNO/BM+Stry application (red trace), CNO+DNQX+AP5/BM+Stry+DNQX+AP5 application (gray trace) and the subtracted  $I_{CNO}/IPSC$  (blue trace). B2 & D2 show the activity evoked by the first pulse (refer to dashed square in B1 or D1) at a faster time scale. Arrows 1, 2 and 3 mark the onsets of the electrical pulse, the EPSCs and the  $I_{CNO}$  (B2)/IPSC (D2), respectively. **C & E**, Plots show EPSC latency and  $I_{CNO}/IPSC$  latency in DREADD experiments (C) and pharmacology experiments (E). **F**, Plot shows RT and HW relationship of the IPSCs (green) and  $I_{CNO}$  (red). The open circles show the result of an individual experiment, and the filled circles (mean) + capped vertical lines (SEM) show the averaged results.

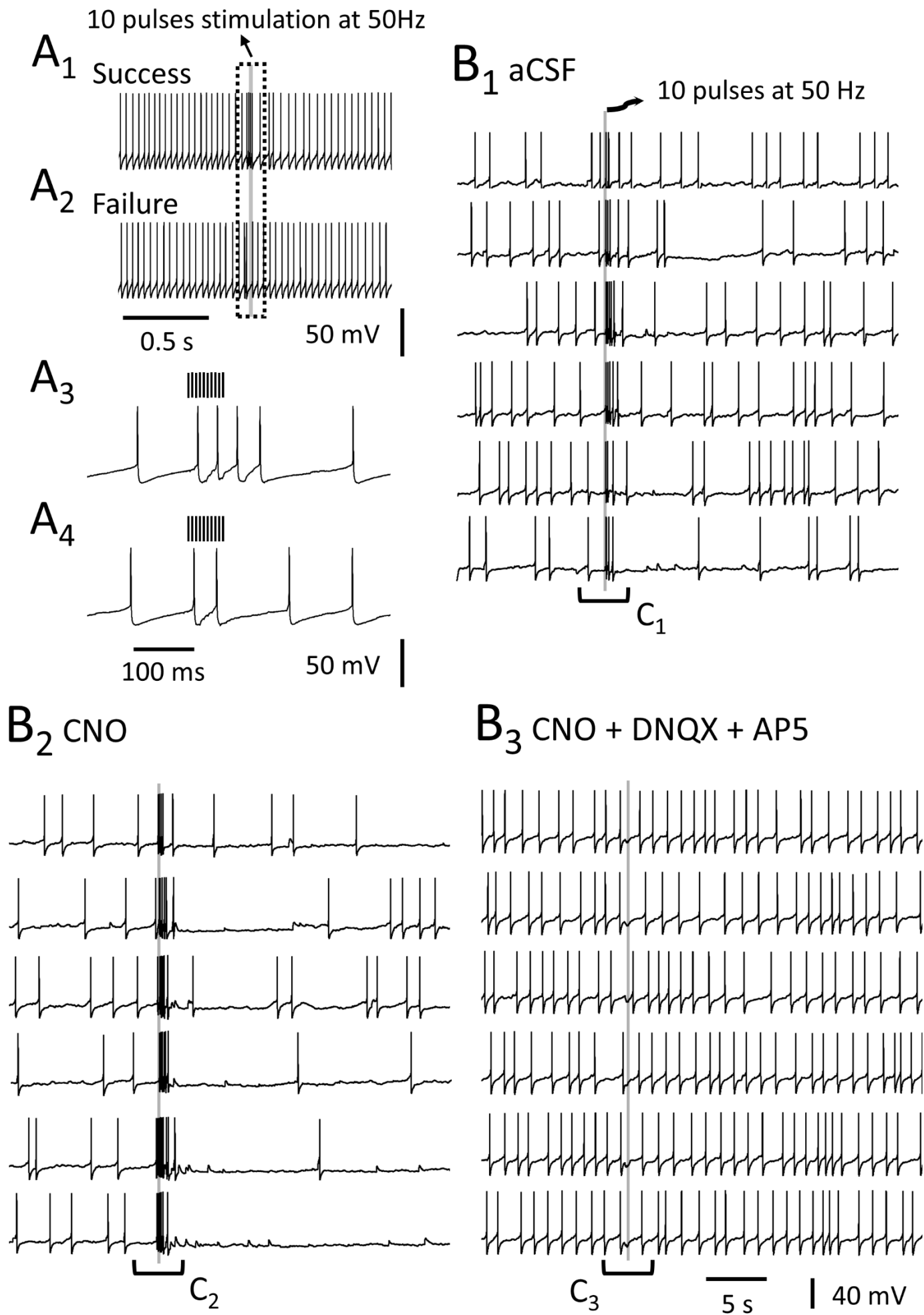


Figure 22

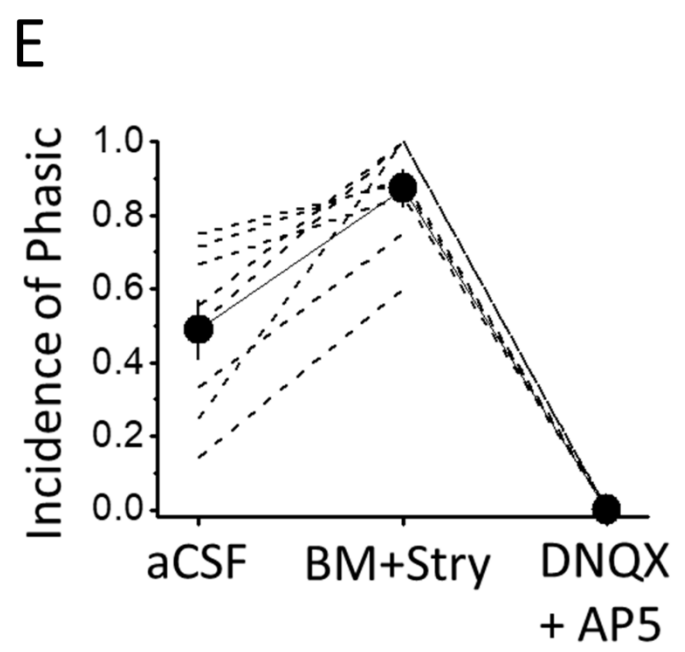
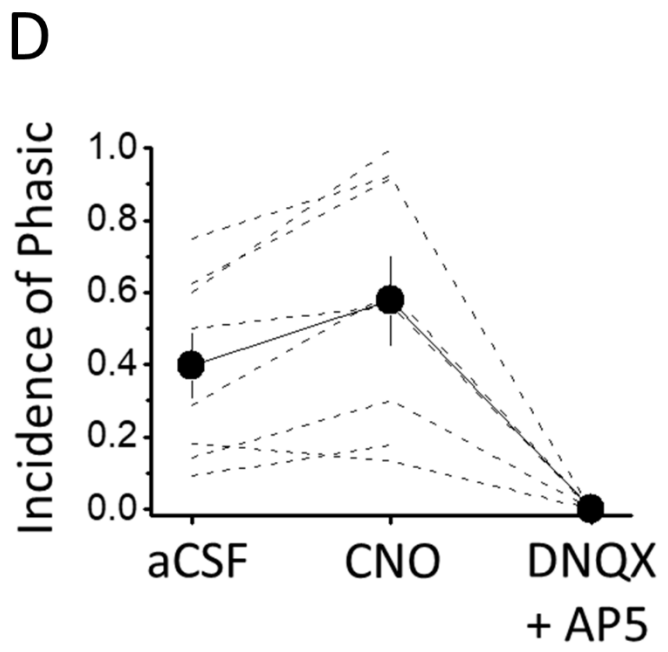
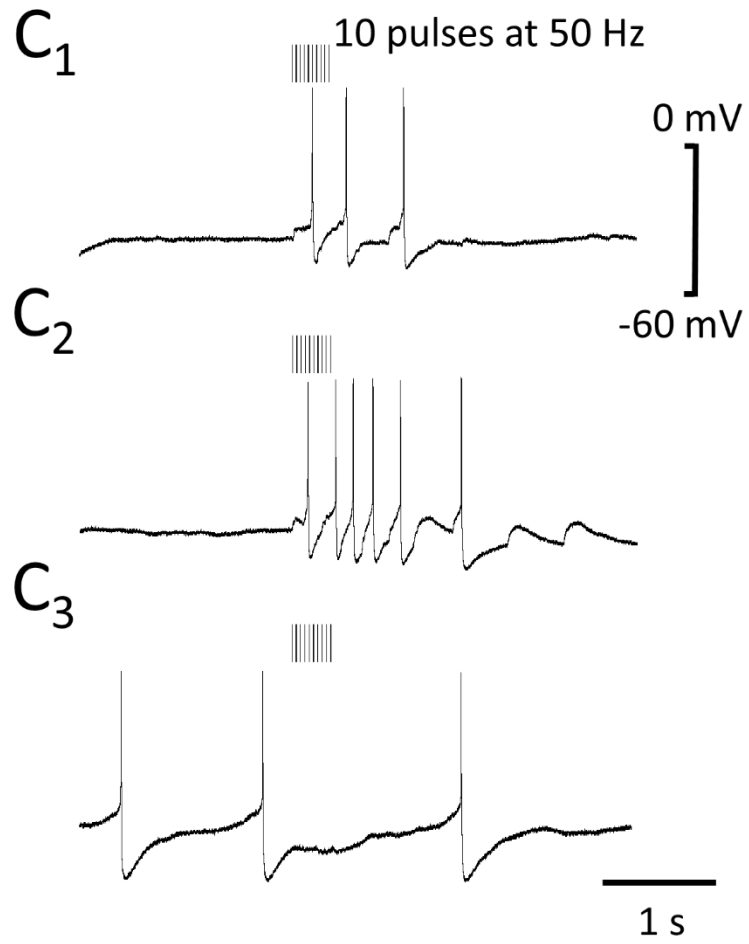
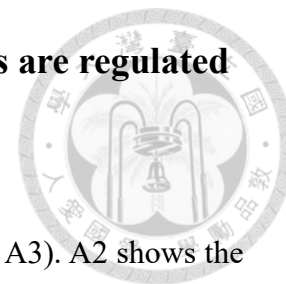


Figure 22

**Figure 22. Evoked phasic activation in LC-NA neurons are regulated by peri-LC I-INs**



*A*, Examples of representative recordings show the raw data (*A1* & *A3*). *A2* shows the episode indicated by dashed box in *A1* and *A4* shows another episode shown in *A3*. *A1* & *A3* demonstrate an evoked phasic activation by a train of 10 electrical pulses at 50 Hz that successful fulfills the detection criteria. While a failure attempt is shown in *A2* & *A4*. The red vertical lines indicate electrical stimulation. *B*, A representative I-clamp experiment shows phasic activity evoked in a LC-NA neuron. *B1-B3* show raw data of 6 consecutive sweeps evoked in aCSF (*B1*), CNO application (*B2*) and CNO+DNQX+AP5 application (*B3*). The red vertical lines indicate electrical stimulation. *C*, Representative recordings show peri-stimuli episodes indicated by the brackets the 6th sweep in *B*; phasic activity was evoked by CNO application but not in aCSF or by CNO+DNQX+AP5 application. For all 6 sweeps shown, phasic activity was evoked in 3 of the 6 sweeps in aCSF (*C1*), 6 of the 6 sweeps by CNO application (*C2*), and 0 of the 6 sweeps by CNO+DNQX+AP5 application (*C3*). *D & E*, Plot shows summarized results of DREADD (*D*) and pharmacology (*E*) experiments. Each blue dashed line represents the result of an individual experiment, and the green circles (mean) + capped vertical lines (SEM) show the averaged results.

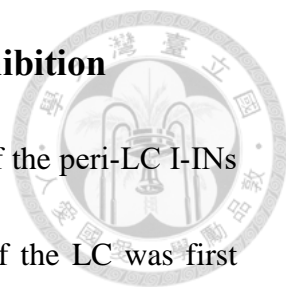
## Section 3



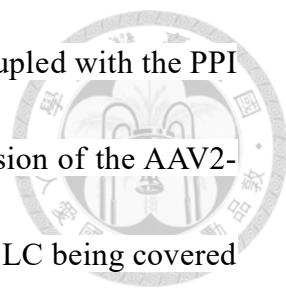
### Functional Implications of peri-LC I-IN

The aim of the section was to find the role of peri-LC I-IN in living animals. My strategy was to focus on the two major functions which the LC was involved in, namely, the sensory processing and cognitive vigilance. First, I and my colleagues used the startle behavior as a model for checking as to whether the peri-LC I-IN affected the sensorimotor gating through the LC-NA neurons. Second, I and my colleagues used the viral anterograde and the trans-synaptic tracing to confirm that the peri-LC I-IN received the inputs from the prefrontal cortex, and hence, can be involved in the cognitive vigilance via helping LC-NA neurons integrate cortical afferents.

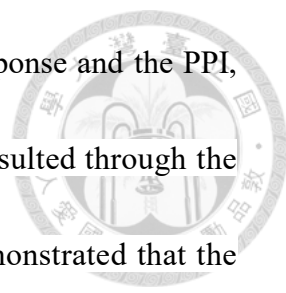
### 3.1 Inhibition of peri-LC I-INs Enhances Prepulse Inhibition



I and my colleagues subsequently examined the potential role of the peri-LC I-INs in controlling behaviors. As aforementioned, the phasic activity of the LC was first found in response to sensory stimuli and further confirmed to affect the sensory processing, even the following cognitive updating of certain stimuli. Based on these reasons, I and my colleagues chose the startle reflex coupled with the PPI as a target of functional investigation in the behavioral level. The startle reflex is a pre-attentional behavior response when encountering the unexpected sensory stimuli, therefore it fits one of the typical ways for triggering the phasic activity in the LC (Waterhouse and Navarra, 2019). In general, the PPI assesses how efficient the neural network filters intrusive irrelevant stimuli were (Braff et al., 2008; Geyer, 2008; Swerdlow et al., 2008). Alsene & Bakshi (2011) showed that increasing the tonic LC activation by cholinergic and glutamatergic agonists could disrupt the PPI through hyper-activating the LC result of the augmented tonic activity and repressed phasic activity. Given that the present results showed that peri-LC I-INs played a role in gating the phasic activity but had no effect on the basal tonic rate, selective inhibition of peri-LC I-INs was hypothesized to promote the PPI but not startle reflex (see **Discussion**).



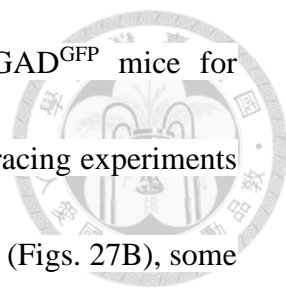
I and my colleagues monitored the auditory startle behavior coupled with the PPI value examining of male  $Vgat^{Cre}$  mice receiving a bilateral infusion of the AAV2-DIO-hM4DiR-mCherry into the LC (Fig. 23). Only mice with the LC being covered bilaterally by the expression of M4Di-mcherry were allowed the proceeding behavior tests (Fig. 24A), The IP administration of CNO significantly increased the PPI compared to vehicle administration tested one week before or after the CNO test (Fig. 25A; Table 6). However, no significant changes in the startle reflex, travel distance, rearing or grooming were noted (Figs. 22A, E; Table 6), demonstrating that only the behavior associated with the LC-NA system, namely, the PPI (Alsene and Bakshi, 2011), was affected. These observations were further confirmed by analyzing the experiments in which the territory of the AAV2 transfection did not cover the LC in either hemisphere. In these cases, the IP administration of CNO had no effect on the PPI or startle reflex compared to vehicle administration (Fig. 24B, 25B; Table 6). The enhancement of the PPI by CNO was not observed when the control AAV2 was injected into both sides of the LC in  $Vgat^{Cre}$  mice (Fig. 25C; Table 6). Finally, CNO alone did not have an effect on the PPI. In naïve animals, the IP administration of CNO had no effect on the PPI compared to vehicle administration (Fig. 25D; Table 6). Mice that received the bilateral lesions of the LC principle neurons



by the local 6-OHDA infusion showed no change in the startle response and the PPI, this result excluded the possibility of the LC independent effect resulted through the different neural circuit (Fig. 26). Together, my findings have demonstrated that the peri-LC I-INs were involved in a cell-population specific, LC-NA neurons dependent and the LC-related behavior, suggested a role in the sensorimotor gating functions of peri-LC I-INs through the LC.

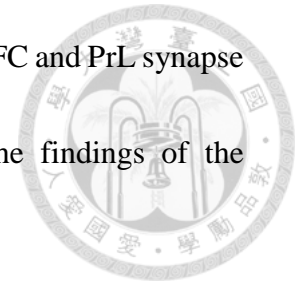
### **3.2 Peri-LC I-INs Receive Axonal Contacts from the OFC and PrL**

As shown, peri-LC I-INs could put their regulation onto the phasic activity. However, a basic assumption was that they received the innervations from the cortex or other brain areas, and such a key feature could explain which brain function they participated in. Here, I and my colleagues aim to confirm as to whether peri-LC I-INs played a potential role in the high cognitive function associated with LC-NA system. In this regard, I assessed the functional contact from the prefrontal cortex onto peri-LC I-INs. The OFC and PrL, parts of the prefrontal cortex, projected to the LC and played crucial roles in the cognitive functions overlapping with those attributed to the LC (Delatour and Gisquet-Verrier, 2000; Dias and Aggleton, 2000; Jodo et al., 1998). I and my colleagues infused the AAV9 viral vector encoding the ChrimsonR tagged with



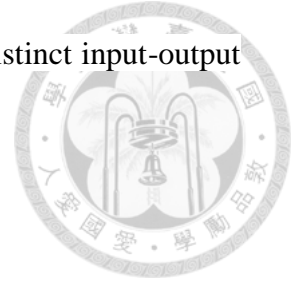
tdTomato (ChriR-tdT) into the left OFC and PrL of TH<sup>Cre</sup>×GAD<sup>GFP</sup> mice for anterograde tracing (Gautron et al., 2013) and repeated the WGA-tracing experiments (Fig. 27A). When the AAV9 transfection occurred within the vOFC (Figs. 27B), some ChriR-tdT fibers were noted in the LC, and their varicosities made contacts not only with LC-NA (WGA<sup>+</sup>/TH<sup>+</sup>) neurons, but also with peri-LC I-INs (TH<sup>-</sup>/WGA<sup>+</sup>/GFP<sup>+</sup> neurons) (Figs. 27 C-E). Compared to the finding with the AAV9 transfection in the vOFC, similar observations were made when the AAV9 transfection occurred within the mOFC plus PrL, but a more extensive innervation covered all of the peri-LC and LC-proper regions, as well as the vast of medial pontine area (Fig. 28; 30), whereas the cases with transfection in the vOFC led to a moderate innervation preferential that occupied the dorsomedial part of the peri-LC region (Figs. 27; 30). To confirm that the ChriR-tdT fibers made functional contacts and did not just pass through the LC as barely appositions, I infused the AAV9 viral vector encoding GFP (Table 3) into the medial prefrontal cortex of TH<sup>Cre</sup> mice and performed the IHC for WGA, GFP, and synaptophysin (Syn), a marker of the synaptic terminal, in a series of experiments. When the AAV9 transfection occurred within the mOFC (Fig. 29A), numerous GFP-labeled fibers were present in the LC and peri-LC (Fig. 29B). In addition, their varicosities exhibited Syn-ir and made contacts with WGA-ir neurons in the medial part

of the peri-LC (Fig. 29C). These results show that axons from the OFC and PrL synapse on both LC-NA neurons and peri-LC I-INs, thus supporting the findings of the feedforward inhibition exerted from them.



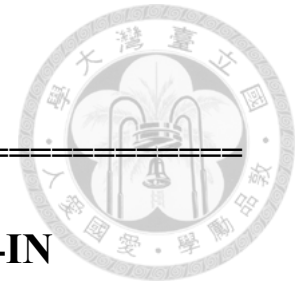
Another important observation was that the projections of the OFC and PrL to the LC showed regional differences (Fig. 30). The IOFC projection was minor (Fig. 30A); the vOFC had a moderate projection with numerous fibers observed in the dorsomedial pons, including the rostral but not the caudal peri-LC (Fig. 30B). In addition, the mOFC and PrL had a substantial projection to the dorsal pons, including the entire LC-proper and the peri-LC (Fig. 30C). Although a small part of the M2 was also transfected in cases with the vOFC was transfected, the labeled fibers located in the peri-LC should mainly represent the vOFC efferent fibers because a small part of the M2 was also transfected in the IOFC in two cases, but the presence of ChR2-tdT-labeled fibers in the peri-LC was rare. Furthermore, in the control experiments in which the AAV9 infusion was aimed at the M2, ChR2-tdT fibers located in the peri-LC were also rare. Interestingly, a large number of axonal terminals from the M2 were located in the ventral pons bilaterally (Fig. 30D), a strikingly different pattern when compared to the

bilateral dorsal pons projection by the vOFC fibers, showing the distinct input-output pattern across prefrontal cortices.



# Figures

---



## Section 3: Functional Implications of peri-LC I-IN

Figure 23. Experiment design of behavior task - startle reflex and PPI -----	175
Figure 24. Bilateral expression profiles of hM4DiR-mcherry in mice involved in behavior task-----	177
Figure 25. Inhibition of peri-LC I-INs enhances prepulse inhibition-----	180
Figure 26. Effects on PPI are done via LC-NA neurons-----	183
Figure 27. Peri-LC I-INs receive axonal contacts from the vOFC-----	185
Figure 28. Peri-LC I-INs receive axonal contacts from the PrL and mOFC--- -----	189
Figure 29. Confirmation of functional connection from mOFC onto peri-LC I-INs by IHC of synaptophysin-----	192
Figure 30. Region-specific projections of the OFC and PrL to the dorsal pontine area-----	194

---

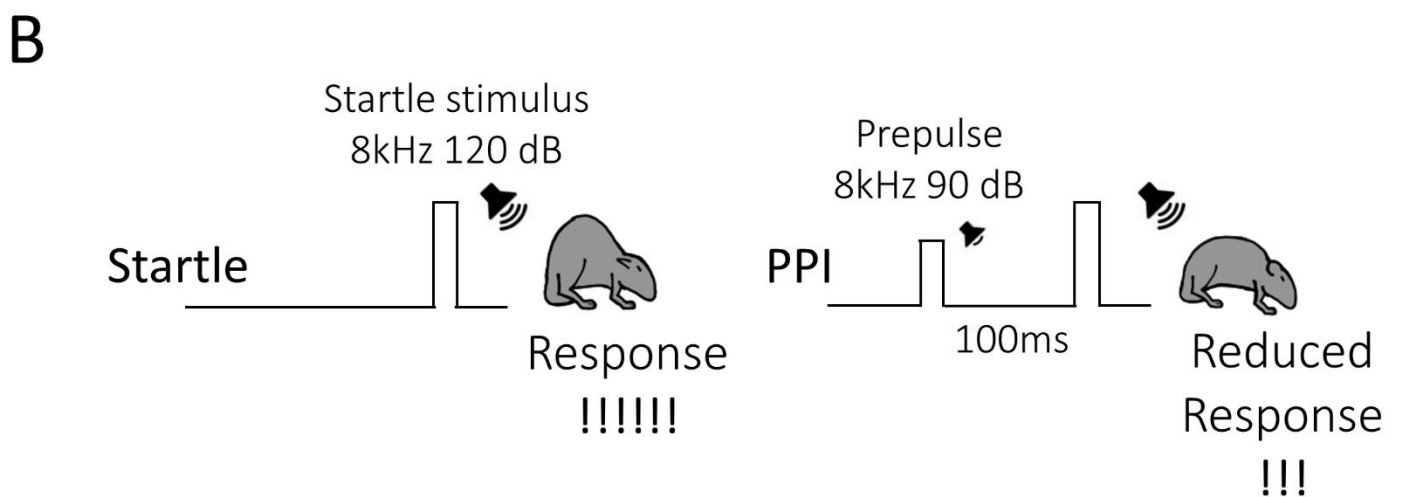
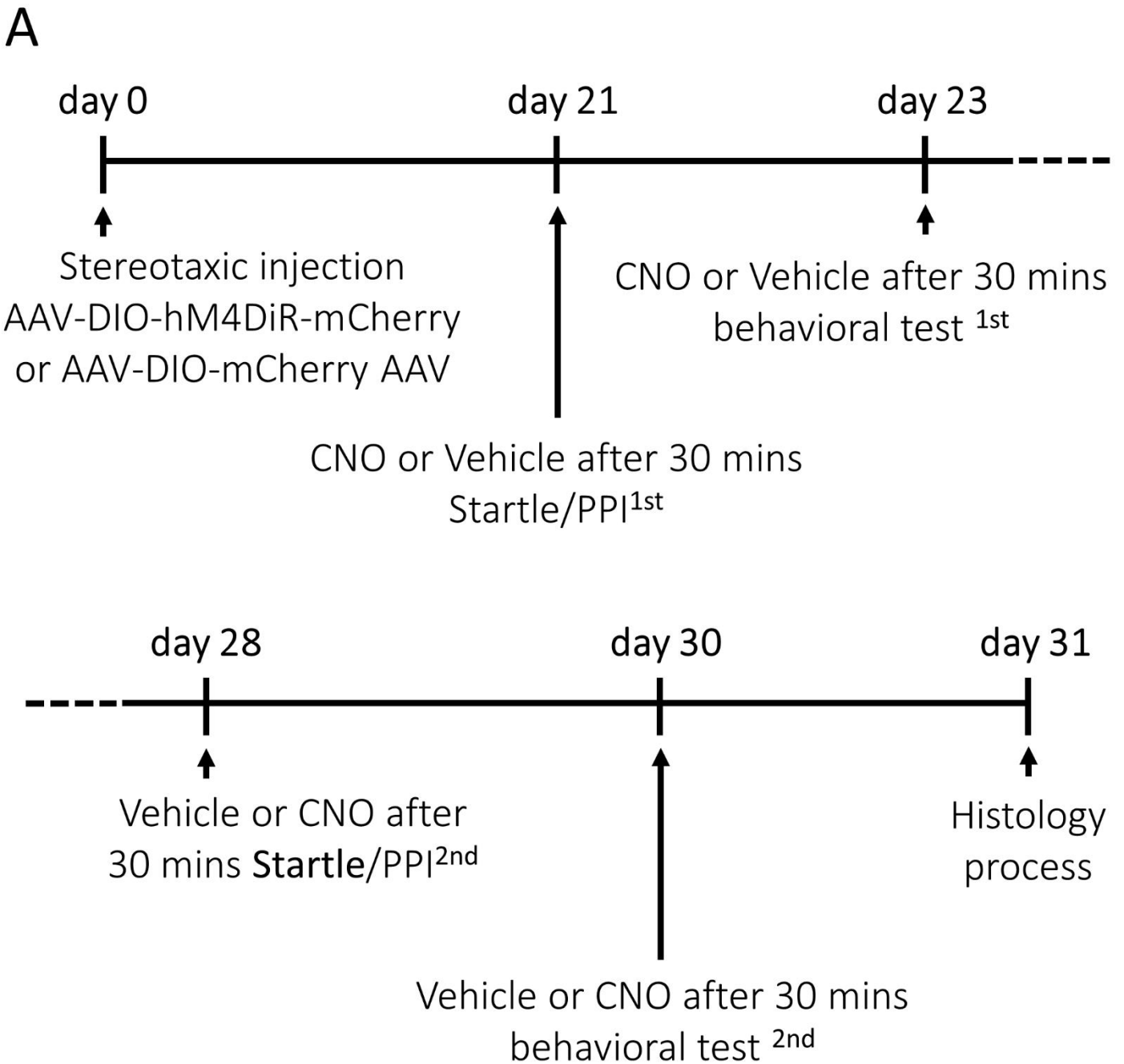


Figure 23

## Figure 23. Experiment design of behavior task - startle reflex and

### PPI

*A*, Chart flow shows the experimental protocol of behavior tests. Note mice engaged in the task are randomly divided into two groups receiving either saline or CNO application first. *B*, schematic plots explain startle reflex and PPI. Stimuli with 120 dB, 40ms burst of 8kHz are used as the startle tone, while weaker stimuli with 80 dB, 20ms burst of 8kHz are used as the prepulse stimuli. The male  $vgat^{cre}$  mice receiving infusions of AAV2-DIO-hM4Di-mcherry into the LC bilaterally were used.



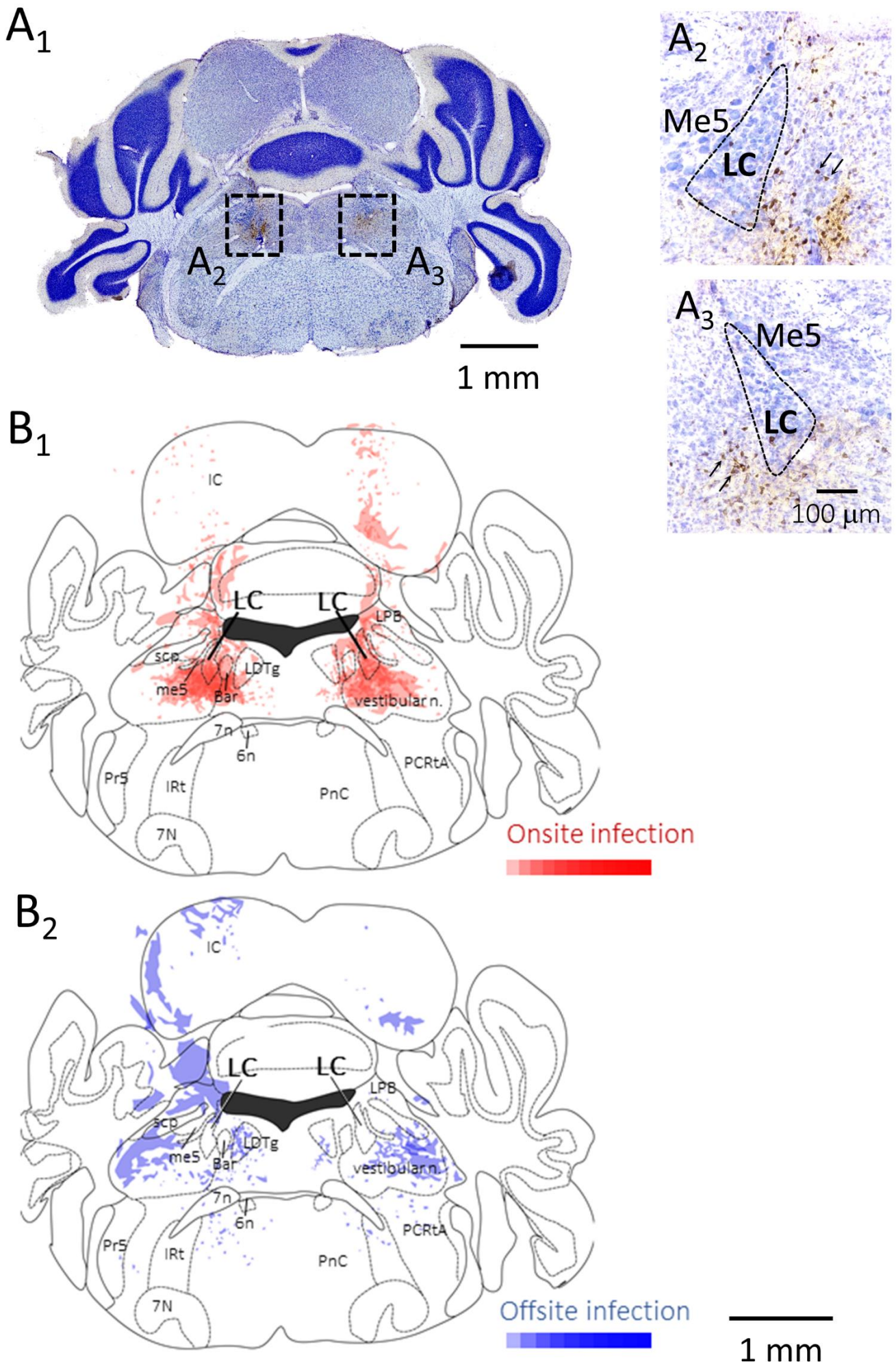
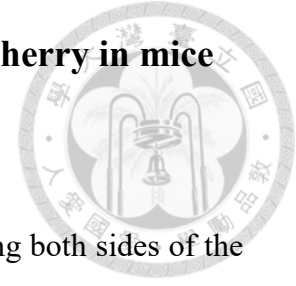


Figure 24

**Figure 24. Bilateral expression profiles of hM4DiR-mcherry in mice involved in behavior task**

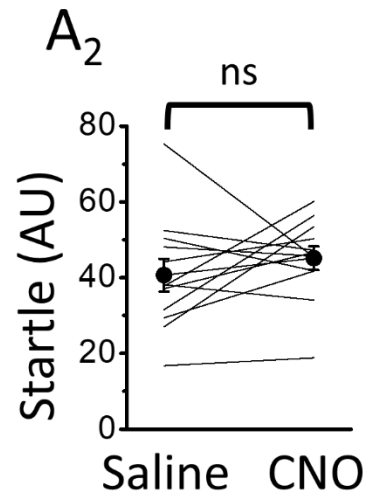
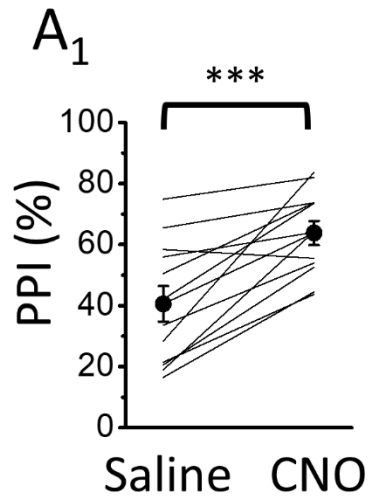


*A*, A representative post hoc IHC shows AAV2 transfection covering both sides of the LC. A1 shows an image of the entire section cut through the pons comprising the LC. The section was stained with anti-mCherry antibodies using DAB as chromagen and the Nissl method. A2 and A3 show a highlighted region comprising the LC as indicated by the dashed squares in A1 at higher magnification. The arrows mark examples of labeled peri-LC I-INs in the medial part of the peri-LC. *B*, Camera lucida drawings show the summarized hM4Di-mCherry expression pattern in this series of experiments. B1 shows the transfection covering both sides of the LC. B2 shows the transfection covering neither side of the LC. The data shown were collected from 12 and 10 animals for B1 and B2, respectively. The trajectory of hM4Di-mCherry expression in 12 animals (red) or 10 animals (blue) is superimposed, and the colors are expressed as a heat chart to indicate the number of times that a given area was transfected by AAV2. The arrangement of heat chart is similar to Fig. 12A and Fig. 17C. Abbreviations: 6n, the 6th nerve; IC, inferior colliculus; IRt, intermediate reticular nucleus; LPB, lateral parabrachial nucleus; Me5, mesencephalic trigeminal nucleus; for other abbreviations, refer to Fig. 12A & 17C. The experiments were performed with Ms. Hsing-Chun Tsai,

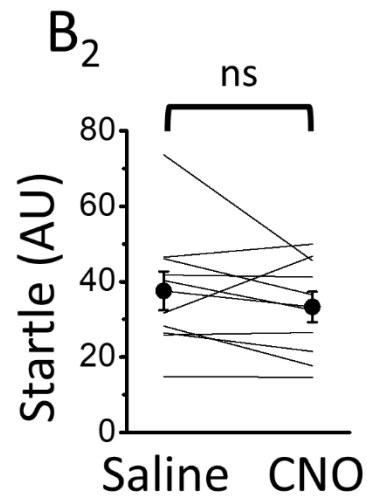
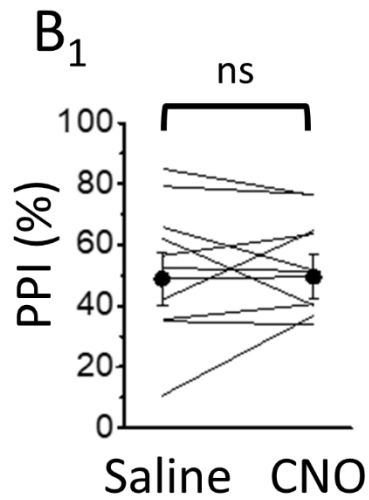
and some of the presented data also formed a part of Ms. Hsing-Chun Tsai's Master thesis (National Taiwan University).



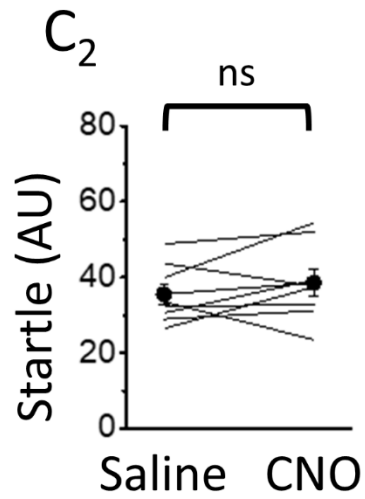
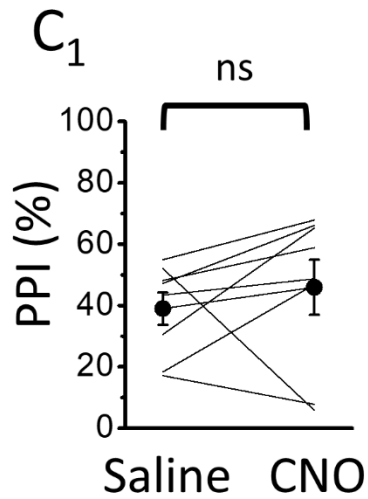
### hM4Di-mCherry<sub>LC</sub>



### hM4Di-mCherry<sub>Offsite</sub>



### mCherry<sub>LC</sub>



### Naïve

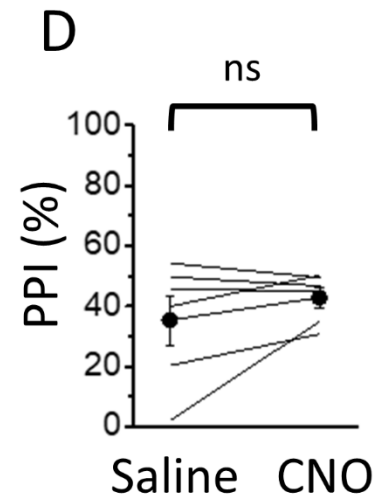


Figure 25

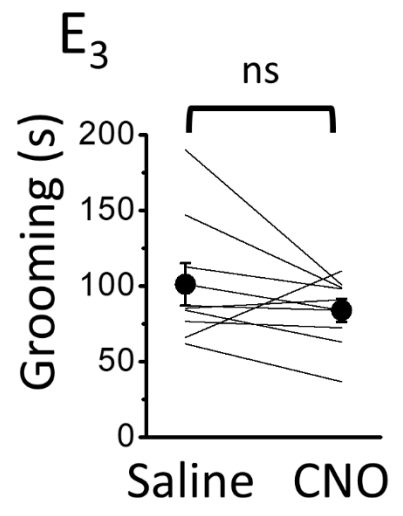
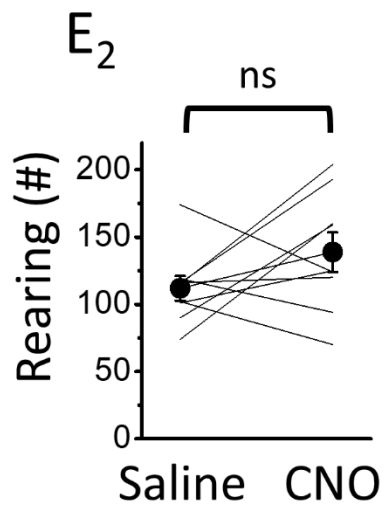
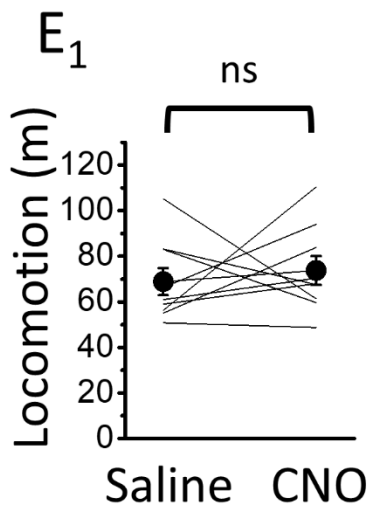
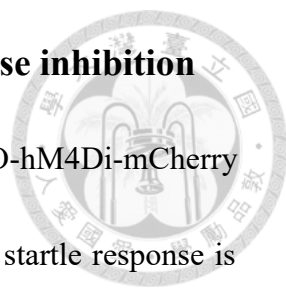


Figure 25

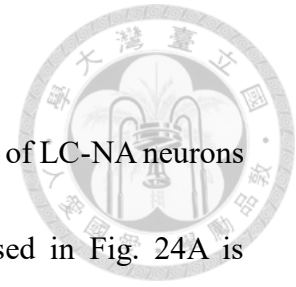
## Figure 25. Inhibition of peri-LC I-INs enhances prepulse inhibition



*A*, Plots show summarized results of behavior tests with AAV2-DIO-hM4Di-mCherry transfections covering the LC. Statistics show that the PPI but not startle response is enhanced by the inhibition of peri-LC I-INs. *B*, Plots show summarized results of PPI and startle with AAV2-DIO-hM4Di-mCherry transfections not covering the LC. *C*. Plots show summarized results from mice that received AAV2-DIO-mCherry transfections. *D*. A plot shows the effect of CNO on PPI results in naïve mice. *E*, General behaviors including locomotion (E1), rearing (E2) and grooming (E3) are not influenced by inhibition of peri-LC I-INs. Note that the significant comparison is observed only in A1, also see Table 6 for statistical information. The lines show the result of an individual experiment, and the filled circles (mean) + capped vertical lines (SEM) show the averaged results. The male *vgat<sup>cre</sup>* mice receiving infusions of AAV2-DIO-hM4Di-mcherry into the LC bilaterally were used. The experiments were performed with Ms. Hsing-Chun Tsai, and some of the presented data also formed a part of Ms. Hsing-Chun Tsai's Master thesis (National Taiwan University).

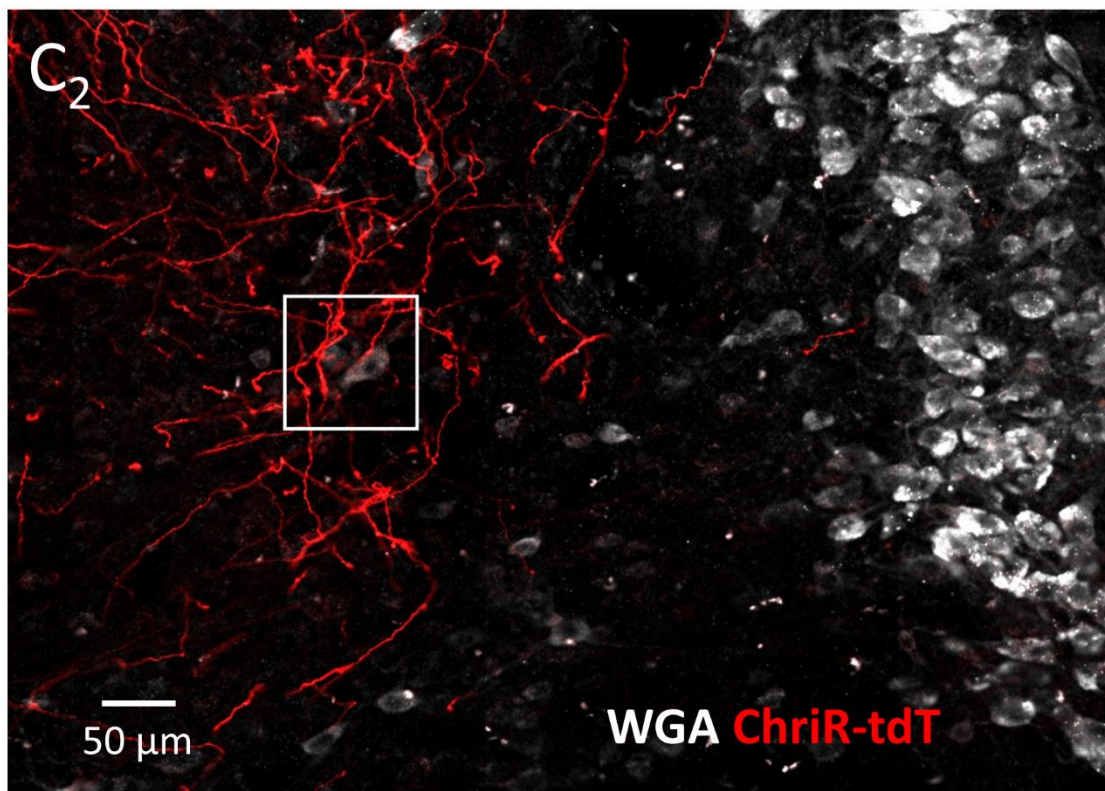
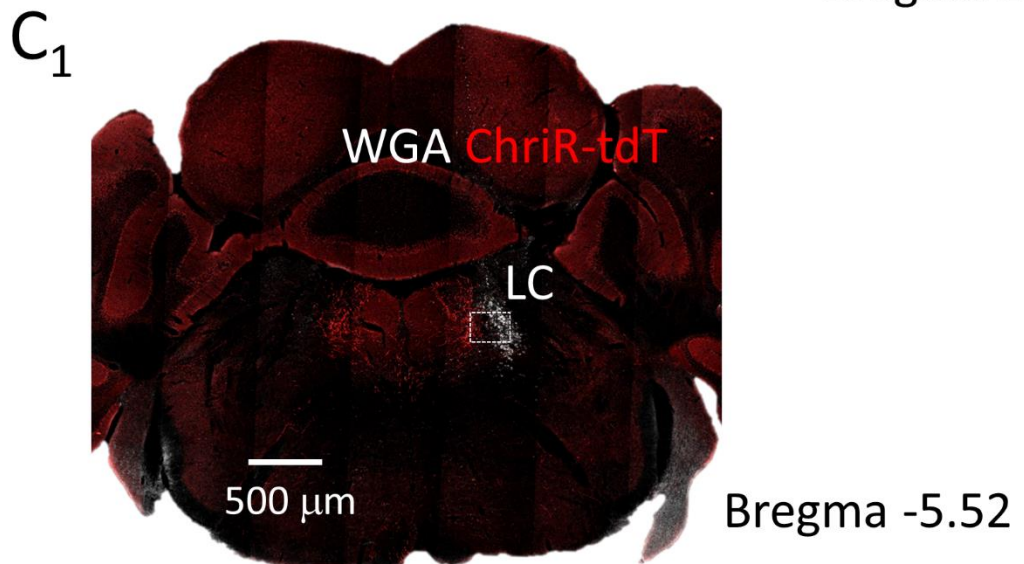
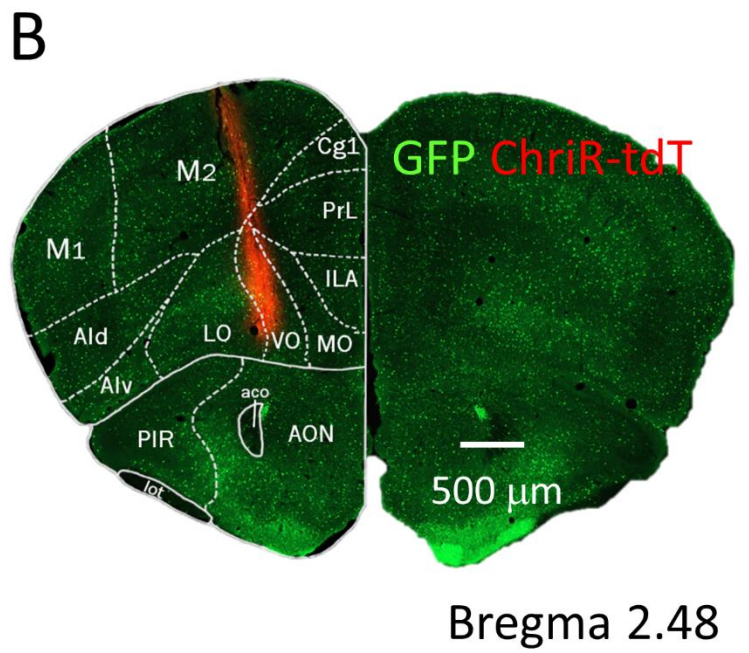
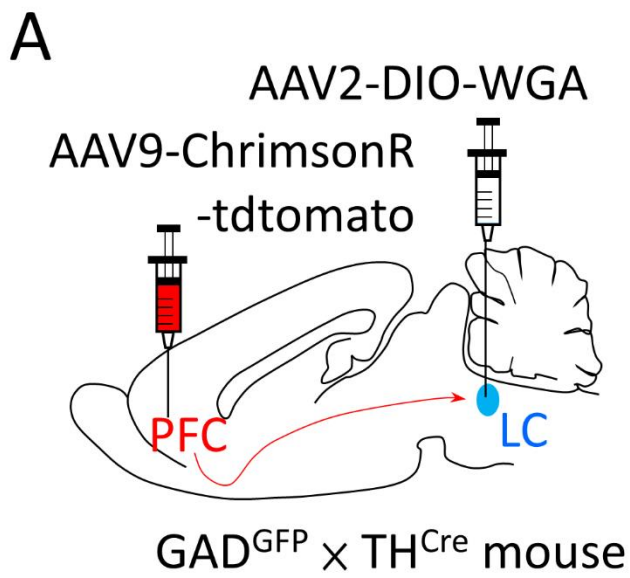


## Figure 26. Effects on PPI are done via LC-NA neurons



**A**, Images from *post-hoc* validation demonstrate the selective lesion of LC-NA neurons by infusion of 6-OHDA. The same protocol of IHC staining used in Fig. 24A is performed. A1 and A2 show the LC with 6-OHDA infusion or vehicle only, respectively.

**B**, Lesion of LC-NA neurons attenuate the positive effect on PPI (B1) and no change in startle response (B2) by the inhibition of peri-LC I-INS. The lines show the result of an individual experiment, and the filled circles (mean) + capped vertical lines (SEM) show the averaged results. The male *vgat<sup>cre</sup>* mice receiving infusions of AAV2-DIO-hM4Di-mcherry into the LC bilaterally and 6-OHDA into the right LC were used. The experiments were performed with Ms. Hsing-Chun Tsai, and some of the presented data also formed a part of Ms. Hsing-Chun Tsai's Master thesis (National Taiwan University).



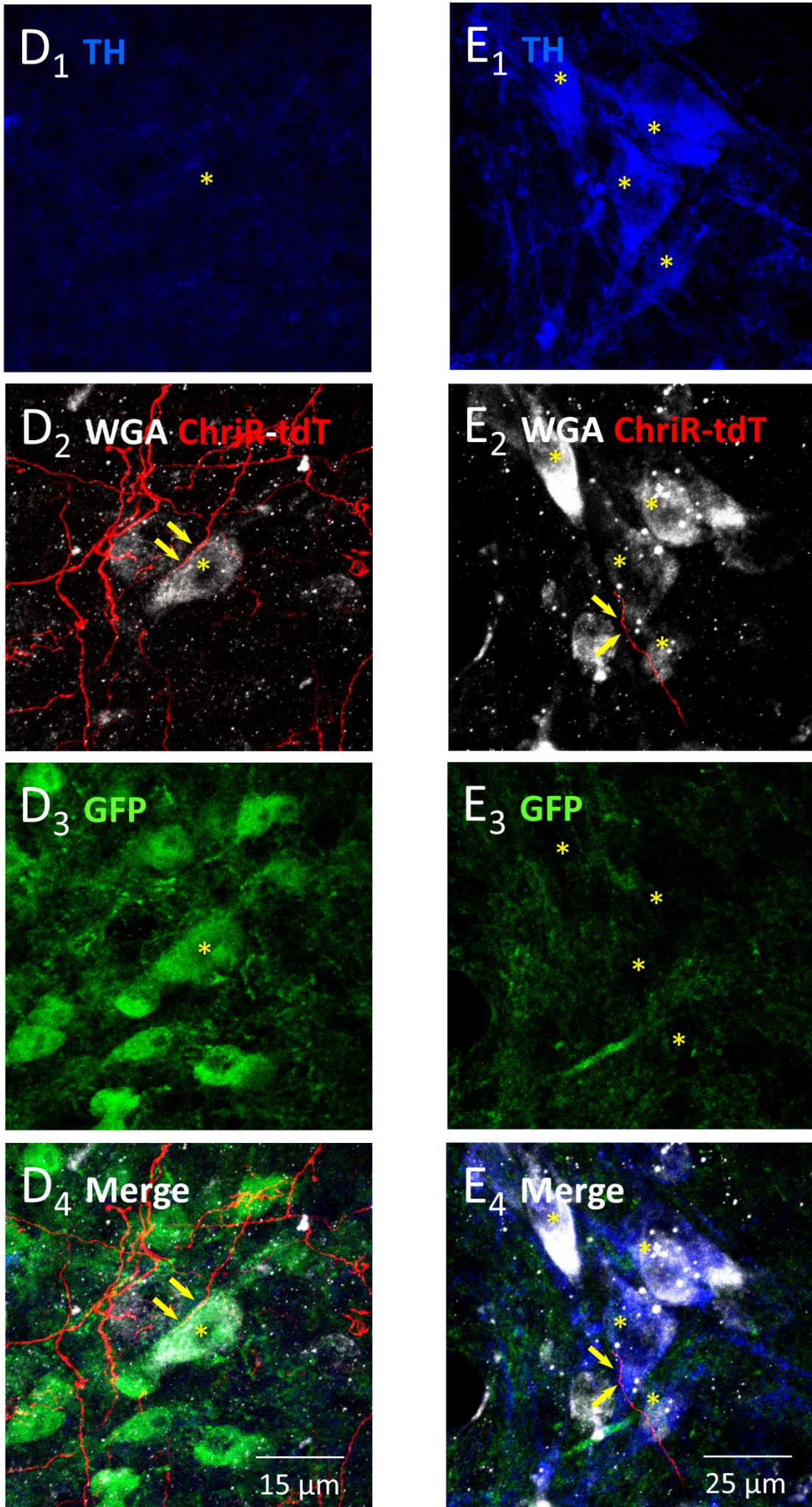
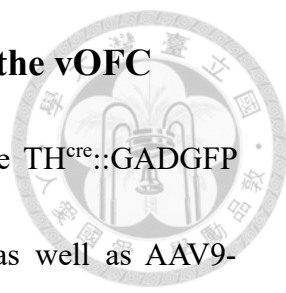


Figure 27

**Figure 27. Peri-LC I-INs receive axonal contacts from the vOFC**



*A*, Schematic diagram shows the experimental arrangements. The TH<sup>cre</sup>::GADGFP mice receiving infusions of AAV2-DIO-WGA into the left LC as well as AAV9-ChrimsonR-TdTomato into the left PFC were used. The target of PFC infusions includes OFCs, PrL and part of M2 according to the stereotaxic coordinates. *B*, A representative experiment shows that AAV9 transfection covered the vOFC and M2. The photograph is a merged immunofluorescent image of GFP (green) and ChriR-tdT (red). The data are from the same experiment in Fig. 30B, as merged immunofluorescent images of WGA (white) and ChriR-tdT (red) in the pontine area. *C*, Fluorescent images show projection pattern from vOFC to the LC. C1 shows the ChriR-tdT labeled fibers in the dorsomedial pons at low magnification (also see Fig. 30B4); C2 shows higher magnification of the LC as indicated by dashed-square in C1. *D*, Images of the same experiment show ChriR-tdT-labeled fibers making contacts with a peri-LC I-IN indicated in C2. The asterisk marks a peri-LC I-IN that showed TH<sup>-</sup> (D1), WGA<sup>+</sup> (D2) and GFP<sup>+</sup> (D3) expression and received axonal contacts from a ChriR-tdT fiber (refer to arrows in D2, D4). *E*, Images show another example of synaptic contacts from vOFC to a LC-NA neuron. The asterisk marks a peri-LC I-IN that showed TH<sup>+</sup> (E1), WGA<sup>+</sup> (E2) and GFP<sup>-</sup> (E3) expression and received axonal contacts from a ChriR-

tdT fiber (refer to arrows in E2, E4). The experiments were performed with Ms. Yu-Shan Kuo, and some of the presented data also formed a part of Ms. Yu-Shan Kuo's Master thesis (National Taiwan University).



A

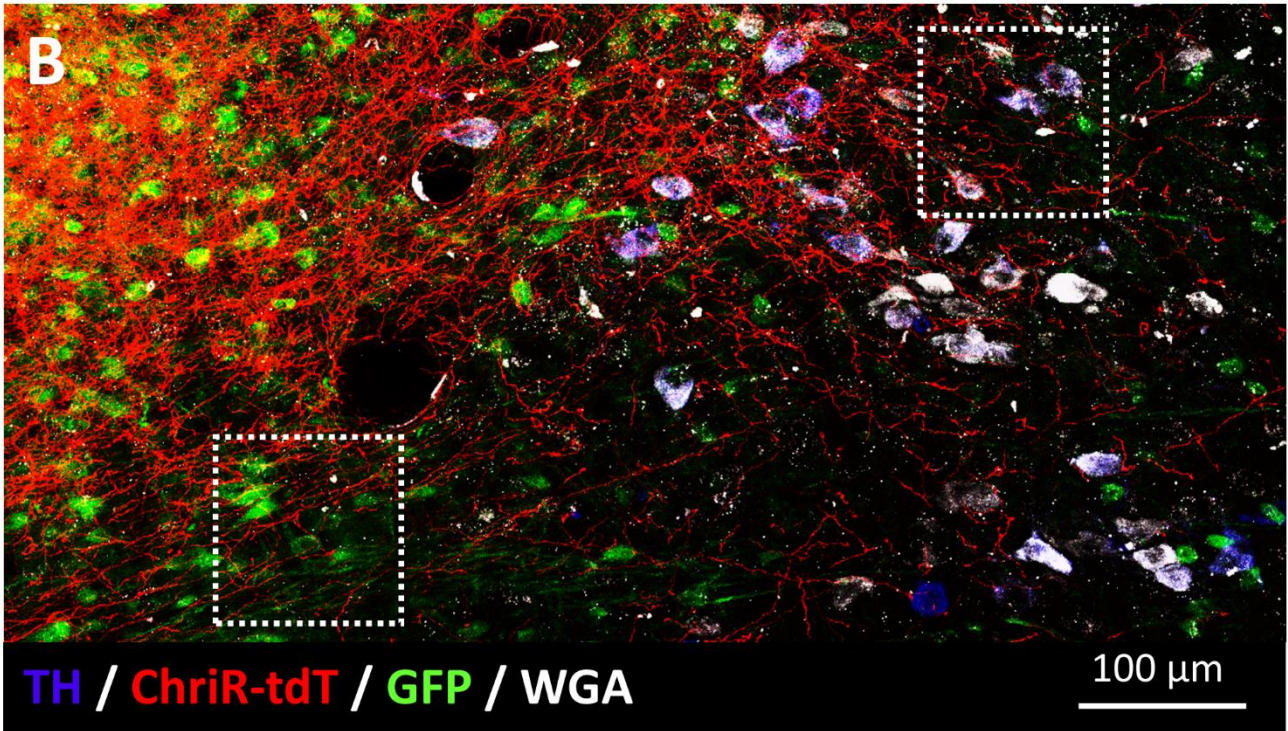
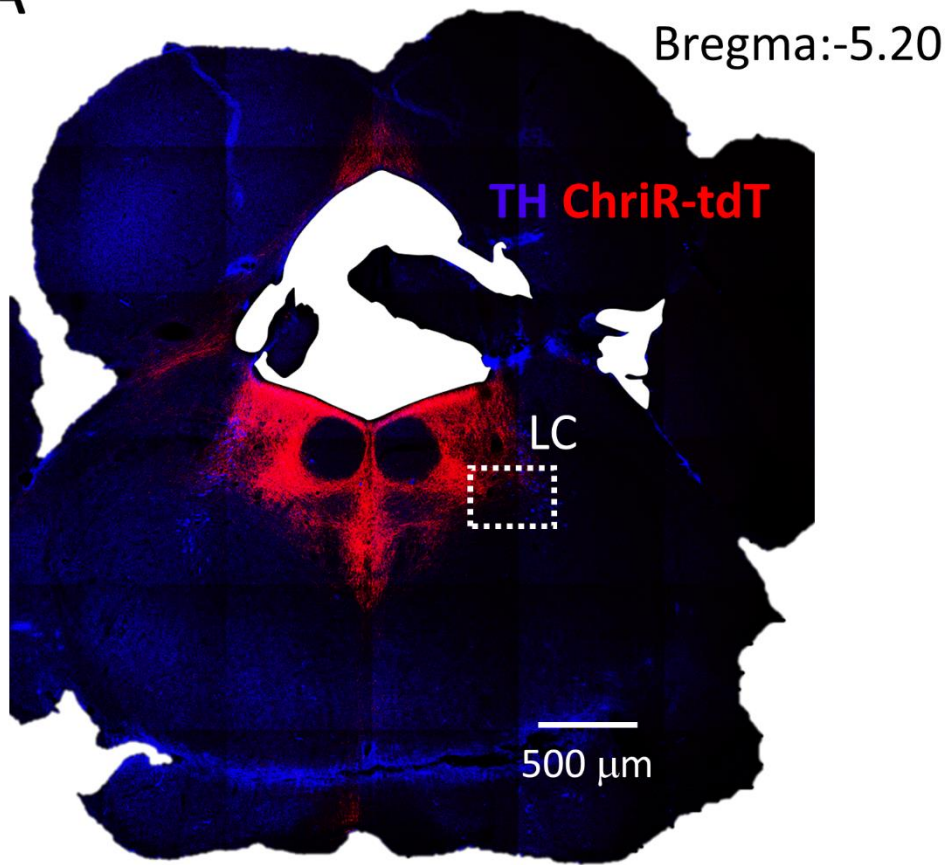


Figure 28

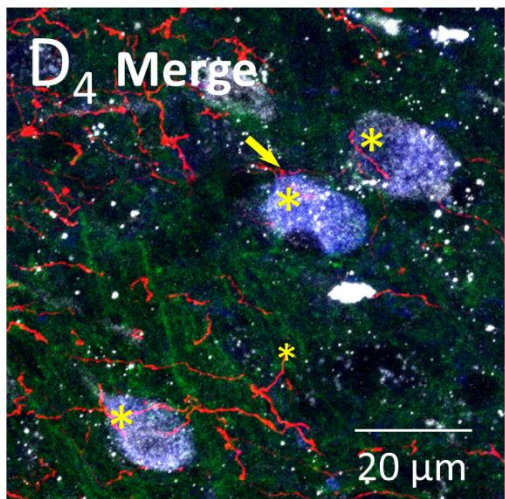
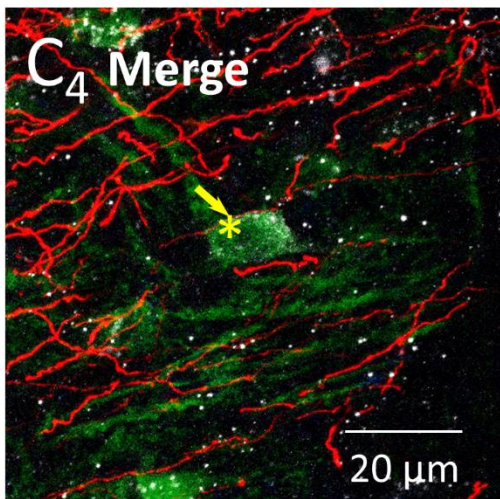
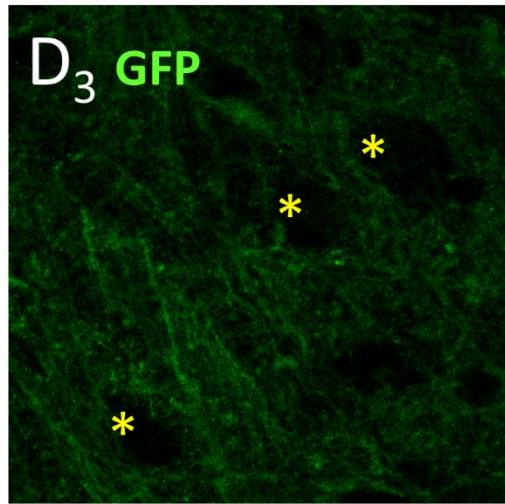
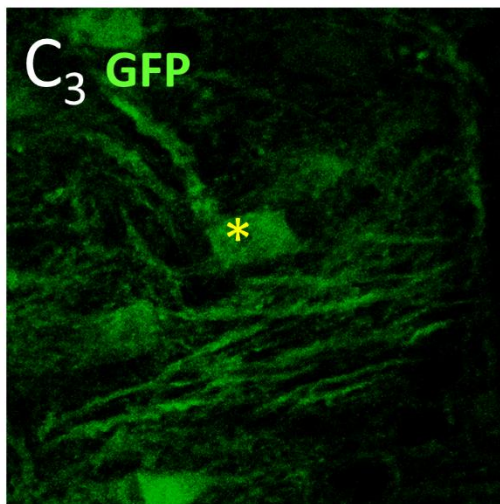
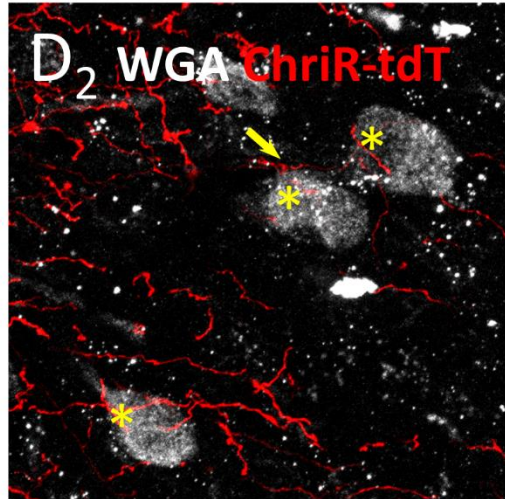
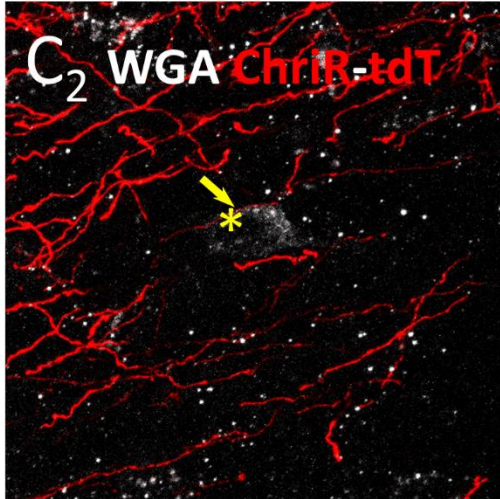
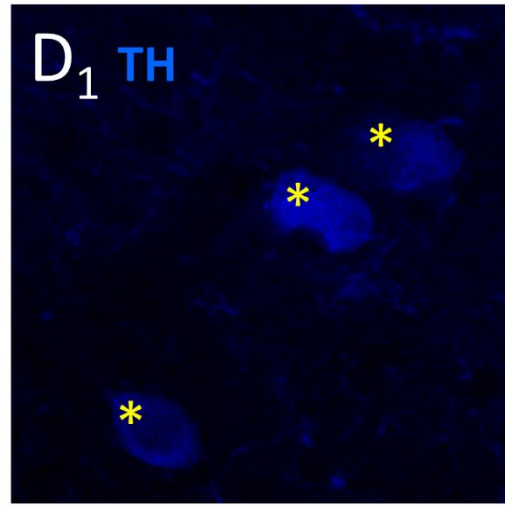
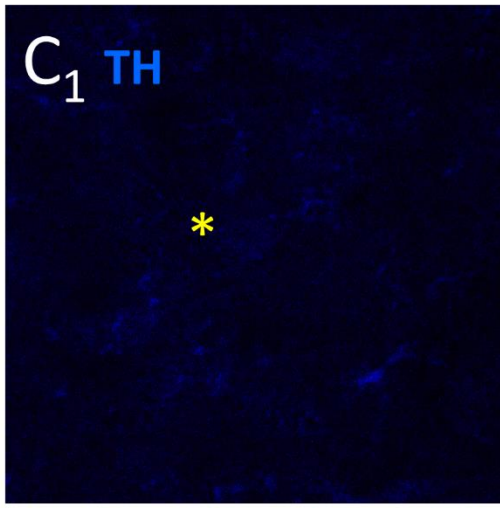


Figure 28

**Figure 28. Peri-LC I-INs receive axonal contacts from the PrL and mOFC**



*A*, A fluorescent image shows an example with the same experimental design shown in Fig. 27A but the AAV is delivered to the PrL and mOFC instead of the vOPC. The TH<sup>cre</sup>::GADGFP mice receiving infusions of AAV2-DIO-WGA into the left LC as well as AAV9-ChrimsonR-TdTomato into the left PFC were used. The photograph is a merged immunofluorescent image of TH (blue) and ChriR-tdT (red). The data are from the same experiment in Fig. 30C as merged immunofluorescent images of WGA (white) and ChriR-tdT (red) in the pontine area. *B*, A fluorescent image show the dashed box indicated in A. Note the extensive projection of axonal fibers from the PrL and mOFC. *C & D*, Images of the same experiment show ChriR-tdT-labeled fibers making contacts with a peri-LC I-IN and some LC-NA neurons indicated in B. The arrangement and labeling follow Fig. 27D & E. The experiments were performed with Ms. Yu-Shan Kuo, and some of the presented data also formed a part of Ms. Yu-Shan Kuo's Master thesis (National Taiwan University).

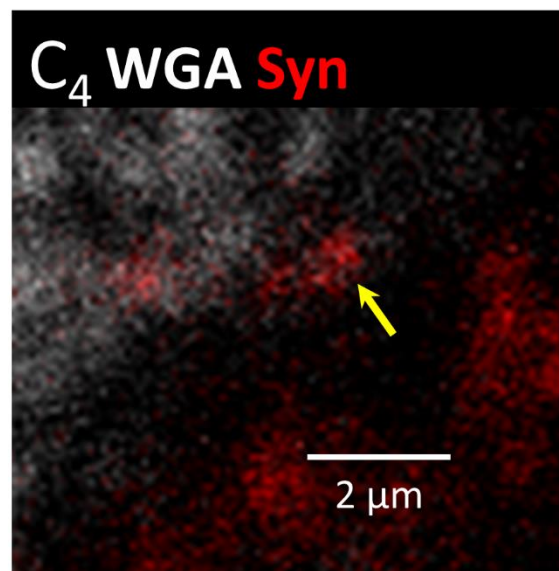
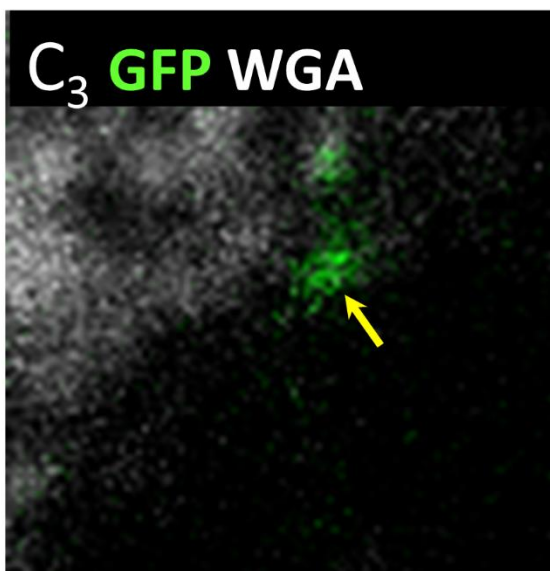
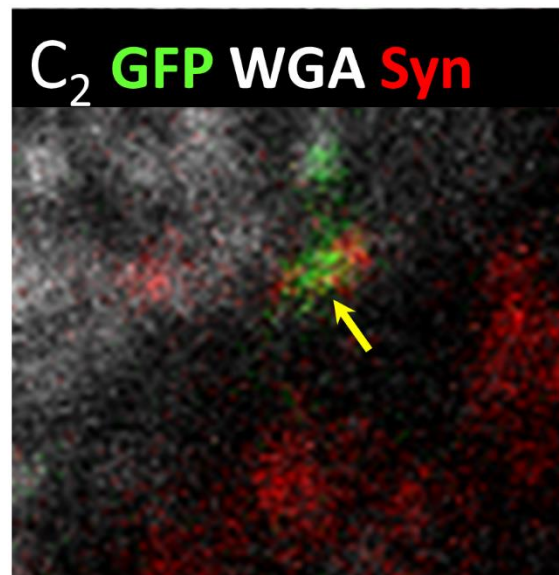
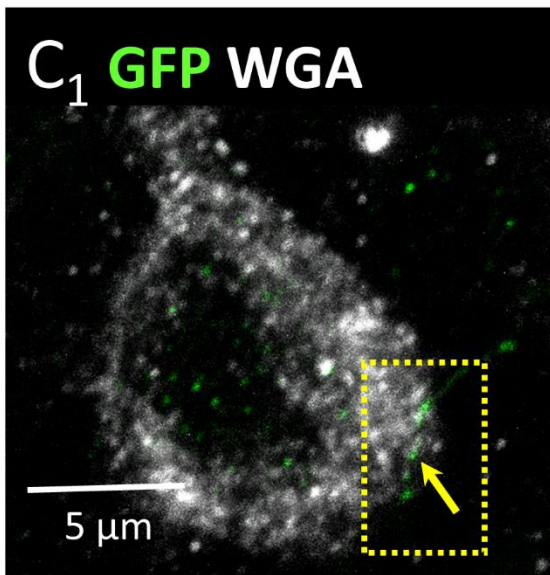
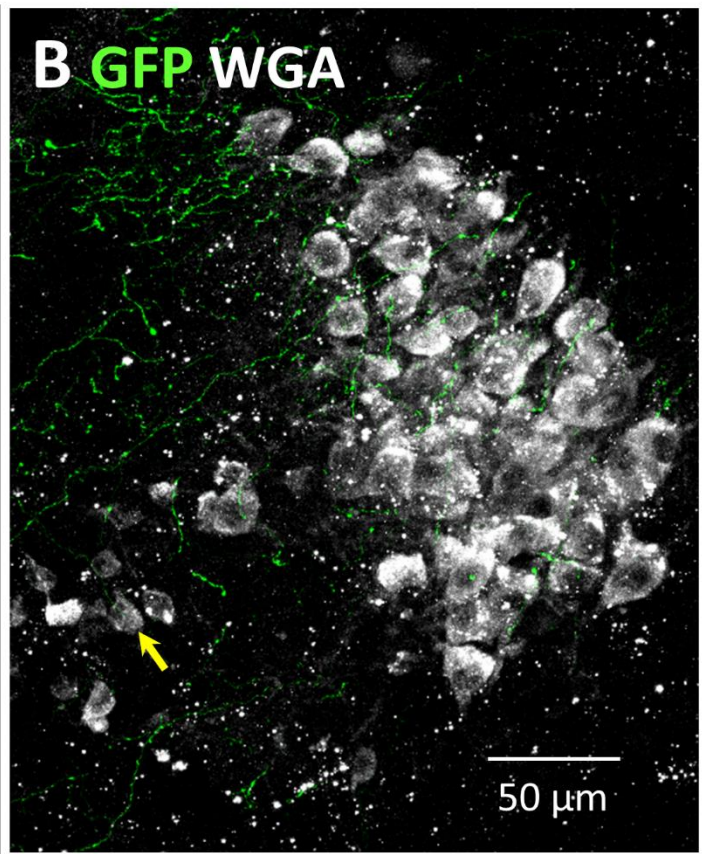
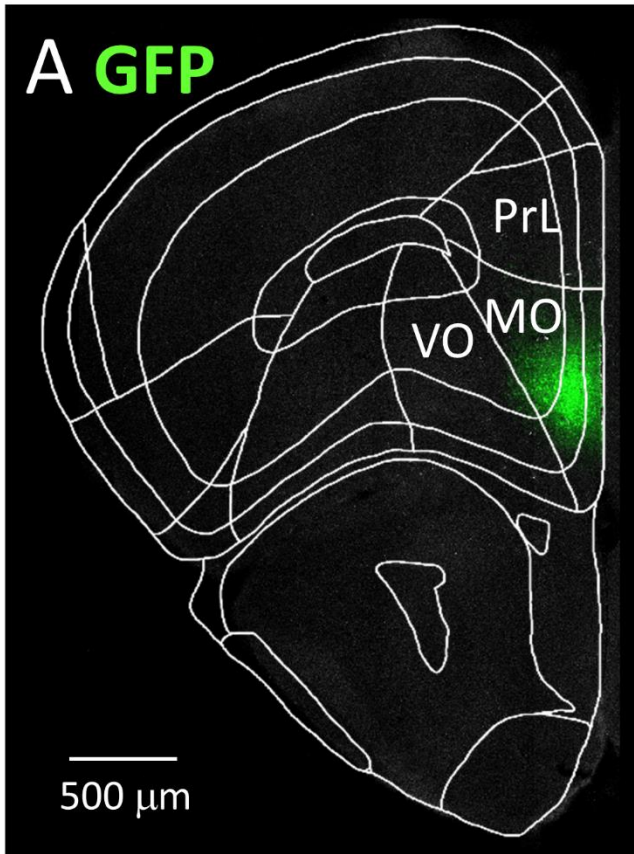
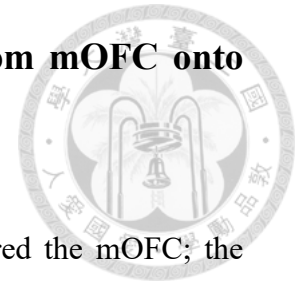
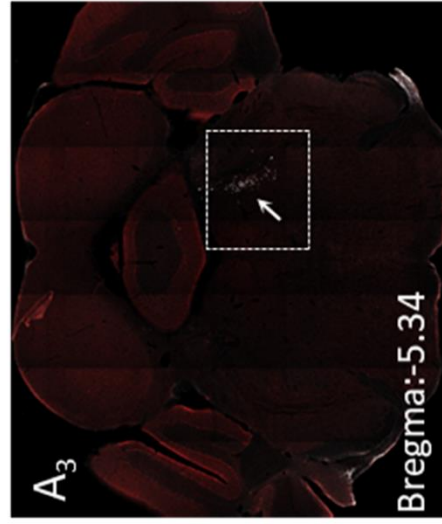
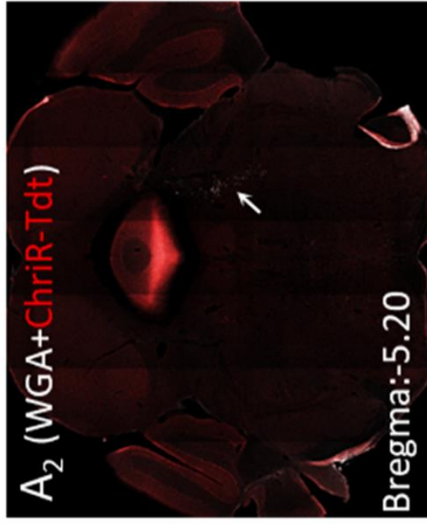
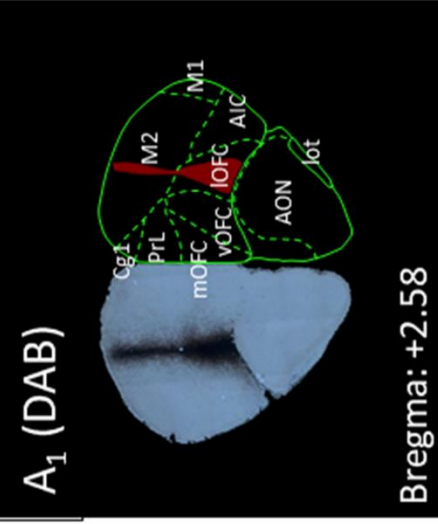
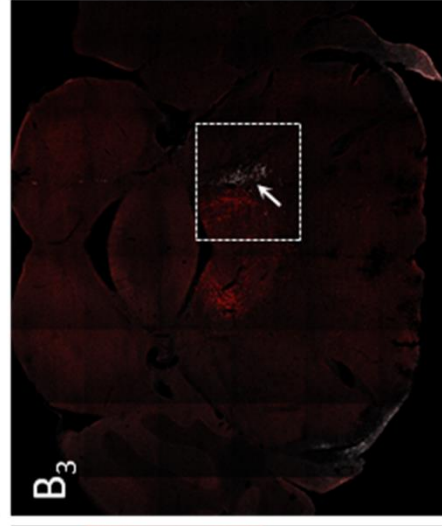
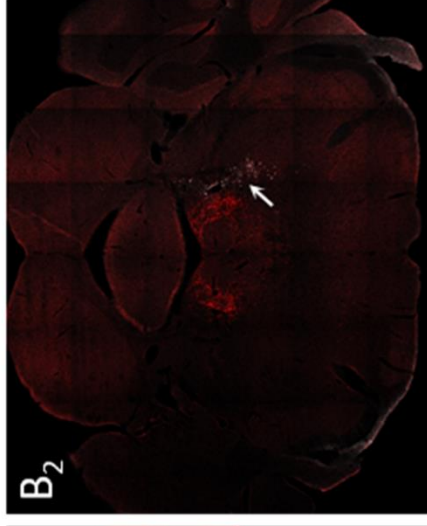
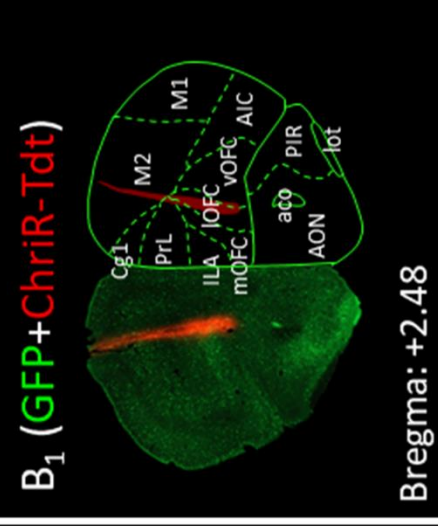
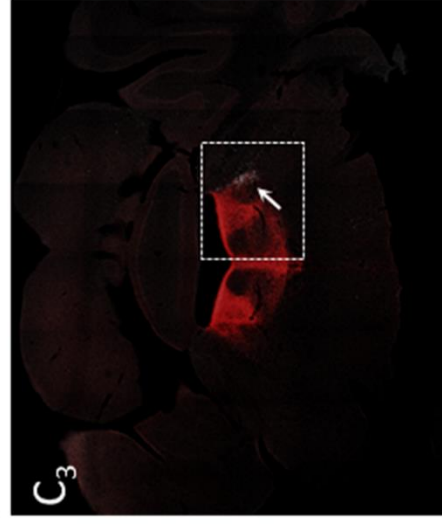
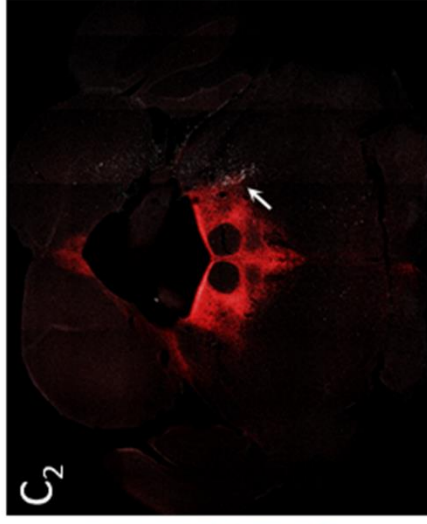
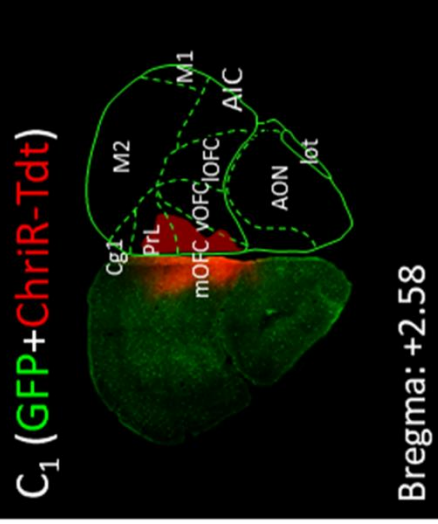
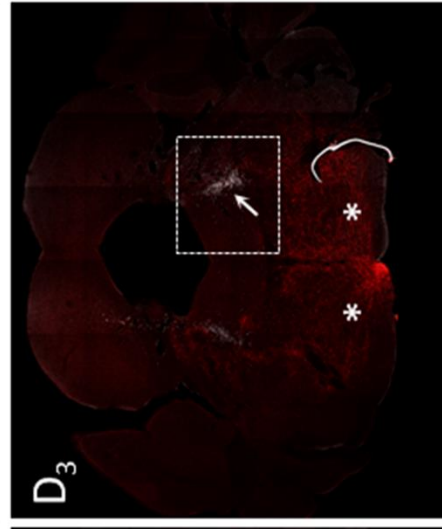
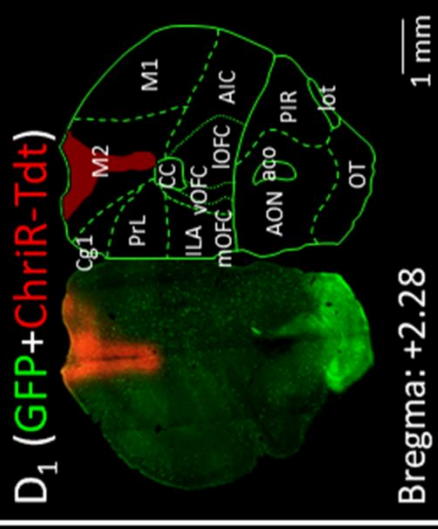


Figure 29

**Figure 29. Confirmation of functional connection from mOFC onto peri-LC I-INs by IHC of synaptophysin**



*A*, A fluorescent image shows that AAV9-GFP transfection covered the mOFC; the territory of virus transfection is shown by the GFP signal (green). The TH<sup>cre</sup> mice receiving infusions of AAV2-DIO-WGA into the left LC as well as AAV9-GFP into the left mOFC were used. ***B & C***, Merged immunofluorescent images of WGA (white) and GFP (green) in the LC and peri-LC from the same experiment shown in *A*. *B* shows WGA-ir LC-NA neurons and INs in peri-LC at low power, the arrow indicates an IN located in the peri-LC with the WGA-ir signal. *C* shows that the same IN receives a functional contact from a GFP-ir fiber at high power (referred to arrow in *C1*). The contact is further enlarged in *C2-C4*. *C3* shows a merged image of WGA and GFP. *C4* shows a merged image of WGA and Syn (*C4*), and *C2* shows a merged image of WGA, GFP and Syn (*C3*). Note the colocalization of Syn-ir and GFP-ir signals in the axonal component forming a close apposition onto the WGA<sup>+</sup> IN. The experiments were performed with Ms. Yu-Shan Kuo.

**IOFC + M2****vOFC + M2****mOFC + PrL****M2**

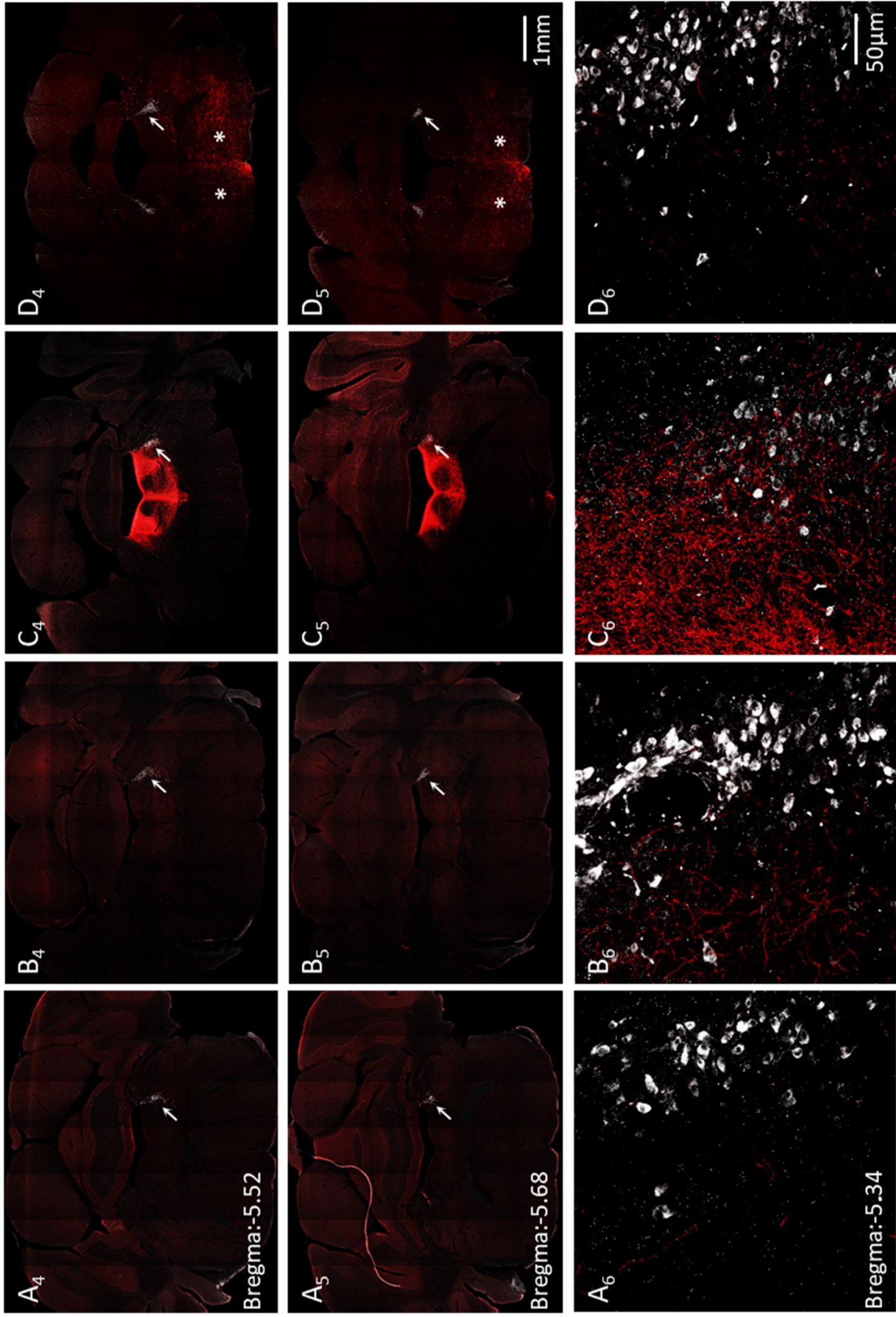
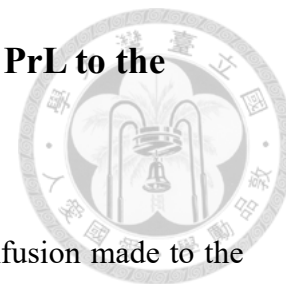


Figure 30

### **Figure 30. Region-specific projections of the OFC and PrL to the dorsal pontine area**



Photographs of Row 1 (A1-D1) show transfection by the AAV9 infusion made to the left OFC/PrL of TH<sup>Cre</sup>×GADGFP mice (left) and the lucida camera drawings (right) according to the Allen Brain Atlas. All photographs shown are a merged immunofluorescent image of GFP (green) and ChriR-tdT (red) with the exception that DAB was used as a chromogen in A1. Photographs of Rows 2-5 show a merged WGA (white) and ChriR-tdT (red) immunofluorescent image in the pontine area at low magnification. The white spot in each photograph marked by arrows shows the location of the LC that consists of a large number of WGA<sup>+</sup> neurons. Dashed-square areas in row 3 are highlighted at higher magnification and shown in Row 6. Columns A-D are representative experiments of AAV9 transfection that covered the lOFC & M2 (A), vOFC & M2 (B), mOFC & PrL (C), and M2 (D). Abbreviations: aco: anterior commissure; AIC: anterior insular cortex; AON: anterior olfactory nucleus; cc: corpus callosum; Cg1: anterior cingulate cortex; ILA: infra-limbic cortex; lOFC: lateral orbitofrontal cortex; lot: lateral olfactory tract; M1: primary motor cortex; M2: secondary motor cortex; mOFC: medial orbitofrontal cortex; OT: olfactory tubercle; PIR: piriform cortex; PrL: prelimbic cortex; vOFC: ventral orbitofrontal cortex. The

experiments were performed with Ms. Yu-Shan Kuo, and some of the presented data also formed a part of Ms. Yu-Shan Kuo's Master thesis (National Taiwan University).



## Section 4



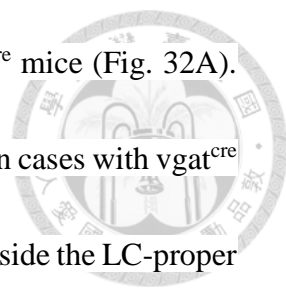
### **Positive Evidence of near LC ENs in Regulation of LC Phasic Activation**

In this section I go back to the LC E-INs. I used the optogenetic and the GCaMP6s calcium imaging techniques for the selective target of a specific population of cells.

The investigation on E-INs of the LC provides preliminary but positive results to support the role of the LC E-INs in recruiting or generating sPLAs. However, further investigation and effort is still required to complete my research.

#### 4.1 Excitatory Connection from near LC E-INs onto LC-NA Neurons

In order to target the E-INs in the LC, *vglut2<sup>cre</sup>* transgenic mice were used. I first checked the expression of the Cre recombinase in cells supposed to be E-INs secreting glutamatergic vesicles via the *vglut2* transporter. As previously displayed, cross-mating of *vglut2<sup>cre</sup>* and normal Cre-reporter mice showed a high co-localization of the TH and reporter protein in LC-NA neurons, raised an issue of the genetic lineage of the *vglut2* gene in embryonic LC-NA neurons (Verstegen et al., 2017). Therefore, I refused the usage of reporter mice in my experiments. As the AAV infusions to the *vgat<sup>cre</sup>* mice, the AAV2-DIO-mcherry was injected into the LC of adult *vglut2<sup>cre</sup>* mice of 5-6 weeks old (Fig. 31A). When the mcherry expressing territory covered the LC proper (four hemispheres from two mice), an opposite result was obtained using the IHC as a very little population of TH<sup>+</sup>/mcherry<sup>+</sup> LC-NA neurons. The cell population with the colocalization shows an average of three cells ranging from 0 – 6 for each hemisphere (Fig. 31B, C; 4 hemisphere from 2 mice). As I showed the auto-flipped Cre function in the control experiments with the same AAV, the contamination of Cre expression was too little to interfere in my experiment (Fig. 17B).

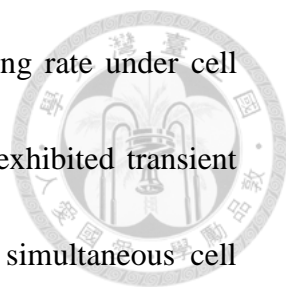


Next, I infused the AAV2-ChR2-eYFP into the LC of *vglut2<sup>cre</sup>* mice (Fig. 32A). The *Post hoc* IHC showed different patterns when compared to that in cases with *vgat<sup>cre</sup>* mice but shared a common feature of fewer non-noradrenergic INs inside the LC-proper (Figs. 9C; 32B). The extensive expression in the Me5, LdTg, and other areas depending on the infusion target, reflected the heterogeneity of eYFP<sup>+</sup> cells including excitatory neurons of the adjacent nuclei and putative LC E I-INs, so a better way was to introduce a mouse line with *vglut2* promoter driven fluorescence for the compatibility of the viral WGA tracing experiments. Theoretically, all of excitatory cells with spontaneous firing and functional contacts onto LC-NA neurons could be necessary for driving the sPLA. In order to prevent the omission of possible origin of the sPLA, I pooled these excitatory neurons as LC E-INs (or simply E-INs) regardless which nuclei they belonged to. In brain slices with E-INs expressing ChR2-eYFP, a single blue light illumination evoked an EPSC in LC-NA neurons, which was subsequently blocked by adding DNQX plus AP5. The complete suppression of light evoked EPSCs showed the glutamatergic transmissions from presumed E-INs expressing ChR2 onto LC-NA neurons (Figs. 32C, D). The mean latency of the EPSC was about 2ms ( $2.07 \pm 0.06$  ms,  $n = 9$  cells; Fig. 32E) with a small variation, indicated a monosynaptic contact, however, additional experiments are required to confirm this monosynaptic connection as shown in Fig. 10.

The paired pulse of light illuminations caused a paired EPSCs with the PPR of  $0.87 \pm 0.14$  ( $n = 8$  cells) with a considerable variation (Fig. 32F, G). Together, my results confirm the functional connection from local E-INs onto LC-NA neurons by using glutamatergic transmissions.

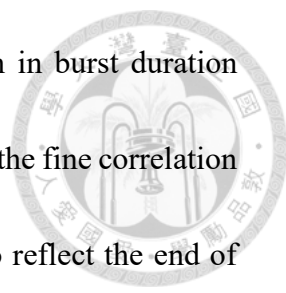
## 4.2 Spontaneous Activity of LC E-INs

Despite the functional contact, E-INs must exhibit spontaneous firing if they participate in the generation of the sPLA. In regard of the mass and heterogeneity of E-INs, I introduced the calcium image technique for a quick selecting and screening of active E-INs in the brain slice (Fig. 33A). The GCaMP6s protein, a potent calcium indicator, was expressed in E-INs by transfections of the AAV5-DIO-GCaMP6s bilaterally infused into the LC of *vglut2<sup>cre</sup>* mice (Figs. 33C, D). Numerous E-INs exhibited the GCaMP6s signal in normal aCSF condition and were supposed to actively fire APs. Many of active E-INs were resistant to the application of 2.5mM Kynurenic acid (KA), a competitive antagonist of AMPA and NMDA receptors, showing that they could intrinsically generate APs. Interestingly, I observed two types of E-INs by the distinct pattern of calcium activity in the presence of KA. First, cells with constant GCaMP6s activities typically belonged to the tonic firing or non-burst E-INs, which



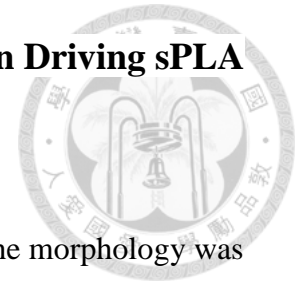
were exhibiting continuous AP firing with fluctuations of the firing rate under cell attachment recording (Fig. 33C-E). Second, cells that repeatedly exhibited transient flashes of the GCaMP6s signal were classified as burst E-INs, simultaneous cell attachment recordings showed repeated bursts in about 20-80 Hz of the AP firing correspondent to the fluorescent flashes (Fig. 31C, D, F). In addition to the soma, dendrites with GCaMP6s signals also showed identical patterns that were likely due to the back propagation of spontaneous APs from the soma at different focus plane. Hence, the dendrite with fluorescent signals were counted as statistic units in further analysis (Fig. 33D). The raw video of Fig. 33D demonstrates a lucky example that an intact back propagated AP occurs in soma and proximal dendrite.

The burst E-INs served as a potent candidate in driving the sPLA because of the spontaneous transient activation. I further analyzed the detailed timing relationship of the bursts and the correspondent GCaMP6s fluorescence (Fig. 33A, B). The fine alignment showed that the first AP in a burst from E-IN always occurred prior to the detection of the meaningful fluorescent rising, this time delay for fluorescent detecting was  $0.12 \pm 0.02$  s ( $n = 7$  cells, Fig. 34C) and the mean duration of bursts was  $1.57 \pm 0.60$  s, ( $n = 7$  cells, Fig. 34D). The low variation underlying the detecting latency allowed

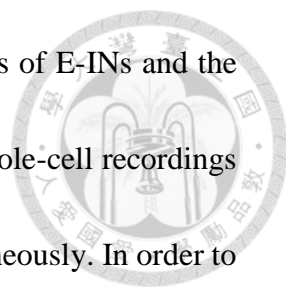


us to monitor the burst activity in E-INs, while the high variation in burst duration reflected the heterogeneous composition of the burst E-INs. Though the fine correlation with the beginning of E-IN bursts, the fluorescent activity failed to reflect the end of bursts. My results showed a long lasting plateau of fluorescence after a burst generated (Fig. 34A). As for the fine alignment, I was able to monitor the activity across the corpious E-INs in brain slices simultaneously without any pipette recording. However, I failed to record stable bursts under whole-cell recordings onto the burst E-INs, as this may be due to the diffusion of ion concentrations or essential molecules, such as the cAMPs for the hyperpolarization-activated cyclic nucleotide-gated (HCN) channel, which maintain the rhythmic pace-making in the sinoatrial node of heart and some neurons (Fig. 33G). Thus increasing the difficulty on the investigation of the channel composition on the burst E-INs enabling the pace making feature. I believe that the clear dissection of this putative critical channel is a crucial step for further understanding the role of LC E-INs.

### 4.3 Preliminary but Positive Evidence of Burst E-IN in Driving sPLA in LC-NA Neurons

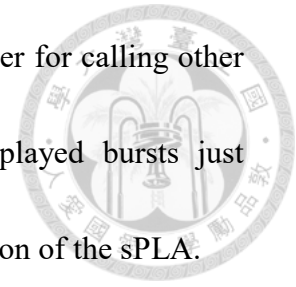


After the 6 cases of whole cell recordings on the burst E-INS, the morphology was reconstructed by the *post hoc* DAB staining (Fig. 36A, F). One case out of five brain slices demonstrated two recoded E-INS displaying some local axon projections covering a limited space inside the LC-proper (Fig. 36B, C). Even though lacks counter stain for identifying the LC, the adjacent large soma with dense assembly and a transparent appearance, as well as the online phase contrast photo at lower magnification showed the inside-LC location of the recorded E-INS (Fig. 36 B-E). Some of the bouton-like, swollen structures were found along the axons and formed close appositions to the large cells in the LC-proper, supposed to be candidates of synaptic contacts (Fig. 36G). The results provided positive evidence of the local innervations from burst E-INS onto LC-NA neurons. Nevertheless, more experiments are required to confirm the functional connection, and the best way here is to perform this with the electron microscope for a solid judgment of the functional contact from the LC burst E-INS.



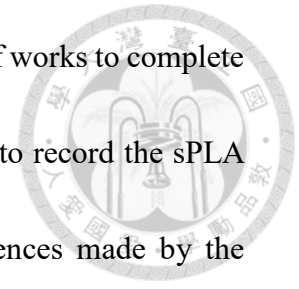
Finally, I tested the relationship between the spontaneous bursts of E-INs and the sPLA in the principle neurons. Therefore, I performed V-clamp whole-cell recordings on LC-NA neurons and monitored the activity of the E-INs simultaneously. In order to increase the incidence of sPLAs, 1  $\mu$ M Stry and 100  $\mu$ M picrotoxin, an antagonist of GABA<sub>A</sub> receptors, were perfused into the recording bath. My data showed the difficulty in pairing the sPLA and E-INs' activity as most of the bursts failed to trigger fast EPSCs or large sEPSCs, which indicated the low or weak connection rate from E-INs onto LC-NA neurons, or may be due to the necessity of synchronous bursts among E-INs for the sPLA generation. Moreover, my video lasted only 100-300 seconds, so the sPLA had not occurred in many recording traces (see the coincidence of the sPLA in Table 4), only one out of six cells from six slices among attempts using 10 mice showed some positive results (Fig. 35A). In this case, many cells fired bursts in high correlation to the large sEPSC, but most of them showed their burst just after the large sEPSC onset and were supposed not to be the executor of the sPLA. In contrast, there were two ROIs containing two dendrites displayed bursts which were just prior to the large EPSCs, showing about 300-400 ms in calculation of the large EPSCs latency from the supposed onsets of the bursts firing, except that only one burst was located near the onset of a large EPSC (Fig. 35B). The long latency implied that the given E-INs may not be the

direct synaptic source to start the sPLAs, but could act as a recruiter for calling other cells behaving as executors of the sPLA. For those cells displayed bursts just proceeding the large EPSCs, as they may contribute to the summation of the sPLA.



As the large sEPSC shown in Fig. 3, the sPLA was likely composed by the EPSCs in a high temporal summation if the LC E-INs could generate the sPLA. And the cell attachment recordings on burst E-INs showed 20-80Hz AP firings within a burst. Therefore, I performed the optogenetic experiments again as aforementioned (Fig. 32). The light stimulation protocol was adjusted into trains at high frequency aiming to test the capability of E-INs for driving the LC phasic activations. In the V-clamp configuration, 20 light pulses at 20 or 50 Hz resulted in a compound EPSC similar to the intact large sEPSC (Figs. 3B; 37A, B), when switched to the I-clamp condition, 10 light pulses at 20Hz was enabled to evoke a phasic activation followed by a silent period resembling the natural LC phasic activation (Fig. 37C, D). The conceptual experiments demonstrated that the burst activity of LC burst E-INs was able to trigger phasic activations in LC-NA neurons. However, I cannot exclude those excitatory neurons that exhibit silent activity in brain slices. A further experiment selectively manipulating the burst E-INs is required. Together, my work has offered a preliminary result in roles of

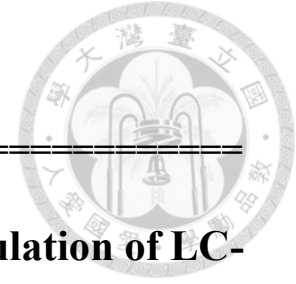
LC E-INs onto the generation of sPLAs. However, it remains a lot of works to complete for my investigation, as some of the critical experiments could be to record the sPLA in vitro or monitor the LC activity in vivo, as to see the differences made by the manipulations of the neural activity of the E-INs.



# Figures

---

---



## Section 4: Possible Role of near LC ENs in Regulation of LC-NA Neurons Using Calcium Imaging

Figure 31. Targeting excitatory neurons near LC using *Vglut2<sup>cre</sup>* mice-----209

Figure 32. Functional glutamatergic connections from LC E-INs onto LC-NA neurons-----211

Figure 33. Calcium imaging using GCaMP6s indicator demonstrates two groups of LC E-INs-----213

Figure 34. Simultaneous alignment of spontaneous burst and calcium activity in burst LC E-INs-----217

Figure 35. Preliminary results in alignment of burst related calcium activity in E-INs and large sEPSC in LC-NA neurons-----219

Figure 36. Reconstructed morphology of E-INs shows an evidence of synaptic contacts onto LC-NA neurons-----221

Figure 37. Train of optical stimulations on LC E-INs can evoke phasic activations in LC-NA neurons-----224

---

---

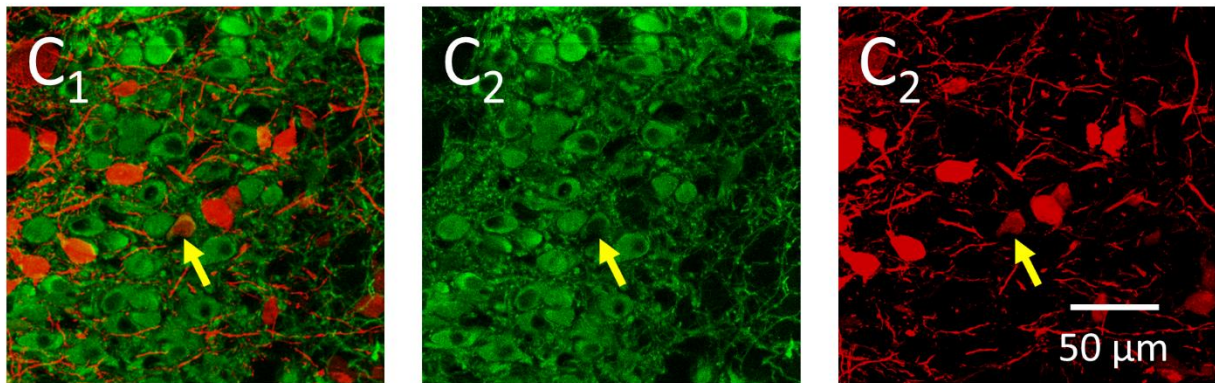
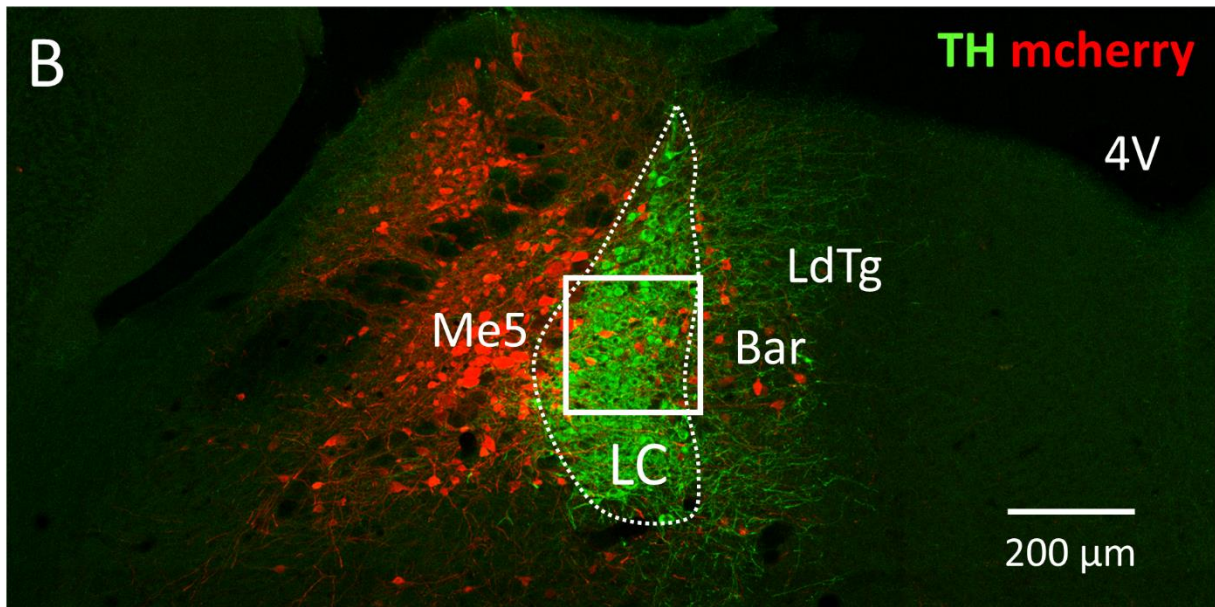
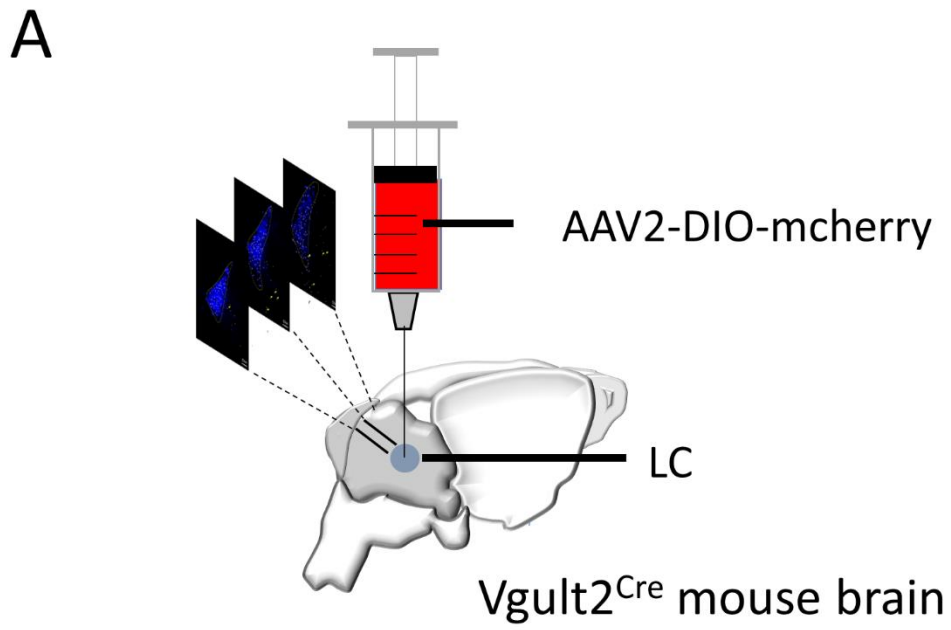
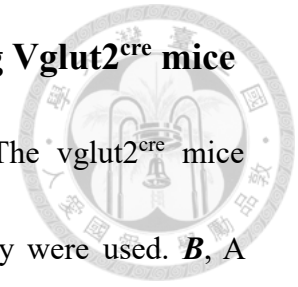


Figure 31

**Figure 31. Targeting excitatory neurons near LC using Vglut2<sup>cre</sup> mice**

*A*, Schematic diagram shows the experimental arrangements. The vglut2<sup>cre</sup> mice receiving infusions of AAV2-DIO-mcherry into the LC bilaterally were used. *B*, A representative image shows a merged immunofluorescent image of TH (green) and mcherry (red) in the dorsal pontine area at low magnification. Note many mcherry<sup>+</sup> glutamatergic neurons located near the LC. *C*, Signals of TH-ir and mcherry-ir exhibit a low possibility of fluorescent co-localization. Images show the box region in *B* as fluorescent profiles of TH (*C2*), mcherry (*C3*) and the merged image (*C1*). The arrow shows a LC-NA neuron with both TH-ir and mcherry-ir signals.



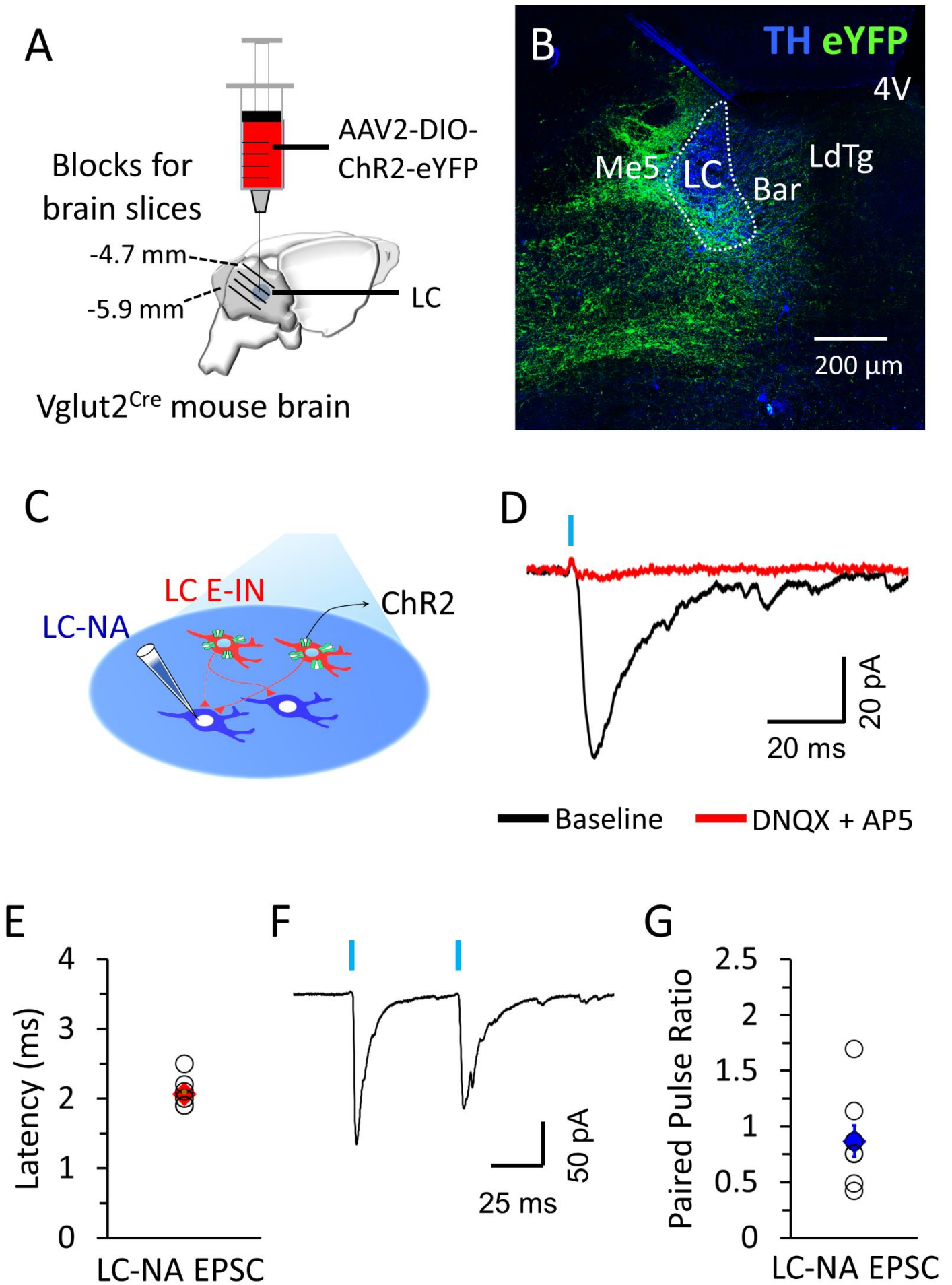


Figure 32

**Figure 32. Functional glutamatergic connections from LC E-INs onto LC-NA neurons**



*A*, Schematic diagram shows the arrangement of experiments. The *vglut2<sup>cre</sup>* mice receiving infusions of AAV2-DIO-ChR2-eYFP into the LC bilaterally were used. *B*, Representative fluorescent image shows post hoc IHC that validates ChR2-eYFP expression near the LC-proper. Note that ChR2-eYFP<sup>+</sup> neurons are located in nearby nuclei, including Bar, Me5 and LdTg. *C*, Schematic diagram shows the experimental arrangements of optogenetics. *D*, Photostimulation of the slice, as indicated by the blue rectangle, evoked EPSCs in the LC-NA neuron. The evoked EPSCs are further blocked by application of DNQX plus AP5. *E*, A plot summarizes the onset of evoked EPSCs from the light pulses (*n* = 9 cells obtained in 3 slices from 2 mice), *F & G*, Paired EPSCs evoked by two light pulses (interval = 50 ms) show the paired pulse ratio of the synaptic transmission. *F* demonstrates a representative trace and the summarized results are shown in *G*. In *E* and *G*, each circle in the plots presents result from a neuron, the diamond (mean) + capped vertical lines (SEM) show the averaged results.

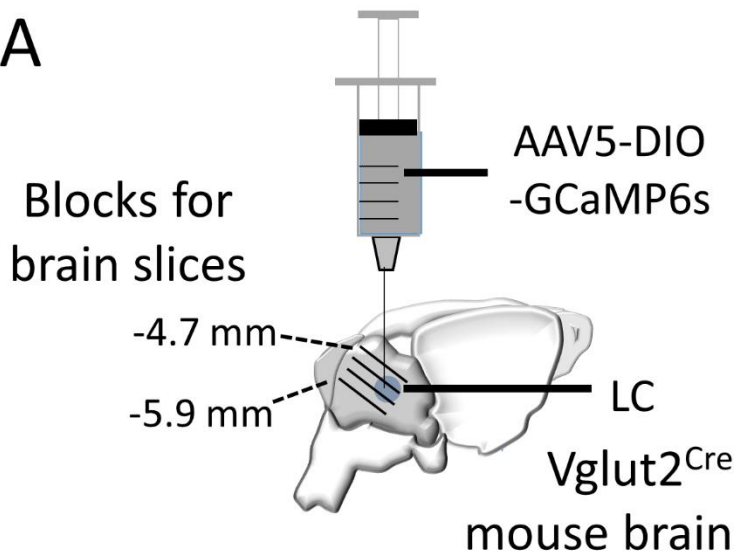
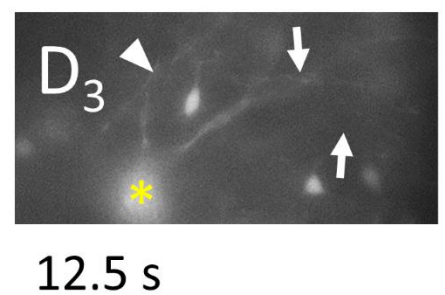
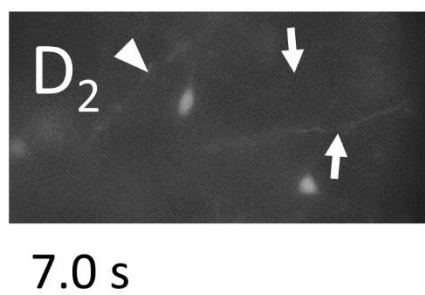
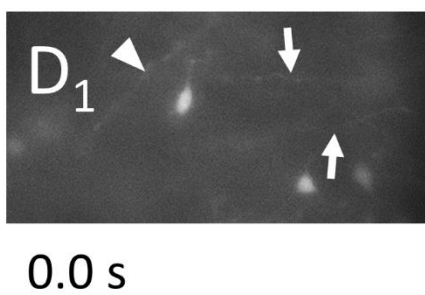
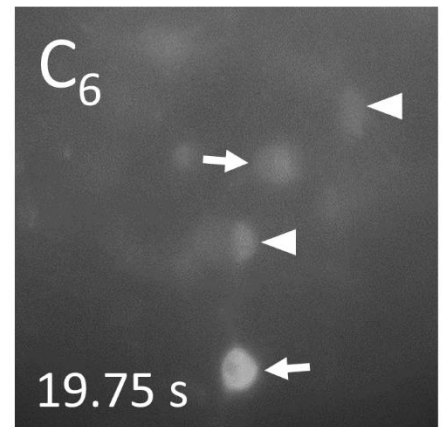
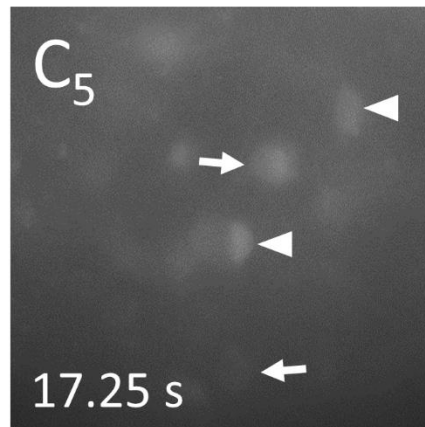
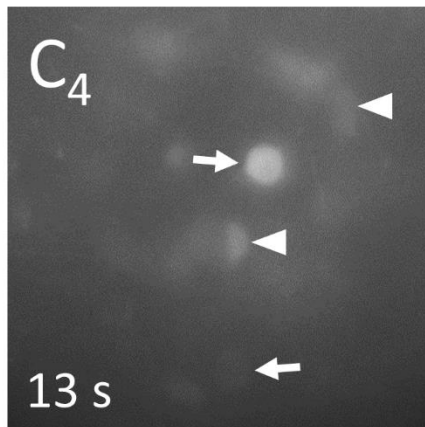
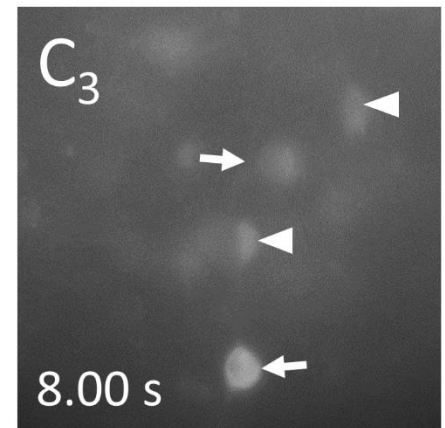
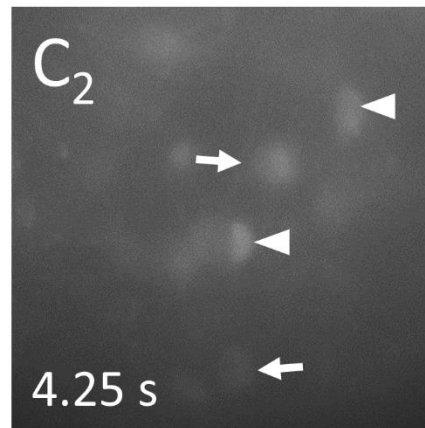
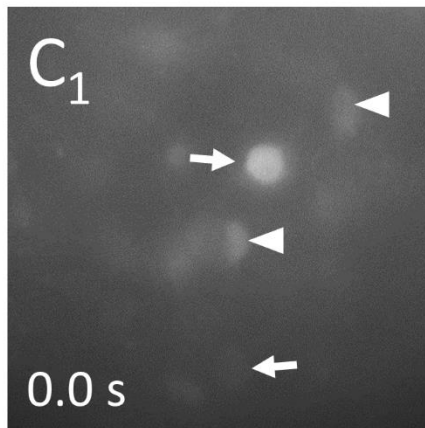
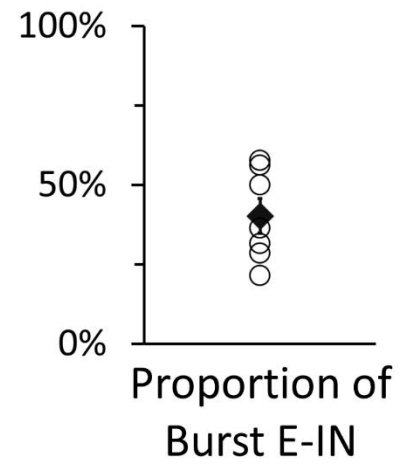
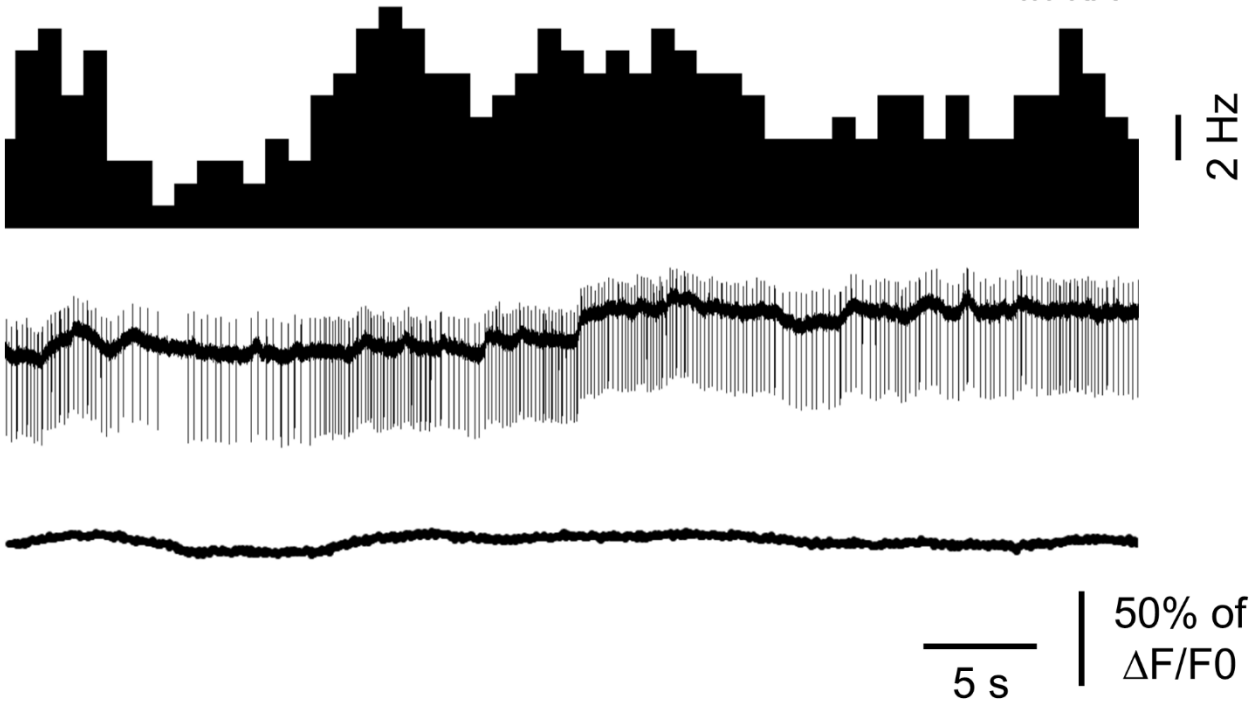
**A****B**

Figure 33

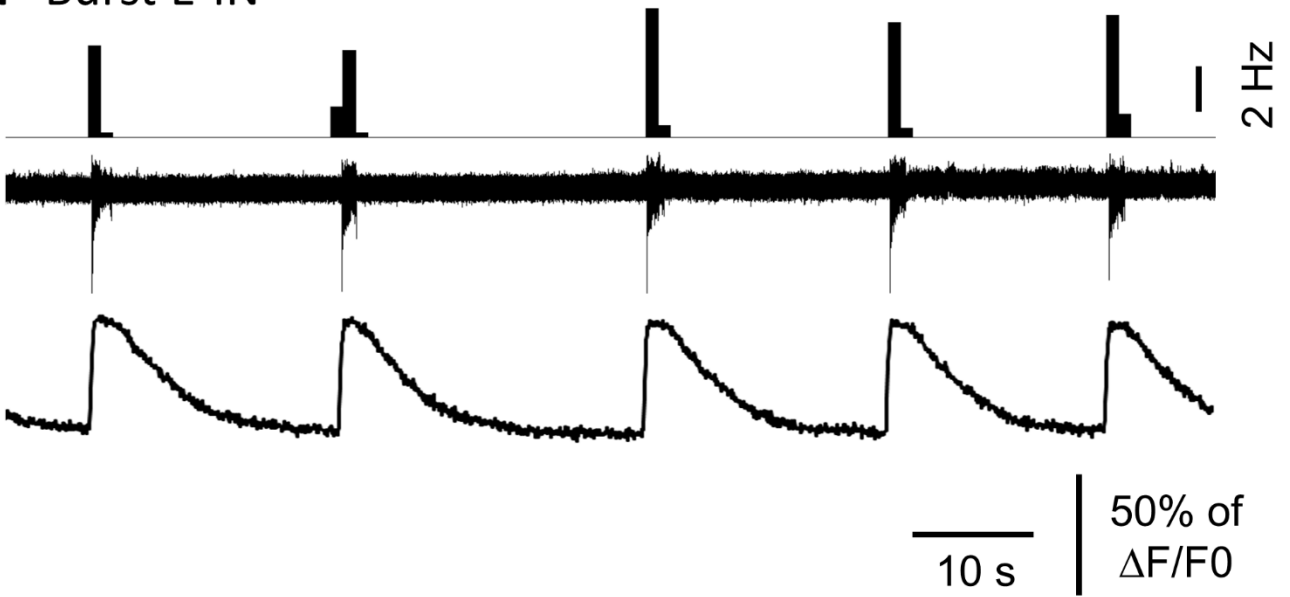
### E Tonic E-IN

in KA



### F Burst E-IN

in KA



### G

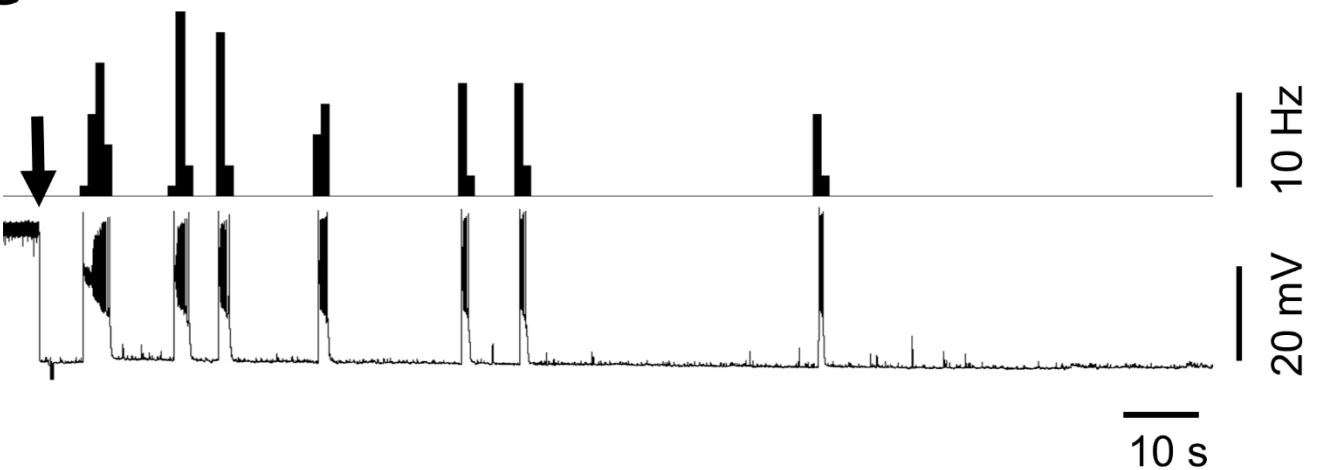
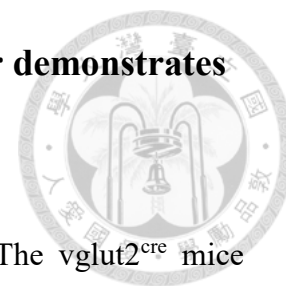


Figure 33

**Figure 33. Calcium imaging using GCaMP6s indicator demonstrates two groups of LC E-INs**



**A**, Schematic diagram shows the arrangement of experiments. The *vglut2<sup>cre</sup>* mice receiving infusions of AAV5-DIO-GCaMP6s into the LC bilaterally were used. **B**, Plot summarizes the proportion of burst neurons in GCaMP6s signal<sup>+</sup> cells near the LC in brain slices. Each circle in the plots presents result from a neuron, the diamond (mean) + capped vertical lines (SEM) show the averaged results. **C**, Representative fluorescent images show two groups of E-INs by the difference in GCaMP6s fluorescent flashings. C1 to C6 are gathered from a video and the time points from the beginning are labeled. Arrows and arrowheads indicate burst E-INs with spontaneous fluorescence fluctuations and tonic E-INs with a relative stable calcium activity, respectively. Note the burst E-INs shown in C exhibit a burst rhythm with 10-20 s as the inter-burst interval. **D**, Back propagating APs are monitored in dendrites of E-INs, even though the soma is not located in the same focus plane. D1 to D3 are gathered from a video and the time points from the beginning are labeled. Arrows and arrowheads indicate the calcium activity of given dendrites with back propagated APs and a constant fluorescence, respectively. The asterisk shows a burst E-IN and the antidromic activity in its proximal dendrite is also observed (the top right arrow). **E**, A representative cell-attachment



recording of a tonic E-IN demonstrates the relative continuous AP firing with some fluctuations underlying a stable calcium activity. The top histogram shows the firing rate, the middle trace shows raw data of cell-attachment and the bottom trace displays the fluorescent signals. **F**, A representative cell-attachment recording of a burst E-IN. The arrangement and labeling are follow the same way as E. Note the spontaneous bursts and corresponding calcium activities. The recordings shown in E &F are performed under KA application, reflecting the intrinsic origin of the spontaneous tonic firing and bursts. **G**, A representative whole cell recording of a burst E-IN show the decline of burst ability after the stable recording is obtained.

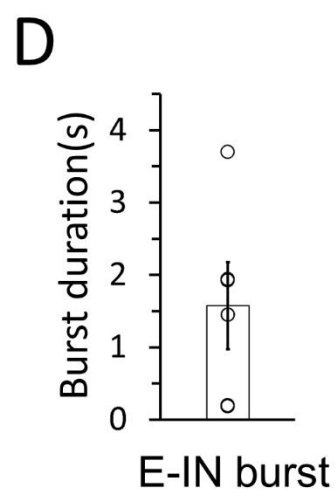
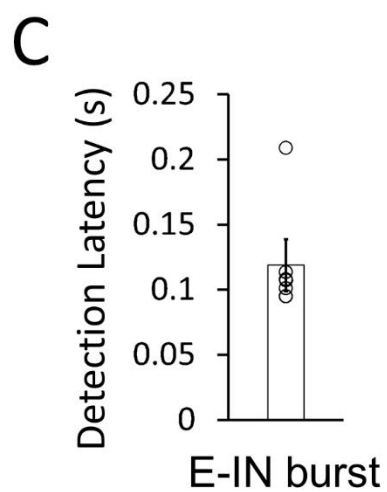
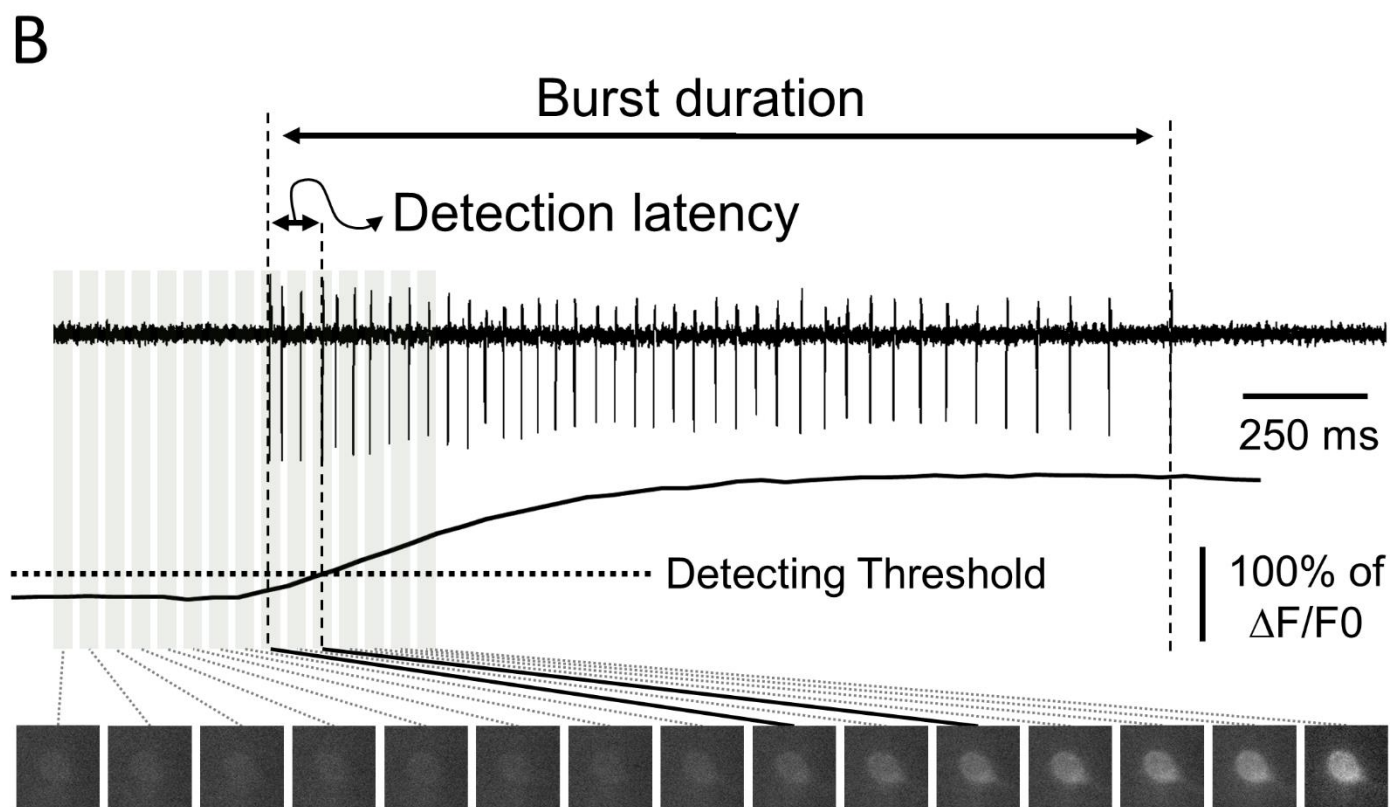
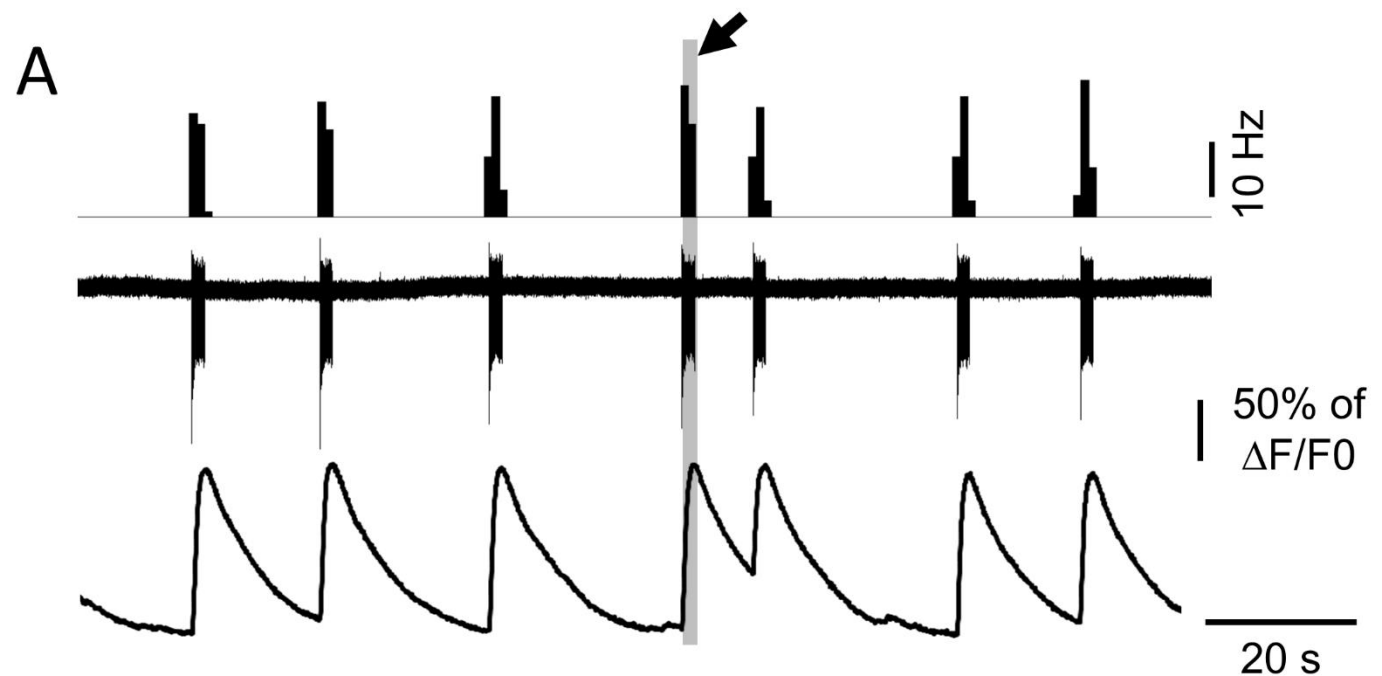
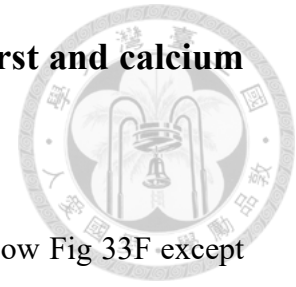


Figure 34

**Figure 34. Simultaneous alignment of spontaneous burst and calcium activity in burst LC E-INs**



*A*, A representative recording of a burst E-IN, the arrangement follow Fig 33F except the arrow and red vertical line indicate one of spontaneous bursts. *B*, Alignment of the burst indicated in *A* and the peri-event calcium activity. Grey rectangles show the exposure time of a serious of image acquisitions and the consecutive images are shown beneath the trace. Labels display the detecting threshold of burst-related calcium activity as well as calculations of detection latency and burst duration. Note the calcium signals show a slower onset and a prolonged plateau after the burst firing. *C & D*, Plots summarize the results of calculated detection latency and burst duration from 7 cells (obtained in 3 slices from 2mice). Each circle in the plots presents result from a neuron, the bar (mean) + capped vertical lines (SEM) show the averaged results.

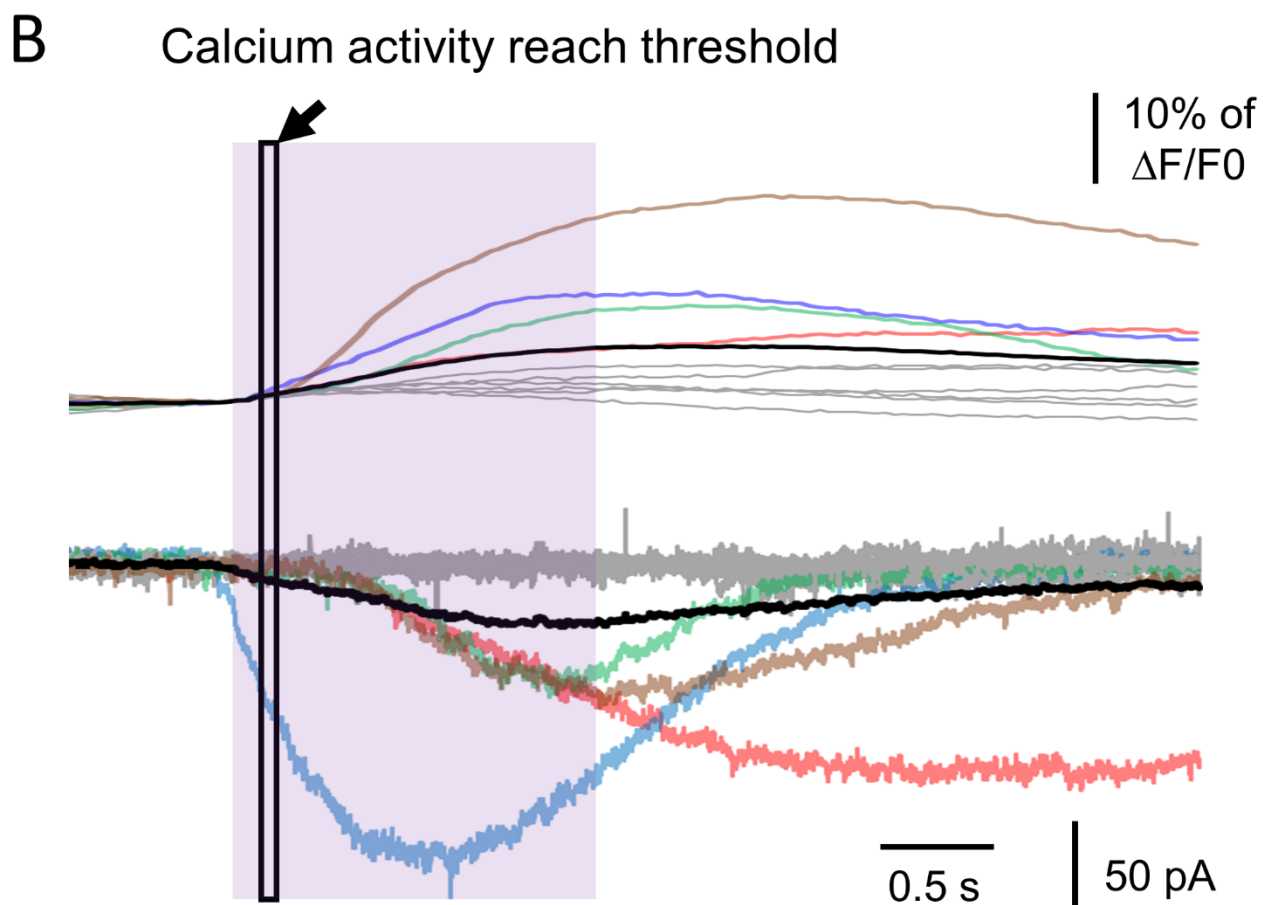
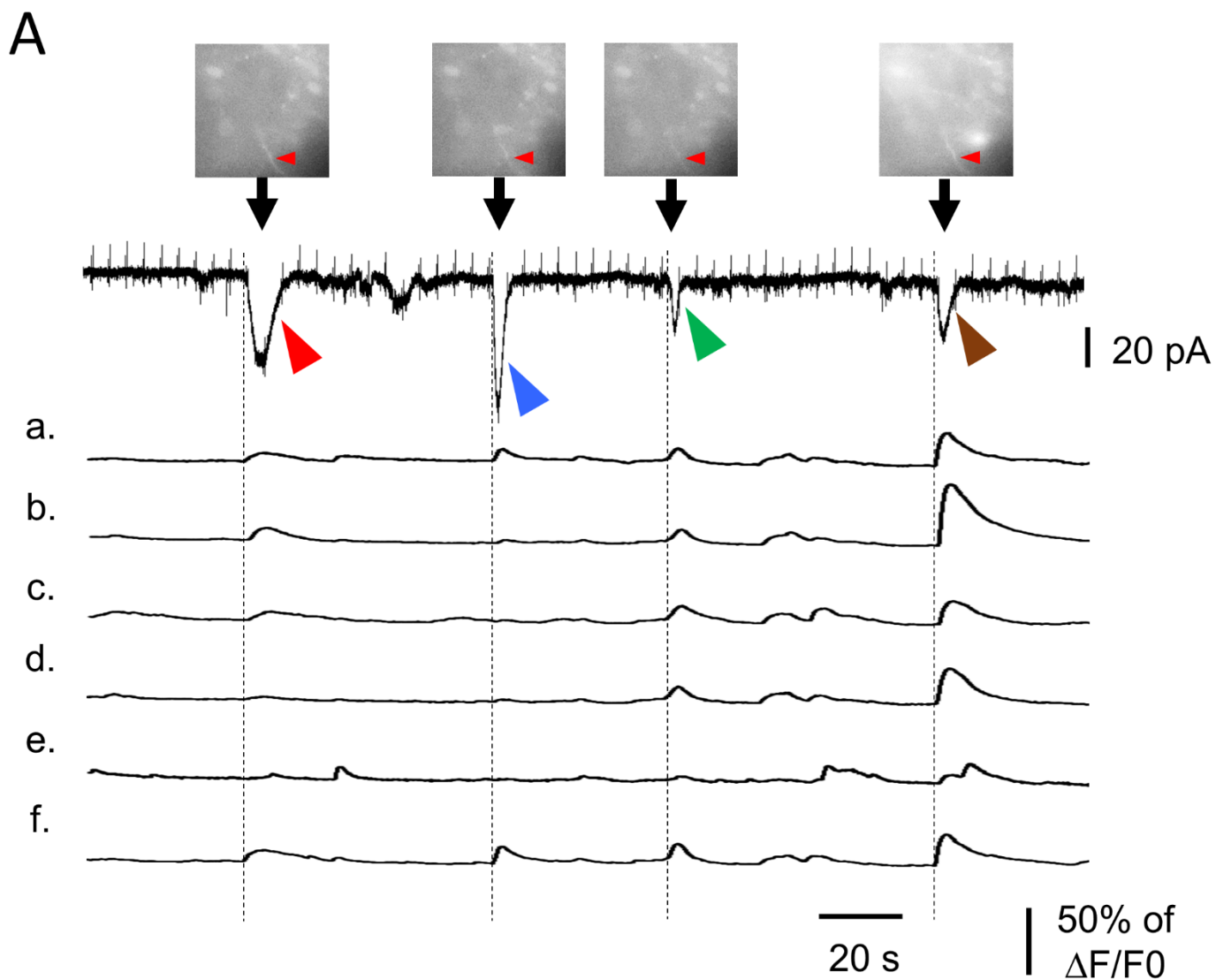
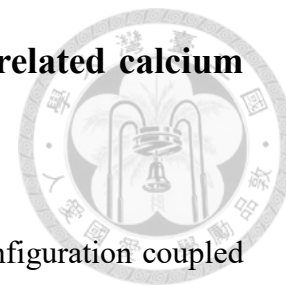


Figure 35

**Figure 35. Preliminary results in alignment of burst related calcium activity in E-INs and large sEPSC in LC-NA neurons**



**A**, A representative recording of a LC-NA neurons in V-clamp configuration coupled with a simultaneous calcium activity recording of many E-INs. The top trace shows the recording of a LC-NA neuron exhibiting many large sEPSC (arrowheads). The bottom traces show the trace of  $\Delta F/F_0$  from six ROIs (a-f), the trace a-d are obtained from the soma and the e & f are from the dendrites with back propagated APs. The vertical lines demonstrate the close timing relationship between large sEPSCs and burst-related calcium activity events. Photos above the V-clamp trace show examples of the raw images during the large sEPSC expressing. The red arrowhead indicates a dendrite with calcium activity from the trace f. **B**, An alignment of detected activity in trace f of A (top) and the peri-event traces from the recording of the LC-NA neuron (bottom). The black box denotes the data point that traces over the detection threshold and the purple rectangle shows the putative bursting period of the E-IN. Note that many large sEPSC show a considerable onset latency. Colored traces in B denote the pairs of burst-related calcium activity in the E-IN and the large sEPSC in the LC-NA neuron. The large sEPSCs in A are marked by the arrowheads with the same color. The grey traces present each of other burst events, and the black trace denotes the average result.

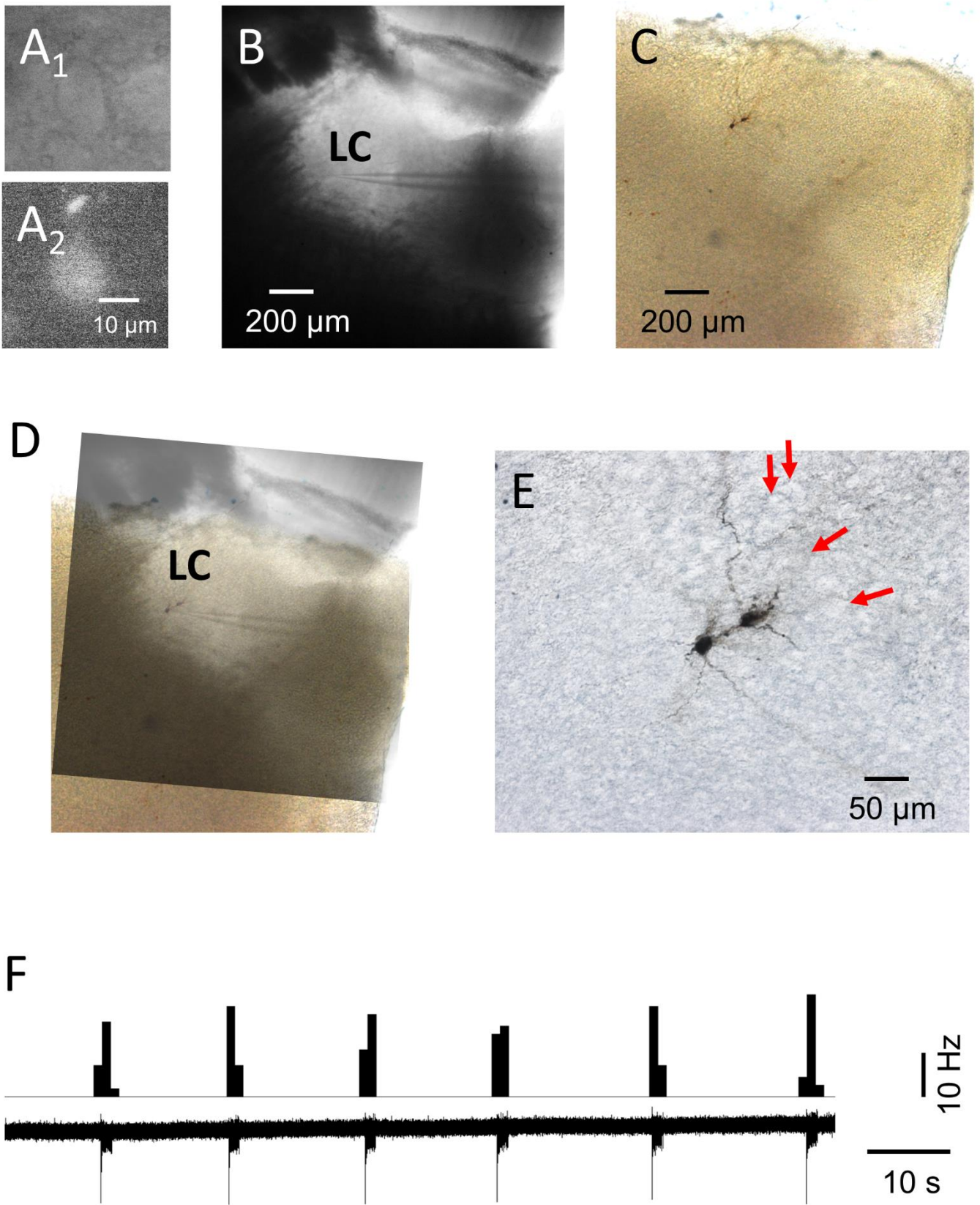


Figure 36

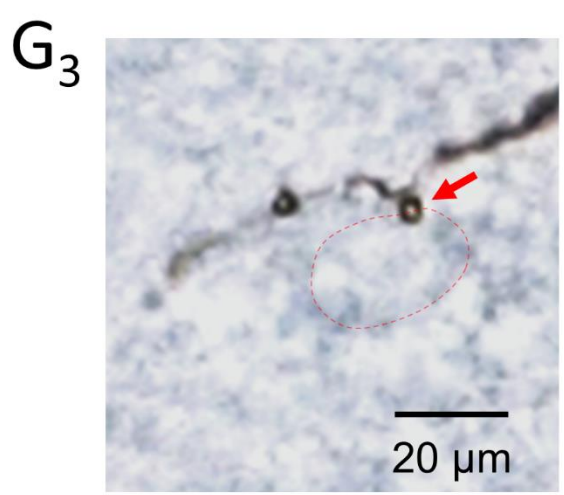
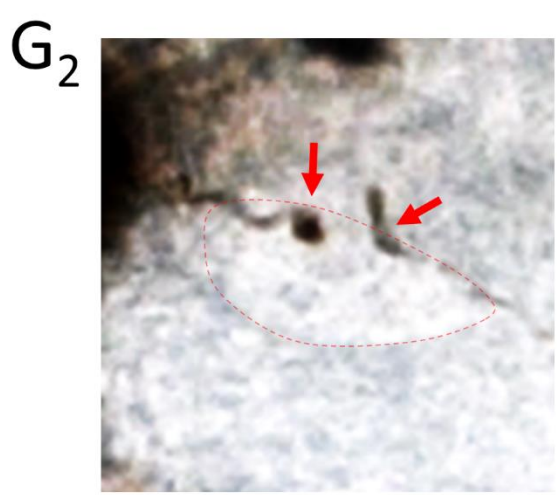
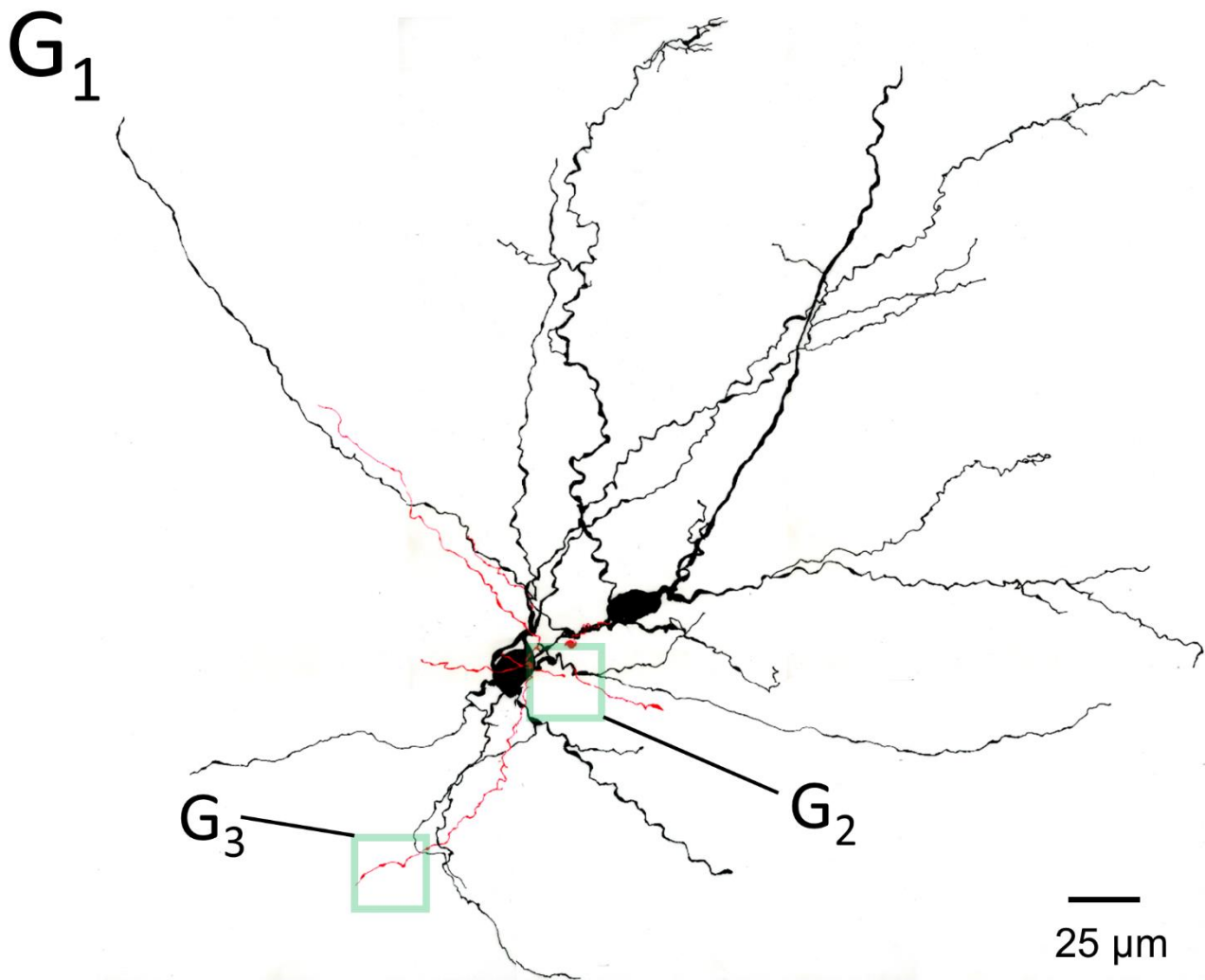
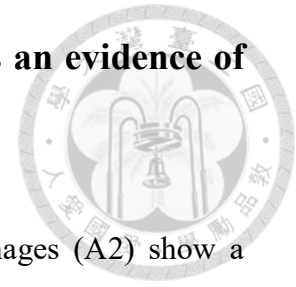


Figure 36

**Figure 36. Reconstructed morphology of E-INs shows an evidence of synaptic contacts onto LC-NA neurons**



**A**, Representative online phase contrast (A1) and fluorescent images (A2) show a recording from a GCaMP6s<sup>+</sup> neuron. **B**, A representative online phase contrast image with lower magnification shows the location of recorded E-IN is inside the LC-proper. **C**, A representative photo with lower magnification displays the *post hoc* IHC of the biocytin for the morphology reconstruction of the same E-IN. **D**, A superimposed image from B and C confirms the intra-proper location of the E-INs. **E**, The same photo with higher magnification shows two recorded E-INs in the slice. Note the arrows near the recorded cell indicate some large cell in a compact arrangement, being supposed as LC-NA neurons. **F**, A representative cell attachment recording coupled with calcium imaging of the same cell exhibiting obvious bursts spontaneously. **G**, The camera lucida drawing of the reconstructed morphology (G1). G2 & G3 show the box regions in G1. Note that many bouton-like, swollen structures (Arrows) along the short axon make close appositions onto the large fusiform cells supposed to be LC-NA neurons.

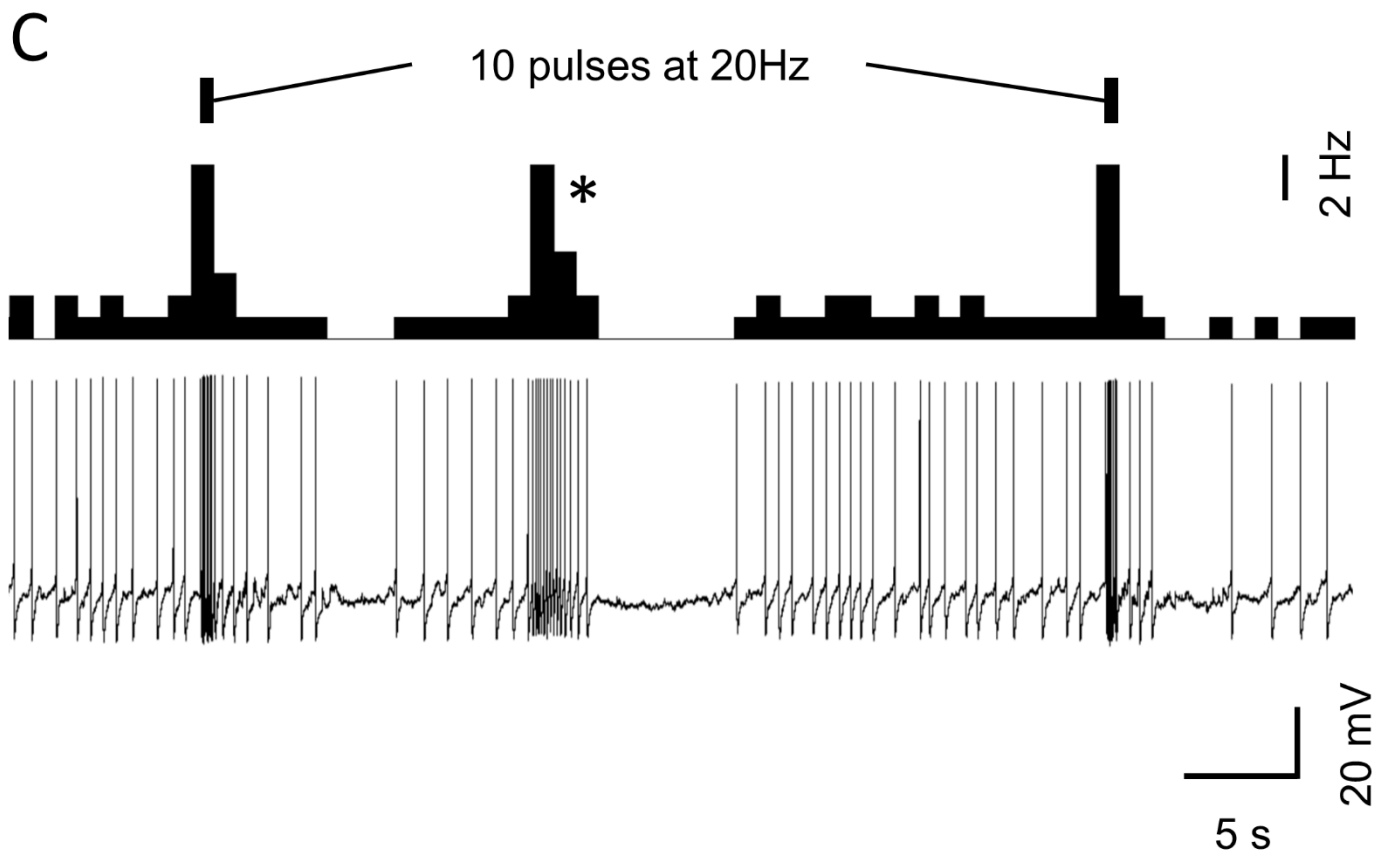
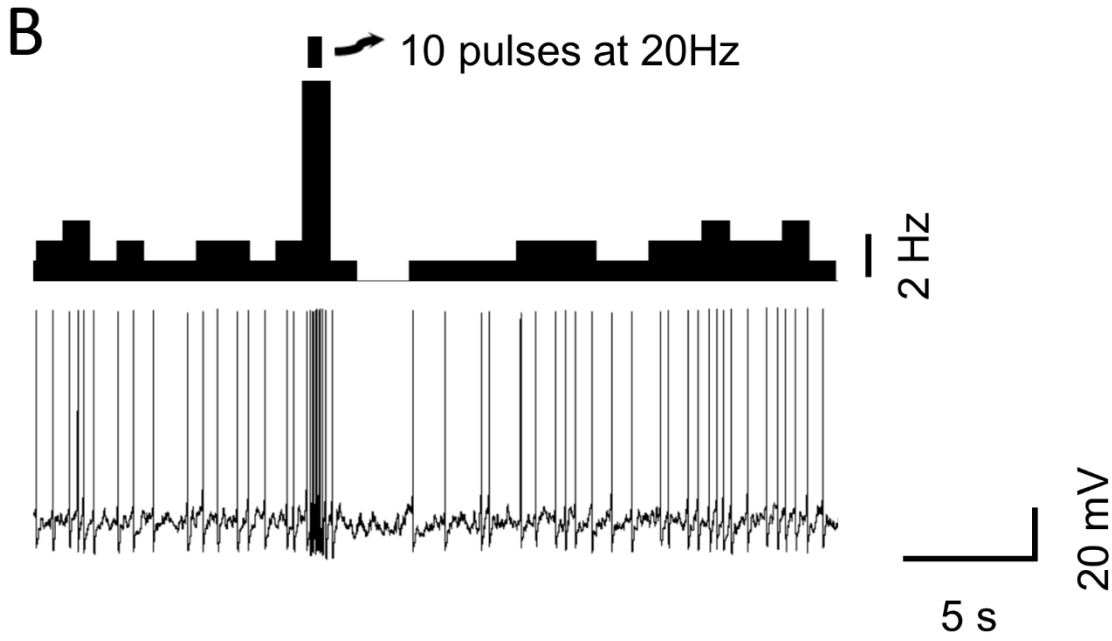
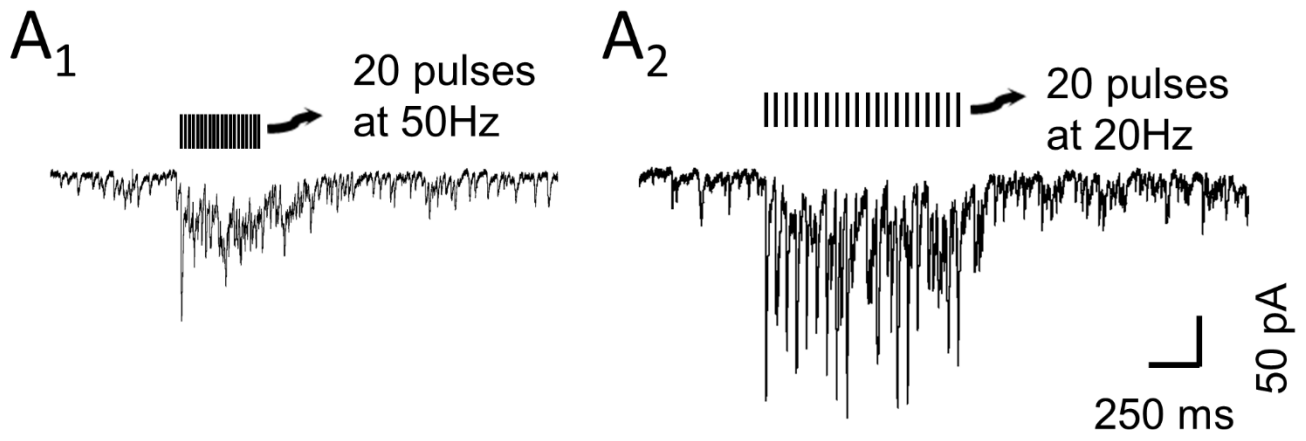
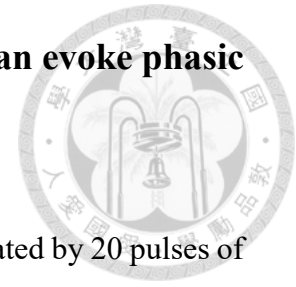


Figure 37

**Figure 37. Train of optical stimulations on LC E-INs can evoke phasic activations in LC-NA neurons**



*A*, Representative traces in V-clamp show compound EPSCs summated by 20 pulses of optical stimulations at 50 Hz (A1) and 20 Hz (A2). The blue rectangles denote illuminations of blue light. *B*, 10 pulses of light illuminations at 20 Hz elicit a phasic activation in representative recording on a LC-NA neuron. The top histogram and the bottom trace show the firing rate and I-clamp trace. *C*, A representative recording from another LC-NA neuron under same stimulation protocol that exhibit few sPLA. Note the sPLA doesn't show no obvious relationship to the evoked phasic activations. In *B* & *C*, rectangles above the histogram indicate the optical stimulations. In this series of experiments, the *vglut2<sup>cre</sup>* mice receiving infusions of AAV2-DIO-ChR2-eYFP into the LC bilaterally were used.

# Discussion



---

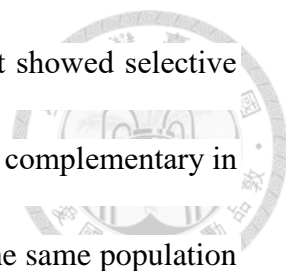
<b>1. General Discussion</b>	<b>228</b>
<b>2. Mechanisms for Specific Noradrenergic Modulation</b>	<b>230</b>
<b>3. LC-INs in interactions between Phasic and Tonic Activity</b>	<b>233</b>
<b>4. of Cell Types of LC INs- Limited Understanding</b>	<b>237</b>
<b>5. PPI Results and the Functional Implications</b>	<b>240</b>
<b>6. Involvement of LC INs in Cognitive Function</b>	<b>243</b>
<b>7. Consideration and Interpretations of Technical Limitation</b>	<b>244</b>
<b>8. Future Improvements and Perspectives of Investigation on Roles of LC E-INs</b>	<b>247</b>
<b>9. Conclusion</b>	<b>251</b>

---

## 1. General Discussion



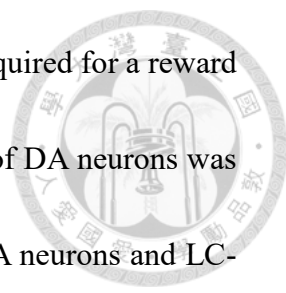
LC-NA neurons exhibit sPLA in brain slice preparations. I demonstrated that the observed sPLA was enhanced by blockade of GABA<sub>A</sub>Rs and GlyRs but was suppressed by blockade of glutamatergic transmissions. These observations suggested the presence of a local circuit that contains E-INs to drive sPLA and I-INs to modulate the activity. On the basis of the following facts, I deduce that the sPLA might be analogous to phasic LC activation observed in animal studies. First, I adapted the criteria modified from those commonly used to detect phasic LC activation in previous studies on rats (Bouret et al., 2003; Darling et al., 2011; Devilbiss and Waterhouse, 2011). Second, sPLA was frequently followed by a lasting inhibition of the background activity, an important feature that characterizes phasic LC activation in living rats (Bouret and Sara, 2004; Clayton et al., 2004; Bari and Aston-Jones, 2013; Marzo et al., 2013). Finally, Breton-Provencher and Sur (2019) reported a group of GABAergic I-INs in the medial part of the peri-LC in mice as demonstrated in this study; however, Jin et al. (2016) report that GABAergic I-INs were located in the dorsomedial part of the peri-LC in the same species. Breton-Provencher and Sur (2019) further demonstrated that the GABAergic I-INs regulate LC-dependent pupil dilation, which has been proven to intimately correlate with phasic LC activation in rodents and primates (Aston-Jones and



Cohen, 2005; Geva et al., 2013; Joshi et al., 2016). My results that showed selective inhibition of peri-LC I-INs enhance sPLA and provide complementary in vitro evidence to support the conclusion. In addition, the fact that the same population of I-INs regulates sPLA in vitro and LC-dependent pupil dilation in vivo further supports the argument that sPLA might be analogous to phasic LC activation in animals. Moreover, my results also demonstrate that sPLA analyses in brain slices might provide a potential model for exploring the molecular and cellular mechanisms that underlie phasic LC activation. By analyzing sPLA and the evoked phasic activity in vitro, I showed that peri-LC I-INs exerted feedforward inhibition of LC-NA neurons via GABAergic and glycinergic transmission and could gate phasic activation. In addition to the peri-LC I-INs, I also found a population of E-INs located near the LC exhibited intrinsic burst firing spontaneously. By using optogenetics and calcium imaging techniques, my preliminary data provide a positive evidence for the involvement of LC E-INs in generation of sPLAs in brain slices. My works show a LC local circuit comprising both E-INs and I-INs, and its potent role in regulating the phasic activation of LC-NA neurons.

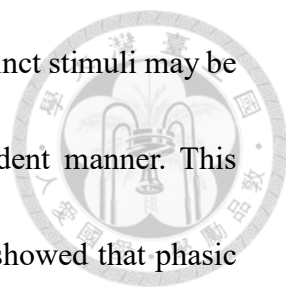
## 2. Mechanisms for Specific Noradrenergic Modulation

During wakefulness, LC-NA neurons also exhibit the other activation pattern, namely, tonic activation. In animals engaged in a 2-alternative forced choice task, an increase in tonic LC activation is observed when utility in the task wanes (Aston-Jones et al., 1994, 1998). As aforementioned in introduction, it is hypothesized that tonic hyperactivity of the LC-NA system could widely increase the gain of neuronal networks that could cause the animals to be distracted by irrelevant stimuli in the environment, then subsequently disengage from the current task and a search for alternative behaviors (Aston-Jones and Cohen, 2005). The results of a recent computational study support the roles of tonic and phasic activation of LC-NA neurons in regulation of behaviors (Sales et al., 2019). This study establishes a model suggests that the activity of LC-NA neurons reflects the magnitude of cognitive prediction error and helps individuals to update their high level estimation models quickly according to new observations in a classical forced choice task. The feedback of prediction error foreshadows efforts for counteracting unexpectancy, subsequently optimizes learning efficiency and behavior plasticity through NA release. This role of the LC-NA neurons shows its similarity to DA neurons in midbrain which respond to the prediction error of reward obtains (Montague et al. 2004). A recent study in monkey showed that the phasic



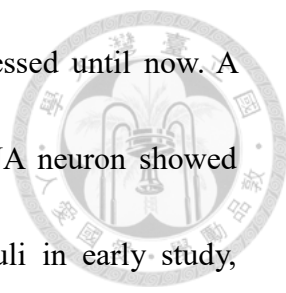
responses of LC-NA neurons were more dependent on the policy required for a reward than the reward itself in a multiple choice task. And the activation of DA neurons was prior to the LC's, suggesting a decisive and a motivated role for DA neurons and LC-NA neurons, respectively. These findings may well isolate roles of the LC in evaluating valuable uncertainty for a given reward, not the reward itself because it is already known, whereas the midbrain DA neurons demonstrated good correlations with both reward and effort (Varazzani, et al. 2015).

However, the LC-NA neurons naturally responds to multi-dimensional stimuli more than single type of given tasks in a more complex environment. It is an interesting question that how the LC-NA neurons prevent a global modulation regardless where stimuli sufficient for phasic activations through the broader projection. As studies on rodents used similar stimulation approaches on the LC-NA neurons, different outcomes in behavior were yield depending on what kinds of experimental design that animal was in engaged in (Carter et al., 2010; McCall et al., 2015; Aston-jones et al., 2017). A reasonable explanation is that the neural network receives stronger updating if it is occupying the most of attention resource, such as a prediction error to the mPFC or a salient tone to the A1 and the thalamus. Hence the discrepancy amongst the updating



contents by phasic activations of LC-NA neurons in response to distinct stimuli may be determined by the current allocating of attention in a use-dependent manner. This hypothesis can be partially supported by studies on living rodents showed that phasic activations enhanced the signal-to-noise ratio in response to given non-noxious stimuli (Berridge and Waterhouse, 2003; Devilbiss and Waterhouse, 2004; Linster et al., 2011; Devilbiss and Waterhouse, 2012). Also, activations of  $\beta$ -ARs differentially increase pyramidal cells receiving a train of excitatory inputs but yield quite small effects on silent cells in brain slices from rats (McCormick et al., 1991; McCormick et al., 1993). In addition to the use-dependent manner underlying current attention, the specific target of LC-NA system may be done by differential activations of subsets of LC-NA neurons with different projecting preference. Experiments required for addressing this issue is to see whether these subsets also receive differential inputs as the their efferents, but supposed not in cases of targets within the same subset.

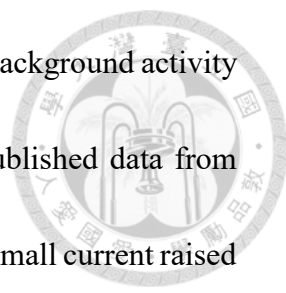
Another way for the specific noradrenergic modulation might be reached through the modular organization of LC-NA neurons with different projection preferences (Schwarz et al., 2015; Hirschberg et al., 2017; Uematsu et al., 2017). This hypothesis is built on the different afferent compositions onto LC-NA neurons depending on the



efferent they send, though this issue has not been properly addressed until now. A limited but inspiring evidence is the unit recordings of the LC-NA neuron showed different phasic activations in response to various sensory stimuli in early study, showing the heterogeneous effect from different stimuli in a single LC-NA neuron (Aston-jones and Blomm, 1981). Based on the speculation, it is not surprising that a given stimulus can activate a broad population of LC-NA neurons in different degrees, but how large is the differential effect among LC-NA neurons that belonged to different efferent group will be raised as a critical question.

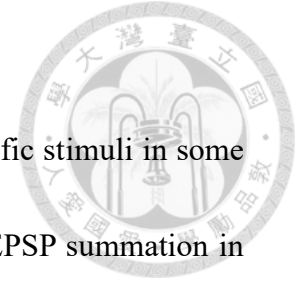
### **3. LC-INs in Interactions between Phasic and Tonic Activity**

On the other hand, the LC-NA neuron spends many of time expressing tonic activity, especially in facing fairly new situations that is full of unexpected events and unexplored resources. The unanswered question is why the same set of neural networks cannot evoke a LC phasic activation when share similar resource of attention during the exploration. This can be done by many hypothesized explanations. First, the intrinsic property of LC-NA neurons causes the negative relationship between the phasic activation and the hyperactive tonic activity. Studies on rats showed the enhanced LC tonic activity by CRF infusions but not the sensory stimuli induced phasic



activity, resulted a relatively weak phasic activation setting on high background activity (Valentino and Foote, 1987; Valentino and Foote, 1988). My unpublished data from brain slice recordings also indicate that the prolonged application of small current raised tonic activity but showed less effect on phasic activations induced by playback of large sEPSC. Moreover, Brown and Moehlis proposed a computational model and reported that the phasic activity was mainly caused by increasing firing of cells with low spiking rate, and thus the phasic activation could be interfered by the hyperactive tonic firing (Brown and Moehlis, 2004).

Second, LC phasic activations are caused by the specific excitatory input. Although the PrL unit didn't show obvious burst activity in response to the CS+ stimuli in the forced choice task, a transient phasic activation could be evoked by synchronization in a specific population of cells that projected to the LC. Previous computational studies suggested a role of excitatory input on the LC phasic activity (Brown and Moehlis, 2004; Howells et al., 2012; Seo and Bruchas, 2017). But these studies cannot show the circuitry mechanism for the excitatory afferents to the LC. Shortly, more researches are required for the further understanding about how different brain areas amplify the specific salience and cause phasic activations of LC-NA neurons.



Third, I hypothesize the LC local circuit help amplify the specific stimuli in some degree. This synergistic role may be achieved via enhancing the EPSP summation in dendrites under assistance of local E-IN or facilitating phasic emergence by a general activation of I-IN induced background inhibition. However, my results show a role of feedforward inhibition of peri-LC I-INs that gates excitatory input for phasic activity generation, it requires a precise activation of peri-LC I-INs corresponding to given stimuli. Although Breton-Provencher and Sur proposed a regulatory role of supposed same population of I-INs that receives more PFC afferents than LC-NA neurons, they suggested a reduction on evoked LC phasic activity by optical stimulation of the PFC as the regulatory outcome from I-INs. In fact, the startle stimuli transport to the LC through cochlear nucleus and subsequent brainstem pathway, so it raised an important issue that the stimulation of PFC can also cause an occupance of a considerable resource of attention and thus repel the startle tone induced phasic activity theoretically (Breton-Provencher and Sur, 2019). These arguments suggest a bidirectional roles of peri-LC I-INs in regulation of the phasic activity according to the temporospatial activating specificity of them. As shown in the previous study, the local GABAergic INs counteracted the plateau potential in dendrites of striatal medium spiny cells depending

on the temporospatial encountering of EPSPs and IPSPs. And this regulation may be conducted by the recruitment of  $Mg^{2+}$  blockade in NMDA receptors (Du et al., 2017).

So the timing accuracy of I-INs activations is likely to act as a crucial parameter for their effect on the forthcoming LC phasic activation. I cannot address this issue because the E-INs is the only intact excitatory source for the phasic activation, however, a selective stimulation of long distance afferents is a feasible way in the future.

The local circuit also provides an interface for multi-dimensional regulations from many brain areas, and helps individuals integrate different functions required these brain areas. In this regard, an essential experiment is to analyze afferents for local INs, and similar investigations were made on the VTA in mice (Morales and Margolis, 2017). As cases in VTA, it could be a spectrum between two putative patterns, the convergent and divergent which represent a common innervations form multiple upstream to the same cell and a divisions of cell populations for a specific innervation, respectively.

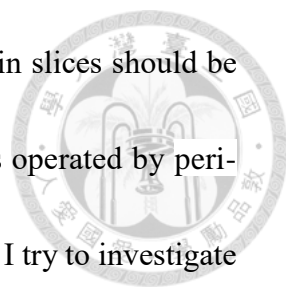
Besides, the local circuit may also project axon collaterals to other brain region subsequently regulate brain functions that the LC is involved in. It has been reported in mice recently that populations of non-dopaminergic cells in VTA project axons out of



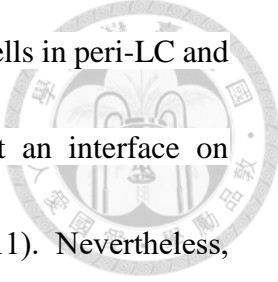
midbrain, form a complex projection system combining different transmitter secretions (Qi et al. 2016; Morales and Margolis, 2017; Paul et al., 2019). For example, projections to nucleus accumbens from VTA glutamatergic cell drive aversion through GABAergic INs they target (Qi et al., 2016). The new data from McCall and his colleagues supported that the direct activation of fibers from VTA glutamatergic cells inside the LC drove a transient aversive behavior and showed aversive memory after repeats (McCall et al., 2019). Based on the network with multi-type cells, it is found in mice that afferents to the VTA demonstrated innervating preferences to different type of cells and provided a more delicate framework in regulation of the reward function as mentioned above (Lammel et al., 2012; Barbano et al. 2020). Since I don't know whether the LC INs exhibit similar profiles as non-dopaminergic cells in VTA, but it still can be a good direction for the future work. Cases in other regions can offer good examples for the investigation on LC INs.

#### **4. Cell Types of LC INs - Limited Understanding**

The observation that revealed that sPLA no longer occurred when glutamatergic transmissions were blocked raised another argument regarding the components of the proposed local circuit. In addition to peri-LC I-INs, the circuit should involve peri-LC



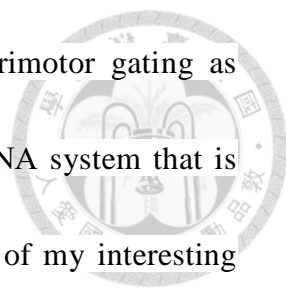
E-INs to drive sPLA. Namely, the sPLA incidence observed in brain slices should be determined by the excitatory-inhibitory balance of LC-NA neurons operated by peri-LC I-INs and LC E-INs in the circuit. In the final part of this thesis, I try to investigate these E-INs by multiple approaches. Although not fully examined, anatomical evidence implies the existence of local LC E-INs that make functional connections with LC-NA neurons. Consistent with my observations, Verstegen and her colleagues reported a population of both inhibitory and excitatory neurons in the gap between the LC proper and the Barrington nucleus in mice as I mentioned above (Verstegen et al., 2017). This is the region where most of the TH<sup>-</sup>/WGA<sup>+</sup> neurons were located in results of WGA-tracing experiment. The authors also showed a population of glutamatergic neurons in this region which express the FoxP2 transcription factor, since both inhibitory and glutamatergic neurons showed FoxP2<sup>+</sup> around the LC in a regional dependent manner. Given that I showed that neurons expressing GFP accounted for only approximately 20% of TH<sup>-</sup>/WGA<sup>+</sup> neurons, it is very likely that some of the TH<sup>-</sup>/WGA<sup>+</sup> neurons that did not express GFP were glutamatergic. In support of this argument, I obtained preliminary evidence demonstrating that a portion of TH<sup>-</sup>/WGA<sup>+</sup>/GFP<sup>-</sup> neurons were immunoreactivity to anti-FoxP2 antibody. This population of INs could be the same population of glutamatergic INs expressing FoxP2 as reported by Verstegen and her



colleagues. Interestingly, a study on mice reported that the FoxP2<sup>+</sup> cells in peri-LC and parabrachial region project axons into the VTA and may exert an interface on reciprocal connections between LC and VTA (Miller et al., 2011). Nevertheless, specific cell markers in the LC remain fairly unclear, in addition to the FoxP2 expressing cells, studies on rodents showed the makers of neuropeptide Y (NPY) expressing in the peri-LC INs and the NPY was reported to related to arousal and anxiety that were deemed as one of the LC's functions. As a limited evidence showed that NPY<sup>+</sup> cells were excited by the CRF and the activation of NPY receptor and the infusion of NPY into the LC introduced the anxiolytic behavior in rat (Kask et al., 1998; Xu et al., 2004; Jüngling et al., 2012; Zitnik, 2016; Versteegen et al., 2017). there are many peri-LC INs that cannot be identify because of the limited understanding of the cell types. In my experiments, I face the physical leakages of infused AAVs because only general markers such as Vgat and Vglut2 gene are available instead of specific markers. In conclusion, to investigate the role of LC INs systematically, more experiments are still required to reveal different cell types and markers.

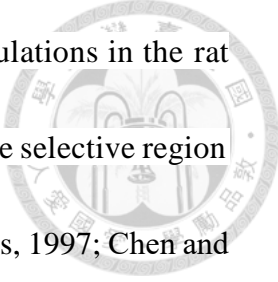
## 5. PPI Results and the Functional Implications

In this study, I also tested the effect of inhibiting peri-LC I-INs, which exert feedforward inhibition of LC-NA neurons, on behaviors that are regulated by the LC-NA system. The PPI was chosen as the study model because it is a commonly used operational measure of sensorimotor gating, a preattentive form of information processing by which organisms defend salient signals from competition by extraneous stimuli (Braff et al., 2008; Geyer, 2008; Swerdlow et al., 2008). Therefore, a change in the intrinsic mechanisms of preconscious information filtering, namely, a change in sensorimotor gating, is expected to accompany manipulation of LC tonic and phasic activation. In support of this argument, Alsene and Bakshi showed that increasing LC tonic activation with cholinergic and glutamatergic agonists resulted in a disruption of PPI in an anatomically, behaviorally, and neurochemically specific manner (Alsene and Bakshi, 2011). The noradrenergic modulation on the PPI are processed through PPTg which elicits a direct inhibition of the startle reflex circuit in nucleus reticularis pontis caudalis (PnC) from the LC (Fendt et al., 2001; Swerdlow et al., 2008). The interpretation of these observations is that given the conceptualization of sensorimotor gating as a mechanism that defends higher order cognitive processes by filtering out potentially intrusive irrelevant stimuli (Braff et



al., 2008; Geyer, 2008; Swerdlow et al., 2008), deficient sensorimotor gating as indexed by PPI could arise from tonic hyperactivity of the LC-NA system that is thought to conflict with phasic activations to some degree. One of my interesting findings using *ex vivo* recordings is that peri-LC I-INs exert a regulation mainly on the LC phasic activity but less on the tonic activity; whereas the blockade of GABA<sub>B</sub> receptor yields an opposite effect with enhanced tonic activities only. Based on the argument, I predicted that improved sensorimotor gating as indexed by PPI could arise from reducing the threshold of phasic activation. Given that the results demonstrated that selective inhibition of peri-LC I-INs did not alter the basal tonic rate but enhanced sPLA and the evoked phasic activity, PPI improvement via similar manipulation of peri-LC I-INs activity fulfilled my expectation. Moreover, my results suggest that the identified peri-LC I-INs play a role in integrating inputs to LC-NA neurons and gating phasic activity.

Nowadays, scientists can manipulate the activity of LC-NA neurons using classical or modern techniques. Common approaches for stimulations include the infusion of agonists or antagonists for many receptors that increases the tonic activity of LC-NA neurons broadly in rodents (Berridge et al., 1993; Berridge and Waterhouse



2003; Alsene and Bakshi, 2011; Grella et al., 2019); electrical stimulations in the rat LC or brain regions that project to the LC mimic the activation of the selective region in a timing specific manner (Ennis et al., 1992; Jodo and Aston-Jones, 1997; Chen and Sara, 2007) and optical stimulations on LC-NA neurons or afferents to the LC enable a highly flexible manipulation than other approaches in mice (Carter et al., 2010; McCall et al., 2015; Vazey et al., 2018; Hayat et al., 2020). However, neither of these method can differentially reduce the threshold of LC phasic activations but put less effect on the tonic activity as the suppression of peri-LC I-INs results in. According to the adaptive gain theory, so I observe a unique condition that stimuli are easier to be selected by LC phasic activations but far from the generally high gain by enhanced tonic activity. A possible expectation is that individuals under this condition show more frequent switches in behavior in response to the distractive stimuli with a moderate intensity. Repeated phasic activations drive shifts in brain network may interfere the normal learning process by the excessive updating of irrelevant information in facing more complex choices. Together, my study provides a valuable model that can help scientists in this field to further reveal more details of the LC phasic activity.

## 6. Involvement of LC INs in Cognitive Function

To test whether peri-LC I-INs also play a role in high cognitive function associated with the LC-NA system, I examined whether these INs received direct contacts from axonal terminals of the OFC and PrL. Previous studies on rats showed that phasic LC activation is more tightly aligned with the subsequent behavioral response than the preceding onset of a task-related stimulus (Bouret and Sara, 2004; Rajkowaski et al., 2004); therefore, it is believed that the LC-NA system responds with phasic activation to facilitate the behavioral responses upon receiving cortical inputs signaling the outcome of the decision processes that represent the recognition of a stimulus associated with reward in the task (Aston-Jones and Cohen et al., 2005; Bouret and Sara, 2005). Given that the OFC and the PrL play crucial roles in the evaluation of the reward of stimuli and decision-making processes (O'Doherty et al., 2002; Roesch et al., 2004; Lipems et al. 2015; Zeeb et al., 2015), my results that showed concomitant innervations of the OFC and PrL efferent fibers onto LC-NA neurons and peri-LC I-INs together with the above-described in vitro physiological data suggest that peri-LC I-INs might be involved in integrating the cortical inputs signaling the recognition of the stimulus associated with a reward onto LC-NA neurons and gating the phasic activation. Nevertheless, further evidence is

required to support the argument. Specifically, evidence indicates that inhibition of peri-LC I-INs using the hM4DiR DREADD method could alter the performance of animals engaged in a Go-NoGo or 2-alternative forced choice task. Moreover, my preliminary data also show a population of supposed glutamatergic LC E-INs forming functional connections to LC-NA neurons receive innervations from the PFC. But more experiments are required to reveal the role of LC E-INs in regulation of LC activity and the choice task performance.

## **7. Consideration and Interpretations of Technical Limitation**

It should be noted that some technical issues in this study require further consideration. Although the same stereotaxic coordinate was used to infuse AAV2-DIO-WGA and AAV2-DIO-hM4DiR-mCherry into the LC, I could not interpret I-INs expressing hM4DiR-mCherry in the DREADD experiments specifically as TH<sup>-</sup>/WGA<sup>+</sup>/GAD<sup>+</sup> neurons in the WGA-tracing experiments. It is possible that some I-INs were located in the peri-LC and exhibited polysynaptic connections with LC-NA neurons. In practice, these I-INs were also transfected by AAV2-DIO-hM4DiR-mCherry; therefore, they should contribute to sPLA enhancement upon CNO application in the hM4DiR DREADD experiments. In addition, further consideration

is also needed for the interpretation of the results showing that the inhibition of peri-LC I-INs by hM4DiR DREADD increased the sPLA incidence but had no effect on the background tonic rate. Given that the majority of peri-LC I-INs could spontaneously discharge APs in slices, LC-NA neurons were expected to receive tonic inhibition, and removal of tonic inhibition using the hM4DiR DREADD method was expected to increase the background tonic rate.

In regard to this issue, I propose two interpretations. First, pontine NA neurons express numerous A-type  $K^+$  channels that operate at a subthreshold voltage (Williams et al., 1984; Forsythe et al., 1992; Min et al., 2008). Accordingly, it is possible that CNO application did increase the excitability of LC-NA neurons; however, the extent was not sufficient to overcome the subthreshold A-type  $K^+$  current and to produce a significant increase in the basal tonic rate. I demonstrated that the large sEPSC recorded in LC-NA neurons were likely to drive sPLA because a high correlation was noted between the incidences of the two events. As displayed in Fig. 3E, about 20% of large sEPSC failed to cause a detectable sPLA, and was exaggerated in the application of BM plus Stry which induced lots of undetectable fluctuations in the firing rate. This

phenomenon suggested an intrinsic filtering mechanism which echoed to my interpretation of the A-type channel gated excitability.

Second, the large sEPSC could not easily drive sPLA under normal conditions because they also simultaneously recruited peri-LC I-INs to counteract their excitatory effect on LC-NA neurons by the regulation of  $Mg^{2+}$  blocks in dendrites of LC-NA neurons. This finding might explain why inhibition of peri-LC I-INs increased the incidence of sPLA. Without the large sEPSC inputs, IPSPs from peri-LC I-INs may be not strong enough to affect the pace maker rhythm in the soma of LC-NA neurons because of the small driving force underlying IPSPs. Certainly, it is possible that the increase in sPLA incidence upon CNO application also included a presynaptic mechanism; namely, peri-LC I-INs might also synapse on the terminals of the presumed LC E-INs as well as other I-INs that might exhibit the same presynaptic modulation of sPLA via polysynaptic connections.

## 8. Future Improvements and Perspectives of Investigation on Roles of LC E-INs

The complete elimination of sPLA by DNQX+AP5 application reflects a putative E-IN population driving the sPLA. As showed in chapter 4 of the results section, I have made some efforts to reveal the role of LC E-INs. However, there are still lots of arduous work waiting for more efforts. First, I used *vglut2<sup>cre</sup>* mice to target glutamatergic neurons near the LC, but I cannot identify and isolate real E-INs forming functional contacts onto LC-NA neurons. Specifically, a mouse line of *vglut2*-reporter cross *TH<sup>cre</sup>* could be compatible with viral-WGA tracing techniques for identification of the functional interneuron pool. And there's another issue that the principle neurons in near nuclei can also send contacts onto LC-NA neurons. An early study suggested that LC-NA neurons receive CRF innervations from principle neurons in Barrington's nucleus which were found to secrete glutamate recently (Valentino et al., 1992; Verstegen et al., 2019). Second, many improvements are required for the optogenetic experiments. Fig. 29B shows a large transfection territory of ChR2-eYFP, more attempts should be made with proper ChR2-eYFP expressing areas. And the application of cocktail of receptor antagonists can prevent polysynaptic contaminations from multi-type transmissions activated by the local E-INs. For example, the synchronous firing of



local glutamatergic source is supposed to cause an overall activation of LC-NA neurons and some I-INs that can lead to inhibitions counteracting the EPSP summation through  $\alpha 2$ -ARs, GABA<sub>A</sub> and glycine receptors. The bath application of selective antagonists such as clonidine, BM and Stry can prevent this contamination. Third, I should provide images containing both reconstructed burst ENs and TH-ir signals, so thus confirm the functional contacts between them by using the IHC of synaptic markers or electron microscope. An alternative way with long-term benefits is to find the mechanism underlying spontaneous bursts in E-INs, then the key channel or structural protein may serve as a better marker to address them. Fourth, I have tried to manipulate the E-IN activity via many approaches, including the viral induced eNpHR 3.0 expressing or both excitatory (hM3DqR) and inhibitory (hM4DiR) system, the chaotic results show that hM3DqR activation causes a complete silence by over-excitation in E-INs, while eNpHR 3.0 and hM4DiR lead to the moderate repression and a mixture of bidirectional effects, respectively. These unpredicted data may be due to the unique channel composition in burst E-INs or the leakage of light spectrum in the current instrument setup. Even so, I can suppress E-INs by activating hM3DqRs to see the influence on the sPLA, this experiment may tell the overall contribution of E-INs. Fifth, I still don't know the real contribution of glutamate receptors on the membrane of LC-NA



neurons in sPLAs, this can be resolved by adding intracellular blockers for these receptors. According to the slower kinetics and longer time-span of sPLAs, it cannot exclude the possibility of the peptidergic or other transmission origin of sPLAs by activations of metabotropic receptors. Despite of above speculations, my data do support the necessity of local E-INs in the generation of sPLAs. Sixth, even though the alignment of the calcium activity in E-INs and the electrophysiology recording in LC-NA neurons, it raises a considerable random error in alignment accuracy in the current imaging system because of the inter-frame interval (50 ms) and the blurred image when the ROI appears in different focus. Seventh, in vivo unit recordings or the pupillometry monitoring the activity of LC-NA neurons can provide a definitive evidence that reveal whether LC E-INs are involved in the natural activity fluctuating of LC-NA neurons. This could be very important that I don't know how large does the sPLA in brain slices contribute to the intact phasic activity of LC-NA neurons in living animals. According to my imagination that is based on the current facts and evidence, local LC INs may show their importance in behaviors related to subtle shifts of attentions. Technically, I still need more practice tests for methods used for manipulations of ENs, but it is worth to keep putting efforts on this issue.



The aim of investigation in LC E-INs is to reveal mechanisms underlying the phasic activations of LC-NA neurons. I have delineated the hypothesis of indirect origin of phasic activity, it is very interesting to test whether the LC E-INs is involved in. For the functional implications of E-INs, it's necessary to know which afferent innervation making synaptic contacts onto E-INs. Actually, I have done experiments that show the direct synaptic contact from the medial PFC onto some E-INs by an alternative way of WGA tracing experiments. Moreover, I notice that the principle neurons of Barrington's nuclei are also glutamatergic and a portion of them exhibit spontaneous burst with a long duration and is highly related to the micrition function in the living animal. Regard to the medial-to-LC location of these cells, I perhaps consider some of them as burst E-INs in my experiment. However, I find the burst E-INs in a broader area near the LC, reflecting that the burst firing pattern could be a general feature in the dorsal pontine region, and the micturition impulses related to Barrington's nuclei could also contribute to the phasic activation of LC-NA neurons. As the neural network with multi-types cells in the VTA was introduced in previous sections, I propose a LC nucleus comprising both E-INs and I-INs and is more complex than the current understanding of a fairly homogeneous nucleus. I think this putative network provide a

new insight in interpreting the integration of multiple afferents. In this thesis, I present some preliminary data and perspectives for the future work.



## 9. Conclusion

In conclusion, based on the results of the present study, I propose the existence of a local circuit that functions as a generator of a primitive form of phasic LC activation termed sPLA and a modulator of the primitive activity. Given that LC-NA neurons receive inputs from various brain regions (Schwarz et al., 2015) that have different activity patterns, I propose that the local circuit could integrate and accommodate the inputs of various activity patterns to LC-NA neurons and drive LC output with phasic activation of adequate timing and strength to help optimize behaviors. I located the inhibitory component of the circuit, namely peri-LC I-INs, and provide evidence demonstrating that peri-LC I-INs possess the functional features to reflect their role as a modulator of phasic LC activation in the circuit. The evidence indicates that stimulation of excitatory inputs to LC-NA neurons also recruits peri-LC I-INs to exert feedforward inhibition, selective inhibition of peri-LC I-INs enhances sPLA in vitro that resembles phasic activation of LC-NA neurons in vivo, selective inhibition of peri-LC I-INs promotes sensorimotor gating, and peri-LC I-INs receive direct axonal

contacts from cortical areas involved in evaluating the reward of the stimuli and decision-making processes. Although my works mainly concentrate on peri-LC I-INs, I also spend some efforts on LC E-INs and find a positive evidence showing the connection from LC E-INs to the principle neurons.

# Tables



---

**Table 1. Mouse lines used for individual experiments-----254**

**Table 2. Number of animals, brain slices and cells for individual experiments-----255**

**Table 3. AAVs used for individual experiments-----256**

**Table 4. Regulation of sPLA-----257**

**Table 5. Comparison of GlyR and GABAAR mediated IPSC components-----258**

**Table 6. Effects of inhibiting LC-INs with hM4Di DREADD on behaviors-----259**

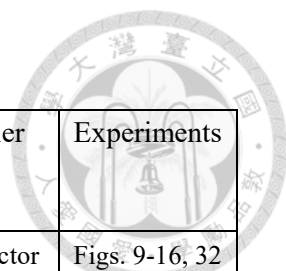
**Table 1 Mouse lines used for individual experiments**

Mouse line	Strain	Supplier	Experiments
VGAT-cre (STOCK <i>Slc32a1</i> <sup>tm2(cre)Lowl</sup> /J)	129S2/SvPas	Jackson Laboratory Bar Harbor, ME USA	Figs. 1-4, 9-22
VGAT-cre (B6J.129S6(FVB)- <i>Slc32a1</i> <sup>tm2(dre)Lowl</sup> /MwarJ)	C57BL/6J	Jackson Laboratory Bar Harbor, ME USA	Fig. 23-26
TH-cre (B6.Cg- <i>7630403G23RiK</i> <sup>Tg(Th- cre)1Tmd</sup> /J)	C57BL/6J	Jackson Laboratory, Bar Harbor, ME USA	Figs. 5-8, 27-30
VGlut2c-re (B6J.129S6(FVB)- <i>Slc17a6</i> <sup>tm2(cre)Lowl</sup> /MwarJ)	C57BL/6J	Jackson Laboratory, Bar Harbor, ME USA	Figs. 31-37
GAD67-GFP	C57BL/6J	Yuchio Yanagawa <sup>†</sup>	Figs. 5-8, 15, 16, 27, 28 & 30
wt	129S2/SvPas	BioLASCO, Co., Ltd Taipei, Taiwan	Figs. 1-4, 9-22
wt	C57BL/6J	NLAC, Taipei, Taiwan	Fig. 5-8, 23-37

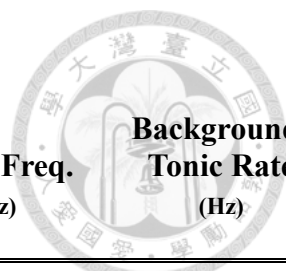
<sup>†</sup> Department of Genetic and Behavioral Neuroscience, Gunma University Graduate School of Medicine, Maebashi, Japan.

**Table 2. Number of animals, brain slices and cells for individual experiments**

Experiments	Animals	Slices	Cells
Figs. 1-4, Recordings of LC-NA neurons and synaptic regulation of sPLA in brain slices.	43	56	58
Figs. 5-8, Localization of peri-LC I-INs making functional connections with LC-NA neurons by viral-genetic WGA tracing.	11	NA	NA
Figs. 9-14, Characterization of synaptic transmission at peri-LC I-INs onto LC-NA neurons using an optogenetic method.	47	54	86
Figs. 15-16, Classification of peri-LC I-INs and reconstruction of the cell morphology.	30	34	63
Figs. 17-20, Inhibition of peri-LC I-INs with hM4DiR DREADD enhanced PLA in LC-NA neurons.	23	21	22
Figs. 21-22, Electrical stimulation of glutamatergic inputs recruits peri-LC I-INs to regulate phasic activity in LC-NA neurons.	27	31	31
Figs. 23-26, Inhibition of peri-LC I-INs enhances prepulse inhibition.	42	NA	NA
Figs. 27-30, Peri-LC I-INs receive axonal contacts from the OFC and PrL/Region-specific projections of the OFC and PrL to the dorsal pontine area.	7	NA	NA
Figs. 31-37, Investigation of of near LC ENs in regulation of the sPLA.	16	15	26

**Table 3. AAVs used for individual experiments**


AAVs	Stereotype	Titer (vg/mL) ×10 <sup>12</sup>	Injection Volume (nL)	Survival Time (weeks)	Supplier	Experiments
AAV2-eF1α-DIO-ChR2(H134R)-eYFP	2	1-8	20-40	3-8	UNC vector Core, NC, USA	Figs. 9-16, 32 & 37
AAV2-hsyn-DIO-hM4Di-mcherry	2	1-8	20-40	3-8	UNC vector Core, NC, USA	Figs. 17-19, 21-26
AAV2-CMV-cre-GFP	2	1-8	na.	na.	UNC vector Core, NC, USA	Fig. 29
AAV2-hsyn-DIO-mCherry	2	1-8	20-40	3-8	UNC vector Core, NC, USA	Figs. 17, 23-26, 31
AAV9-CMV-DIO-WGA	2	0.1-0.2	80-200	8-12	NTU CBT-LS-AAV Core, Taipei, Taiwan	Figs. 5-8, 27-30
AAV2-eF1α-DIO-eYFP	2	1-8	80-200	3-8	UNC vector Core, NC, USA	Figs. 6-7
AAV9-hsyn-ChrimsonR-tdTomato	9	0.1-0.2	80-120	3-8	NTU CBT-LS-AAV Core, Taipei, Taiwan	Figs. 27, 28 & 30
AAV9-CAG-GFP	9	0.1-0.2	80-120	3-8	NTU CBT-LS-AAV Core, Taipei, Taiwan	Fig. 29
AAV5-hsyn-DIO-GCaMP6s	5	1-8	40-80	4-12	UNC vector Core, NC, USA	Figs. 33-36

**Table 4. Regulation of sPLA**


<b>Drug</b>		<b>PLA Incidence (#/10 minutes)</b>	<b>AP #</b>	<b>Mean Freq. (Hz)</b>	<b>Background<sup>a</sup> Tonic Rate (Hz)</b>
Vehicle (aCSF) (n = 12 cells)	Baseline	4.6±1.9 <sup>b</sup>	5.6±1.0	9.8±0.7	1.19±0.12
	Drug	4.2±2.0	9.4±2.3	9.6±0.9	1.23±0.12
	Ratio	0.79±0.27	2.26±0.79	0.99±0.08	1.07±0.08
DNQX+AP5 (n = 9 cells)	Baseline	3.2±1.4	NA <sup>c</sup>	NA	1.44±0.13
	Drug	0±0			1.68±0.14
	Ratio	0±0*			1.21±0.11 <sup>ns</sup>
BMC+Stry (n= 10 cells)	Baseline	5.4±2.2	5.3±0.9	8.8±0.8	1.28±0.13
	Drug	14.6±5.2	8.6±1.4	9.5±0.9	1.89±0.25
	Ratio	4.88±2.55*	1.66±0.14 <sup>ns</sup>	1.11±0.12 <sup>ns</sup>	1.52±0.15**
CNO-mCherry (n = 11 cells)	Baseline	2.4±0.4	5.4±0.7	7.4±0.4	1.64±0.17
	Drug	2.4±0.9	6.0±1.5	8.1±0.9	1.52±0.27
	Ratio	1.03±0.30 <sup>ns</sup>	1.24±0.28 <sup>ns</sup>	1.14±0.17 <sup>ns</sup>	0.92±0.11 <sup>ns</sup>
CNO-hM4Di-mCherry (n = 11 cells)	Baseline	3.8±0.9	4.4±0.4	7.9±0.4	1.58±0.14
	Drug	9.4±2.2	6.7±1.3	7.9±0.5	1.84±0.12
	Ratio	2.53±0.46**	1.52±0.75 <sup>ns</sup>	1.01±0.05 <sup>ns</sup>	1.21±0.09 <sup>ns</sup>
CGP (n = 10 cells)	Baseline	5.7±3.0	4.4±0.8	7.8±0.7	1.25±0.17
	Drug	8.5±4.4	5.3±0.8	7.3±0.5	1.70±0.27
	Ratio	1.47±0.62 <sup>ns</sup>	1.43±0.31 <sup>ns</sup>	0.99±0.11 <sup>ns</sup>	1.36±0.13*

<sup>a</sup>For an individual LC-NA neuron, the background tonic rate is measured by taking the average of instant firing frequency at baseline or during drug application with the detected PLA removed.

<sup>b</sup>Each cell shows data at baseline (upper), drug application (middle), and ratio of the drug application to the baseline (bottom).

<sup>c</sup>NA: Not applicable

Asterisk indicates significant difference in ratio compared to the vehicle group at  $p < 0.05$  (\*) and  $p < 0.01$  (\*\*) using Kruskal-Wallis test followed by post hoc Dunn-Bonferroni test; ns denotes no significant difference.

**Table 5. Comparison of GlyR and GABA<sub>A</sub>R mediated IPSC components**



IPSC Amplitude

(n=12)

GlyR 18.7 ± 5.1 pA<sup>ns</sup>

GABA<sub>A</sub>R 17.4 ± 3.2 pA<sup>ns</sup>

Charge Transfer

(n=12)

GlyR 0.48 ± 0.12 μC<sup>ns</sup>

GABA<sub>A</sub>R 0.52 ± 0.11 μC<sup>ns</sup>

Rising time

(n=11)

GlyR 2.26 ± 0.42 ms<sup>ns</sup>

GABA<sub>A</sub>R 2.93 ± 0.39 ms<sup>ns</sup>

Delay Time Constant

(n=12)

GlyR 24.5 ± 1.6 ms<sup>ns</sup>

GABA<sub>A</sub>R 28.6 ± 5.3 ms<sup>ns</sup>

Paired Pulse Ratio

Control

(n=17)

0.44 ± 0.08<sup>ns</sup>

GlyR

(n=7)

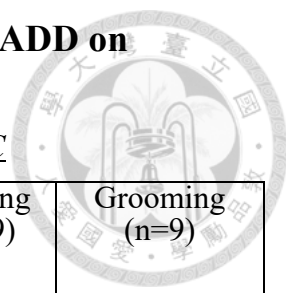
0.57 ± 0.16<sup>ns</sup>

GABA<sub>A</sub>R

(n=4)

0.57 ± 0.16<sup>ns</sup>

**Table 6. Effects of inhibiting LC-INs with hM4Di DREADD on behaviors**



*AAV2-hM4DiR-mCherry transfections covering both sides of the LC*

	PPI (n=12)	Startle (n=12)	Travel Distance (n=9)	Rearing (n=9)	Grooming (n=9)
CNO	63.8±3.8%*	45.1±3.1 AU <sup>†</sup>	73.78±6.4m	139±15	83.9±7.7s
Vehicle	40.6±5.8%*	40.7±4.3 AU	68.9±6.0m	112±9	101.2±14.1s

*AAV2-hM4DiR-mCherry transfections covering neither side of the LC*

	PPI (n=10)	Startle (n=10)
CNO	49.6±7.3%	33.3±4.0AU
Vehicle	49.0±8.7%	37.5±5.1AU

*AAV2-mCherry transfections covering both sides of the LC*

	PPI (n=8)	Startle (n=8)
CNO	45.9±9.0%	38.5±3.7AU
Vehicle	39.0±5.3%	35.6±2.8AU

*Naïve*

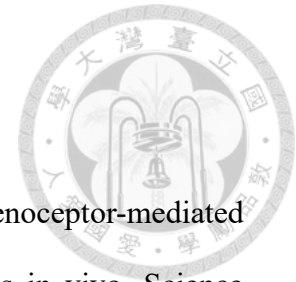
	PPI (n=6)	Startle (n=6)
CNO	42.9±3.3%	36.1 0±6.1AU
Vehicle	35.4±8.2%	32.7±2.8AU

*6-OHDA*

	PPI (n=7)	Startle (n=7)
CNO	50.4±4.3%	36.3±5.0AU
Vehicle	51.6±3.6%	32.8±2.9AU

\*Significant difference at  $p < 0.001$  using paired- $t$  test; <sup>†</sup> AU, arbitrary unit.

## Reference



Aghajanian G. K. and VanderMaelen C. P. (1982). Alpha 2-adrenoceptor-mediated hyperpolarization of locus coeruleus neurons: intracellular studies in vivo. *Science* 215(4538), 1394-6

Aghajanian G. K. and Wang Y. Y. (1986). pertussis toxin blocks the outward currents evoked by opiate and alpha 2-agonists in locus coeruleus neurons. *Brain Res.* 371(2), 390-4.

Alsene, K.M., and Bakshi, V.P. (2011). Pharmacological stimulation of locus coeruleus reveals a new antipsychotic-responsive pathway for deficient sensorimotor gating. *Neuropsychopharmacology* 36, 1656-67.

Alvarez-Maubecin V., García-Hernández F., Williams J. T. and Van Bockstaele E. (2000). Functional Coupling between Neurons and Glia. *J. Neurosci.* 20 (11), 4091-98.

Alvarez V. A., Chow C. C., Van Bockstaele E. and Williams J. T. (2002). Frequency-dependent synchrony in locus ceruleus: Role of electrotonic coupling. *PNAS* 99(6), 4032-36.

Aoki C., Venkatesan, Go C. G., Forman R. and Kurose H. (1998). Cellular and subcellular sites for noradrenergic action in the monkey dorsolateral prefrontal cortex as revealed by the immunocytochemical localization of noradrenergic receptors and

axons. *Cereb. Cortex* 8(3), 269-77.



Arcos D., Sierra A., Nuñez A., Flores G., Aceves J. and Arias-Montaña JA. (2003). Noradrenaline increases the firing rate of a subpopulation of rat subthalamic neurones through the activation of  $\alpha 1$ -adrenoceptors. *Neuropharmacol.* 45(8), 1070-79.

Armstrong-James M. and Fox K. (1983). Effects of ionophoresed noradrenaline on the spontaneous activity of neurons in rat primary somatosensory cortex. *J. Physiol.* 335, 427-47.

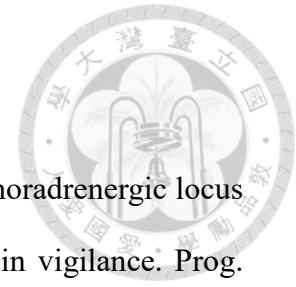
Arnsten A.F., Goldman-Rakic P. S. (1984). Selective prefrontal cortical projections to the region of the locus coeruleus and raphe nuclei in the rhesus monkey. *Brain Res.* 306(1-2), 9-18.

Aston-Jones G. and Bloom F. E. (1981). Norepinephrine-containing locus coeruleus neurons in behaving rats exhibit pronounced responses to non-noxious environmental stimuli. *J. Neurosci.* 1(8), 887-900.

Aston-Jones G., Foote S. L. and Segal M. (1985). Impulse conduction properties of noradrenergic locus coeruleus axons projecting to monkey cerebrocortex. *Neuroscience* 15, 765-77.

Aston-Jones G., Akaoka H., Charléty P. and Chouvet G. (1991). Serotonin selectively attenuates glutamate-evoked activation of noradrenergic locus coeruleus neurons. *J.*

Neurosci. (3), 760-9.



Aston-Jones G., Chiang C. and Alexinsky T. (1991). Discharge of noradrenergic locus coeruleus neurons in behaving rats and monkeys suggests a role in vigilance. *Prog. Brain Res.* 88, 501-20.

Aston-Jones G., Rajkowski J., Kubiak P. and Alexinsky T. (1994). Locus coeruleus neurons in monkey are selectively activated by attended cues in a vigilance task. *J. Neurosci.* 14(7), 4467-80.

Aston-jones G., Rajkowski J. and Kubiak P. (1997). Conditioned responses of monkey locus coeruleus neurons anticipate acquisition of discriminative behavior in a vigilance task. *Neurosci.* 80(3), 697-715.

Aston-Jones G., Zhu Y. and Card J. P. (2004). Numerous GABAergic afferents to locus coeruleus in the pericerulear dendritic zone: possible interneuronal pool. *J. Neurosci.* 24(9), 2313-21.

Aston-Jones G., and Cohen J.D. (2005). An integrative theory of locus coeruleus-norepinephrine function: adaptive gain and optimal performance. *Annu. Rev. Neurosci.* 28, 403-450.

Aston-Jones G. (2013). Behavioral functions of locus coeruleus derived from cellular attributes. *Physiological Psychology* 13, 118-26.



Baghdoyan H. A., Mallios V. J., Duckrow R. B., Mash D. C. (1994). Localization of muscarinic receptor subtypes in brain stem areas regulating sleep. *Neuroreport* 5(13), 1631-4.

Bangasser D. A., Zhang XY., Garachh V., Hanhauser E. and Valentino R. J. (2011). Sexual dimorphism in locus coeruleus dendritic morphology: A structural basis for sex differences in emotional arousal. *103*(3-4), 342-51.

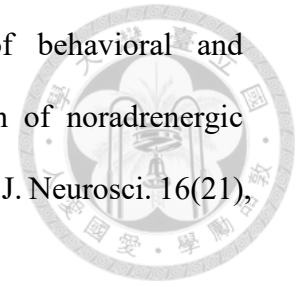
Barbano M. F., Wang HL. Zhang S., Miranda-Barrientos J., Estrin D. J., Figueroa-González A., Liu B., Barker D. J., Morales M. (2020). VTA glutamatergic neurons mediate innate defensive behaviors. *Neuron* In Press.

Bari A. and Aston-Jones G. (2013). Atomoxetine modulate spontaneous and sensory-evoked discharge of locus coeruleus neurons. *Neuropharmacology* 64, 53-64.

Bergles D. E., Doze V. A., Madison D. V. and Smith S. J. (1996). Excitatory actions of norepinephrine on multiple classes of hippocampal CA1 interneurons. *J. Neurosci.* 16(2), 572-85.

Berridge C. W. and Foote S. L. (1991). Effects of locus coeruleus activation on electroencephalographic activity in neocortex and hippocampus. *J. Neurosci.* 11(10), 3135-45.

Berridge C. W. and Foote S. L. (1996a). Enhancement of behavioral and electroencephalographic indices of waking following stimulation of noradrenergic beta-receptors within the medial septal region of the basal forebrain. *J. Neurosci.* 16(21), 6999-7009.



Berridge C. W., Bolen S. J., Manley M. S. and Foote S. L. (1996b). Modulation of Forebrain electroencephalographic activity in halothane-anesthetized rat via actions of noradrenergic beta-receptors within the medial septal region. *J. Neurosci.* 16(21), 7010-20.

Berridge C. W. and Abercrombie E. D. (1999). Relationship between locus coeruleus discharge rates and rates of norepinephrine release within neocortex as assessed by in vivo microdialysis. *Neurosci.* 93(4), 1263-70.

Berridge C. W. and Waterhouse B. D. (2003). The locus coeruleus-noradrenergic system: modulation of behavioral state and state-dependent cognitive processes. *Brain Res.* 42(1), 33-84.

Braff D.L., Greenwood T.A., Swerdlow N.R., Light G.A. and Schork, N.J. (2008). Advances in endophenotyping schizophrenia. *World Psychiatry* 7,11–18.

Berridge C. W., Schmeichel B. E. and España R. A. (2012). Noradrenergic modulation of wakefulness/arousal. *Sleep Med. Rev.* 16(2), 187-97.

Branchereau P., Van Bockstaele E. J., Chan J. and Pickel V. M. (1996). Pyramidal neurons in rat prefrontal cortex show a complex synaptic response to single electrical stimulation of the locus coeruleus region: Evidence for antidromic activation and GABAergic inhibition using in vivo intracellular recording and electron microscopy. *J. Neurosci.* 22(4), 313-331.

Bröcher S., Artola A. and Singer W. (1992). Agonists of cholinergic and noradrenergic receptors facilitate synergistically the induction of long-term potentiation in slices of rat visual cortex. *Brain Res.* 573(1), 27-36.

Boehm S. (1999). Presynaptic  $\alpha$ 2-adrenoceptors control excitatory, but not inhibitory, transmission at rat hippocampal synapses *J. Physiol.* 519(2), 439-49.

Bogerts B. (1981). A brainstem atlas of catecholaminergic neurons in man, using melanin as a natural marker. *J Comp Neurol* 197, 63–80.

Bouret S. and Sara S. J. (2002). Locus coeruleus activation modulates firing rate and temporal organization of odour-induced single-cell responses in rat piriform cortex. *Eur. J. Neurosci.* 16(12), 2371-82.

Bouret S., Duvel A., Onat S. and Sara S. J. (2003). Phasic activation of locus ceruleus neurons by the central nucleus of the amygdala. *J. Neurosci.* 23(8), 3491-97.

Bouret S. and Sara S. J. (2004). Reward expectation, orientation of attention and locus

coeruleus-medial frontal cortex interplay during learning. *Eur. J. Neurosci.* 20, 791-802.

Bouret S. and Sara S. J. (2005). Network reset: a simplified overarching theory of locus coeruleus noradrenaline function. *TRENDS in Neurosci.* 28, 574-82.

Carlsson A, Falck B. and Hillarp N. (1962). NA: Cellular localization of brain monoamines. *Acta. Physiol. Scand. Suppl.* 56, 1-28.

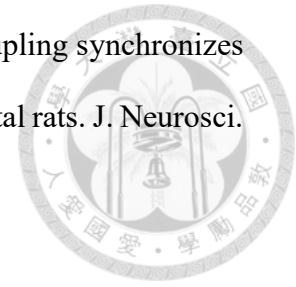
Carter M. E., Yizhar O., Chikahisa S., Nguyen H., Adamantidis A., Nishino S., Deisseroth K. and de Lecea L. (2010). Tuning arousal with optogenetic modulation of locus coeruleus neurons. *Nat. Neurosci.* 13(12), 1526-33.

Chan-Palay V. and Asan E. (1989). Quantitation of catecholamine neurons in the locus coeruleus in human brains of normal young and older adults and in depression. *J. Comp. Neurol.* 287, 357-372.

Chandler D. J., Waterhouse B. D., and Gao W.-J. (2014). New perspectives on catecholaminergic regulation of executive circuits: evidence for independent modulation of prefrontal functions by midbrain dopaminergic and noradrenergic neurons. *Front. Neural Circuits* 8:53.

Chen FJ. and Sara S. J. (2007). Locus coeruleus activation by foot shock or electrical stimulation inhibits amygdala neurons. *Neurosci.* 144(2), 472-81.

Christie M. J., Williams J. T. and North R. A. (1989). Electrical coupling synchronizes subthreshold activity in locus coeruleus neurons in vitro from neonatal rats. *J. Neurosci.* 9(10), 3584-9.



Christi M. J. and Jelinek H. F. (1993). Dye-coupling among neurons of the rat locus coeruleus during postnatal development. *J. Neurosci.* 13(1), 129-37.

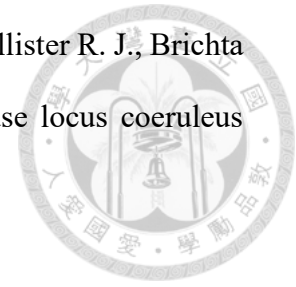
Ciombor K. J., Ennis M. and Shipley M. T. (1999). Norepinephrine increases rat mitral cell excitatory responses to weak olfactory nerve input via alpha-1 receptors in vitro. *J. Neurosci.* 19(2), 595-606.

Clayton, E.C., Rajkowski, J., Cohen, J.D., and Aston-Jones, G. (2004) Phasic activation of monkey locus coeruleus neurons by simple decision in a forced-choice task. *J. Neurosci.* 24, 9914-9920.

Dahlström A. and Fuxe K. (1964). Evidence for the existence of monoamine-containing neurones in the central nervous system. I. Demonstration of monoamines in the cell bodies of brain stem neurones. *Acta Physiol Scand* 62-232, 1-55.

de Freitas R. L., Medeiros P., da Silva J. A., Oliveira R. C., Oliveira R., Ullah F., Khan A. U. and Coimbra N. C. (2016). The  $\mu$ 1-opioid receptor and 5-HT<sub>2A</sub>- and 5HT<sub>2C</sub>-serotonergic receptors of the locus coeruleus are critical in elaborating hypoalgesia induced by tonic and tonic-clonic seizures. *J. Neurosci.* 36, 133-145.

de Oliveira R. B., Howlett M. C. H., Gravina F. S., Imtiaz M. S., Callister R. J., Brichta A. M. and van Helden D. F. (2010). Pacemaker currents in mouse locus coeruleus neurons. *Neurosci.* 170(1), 166-77.



de Oliveira R. B., Gravina F. S., Lim R., Brichta A. M., Callister R. J. and van Helden D. F. (2011). Developmental changes in pacemaker currents in mouse locus coeruleus neurons. *Brain Res.* 1425, 27-36.

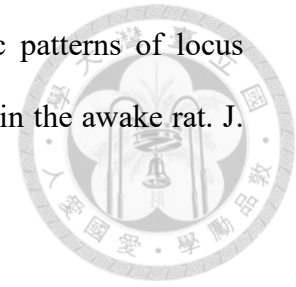
Descarries L., Watkins K. C. and Lapierre Y. (1997). Noradrenergic axon terminals in the cerebral cortex of rat. III. Topometric ultrastructural analysis. *Brain Res.* 133(2), 197-222.

Devilbiss D. M. and Waterhouse B. D. (2000). Norepinephrine exhibits two distinct profiles of action on sensory cortical neuron responses to excitatory synaptic stimuli. *Synapse* 37(4), 273-82.

Devilbiss D. M. and Waterhouse B. D. (2004). The effects of tonic locus ceruleus output on sensory-evoked responses of ventral posterior medial thalamic and barrel field cortical neurons in the awake rat. *J. Neurosci.* 24(48), 10773-85.

Devilbiss D. M., Page M. E. and Waterhouse B. D. (2006). Locus ceruleus regulates sensory encoding by neurons and networks in waking animals. *J. Neurosci.* 26(39), 9860-72.

Devilbiss D. M. and Waterhouse B. D. (2011). Phasic and tonic patterns of locus coeruleus output differentially modulate sensory network function in the awake rat. *J. Neurophysiol.* 105(1), 69-87.



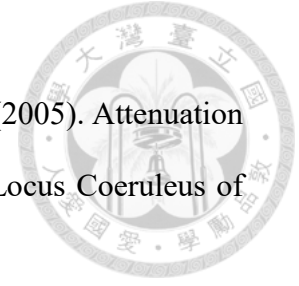
Devilbiss D. M., Waterhouse B. D., Berridge C. W. and Valentino R. (2012). Corticotropin-releasing factor acting at the locus coeruleus disrupts thalamic and cortical sensory-evoked responses. *Neuropsychopharmacol.* 37(9), 2020-30.

Devilbiss D. M. (2019). Consequences of tuning network function by tonic and phasic locus coeruleus output and stress: Regulating detection and discrimination of peripheral stimuli. *Brain Res.* 1709, 16-27.

Devoto P., Flore G., Pani L. and Gessa G. L. (2001). Evidence for co-release of noradrenaline and dopamine from noradrenergic neurons in the cerebral cortex. *Mol. Psychiatry* 6, 657-64.

Devoto P., Flore G., Saba P., Fà M. and Gessa G. L. (2005). Co-release of noradrenaline and dopamine in the cerebral cortex elicited by single train and repeated train stimulation of the locus coeruleus. *BMC Neurosci.* 6, 31.

Dinh L., Nguyen T., Salgado H. and Atzori M. (2009). Norepinephrine homogeneously inhibits  $\alpha$ -amino-3-hydroxyl-5-methyl-4-isoxazole-propionate- (AMPA-) mediated currents in all layers of the temporal cortex of the rat. *Neurochemical Res.* 34, 1896-1906.



Dizgah I. M., Karimian S. M., Zarrindast M. R. and Sohanaki H. (2005). Attenuation of Morphine Withdrawal Signs by a D1 Receptor Agonist in the Locus Coeruleus of Rats. *Neuroreport* 16(15), 1683-6.

Duszkiewicz A. J., McNamara C. G., Takeuchi T. and Genze L. (2019). Novelty and dopaminergic modulation of memory persistence: a tale of two systems. *Trends in Neurosci.* 42(2), 102-14.

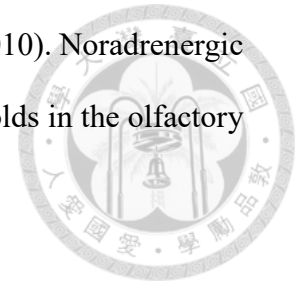
Egan T. M. and North R. A. (1986). Actions of Acetylcholine and Nicotine on Rat Locus Coeruleus Neurons in Vitro. *Neurosci.* 19(2), 565-71.

Elman J. A., Panizzon M. S., Hagler D. J., Eyler L. T., Granholm E. L. and Fennema-Notestine C. (2017). Task-evoked pupil dilation and BOLD variance as indicators of locus coeruleus dysfunction. *Cortex* 97, 60-9.

Ennis M., Aston-Jones G. and Shiekhattar R. (1992). Activation of locus coeruleus neurons by nucleus paragigantocellularis or noxious sensory stimulation is mediated by intracoerulear excitatory amino acid neurotransmission. *Brain Res.* 598(1-2), 185-95.

Ennis M. and Aston-Jones G. (1988). Activation of locus coeruleus from nucleus paragigantocellularis: a new excitatory amino acid pathway in brain. *J. Neurosci.* 8(10), 3644-3657.

Escanilla O., Arrellanos A., Karnow A., Ennis M. and Linster C. (2010). Noradrenergic modulation of behavioral odor detection and discrimination thresholds in the olfactory bulb. *Eur. J. Neurosci.* 32(3), 458-68.



Eschenko O. and Sara S. J. (2008). Learning-dependent, transient increase of activity in noradrenergic neurons of locus coeruleus during slow wave sleep in the rat: brain stem-cortex interplay for memory consolidation? *Cereb. Cortex* 18(11), 2596-603.

Eshel N., Bukwich M., Rao V., Hemmelder V., Tian J. and Uchida N. (2015). Arithmetic and local circuitry underlying dopamine prediction errors. *Nature* 525, 243-6.

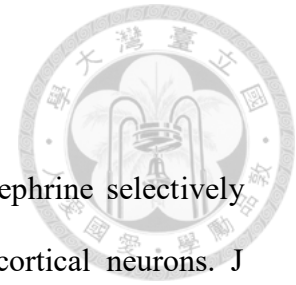
Farb C. R., Chang W. and LeDoux J. E. (2010). Ultrastructural Characterization of Noradrenergic Axons and Beta-Adrenergic Receptors in the Lateral Nucleus of the Amygdala. *Front. Behav. Neurosci.* 4(162).

Félix Vicq d'Azyr (1793). *Instruction sur la manière d'inventorier et de conserver, dans toute l'étendue de la République, tous les objets qui peuvent servir aux arts, aux sciences et à l'enseignement.* de l'imprimerie nationale.

Fendt M., Li L. and Yeomans J. S. (2001). Brain stem circuits mediating prepulse inhibition of the startle reflex. *Psychopharmacol.* 156(2-3), 216-24.

Florin-Lechner S. M., Druhan J. P., Aston-Jones G. and Valentino R. J. (1996). Enhanced norepinephrine release in prefrontal cortex with burst stimulation of the locus

coeruleus. 742(1-2), 89-97.



Foehring R. C., Schwindt P. C. and Crill W. E. (1989). Norepinephrine selectively reduces slow  $\text{Ca}^{2+}$ - and  $\text{Na}^{+}$ -mediated  $\text{K}^{+}$  currents in cat neocortical neurons. *J Neurophysiol.* 61(2), 245-56.

Foote S. L., Freedman R. and Oliver A. P. (1975). Effects of putative neurotransmitters on neuronal activity in monkey auditory cortex. *Brain Res.* 86(2), 229-42.

Foote S. L., Aston-Jones G. and Bloom F. E. (1980). Impulse activity of locus coeruleus neurons in awake rats and monkeys is a function of sensory stimulation and arousal. *PNAS* 77(5), 3033-37.

Foote S. L. and Morrison J. H. (1987) Extrathalamic modulation of cortical function, *Annu Rev Neurosci* 10,67–95.

Foote S. L. and Berridge C. W. (2019). New developments and future directions in understanding locus coeruleus - Norepinephrine (LC-NE) function. *Brain Res.* 1709, 81-84.

Forsythe I. D., Linsdell P. and Stanfield P. R. (1992). Unitary A-currents of Rat Locus Coeruleus Neurones Grown in Cell Culture: Rectification Caused by Internal  $\text{Mg}^{2+}$  and  $\text{Na}^{+}$ . *Physiol.* 451, 553-83.

Gautron L., Rutkowski J.M., Burton M.D., Wei W., Wan Y. and Elmquist, J.K. (2013). Neuronal and nonneuronal cholinergic structures in the mouse gastrointestinal tract and spleen. *J. Comp. Neurol.* 521, 3741-3767.



George M. J. (1992). Modification of receptive fields of posteromedial barrel subfield neocortical single units by known concentrations of iontophoretically applied noradrenaline in the rat. *Int. J. Neurosci.* 65(1-4), 69-81.

Gerfen C. R., O'Leary D. D. M. and Cowan W. M. (1982). A note on the transneuronal transport of wheat-germ agglutinin-conjugated horseradish peroxidase in the avian and rodent visual system. *Exp. Brain Res.* 48, 443-48.

Gervasoni D., Darracq L., Fort P., Soulière F., Chouvet G. and Luppi P-H (1998). Electrophysiological evidence that noradrenergic neurons of the rat locus coeruleus are tonically inhibited by GABA during sleep. *Eur. J. Neurosci.* 10(3), 964-70.

Geva R., Zivan M., Warsha A. and Olchik D. (2013). Alerting, orienting or executive attention networks: differential patterns of pupil dilations. *Front. Behav. Neurosci.* 7, 145.

Gervasoni D., Darracq L., Fort P., Soulière F., Chouvet G. and Luppi P-H. (1998). Electrophysiological evidence that noradrenergic neurons of the rat locus coeruleus are tonically inhibited by GABA during sleep. *Eur. J. Neurosci.* 10(3), 964-70.

Geyer M. A. (2008). Developing translational animal models for symptoms of

schizophrenia or bipolar mania. *Neurotox Res.* 14, 71-78.



Ghasemia M. and Mehranfard N. (2018). Mechanisms underlying anticonvulsant and proconvulsant actions of norepinephrine. *Neuropharmacol.* 137, 297-308.

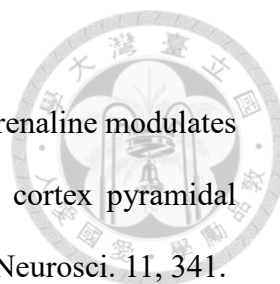
Glennon E., Carcea I., Martins A. R. O., Multani J., Shehu I., Svirsky M. A. and Froemke R. C. (2019). Locus coeruleus activation accelerates perceptual learning. *Brain Res.* 1709, 39-49.

Goldstein D. S. (1997). Catecholamine receptors and signal transduction. *Advances in Pharmacology* (42), 379-90.

Grant S. J., Aston-Jones G. and Redmond Jr D. E. (1988). Responses of primate locus coeruleus neurons to simple and complex sensory stimuli. *Brain Res. Bull.* 21(3), 401-10.

Grella S. L., Neil J. M., Edison H. T., Strong V. D., Odintsova I. V., Walling S. G., Martin G. M., Marrone D. F. and Harley C. W. (2019). Locus coeruleus phasic, but not tonic, activation initiates global remapping in a familiar environment. *J. Neurosci.* 39(3), 445-55.

Grenhoff J., North R. A. and Johnson S. W. (1995). Alpha1-adrenergic effects on dopamine neurons recorded intracellularly in the rat midbrain slice. *Eur. J. Neurosci.* 7(8), 1707-13.



Grzelka K., Kurowski P., Gawlak M. and Szulczyk P. (2017). Noradrenaline modulates the membrane potential and holding current of medial prefrontal cortex pyramidal neurons via  $\beta$ 1-adrenergic receptors and HCN channels. *Front Cell Neurosci.* 11, 341.

Havekes R., Canton D. A., Park A. J., Huang T., Nie T, Day J. P., Guercio L. A., Grimes Q., Luczak V., Gelman I. H., Baillie G. S., Scott J. D. and Abel T. (2012). Gravin orchestrates protein kinase A and  $\beta$ 2-adrenergic receptor signaling critical for synaptic plasticity and memory. *J. Neurosci.* 32(50), 18137-49.

Hayat H., Regev N., Matosevich N., Sales A., Paredes-Rodriguez E., Krom A. J., Bergman L., Li Y., Lavigne M., Kremer E. J., Yizhar O., Pickering A. E. and Nir Y. (2020). Locus coeruleus norepinephrine activity mediates sensory-evoked awakenings from sleep. *Sci. Adv.* 6(15), eaaz4232.

Hervé-Minvielle A. and Sara S. J. (1995). Rapid habituation of auditory responses of locus coeruleus cells in anaesthetized and awake rats. *Neuroreport* 6(10), 1363-8.

Hieble J. P., Bylund D. B., Clarke D. E., Eikenburg D. C., Langer S. Z., Lefkowitz R. J., Minneman K. P. and Ruffolo Jr R. R. (1995). International union of pharmacology. X. recommendation for nomenclature of alpha 1-adrenoceptors: consensus update. *Pharmacol. Rev.* 47(2), 267-70.

Hillman K. L., Doze V. A. and Porter J. E. (2007).  $\alpha$ 1A-adrenergic receptors are

functionally expressed by a subpopulation of cornu ammonis 1 interneurons in rat hippocampus. *J. Pharmacol. Exp. Ther.* 321(3), 1062-68.



Hillman K. L., Lei S., Doze V. A. and Porter J. E. (2009). Alpha-1A adrenergic receptor activation increases inhibitory tone in CA1 hippocampus. *Epilepsy Res.* 84(2-3) 97-109.

Hirata A., Aguilar J., Castro-Alamancos M. A. (2006). Noradrenergic Activation Amplifies Bottom-Up and Top-Down Signal-To-Noise Ratios in Sensory Thalamus. *J. Neurosci.* 26(16), 4426-36.

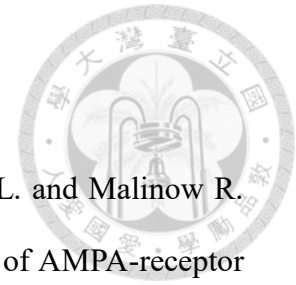
Hirschberg S., Li Y., Randall A., Kremer E. J. and Pickering A. E. (2017). Functional dichotomy in spinal- vs prefrontal-projecting locus coeruleus modules splits descending noradrenergic analgesia from ascending aversion and anxiety in rats. *eLife* 6, e29808.

Hobson, J.A., McCarley, R.W., and Wyzinski, P.W. (1975). Sleep cycle oscillation: reciprocal discharge by two brainstem neuronal groups. *Science* 189, 55-58.

Hopkins W. F. and Johnston D. (1984). Frequency-dependent noradrenergic modulation of long-term potentiation in the hippocampus. *Science* 226(4672), 350-52.

Howells F. M., Stein D. J. and Russell V. A. (2012). Synergistic tonic and phasic activity of the locus coeruleus norepinephrine (LC-NE) arousal system is required for optimal

attentional performance. *Metab. Brain Dis.* 27(3), 267-74.



Hu H., Real E., Takamiya K., Kang M-G, Ledoux J., Huganir R. L. and Malinow R. (2007). Emotion enhances learning via norepinephrine regulation of AMPA-receptor trafficking. *Cell* 131(1) 160-73.

Huang HP., Zhu FP., Chen XW., Xu ZQ. D., Zhang CX. and Zhou Z. (2012). Physiology of quantal norepinephrine release from somatodendritic sites of neurons in locus coeruleus. *Front. Mol. Neurosci.* 5, 29.

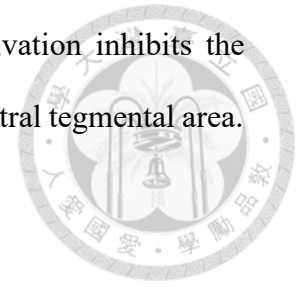
Huang SY., Treviño M., He K., Ardiles A., de Pasquale R., Guo Y., Palacios A., Huganir R. and Kirkwood A. (2012) Pull-push neuromodulation of LTP and LTD enables bidirectional experience-induced synaptic scaling in visual cortex. *Neuron* 73(3), 497-510.

Hung WC., Chu, YL., Tsai ML., Wong SB., Min MY., Chen RF. and Yang HW. (2020). GABAB receptor-mediated tonic inhibition of locus coeruleus neurons plays a role in deep anesthesia induced by isoflurane. *NeuroReport* 31(7), 557-64.

Hurley L. M., Devilbiss D. M. and Waterhouse B. D. (2004). A matter of focus: monoaminergic modulation of stimulus coding in mammalian sensory networks. *Curr. Opin. Neurobiol.* 14(4), 488-95.

Inyushin M. U., Arencibia-Albite F., Vázquez-Torres R., Vélez-Hernández M.E. and

Jiménez-Rivera C.A. (2010). Alpha-2 noradrenergic receptor activation inhibits the hyperpolarization-activated cation current (I<sub>h</sub>) in neurons of the ventral tegmental area. *Neurosci.* 167(2), 287-97.



Imai H., Steindler D. A. and Kitai S. T. (1986). The organization of divergent axonal projections from the midbrain raphe nuclei in the rat. *J. Comp. Neurol.* 243, 363-380.

Ishida Y., Hashiguchi H., Takeda R., Ishizuka Y., Mitsuyama Y., Kannan H., Nishimori T. and Nakahara D. (2002). Conditioned-fear stress increases fos expression in monoaminergic and GABAergic neurons of the locus coeruleus and dorsal raphe nuclei. *Synapse* 45(1), 46-51.

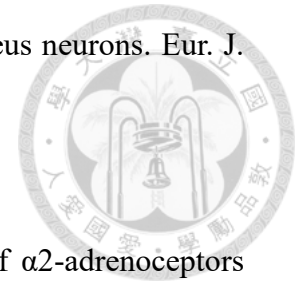
Ishimatsu M. and Williams J. T. (1996). Synchronous activity in locus coeruleus results from dendritic interactions in pericoerulear regions. *J. Neurosci.* 16(16), 5196-5204.

Ito S., Stuphorn V., Brown J. W. and Schall J. D. (2003). Performance monitoring by the anterior cingulate cortex during saccade countermanding. *Science* 302, 120 -22.

Janitzky K., Lippert M. T., Engelhorn A., Tegtmeyer J., Goldschmidt J., Heinze H. and Ohl F. W. (2015). Optogenetic silencing of locus coeruleus activity in mice impairs cognitive flexibility in an attentional set-shifting task. *Front. Behav. Neurosci.* 9, 286.

Jedema H. P., Gold S. J., Gonzalez-Burgos G., Sved A. F., Tobe B. J., Wensel T. G. and Grace A. A. (2008). Chronic cold exposure increases RGS7 expression and decreases

$\alpha$ 2-autoreceptor-mediated inhibition of noradrenergic locus coeruleus neurons. *Eur. J. Neurosci.* 27(9), 2433-43.



Ji X. H., Ji J. Z., Zhang H. and Li B. M. (2008). Stimulation of  $\alpha$ 2-adrenoceptors suppresses excitatory synaptic transmission in the medial prefrontal cortex of rat. *Neuropsychopharmacol.* 33, 2263-71.

Jishage K., Ueda O., Suzuki H. and Tabuchi K. (1999). A genetic approach to visualization neurotechnique of multisynaptic neural pathways using plant lectin transgene. *Neuron* 22, 33-41.

Jodo, E. and Aston-Jones, G. (1997). Activation of locus coeruleus by prefrontal cortex is mediated by excitatory amino acid inputs. *Brain Res.*, 768, 327-332.

Jodo, E., Chiang, C. and Aston-Jones, G. (1998). Potent excitatory influence of prefrontal cortex activity on noradrenergic locus coeruleus neurons. *Neuroscience*, 83, 3-79.

Joe G. and Russell J. B. (1964). Histochemical demonstration of norepinephrine at a fine structure level. *J. Histochem. Cytochem.* 12, 197-209.

Jones B. E. (1990). Immunohistochemical study of choline acetyltransferase-immunoreactive processes and cells innervating the pontomedullary reticular formation in the rat. *J Comp Neurol.* 295(3), 485-514.



Jones B. E. (1991a). The Role of Noradrenergic Locus Coeruleus Neurons and Neighboring Cholinergic Neurons of the Pontomesencephalic Tegmentum in Sleep-Wake States. *Prog. Brain Res.* 88, 533-43.

Jones B. E. (1991b). Paradoxical Sleep and Its Chemical/Structural Substrates in the Brain. *Neurosci.* 40(3), 637-56.

Joshi S., Li Y., Kalwani R. M. and Gold J. I. (2016). Relationships between pupil diameter and neuronal activity in the locus coeruleus, colliculi, and cingulate cortex. *Neuron* 89, 221–234.

Jüngling K., Liu X., Lesting J., Coulon P., Sosulina L., Reinscheid R. K. and Pape H-C (2012). Activation of Neuropeptide S-expressing neurons in the locus coeruleus by corticotropin-releasing factor. *J. Physiol.* 590(16), 3701-17.

Jurgens C. W. D., Boese S. J., King J. D., Pyle S. J., Porter J. E. and Doze V. A. (2005). Adrenergic receptor modulation of hippocampal CA3 network activity. *Epilepsy Res.* 66(1-3), 117-28.

Kask A., Rägo L. and Harrob J. (1998). Anxiolytic-like effect of neuropeptide Y (NPY) and NPY13–36 microinjected into vicinity of locus coeruleus in rats. *Brain Res.* 788(1-2), 345-48.

Katsuki H., Izumi Y., and Zorumski C. F. (1997). Noradrenergic regulation of synaptic plasticity in the hippocampal CA1 region. *J. Neurophysiol.* 77(6), 3013-20.

Kaur S., Saxena R. N. and Mallick B. N. (1997). GABA in locus coeruleus regulates spontaneous rapid eye movement sleep by acting on GABA<sub>A</sub> receptors in freely moving rats. *Neurosci. Lett.* 223(2), 105-8.

Kawaguchi Y. and Shindou T. (1998). Noradrenergic excitation and inhibition of GABAergic cell types in rat frontal cortex. *J. Neurosci.* 18(17), 6963-76.

Kawahara H., Kawahara Y., Westerink B. H. C. (2001). The noradrenaline–dopamine interaction in the rat medial prefrontal cortex studied by multi-probe microdialysis *Eur. J. Pharmacol.* 418(3), 177-86.

Kayama Y., Negi T., Sugitani M. and Iwama K. (1982). Effects of locus coeruleus stimulation on neuronal activities of dorsal lateral geniculate nucleus and perigeniculate reticular nucleus of the rat. *Neurosci.* 7(3), 655-66.

Kayama Y. (1985). Ascending, descending and local control of neuronal activity in the rat lateral geniculate nucleus. *Vision Res.* 25(3), 339-47.

Kazumasa W., Keisuke T., Makoto O., Fabio A. Z., Luigi Z., and Shosuke I. (2015). Norepinephrine and Its metabolites are involved in the synthesis of neuromelanin derived from the locus coeruleus. *J Neurochem.* 135(4), 768-76.



Kempadoo K. A., Mosharov E. V., Choi S. J., Sulzer D. and Kandel E. R. (2016). Dopamine release from the locus coeruleus to the dorsal hippocampus promotes spatial learning and memory. *PNAS* 113(51), 14835-40.

Kirkwood A., Rozas C., Kirkwood J., Perez F. and Bear M. F. (1999). Modulation of long-term synaptic depression in visual cortex by acetylcholine and norepinephrine. *J. Neurosci.* 19(5), 1599-1609.

Kitahama K., Nagatsu I., Geffard M. and Maeda T. (2000). Distribution of dopamine-immunoreactive fibers in the rat brainstem. *J. Chem. Neuroanat.* 18, 1-9.

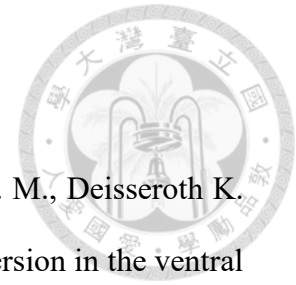
Kobayashi M., Sasabe T., Shiohama Y. Koshikawa N. (2008). Activation of  $\alpha$ 1-adrenoceptors increases firing frequency through protein kinase C in pyramidal neurons of rat visual cortex. *Neurosci. Letters*, 430(2), 175-80.

Kokaia M., Bengzon J., Kale'n P. and Lindvall O. (1989). Noradrenergic mechanisms in hippocampal kindling with rapidly recurring seizures. *Brain Res.* 491(2), 398-402.

Labarrera C., Deitcher Y., Dudai A., Weiner B., Amichai A. N., Zylbermann N. and London M. (2018). Adrenergic modulation regulates the dendritic excitability of layer 5 pyramidal neurons in vivo. *Cell Report*, 23(4), 1034-44.

Laing M. and Bashir Z. I. (2014).  $\beta$ -Adrenoceptors and synaptic plasticity in the

perirhinal cortex. *Neurosci.* 273(100), 163-73.



Lammel S., Lim B. K., Ran C., Huang K. W., Betley M. J., Tye K. M., Deisseroth K. and Malenka R. C. (2012). Input-specific control of reward and aversion in the ventral tegmental area. *Nature* 491, 212–217.

Law-Tho D., Crepel F., Hirsch J. C. (1993). Noradrenaline decreases transmission of NMDA- and non-NMDA-receptor mediated monosynaptic EPSPs in rat prefrontal neurons in vitro. *Eur. J. Neurosci.* 5(11), 1494-1500.

Lazarov N. E., Schmidt U., Wanner I. and Pilgrim C. (1998). Mapping of D1 Dopamine Receptor mRNA by Non-Radioactive in Situ Hybridization. *Histochem. Cell Biol.* 109(3), 271-9.

Lee A., Rosin D. L., Van Bockstaele E. (1998a).  $\alpha$ 2A-adrenergic receptors in the rat nucleus locus coeruleus: subcellular localization in catecholaminergic dendrites, astrocytes, and presynaptic axon terminals. *Brain Res.* 795(1-2), 157-69.

Lee A., Diane L. Rosin D. L. and Van Bockstaele E. (1998b). Ultrastructural evidence for prominent postsynaptic localization of  $\alpha$ 2C-adrenergic receptors in catecholaminergic dendrites in the rat nucleus locus coeruleus. *J. Comp. Neurol.* 394(2) 218-29.

Lee H. K. and Kirkwood A. (2007). Neuromodulators control the polarity of spike-

timing-dependent synaptic plasticity. *Neuron* 55(6), 919-29.



Lei S., Deng P. Y., Porter J. E. and Shin H. S. (2007). Adrenergic facilitation of GABAergic transmission in rat entorhinal cortex. *Neuroscience* 98(5), 2868-77.

Lewis D. A. and Morrison J. H. (1989). Noradrenergic innervation of monkey prefrontal cortex: A dopamine- $\beta$ -hydroxylase immunohistochemical study. *J. Comp. Neurol.* 282(3), 317-30.

Léna C., d'Exaerde A. de K., Cordero-Erausquin M., Le Novère N., Arroyo-Jimenez M. del M. and Changeux J. (1999). Diversity and distribution of nicotinic acetylcholine receptors in the locus ceruleus neurons. *PNAS* 96(21), 12126-31.

Lewis D. A., Campbell M. J., Foote S. L., Goldstein M. and Morrison J. H. (1987). The distribution of tyrosine hydroxylase-immunoreactive fibers in primate neocortex is widespread but regionally specific. *J Neurosci.* 7(1), 279–290.

Lin Y., Quartermain D., Dunn A. J., Weinshenker D., and Stone E. A. (2008). Possible Dopaminergic Stimulation of Locus Coeruleus  $\alpha$ 1-adrenoceptors Involved in Behavioral Activation. *Synapse* 62(7), 516-23.

Lin YW., Min MY., Chiu TH. and Yang HW. (2003). Enhancement of associative long-term potentiation by activation of beta-adrenergic receptors at CA1 synapses in rat hippocampal slices. *J. Neurosci.* 23(10), 4173-81.



Linster C., Nai Q. and Ennis M. (2011). Nonlinear effects of noradrenergic modulation of olfactory bulb function in adult rodents. *J. Neurophysiol.* 105(4), 1432-43.

Liu W., Yuen E. Y., Allen P. B., Feng J., Greengard P. and Yan Z. (2006). Adrenergic Modulation of NMDA receptors in prefrontal cortex is differentially regulated by RGS proteins and spinophilin. *PNAS* 103(48), 18338-43.

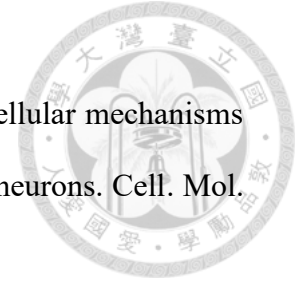
MacDonald E., Kobilka B. K. and Scheinin M. (1997). Gene targeting - homing in on alpha 2-adrenoceptor-subtype function. *Trends Pharmacol. Sci.* 18(6), 211-19.

Madison D. V. and Nicoll R. A. (1982). Noradrenaline blocks accommodation of pyramidal cell discharge in the hippocampus. *Nature*, 636-38.

Madison D. V. and Nicoll R. A. (1988). Norepinephrine decreases synaptic inhibition in the rat hippocampus. *Brain Res.* 442(1), 131-38.

Maeda T., Kitahama K. and Geffard M. (1994). Dopaminergic innervation of rat locus coeruleus: a light and electron microscopic immunohistochemical study. *Microsc. Res. Tech.* 29, 211-218.

Mallick B. N., Kaur R. and Saxena R. N. (2001). Interactions between cholinergic and GABAergic neurotransmitters in and around the locus coeruleus for the induction and maintenance of rapid eye movement sleep in rats. *Neurosci.* 104(2), 467-85.



Marzo A., Bai J., Caboche J., Vanhoutte P. and Otani S. (2010). Cellular mechanisms of long-term depression induced by noradrenaline in rat prefrontal neurons. *Cell. Mol. Neurosci.* 169(1), 74-86.

Matschke L. A., Bertoune M., Roeper J., Snutch T. P., Oertel W. H., Rinné S and Decher N. (2015). A concerted action of L- and T-type  $Ca^{2+}$  channels regulates locus coeruleus pacemaking. *Mol. Cell Neurosci.* 68, 293-302.

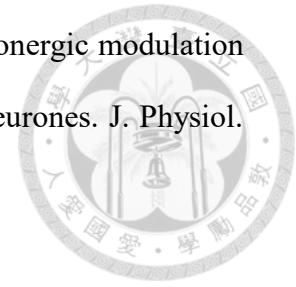
Matschke L. A., Rinné S., Snutch T. P., Oertel W. H., Dolga A. M. and Decher N. (2018). Calcium-activated SK potassium channels are key modulators of the pacemaker frequency in locus coeruleus neurons. *Mol. Cell Neurosci.* 88, 330-41.

McCall J. G., Al-Hasani R., Siuda E. R., Hong D. Y., Norris A. J., Ford C. P., Bruchas M. R. (2015). CRH Engagement of the Locus Coeruleus Noradrenergic System Mediates Stress-Induced Anxiety. *Neuron* 87(3), 605-20.

McCall J. G., Siuda E. R., Bhatti D. L., Lawson L. A., McElligott Z. A., Stuber G. D. and Bruchas M. R. (2017). Locus coeruleus to basolateral amygdala noradrenergic projections promote anxiety-like behavior. *eLife* 6, e18247.

McCormick D. A. and Prince D. A. (1988). Noradrenergic modulation of firing pattern in guinea pig and cat thalamic neurons, in vitro. *J. Neurosci.* 59(3), 978-96.

McCormick D. A. and Pape H. C. (1990). Noradrenergic and serotonergic modulation of a hyperpolarization-activated cation current in thalamic relay neurones. *J. Physiol.* 431(1), 319-42.



McCormick D. A., Pape H. C. and Williamson A. (1991). Actions of norepinephrine in the cerebral cortex and thalamus: implications for function of the central noradrenergic system. *Prog. Brain Res.* 88, 293-305.

McCormick D. A. and Wang Z. (1991). Serotonin and noradrenaline excite GABAergic neurones of the guinea-pig and cat nucleus reticularis thalami. *J. Physiol.* 442, 235-55.

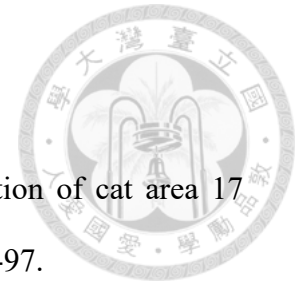
McCormick D. A. (1992a). Cellular mechanisms underlying cholinergic and noradrenergic modulation of neuronal firing mode in the cat and guinea pig dorsal lateral geniculate nucleus. *J. Neurosci.* 12(1), 278-89.

McCormick D. A. (1992b). Neurotransmitter actions in the thalamus and cerebral cortex and their role in neuromodulation of thalamocortical activity. *Prog. Neurobiol.* 39(4), 337-88.

McCormick D. A., Wang Z. and Huguenard J. (1993). Neurotransmitter control of neocortical neuronal activity and excitability. *Cereb. Cortex* 3(5), 387-98.

McDevitt R. A., Szot P., Baratta M. V., Bland S. T., White S. S., Maier S. F. and Neumaier J. F. (2009). Stress-induced activity in the locus coeruleus is not sensitive to

stressor controllability. *Brain Res.* 1285, 109-18.



McLean J. and Waterhouse B. D. (1994). Noradrenergic modulation of cat area 17 neuronal responses to moving visual stimuli. *Brain Res.* 667(1), 83-97.

Mena-Segovia J. and Bolam J. P. (2017) Rethinking the Pedunculo-pontine Nucleus: From Cellular Organization to Function. *Neuron* 94(1), 7-18.

Miller R. L., Stein M. K., and Loewy A. D. (2011). Serotonergic inputs to FoxP2 neurons of the pre-locus coeruleus and parabrachial nuclei that project to the ventral tegmental area. *Neurosci.* 193, 229-40.

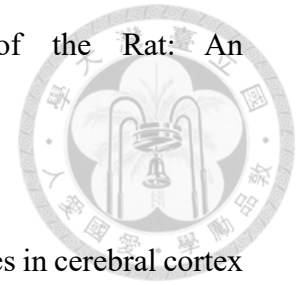
Min MY., Wu YW., Shih PY., Lua HW., Wu Y., Hsu CL., Lia MJ. and Yang HW. (2010). Roles of A-type potassium currents in tuning spike frequency and integrating synaptic transmission in noradrenergic neurons of the A7 catecholamine cell group in rats. *Neurosci.* 168(3), 633-45.

Montague P. R., Hyman S. E. and Cohen J. D. (2004). Computational roles for dopamine in behavioural control *Nature* 431, 760-7.

Morales M. and Margolis E. B. (2017). Ventral tegmental area: cellular heterogeneity, connectivity and behavior. *Nat. Rev. Neurosci.* 18, 73–85.

Morrison J. H., Grzanna R., Molliver M. E. and Coyle J. T. (1978). The Distribution

and Orientation of Noradrenergic Fibers in Neocortex of the Rat: An Immunofluorescence Study. *J. Comp. Neurol.* 181(1), 17-39.



Morrison J. H. and Magistretti P. J. (1983). Monoamines and peptides in cerebral cortex - contrasting principles of cortical organization. *Trends Neurosci.* 6, 146–151.

Morrison J. H. and Foote S. L. (1986). Noradrenergic and serotonergic innervation of cortical, thalamic, and tectal visual structures in old and new world monkeys. *J. Comp. Neurol.* 243, 117-38.

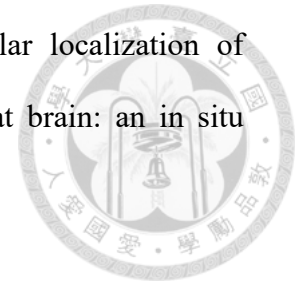
Motaghi S., Sheibani V., Farazifard R. and Joneidi H. (2006). Electrical stimulation of locus coeruleus strengthens the surround inhibition in layer V barrel cortex in rat. *Neurosci. Lett.* 401(3), 280-4.

Murphy P. R., Robertson I. H., Balsters J. H. and O'connell R. G. (2011). Pupillometry and P3 index the locus coeruleus-noradrenergic arousal function in humans. *Psychophysiology.* 48, 1532–43.

Nakazato T. (1987) Locus coeruleus neurons projecting to the forebrain and the spinal cord in the cat. *Neurosci.* 23(2), 529-38.

Nitz D. and Siegel J. M. (1997). GABA release in the locus coeruleus as a function of sleep/wake state. *Neurosci.* 78(3), 795-801.

Nicholas A. P., Pieribone V. A. and Hokfelt, T. (1993). Cellular localization of messenger RNA for beta-1 and beta-2 adrenergic receptors in rat brain: an in situ hybridization study. *Neurosci.* 56, 1023-39.



North R. A. and Williams J. T. (1985). On the potassium conductance increased by opioids in rat locus coeruleus neurones. *J. Physiol.* 364(1), 265-80.

Novitskaya Y., Sara S. J., Logothetis N. K. and Eschenko O. (2016). Ripple-triggered stimulation of the locus coeruleus during post-learning sleep disrupts ripple/spindle coupling and impairs memory consolidation. *Learn Mem.* 23(5), 238-48.

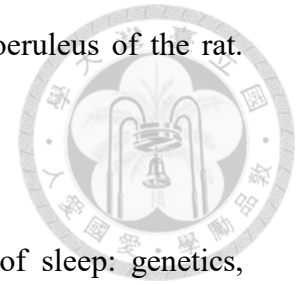
Nowicky A. V., Christofi G. and Bindman L. J. (1992). Investigation of  $\beta$ -adrenergic modulation of synaptic transmission and postsynaptic induction of associative LTP in layer V neurones in slices of rat sensorimotor cortex. *Neurosci. Letters* 137(2), 270-73.

O'Doherty J. P., Deichmann R., Critchley H. D. and Dolan R. J. (2002). Neural responses during anticipation of a primary taste reward. *Neuron* 33, 815-26.

Ornstein K., Milon H., McRae-Degueurce A., Alvarez C., Berger B. and Würzner H. P. (1987). Biochemical and radioautographic evidence for dopaminergic afferents of the locus coeruleus originating in the ventral tegmental area. *J. Neural Transm.* 70, 183-191.

Ortega J. E., Mendiguren A., Pineda J. and Meana J. J. (2012). Regulation of central

noradrenergic activity by 5-HT<sub>3</sub> receptors located in the locus coeruleus of the rat. *Neuropharmacology* 62(8), 2472-79.



Pace-Schott E. F. and Hobson J. A. (2002). The Neurobiology of sleep: genetics, cellular physiology and subcortical networks. *Nat. Rev. Neurosci.* 3, 591-605.

Pal D. and Mallick B. N. (2007). Neural mechanism of rapid eye movement sleep generation with reference to REM-OFF neurons in locus coeruleus. *Indian J. Med. Res.* 125, 721-39.

Pan Z. Z., Grudt T. J. and Williams J. T. (1994). Alpha 1-adrenoceptors in rat dorsal raphe neurons: regulation of two potassium conductances. *J. Physiol.* 478(3), 437-47.

Patt S. and Gerhard L. (1993). A Golgi study of human locus coeruleus in normal brains and in Parkinson's disease. *Neuropathol. Appl. Neurobiol.* 19,519–523.

Parker K. E., Buckley A. R., Stewart S. L., Hunter S. C. and McCall J. G. (2019). Midbrain glutamatergic neurons drive locus coeruleus-mediated negative affect. *Society of Neuroscience 2019 Conference Poster*, 507.15 / X10.

Paul E. J., Tossell K. and Ungless M. A. (2019). Transcriptional profiling aligned with in situ expression image analysis reveals mosaically expressed molecular markers for GABA neuron sub-groups in the ventral tegmental area. *Eur. J. Neurosci.* 50(11), 3732-49.



Piasecik M. T. and Perez D. M. (2001).  $\alpha$ 1-Adrenergic receptors: new insights and directions. *J Pharmacol. Exp. Ther.* 298(2), 403-10.

Pickel V. M., Joh T. H., Reis D. J. (1977). A serotonergic innervation of noradrenergic neurons in nucleus locus coeruleus: demonstration by immunocytochemical localization of the transmitter specific enzymes tyrosine and tryptophan hydroxylase. *Brain Res.* 131, 197-214

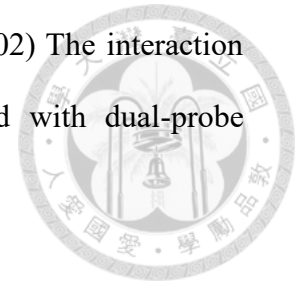
Porrino L. J. and Goldman-Rakic P. S. (1982). Brainstem innervation of prefrontal and anterior cingulate cortex in the rhesus monkey revealed by retrograde transport of HRP, *J Comp. Neurol.* 205:63–76.

Porter J. D., Guthrie B. L. and Sparks D. L. (1985). Selective retrograde transneuronal transport of wheat-germ agglutinin-conjugated horseradish peroxidase in the ocular motor system. *Exp. Brain Res.* 57, 411-16.

Pralong E. and Magistretti P. J. (1995). Noradrenaline increases K-conductance and reduces glutamatergic transmission in the mouse entorhinal cortex by activation of  $\alpha$ 2-adrenoreceptors. *Eur. J. Neurosci.* 7(12), 2370-78.

Price J. L., Amaral D. G. (1981). An Autoradiographic Study of the Projections of the Central Nucleus of the Monkey Amygdala. *J. Neurosci.* 11, 1242-59.

Pudovkina O. L., Cremers T. I. F. H. and Westerink B. H. C. (2002) The interaction between the locus coeruleus and dorsal raphe nucleus studied with dual-probe microdialysis. *Eur. J. Pharmacol.* 445(1-2), 37-42.



Pudovkina O. L., Cremers T. I. F. H. and Westerink B. H. C. (2003). Regulation of the release of serotonin in the dorsal raphe nucleus by  $\alpha 1$  and  $\alpha 2$  adrenoceptors. *Synapse* 50(1), 77-82.

Qi J., Zhang S., Wang HL., Barker D. J., Miranda-Barrientos J., Morales M. (2016). VTA glutamatergic inputs to nucleus accumbens drive aversion by acting on GABAergic interneurons. *Nat. Neurosci.* 19(5), 725-33.

Ramos B. P. and Arnsten A. F. T. (2007). Adrenergic pharmacology and cognition: focus on the prefrontal cortex. *Pharmacol. Ther.* 113(3), 523-36.

Ranjbar-Slamloo Y. and Fazlali Z. (2020). Dopamine and noradrenaline in the brain; overlapping or dissociate functions? *Front. Mol. Neurosci.* 12,334.

Rajkowski J., Majczynski H., Clayton E. C. and Aston-Jones G. (2004). Activation of monkey locus coeruleus neurons varies with difficulty and performance in a target detection task. *J. Neurophysiol.* 92(1), 361-71.

Rash J. E., Olson C. O., Davidson K. G. V., Yasumura T., Kamasawa N. and Nagy J. I. (2007) Identification of connexin36 in gap junctions between neurons in

rodent locus coeruleus. *Neurosci.* 147(4), 938-56.



Rogawski M. A. and Aghajanian G. K. (1980). Modulation of lateral geniculate neurone excitability by noradrenaline microiontophoresis or locus coeruleus stimulation. *Nature* 287(5784), 731-34.

Rodenkirch C., Liu Y., Schriver B. J. and Wang Q. (2019). Locus coeruleus activation enhances thalamic feature selectivity via norepinephrine regulation of intrathalamic circuit dynamics. *Nat. Neurosci.* 22, 120-33.

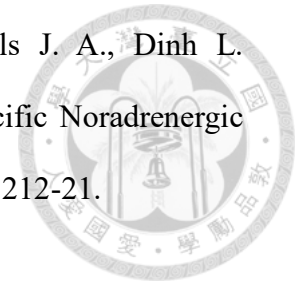
Roesch M. R. and Olson C. R. (2004). Neuronal activity related to reward value and motivation in primate frontal cortex. *Science* 304, 307-10.

Roychowdhury S., Zwierchowski A. N., Garcia-Oscos F., Olguin R. C., Delgado R. S. and Atzori M. (2014). Layer- and area-specificity of the adrenergic modulation of synaptic transmission in the rat neocortex. *Neurochemical Res.* 39, 2377-84.

Rutecki, P. A. (1995). Noradrenergic modulation of epileptiform activity in the hippocampus. *Epilepsy Res.* 20(2), 125-36.

Sales, A. C., Friston, K. J., Jones, M. W., Pickering, A. E. and Moran, R. J. (2019). Locus Coeruleus tracking of prediction errors optimises cognitive flexibility: An Active Inference model. *PLoS Comput. Biol.* 15, e1006267.

Salgado H., Garcia-Oscos F., Patel A., Martinolich L., Nichols J. A., Dinh L. Roychowdhury S., Tseng K. Y. and Atzori M. (2011). Layer-Specific Noradrenergic Modulation of Inhibition in Cortical Layer II/III. *Cereb. Cortex* 21, 212-21.



Salgado H., Garcia-Oscos F., Martinolich L., Hall S., Restom R., Tseng K. Y. and Atzori M. (2012). Pre- and postsynaptic effects of norepinephrine on  $\gamma$ -aminobutyric acid-mediated synaptic transmission in layer 2/3 of the rat auditory cortex. *Synapse* 66(1), 20-28.

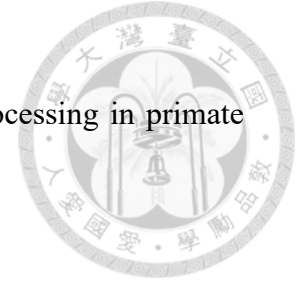
Salgado H., Köhr G. and Treviño M. (2012). Noradrenergic 'tone' determines dichotomous control of cortical spike-timing-dependent plasticity. *Sci. Rep.* 2, 417

Salgado H., Treviño M. and Atzori M. (2016). Layer- and area-specific actions of norepinephrine on cortical synaptic transmission. *Brain Res.* 1641, 163-76.

Sara S. J. and Segal M. (1991). Plasticity of sensory responses of locus coeruleus neurons in the behaving rat: implications for cognition. *Prog. Brain Res.* 88, 571-85.

Sara S. J. and Bouret S. (2012). Orienting and reorienting: the locus coeruleus mediates cognition through arousal. *Neuron*, 130-141.

Scheiderer C. L., Dobrunz L. E. and McMahon L. L. (2004). Novel form of long-term synaptic depression in rat hippocampus induced by activation of  $\alpha 1$  adrenergic receptors. *J. Neurophysiol.* 91(2), 1071-77.



Schultz W., Tremblay L. and Hollerman J. R. (2000). Reward processing in primate orbitofrontal cortex and basal ganglia. *Cereb. Cortex* 10, 272-84.

Schwarz, L.A., Miyamichi, K., Gao, X.J., Bier, K.V., Weissbourd, B., DeLoach, K.E., Ren, J., Ibanes, S., Malenka, R.C., Kremer, E.J. and Luo, L. (2015). Viral-genetic tracing of the input-output organization of a central noradrenaline circuit. *Nature* 524, 88-92.

Segal M., Foote S. L. and Aston-Jones G. (1983). Physiological properties of ascending locus coeruleus axons in the squirrel monkey. *Brain Res.* 274(2), 381-87.

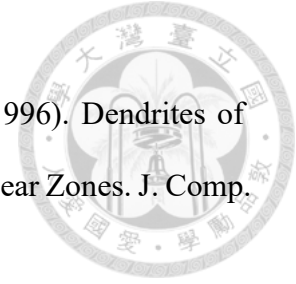
Seo D. and Bruchas M. R. (2017). Polymorphic computation in locus coeruleus networks. *Nat. Neurosci.* 20, 1517-19.

Seol G. H., Ziburkus J., Huang S. Y., Song L., Kim I. T., Takamiya K. Haganir R. L.,

Shane T. R., Marios L., Mohammadali M. S., Martin M. M. and Aaron A. C. (2011).

Félix Vicq d'Azyr (1746–1794): early founder of neuroanatomy and royal French physician. *Child's Nervous System* 27, 1031–1034.

Shen K. Z. and North R. A. (1992). Muscarine increases cation conductance and decreases potassium conductance in rat locus coeruleus neurones. *J Physiol.* 455, 471–485.



Shiple M. T., Fu L., Ennis M., Liu W. L. and Aston-Jones G. (1996). Dendrites of Locus Coeruleus Neurons Extend Preferentially Into Two Pericoerulear Zones. *J. Comp. Neurol.* 365(1), 56-68.

Stanton P. K. and Sarvey J. M. (1985). Depletion of norepinephrine, but not serotonin, reduces long-term potentiation in the dentate gyrus of rat hippocampal slices. *J. Neurosci.* 5(8), 2169-76.

Steininger T. L., Gong H., McGinty D. and Szymusiak R. (2001). Subregional organization of preoptic area /anterior hypothalamic projections to arousal-related monoaminergic cell groups. *J. Comp. Neurol.* 429(4), 638-53.

Stocker M. and Pedarzani P. (2000). Differential distribution of three  $Ca^{2+}$ -activated  $K^{+}$  channel subunits, SK1, SK2, and SK3, in the adult rat central nervous system. *Mol. Cell Neurosci.* 15(5), 476-93.

Sugrue L. P., Corrado G. S. and Newsome W. T. (2004). Matching behavior and the representation of value in the parietal cortex. *Science* 304, 1782-87.

Summers R. J., Papaioannou M., Harris S. and Evans B. A. (1995). Expression of beta 3-adrenoceptor mRNA in rat brain. *Br. J. Pharmacol.* 116,2547-48.

Sutin E. L. and Jacobowitz D. M. (1991). Neurochemicals in the dorsal pontine

tegmentum. *Prog. Brain Res.* 88, 3-14.



Swanson L. W. (1982). The projections of the ventral tegmental area and adjacent regions: a combined fluorescent retrograde tracer and immunofluorescence study in the rat. *Brain Res. Bull.* 9, 321- 353.

Swanson L. W. and Hartman B. K. (1975). The central adrenergic system. An immunofluorescence study of the location of cell bodies and their efferent connections in the rat utilizing dopamine-beta-hydroxylase as a marker. *J. Comp. Neurol.* 163, 467-505.

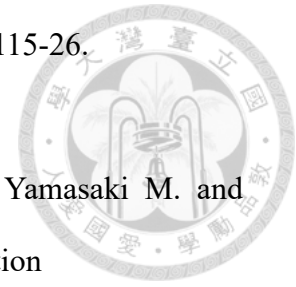
Swerdlow N.R., Weber M., Qu Y., Light G. A. and Braff D.L. (2008). Realistic expectations of prepulse inhibition in translational models for schizophrenia research. *Psychopharmacology* 199, 331–388.

Swift K. M., Gross B. A., Frazer M. A., Bauer D. S., Clark K. J. D., Vazey E. M., Aston-Jones G., Li Y., Pickering A. E., Sara S. J. and Poe G. R. (2018). Abnormal locus coeruleus sleep activity alters sleep signatures of memory consolidation and impairs place cell stability and spatial memory. *Curr. Biol.* 28(22), 3599-3609.

Szabadi E. (2013). Functional neuroanatomy of the central noradrenergic system. *J Psychopharmacol.* 27(10), 964

Takahashi K., Kayama Y., Lin J. S. and Sakai K. (2010). Locus coeruleus neuronal

activity during the sleep-waking cycle in mice. *Neurosci.* 169(3), 1115-26.



Takeuchi T., Duzskiewicz A. J., Sonneborn A., Spooner P. A., Yamasaki M. and Watanabe M. (2016). Locus coeruleus and dopaminergic consolidation of everyday memory. *Nature* 537, 357–362.

Thomas M. J., Moody T. D., Makhinson M. and O'Dell T. J. (1996). Activity-dependent  $\beta$ -adrenergic modulation of low frequency stimulation induced LTP in the hippocampal CA1 region. *Neuron* 17(3), 475-82.

Torontali Z. A., Grace K. P., Horner R. L. and Peever J. H. Cholinergic involvement in control of REM sleep paralysis. *J. Physiol.* 592(7), 1425-26.

Travagli R. A., Dunwiddie T. V. and Williams J. T. (1991). Opioid inhibition in locus coeruleus. *J. Neurophysiol.* 74(2), 519-27

Tronel S., Feenstra M. G. P. and Sara S. J. (2004). Noradrenergic action in prefrontal cortex in the late stage of memory consolidation. *Learn Mem.* 11(4), 453-8.

Uematsu A., Tan B. Z., Ycu E. A., Cuevas J. S., Koivumaa J., Junyent F., Kremer E. J., Witten I. B., Deisseroth K. and Johansen J. P. (2017). Modular organization of the brainstem noradrenaline system coordinates opposing learning states. *Nat. Neurosci.* 20, 1602-11.

Valentino R. J. and Foote S. L. (1987). Corticotropin-releasing factor disrupts sensory responses of brain noradrenergic neurons. *Neuroendocrinology* 45(1), 28-36.

Valentino R. J. and Foote S. L. (1988). Corticotropin-releasing hormone increases tonic but not sensory-evoked activity of noradrenergic locus coeruleus neurons in unanesthetized rats. *J. Neurosci.* 8(3), 1016-25.

Valentino R. J., Page M. E. and Curtis A. L. (1991). Activation of noradrenergic locus coeruleus neurons by hemodynamic stress is due to local release of corticotropin-releasing factor. *Brain Res.* 555(1), 25-34.

Valentino R. J., Page M., Van Bockstaele E. J. and Aston-Jones G. (1992). Corticotropin-releasing factor innervation of the locus coeruleus region: Distribution of fibers and sources of input. *Neurosci.* 48(3), 689-705.

Valentino R. J. and Van Bockstaele E. J. (2001). Opposing regulation of the locus coeruleus by corticotropin-releasing factor and opioids: Potential for reciprocal interactions between stress and opioid sensitivity. *Psychopharmacology* 158, 331-42.

Valentino R. J. and Van Bockstaele E. J. (2008). Convergent regulation of locus coeruleus activity as an adaptive response to stress. *Eur. J. Pharmacol.* 583(2-3), 194-203.

Van Bockstaele E., Colago E. E. and Valentino R. J. (1998). Amygdaloid Corticotropin-

Releasing Factor Targets Locus Coeruleus Dendrites: Substrate for the Co-Ordination of Emotional and Cognitive Limbs of the Stress Response. *J. Neuroendocrinol.* 10(10), 743-57.



Van Bockstaele E., Peoples J. and Valentino R. J. (1999). Anatomic basis for differential regulation of the rostralateral peri-locus coeruleus region by limbic afferents. *J. Neuroendocrinol.* 46(10), 1352-63.

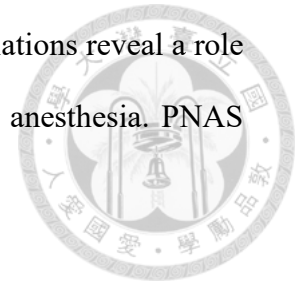
Van Bockstaele E., Garcia-Hernandez F., Fox K., Alvarez V. A. and Williams J. T. (2004). Expression of connexins during development and following manipulation of afferent input in the rat locus coeruleus. *Neurochem. Int.* 45(2-3), 421-28.

Van Bockstaele E. J., Reyes B. A. S. and Valentino R. J. (2010). The locus coeruleus: A key nucleus where stress and opioids intersect to mediate vulnerability to opiate abuse. *Brain Res.* 1314, 162-74.

Van Bockstaele E. J. and Valentino R. J. (2013). Neuropeptide regulation of the locus coeruleus and opiate-induced plasticity of stress responses. *Adv. Pharmacol.* 68, 405-420.

Varazzani C., San-Galli A., Gilardeau S. and Bouret S. (2015). Noradrenaline and dopamine neurons in the reward/effort trade-off: a direct electrophysiological comparison in behaving monkeys. *J. Neurosci.* 35(20), 7866-77.

Vazey E. M. and Aston-Jones G. (2014). Designer receptor manipulations reveal a role of the locus coeruleus noradrenergic system in isoflurane general anesthesia. *PNAS* 111(10), 3859-64.



Vazey E. M., Moorman D. E. and Aston-Jones G. (2018). Phasic locus coeruleus activity regulates cortical encoding of salience information. *PNAS* 115(40), 9439-48.

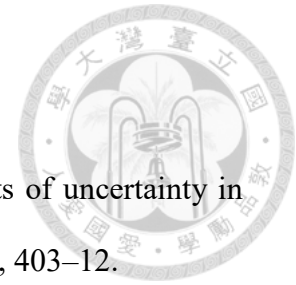
Verret L., Fort P., Gervasoni D., Léger L. and Luppi P. (2006). Localization of the neurons active during paradoxical (REM) sleep and projecting to the locus coeruleus noradrenergic neurons in the rat. *J. Comp. Neurol.* 495(5), 573-86.

Verstegen A. M. J., Vanderhorst V., Gray P. A., Zeidel M. L. and Geerling J. C. (2017). Barrington's nucleus: Neuroanatomic landscape of the mouse "pontine micturition center". *J. Comp. Neurol.* 525(10), 2287-2309.

Verstegen A. M. J., Klymko N., Zhu L., Mathai J. C., Kobayashi R., Venner A., Ross R. A., VanderHorst V. G., Arrigoni E., Geerling J. C. and Zeidel M. L. (2019). Non-Crh glutamatergic neurons in Barrington's nucleus control micturition via glutamatergic afferents from the midbrain and hypothalamus. *Curr. Biol.* 29(17), 2775-89.

Vila-Porcile E., Xu ZQ. D., Mailly P., Nagy F., Calas A., Hökfelt T. and Landry M. (2009). Dendritic synthesis and release of the neuropeptide galanin: Morphological evidence from studies on rat locus coeruleus neurons. *J. Comp. Neurol.* 516(3), 199-

212.



Volz K. G., Schubotz R. I. and von Cramon D. Y. (2005). Variants of uncertainty in decision-making and their neural correlates. *Brain Res. Bull.* 67 (5), 403–12.

Wallace, D.M., Magnuson, D.J., Gray, T.S. (1989) The amygdalobrainstem pathway: selective innervation of dopaminergic, noradrenergic and adrenergic cells in the rat. *Neurosci. Lett.* 97, 252-258.

Wang HY., Kuo ZC., Fu YS., Chen RF., Min MY. and Yang HW. (2015). GABAB receptor-mediated tonic inhibition regulates the spontaneous firing of locus coeruleus neurons in developing rats and in Citalopram-treated rats. *J. Physiol.* 593(1), 161-80.

Waterhouse B. D. and Woodward D. J. (1980). Interaction of norepinephrine with cerebrocortical activity evoked by stimulation of somatosensory afferent pathways in the rat. *Exp. Neurol.* 67(1), 11-34.

Waterhouse B. D., Sessler F. M., Cheng JT., Woodward D. J., Azizi S. A. and Moises H. C. (1988). New evidence for a gating action of norepinephrine in central neuronal circuits of mammalian brain. *Brain Res. Bull.* 21(3), 425-32.

Waterhouse B. D., Azizi S. A., Burne R. A. and Woodward D. J. (1990). Modulation of rat cortical area 17 neuronal responses to moving visual stimuli during norepinephrine and serotonin microiontophoresis. *Brain Res.* 514(2), 276-92.



Waterhouse B. D., Moises H. C. and Woodward D. J. (1998). Phasic activation of the locus coeruleus enhances responses of primary sensory cortical neurons to peripheral receptive field stimulation. *Brain Res.* 790(1-2), 33-44.

Waterhouse B. D. and Navarra R. L. (2019). The Locus coeruleus-norepinephrine system and sensory signal processing: a historical review and current perspectives. *Brain Res.* 1709, 1-15.

Weiner D. M., Levey A. I., Sunahara R. K., Niznik H. B., O'Dowd B. F., Seeman P. and Brann M. R. (1991). D1 and D2 Dopamine Receptor mRNA in Rat Brain. 88(5), 1859-63.

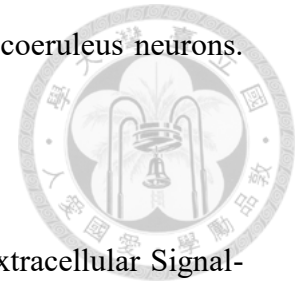
Weinshenker D. and Szot P. (2002). The role of catecholamines in seizure susceptibility: new results using genetically engineered mice. *Pharmacol. Ther.* 94(3), 213-33.

Westlund K.N. and Coulter J.D. (1980). Descending projections of the locus coeruleus and subcoeruleus/medial parabrachial nuclei in monkey: axonal transport studies and dopamine-beta-hydroxylase immunocytochemistry. *Brain Res* 2, 235–264.

Williams, J.T., North, R.A., Shefner, S.A., Nishi, S., and Egan, T.M. (1984) Membrane properties of rat locus coeruleus neurons. *Neurosci.* 13, 137-56.

Williams J. T., Henderson G. and North R. A. (1985). Characterization of  $\alpha$ 2-

adrenoceptors which increase potassium conductance in rat locus coeruleus neurons. *Neurosci.* 14(1), 95-101



Wu RN., Kuo CC., Min MY., Chen RF. and Yang HW. (2020). Extracellular Signal-Regulated Kinases Mediate an Autoregulation of GABA B-Receptor-Activated Whole-Cell Current in Locus Coeruleus Neurons. *Sci. Rep.* 10(1), 7869.

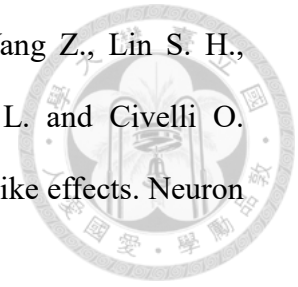
Wyrofsky R. R., Reyes B. A. S., Yu D., Kirby L. G. and Van Bockstaele E. J. (2018). Sex differences in the effect of cannabinoid type 1 receptor deletion on locus coeruleus-norepinephrine neurons and corticotropin releasing factor-mediated responses. *Eur. J. Neurosci.* 48(5), 2118-38.

Wyrofsky R. R., Reyes B. A. S., Zhang XY., Bhatnagar S., Kirby L. G., Van Bockstaele E. J. (2019). Endocannabinoids, stress signaling, and the locus coeruleus-norepinephrine system. *Neurobiol. Stress* 11, 100176.

Xiang L., Harel A., Gao HY., Pickering A. E., Sara S. J. and Wiener S. I. (2019). Behavioral correlates of activity of optogenetically identified locus coeruleus noradrenergic neurons in rats performing T-maze tasks. *Sci. Rep.* 9, 1361.

Xing B., Li YC., and Gao WJ. (2016). Norepinephrine versus dopamine and their interaction in modulating synaptic function in the prefrontal cortex. *Brain Res.* 1641, 217–233.

Xu YL., Reinscheid R. K., Huitron-Resendiz S., Clark S. D., Wang Z., Lin S. H., Brucher F. A., Zeng J., Ly N. K., Henriksen S. J., de Lecea L. and Civelli O. Neuropeptide S: A neuropeptide promoting arousal and anxiolytic-like effects. *Neuron* 43(4), 487-97.



Yamasaki M. and Takeuchi T. (2017). Locus coeruleus and dopamine-dependent memory consolidation. *Neural Plast.* 2017, 8602690

Yang H., Yang J., Xi W., Hao S., Luo B., He X., Zhu L., Lou H., Yu Y., Xu F., Duan S. and Wang H. (2016). Laterodorsal tegmentum interneuron subtypes oppositely regulate olfactory cue-induced innate fear. *Nat. Neurosci.* 19, 283-89.

Yoshihara Y., Mizuno T., Nakahira M., Kawasaki M., Watanabe Y., Kagamiyama H., Jishage K., Ueda O., Suzuki H. and Tabuchi K., et al., (1999). A genetic approach to visualization neurotechnique of multisynaptic neural pathways using plant lectin transgene. *Neuron* 22, 33-41.

Zerbi V., Floriou-Servou A., Markicevic M., Deyn P. P. D., Wenderoth D. and Bohacek J. (2019). Rapid reconfiguration of the functional connectome after chemogenetic locus coeruleus activation. *Neuron* 103(4), 702-718.

Zhang Y., Yu T., Yuan J. and Yu BW. (2015). The ventrolateral preoptic nucleus is required for propofol-induced inhibition of locus coeruleus neuronal activity. *Neurological Sciences* 36, 2177-84.

Zitnik G. A. (2016). Control of arousal through neuropeptide afferents of the locus coeruleus. *Brain Res.* 1641, 338-50.

